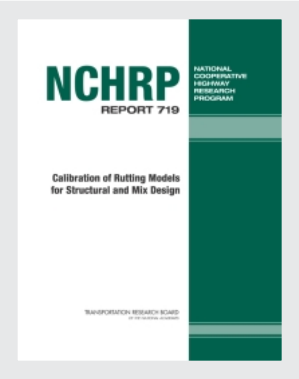

Calibration of Rutting Models for Structural and Mix Design

DETAILS

207 pages | 8.5 x 11 | PAPERBACK
ISBN 978-0-309-21406-3 | DOI 10.17226/22781

AUTHORS

Von Quintus, Harold L.; Mallela, Jagannath; Bonaquist, Ramon; Schwartz, Charles W.; and Carvalho, Regis L

NATIONAL COOPERATIVE HIGHWAY RESEARCH PROGRAM

NCHRP REPORT 719

Calibration of Rutting Models for Structural and Mix Design

Harold L. Von Quintus
APPLIED RESEARCH ASSOCIATES, INC.
Round Rock, Texas

Jagannath Mallela
APPLIED RESEARCH ASSOCIATES, INC.
Round Rock, Texas

Ramon Bonaquist
ADVANCED ASPHALT TECHNOLOGIES, LLC
Sterling, Virginia

Charles W. Schwartz
UNIVERSITY OF MARYLAND
College Park, Maryland

Regis L. Carvalho
DYNATEST CONSULTING, INC.
Upper Marlboro, Maryland

Subscriber Categories
Highways • Materials • Design

Research sponsored by the American Association of State Highway and Transportation Officials
in cooperation with the Federal Highway Administration

TRANSPORTATION RESEARCH BOARD

WASHINGTON, D.C.
2012
www.TRB.org

NATIONAL COOPERATIVE HIGHWAY RESEARCH PROGRAM

Systematic, well-designed research provides the most effective approach to the solution of many problems facing highway administrators and engineers. Often, highway problems are of local interest and can best be studied by highway departments individually or in cooperation with their state universities and others. However, the accelerating growth of highway transportation develops increasingly complex problems of wide interest to highway authorities. These problems are best studied through a coordinated program of cooperative research.

In recognition of these needs, the highway administrators of the American Association of State Highway and Transportation Officials initiated in 1962 an objective national highway research program employing modern scientific techniques. This program is supported on a continuing basis by funds from participating member states of the Association and it receives the full cooperation and support of the Federal Highway Administration, United States Department of Transportation.

The Transportation Research Board of the National Academies was requested by the Association to administer the research program because of the Board's recognized objectivity and understanding of modern research practices. The Board is uniquely suited for this purpose as it maintains an extensive committee structure from which authorities on any highway transportation subject may be drawn; it possesses avenues of communications and cooperation with federal, state and local governmental agencies, universities, and industry; its relationship to the National Research Council is an insurance of objectivity; it maintains a full-time research correlation staff of specialists in highway transportation matters to bring the findings of research directly to those who are in a position to use them.

The program is developed on the basis of research needs identified by chief administrators of the highway and transportation departments and by committees of AASHTO. Each year, specific areas of research needs to be included in the program are proposed to the National Research Council and the Board by the American Association of State Highway and Transportation Officials. Research projects to fulfill these needs are defined by the Board, and qualified research agencies are selected from those that have submitted proposals. Administration and surveillance of research contracts are the responsibilities of the National Research Council and the Transportation Research Board.

The needs for highway research are many, and the National Cooperative Highway Research Program can make significant contributions to the solution of highway transportation problems of mutual concern to many responsible groups. The program, however, is intended to complement rather than to substitute for or duplicate other highway research programs.

NCHRP REPORT 719

Project 9-30A
ISSN 0077-5614
ISBN 978-0-309-21406-3
Library of Congress Control Number 2012936953

COPYRIGHT INFORMATION

NOTICE

The project that is the subject of this report was a part of the National Cooperative Highway Research Program, conducted by the Transportation Research Board with the approval of the Governing Board of the National Research Council.

The members of the technical panel selected to monitor this project and to review this report were chosen for their special competencies and with regard for appropriate balance. The report was reviewed by the technical panel and accepted for publication according to procedures established and overseen by the Transportation Research Board and approved by the Governing Board of the National Research Council.

The opinions and conclusions expressed or implied in this report are those of the researchers who performed the research and are not necessarily those of the Transportation Research Board, the National Research Council, or the program sponsors.

The Transportation Research Board of the National Academies, the National Research Council, and the sponsors of the National Cooperative Highway Research Program do not endorse products or manufacturers. Trade or manufacturers' names appear herein solely because they are considered essential to the object of the report.

Published reports of the

NATIONAL COOPERATIVE HIGHWAY RESEARCH PROGRAM

are available from:

Transportation Research Board
Business Office
500 Fifth Street, NW
Washington, DC 20001

and can be ordered through the Internet at:

http://www.national-academies.org/trb/bookstore

Printed in the United States of America

THE NATIONAL ACADEMIES

Advisers to the Nation on Science, Engineering, and Medicine

The **National Academy of Sciences** is a private, nonprofit, self-perpetuating society of distinguished scholars engaged in scientific and engineering research, dedicated to the furtherance of science and technology and to their use for the general welfare. On the authority of the charter granted to it by the Congress in 1863, the Academy has a mandate that requires it to advise the federal government on scientific and technical matters. Dr. Ralph J. Cicerone is president of the National Academy of Sciences.

The **National Academy of Engineering** was established in 1964, under the charter of the National Academy of Sciences, as a parallel organization of outstanding engineers. It is autonomous in its administration and in the selection of its members, sharing with the National Academy of Sciences the responsibility for advising the federal government. The National Academy of Engineering also sponsors engineering programs aimed at meeting national needs, encourages education and research, and recognizes the superior achievements of engineers. Dr. Charles M. Vest is president of the National Academy of Engineering.

The **Institute of Medicine** was established in 1970 by the National Academy of Sciences to secure the services of eminent members of appropriate professions in the examination of policy matters pertaining to the health of the public. The Institute acts under the responsibility given to the National Academy of Sciences by its congressional charter to be an adviser to the federal government and, on its own initiative, to identify issues of medical care, research, and education. Dr. Harvey V. Fineberg is president of the Institute of Medicine.

The **National Research Council** was organized by the National Academy of Sciences in 1916 to associate the broad community of science and technology with the Academy's purposes of furthering knowledge and advising the federal government. Functioning in accordance with general policies determined by the Academy, the Council has become the principal operating agency of both the National Academy of Sciences and the National Academy of Engineering in providing services to the government, the public, and the scientific and engineering communities. The Council is administered jointly by both Academies and the Institute of Medicine. Dr. Ralph J. Cicerone and Dr. Charles M. Vest are chair and vice chair, respectively, of the National Research Council.

The **Transportation Research Board** is one of six major divisions of the National Research Council. The mission of the Transportation Research Board is to provide leadership in transportation innovation and progress through research and information exchange, conducted within a setting that is objective, interdisciplinary, and multimodal. The Board's varied activities annually engage about 7,000 engineers, scientists, and other transportation researchers and practitioners from the public and private sectors and academia, all of whom contribute their expertise in the public interest. The program is supported by state transportation departments, federal agencies including the component administrations of the U.S. Department of Transportation, and other organizations and individuals interested in the development of transportation. **www.TRB.org**

www.national-academies.org

COOPERATIVE RESEARCH PROGRAMS

CRP STAFF FOR NCHRP REPORT 719

Christopher W. Jenks, *Director, Cooperative Research Programs*
Crawford F. Jencks, *Deputy Director, Cooperative Research Programs*
Edward T. Harrigan, *Senior Program Officer*
Anthony Avery, *Senior Program Assistant*
Eileen P. Delaney, *Director of Publications*
Doug English, *Editor*

NCHRP PROJECT 9-30A PANEL
Field of Materials and Construction—Area of Bituminous Materials

Carl L. Monismith, *University of California – Berkeley, Berkeley, CA* (Chair)
Bouzid Choubane, *Florida DOT, Gainesville, FL*
Shongtao Dai, *Minnesota DOT, Maplewood, MN*
Danny A. Dawood, *The Transtec Group, Mechanicsburg, PA*
Adam J. T. Hand, *Granite Construction, Inc., Sparks, NV*
Julie E. Kliewer, *Arizona DOT – Phoenix Construction Division, Phoenix, AZ*
Leslie Ann McCarthy, *Villanova University, Villanova, PA*
David E. Newcomb, *Texas Transportation Institute, College Station, TX*
Murari M. Pradhan, *Arizona DOT, Phoenix, AZ*
John Bukowski, *FHWA Liaison*
Katherine A. Petros, *FHWA Liaison*
Nelson H. Gibson, *FHWA Liaison*
Frederick Hejl, *TRB Liaison*

FOREWORD

By Edward T. Harrigan
Staff Officer
Transportation Research Board

This report proposes revisions to the *Mechanistic–Empirical Pavement Design Guide* (MEPDG) and software to (1) incorporate three alternative rut-depth prediction models that rely on repeated load (triaxial) permanent deformation or constant height testing to provide the requisite input data, and (2) provide revised coefficients for the original and alternative rut-depth transfer functions or prediction models derived from material properties measured in the laboratory and pavement performance data. Thus, the report will be of immediate interest to engineers in public- and private-sector organizations with responsibility for the structural design and analysis of asphalt concrete (AC) pavements.

NCHRP Project 9-30A, "Calibration of Rutting Models for HMA Structural and Mix Design," was conducted by Applied Research Associates, Inc. (ARA), Round Rock, Texas, with major participation by Advanced Asphalt Technologies, LLC, Sterling, Virginia, and the University of Maryland, College Park, Maryland.

The objective of this research was to recalibrate the AC rutting prediction model in the MEPDG software developed in NCHRP Projects 1-37A and 1-40 with measured material properties and performance data from Long-Term Pavement Performance Program Special Pavement Studies (LTPP SPS) and other full-scale pavement sections, including sections built with modified asphalt binders. The measured material properties included volumetric properties, dynamic modulus, and repeated-load plastic deformation tests (triaxial and shear-based tests). In addition, the project team evaluated three alternative rut-depth transfer functions, programmed them into the MEPDG Version 1.0, and compared the accuracy and goodness of fit of their predicted rut depth results to those obtained with the original (Kaloush) transfer function developed in NCHRP Projects 1-37A and 1-40.

Material properties needed for Input Level 1 were measured on original materials and pavement cores from 45 AC pavement sections from the LTPP SPS-5, SPS-6, and SPS-9, the WesTrack project, the NCAT test track, MnROAD, and I-710 in Long Beach, California. Pavement rutting distress data in the LTPP and other databases were supplemented by forensic examination (including trenching) of pavement sections.

The data from these pavement sections were used for recalibration and validation of the original and three alternative rut-depth transfer functions:

1. Asphalt Institute (modified Leahy) vertical strain and deviator stress transfer function.
2. Verstraeten deviator stress transfer function.
3. WesTrack shear strain and stress transfer function.

A key characteristic of these alternative transfer functions is that they use repeated-load (triaxial) permanent deformation or constant height shear testing to develop the MEPDG input data, in contrast to the original MEPDG transfer function that only requires dynamic modulus (stiffness) mixture testing for Input Level 1.

The research reached several key conclusions. With proper calibration, all four transfer functions accurately simulated the evolution of AC pavement rutting, and there were no statistically or practically significant differences among results obtained with the four functions. All of the transfer functions were calibrated to provide reasonable predictions of rut depth. Finally, for higher traffic conditions and larger rut-depth threshold values or design criteria, conducting repeated load tests to define the plastic deformation properties of AC mixtures is cost effective.

The four transfer functions are implemented in the software program MEPDG Version NCHRP 9-30A produced as a project deliverable. MEPDG Version NCHRP 9-30A is based on MEPDG Version 1.0 produced in NCHRP Project 1-40 and allows the user to choose among the four transfer functions for predicting the rutting behavior of an AC pavement design. All transfer function calibration coefficients are derived from the calibration carried out in the project with measured material properties. Other enhancements or modifications made in MEPDG Version NCHRP 9-30A include (1) the capability to enter mixture- or layer-specific permanent deformation parameters, (2) a fix to the local calibration parameter for unbound aggregate base layers, and (3) incorporation of a normal distribution of truck traffic rather than a uniform distribution between limits of truck wander.

The report fully documents the research leading to MEPDG Version NCHRP 9-30A, and includes six appendixes:

- Appendix A: Proposed Addendum to AASHTO Publication MEPDG-1: *Mechanistic–Empirical Pavement Design Guide, Interim Edition: A Manual of Practice*
- Appendix B: Software Modifications or Alterations to the MEPDG for Predicting Rut Depths
- Appendix C: Step-By-Step Procedure for Adjusting the Global Calibration Parameters of the MEPDG (Kaloush) Rut-Depth Transfer Function
- Appendix D: Dynamic Modulus Test Results
- Appendix E: Repeated-Load Test Results
- Appendix F: Incremental Benefit–Cost Analysis: Comparison of Alternate Transfer Functions and Test Methods

In addition, five appendixes are available for download from the NCHRP Project 9-30A web page at http://apps.trb.org/cmsfeed/TRBNetProjectDisplay.asp?ProjectID=965:

- Appendix G: December 2005 Facilitated Workshop: Executive Summary and Minutes
- Appendix H: User Manual for the M-E_DPM Database
- Appendix I: Simple Performance Test System Instrumentation
- Appendix J: Summary of Data from the Test Sections Used For the Calibration and Validation of MEPDG Version NCHRP 9-30A
- Appendix K: Advanced Materials Characterization and Modeling

The software program MEPDG Version NCHRP 9-30A was provided to the AASHTO Joint Task Force on Pavements and the DARWin-ME Task Force for consideration for adoption in a future version of DARWin-ME.

CONTENTS

Appendices G through K are available to download from the NCHRP Project 9-30A web page at http://apps.trb.org/cmsfeed/TRBNetProjectDisplay.asp?ProjectID=965.

Note: Many of the photographs, figures, and tables in this report have been converted from color to grayscale for printing. The electronic version of the report (posted on the Web at www.trb.org) retains the color versions.

AUTHOR ACKNOWLEDGMENTS

The research described herein was performed under NCHRP Project 9-30A by the transportation sector of Applied Research Associates (ARA), Inc. Mr. Harold L. Von Quintus served as the Principal Investigator on the project.

Mr. Von Quintus was assisted by Mr. Jagannath Mallela as the project manager and engineer on the team. Other management team members and subcontractors included Dr. Charles W. Schwartz, P.E., of the University of Maryland, and Dr. Ramon Bonaquist of Advanced Asphalt Technologies, LCC. Both Dr. Schwartz and Dr. Bonaquist served as Co-Principal Investigators on the project.

In addition, the project management team was supported by many individuals who assisted in the facilitated workshop, software modifications, computational analyses, laboratory testing, field forensic investigations, calibration, and other activities. These individuals are listed as follows:

Applied Research Associates: Dr. Chetana Rao assisted with preparation of the workshop and analysis of the transfer functions. Dr. Alex Gotlif and Dr. Greg Larson were the individuals that made all revisions and upgrades to the software. Mr. Leslie Titus-Glover, Mr. Mark Stanley, and Dr. Suri Sadasivam participated in the data analysis activities and exported data from the Long Term Pavement Performance (LTPP) database for use in the calibration effort. Dr. Chetana Rao, Mr. Ajay Singh, and Mr. Brandon Von Quintus assisted with the local calibration and analysis of the rut-depth transfer functions. Mr. Paul Littleton participated as a member of the forensic investigation team. Ms. Robin Jones provided editorial review and report formatting.

University of Maryland: Dr. Laura Scott participated as the facilitator for the workshop. Dr. Regis L. Carvalho (now with ARA) assisted with conducting the facilitated workshop, developing and populating the Mechanistic–Empirical Distress Prediction Model (M-E_DPM) database, and developing the advanced mixture characterization tools, procedures, and software. The advanced materials characterization and modeling effect were completed under the supervision of Dr. Charles W. Schwartz. The University of Maryland completed all of the advanced modeling activities.

Advanced Asphalt Technologies (AAT): All of the laboratory testing was completed under the supervision of Dr. Ramon Bonaquist. AAT's laboratory technician provided all of the production testing conducted under this project.

North Carolina State University: Dr. Richard Kim assisted in the advanced mixtures characterization studies for the project.

Arizona State University: Dr. Mohamed El Basyouny participated as an independent reviewer of the software modifications made to the *Mechanistic–Empirical Pavement Design Guide*.

Burns Cooley Dennis, Inc.: Mr. Robert Long participated as a member of the forensic investigation team.

One of the major efforts of this study was the facilitated workshop in selecting the rut-depth transfer functions that were to be calibrated and evaluated under Phase III. The team greatly appreciates the time attendees of the workshop spent planning for and attending the workshop. Individuals that participated in this workshop, other than the team members, included Dr. Carl L. Monismith and Mrs. Lorina Popescu with the University of California at Berkeley (Ms. Popescu assisted the team with conducting the workshop and preparation of the meeting minutes); John Bukowski, Katherine A. Petros, and Cheryl Richter with the FHWA; Julie E. Kliewer and Murari M. Pradhan with the Arizona DOT; Dr. Steve Brown (consultant); Leslie Ann McCarthy (Villanova University); Bouzid Choubane (Florida DOT); Shongtao Dai (Minnesota DOT); Danny A. Dawood (the Transtec Group); Adam J. T. Hand (Granite Construction, Inc.); John Haddock (Purdue University); Shmuel Weissman (University of California at Berkeley); Tom Scarpas (Delft University); Per Ullitz (Dynatest); Rey Roque (University of Florida); Linbing Wang (Virginia Tech); and Mohamed El Basyouny (Arizona State University).

The project team also appreciates and acknowledges the support and technical assistance of various agency and contractor personnel that provided field and laboratory data and support for the forensic investigations of multiple test sections included within this study. Those individuals involved in coordination and data collection for specific test sections are listed in the following.

LTPP – MRL: Dr. Sirus Alavi with Transportation Engineers (contractor on the LTPP program) for coordinating, scheduling, and shipping component materials from the LTPP Materials Research Library in Reno, Nevada. These materials were used in the production test program for calibrating the different transfer functions considered and evaluated within the study.

National Center for Asphalt Technology (NCAT): Drs. Nam Tran and Buzz Powell with NCAT for providing measured rut depths and samples of the hot-mix asphalt mixtures placed on specific test sections at the NCAT test track.

Arizona: Ms. Judie Kliewer with the Arizona Department and Mr. Kevin Senn with Nichols Consulting for providing access to and assistance with the forensic investigation of Arizona's LTPP SPS-5 project.

Mississippi: Mr. William Barstis with the Mississippi Department of Transportation and Mr. Gaylon Baumgardner with Paragon Technical Services, Inc., for providing information and additional materials used on Mississippi's LTPP SPS-5 project.

Missouri: Mr. John Donahue with the Missouri Department of Transportation for providing materials and mixture design information for Missouri's LTPP SPS-5 project.

Montana: Ms. Sue Sillick and Mr. Jon Watson with the Montana Department of Transportation for providing materials, mixture data, and access to Montana's LTPP SPS-5, SPS-1, and SPS-9 projects.

Texas: Dr. Fee Fong with the Texas Transportation Institute for assisting with the coordination of the forensic investigation of the Texas SPS-5 project.

Wisconsin: Mr. Steve Krebs and Mrs. Laura Fenley with the Wisconsin Department of Transportation for providing mixture design information and assistance with trenching the Wisconsin SPS-1 and SPS-9 LTPP projects. Dr. Erv Dukatz with Mathy Construction provided additional samples of the fine and coarse aggregate that were used in production to complete the production test program for the Wisconsin projects.

CHAPTER 1

Introduction

1.1 Background

The 1993 *AASHTO Guide for Design of Pavement Structures* is used by most agencies in the United States (AASHTO, 1993) for both new pavement and rehabilitation designs. The 1993 version of the AASHTO design procedure contained many improvements over its predecessor. However, it remained an empirical design procedure with limitations and deficiencies that were addressed in the development of the MEPDG, now deployed as the AASHTO design program DARWin-ME. In addition, analyses completed within SHRP under the Long Term Pavement Performance (LTPP) program showed that the AASHTO design equation does not adequately explain pavement performance (Daleiden et al., 1994).

To overcome the deficiencies and limitations of empirical design procedures, industry has supported and sponsored the development of structural design procedures that are based on mechanistic–empirical (M-E) principles. The latest and most comprehensive one was developed under NCHRP Project 1-37A as the *Guide for Mechanistic–Empirical Design of New and Rehabilitated Pavement Structures* (ARA, Inc., ERES Consultants Division, 2004—referred to hereafter as MEPDG or the *Mechanistic–Empirical Pavement Design Guide*). These procedures use both volumetric and fundamental material properties, such as modulus and strength, to characterize hot-mix asphalt (HMA) and other pavement materials. This is in contrast to the 1993 *AASHTO Guide for Design of Pavement Structures,* which only uses resilient modulus for estimating structural layer coefficient.

A major effort of NCHRP Project 1-37A was the calibration of the distress transfer functions. It was the opinion of the research team that if the design procedure was to be adopted by industry, the design and analysis method would have to demonstrate reasonable accuracy in predicting the performance of actual pavements. As such, over 100 test sections in the LTPP program were used to calibrate the flexible pavement and HMA overlay distress transfer functions included in the MEPDG software. The sections used in the calibration process cover a diverse range of soils, structures, climates, and truck traffic. Unfortunately, these sections also omit common mixture types that are now being used by industry [for example, polymer-modified asphalt (PMA) mixtures, high-percentage recycled-asphalt pavement (RAP) mixtures, asphalt-permeable drainage layers, open-graded friction layers, and warm-mix asphalt (WMA) technology].

A major limitation of that calibration process was the use of default values for the material properties of the HMA and other pavement layers. It was hypothesized that the total error term was heavily affected by the use of global default HMA properties (fracture and plastic or permanent deformation) and dynamic modulus calculated from volumetric properties. Default values had to be used in the calibration process because dynamic modulus (or other laboratory stiffness measurements) and other fundamental tests were not included in the LTPP database at the time of calibration. Thus, it was recommended by the NCHRP Project 1-37A team that the distress transfer functions be checked and recalibrated using material properties measured in the laboratory for the pavement layers and foundation soils. The NCHRP Project 9-19 team made a similar recommendation in developing and validating the simple performance test in support of the Superpave® volumetric design of HMA mixtures and integrating mixture and structural design (Witczak et al., 2002).

NCHRP Project 9-30 was tasked with developing a detailed and practical experimental plan for this effort to improve on the calibration by using laboratory material tests for characterizing the layers for structural design. *NCHRP Research Results Digest 284: Refining the Calibration and Validation of Hot-Mix Asphalt Performance Models: An Experimental Plan and Database,* is a synthesis of the experimental plan that resulted from NCHRP Project 9-30 (Transportation Research Board, 2003b). In addition, NCHRP Project 9-30 identified an analytical technique called *jackknifing* as a means of accomplishing reliable calibration and validation with limited sets of

complete data from full-scale pavement sections. The specific application of jackknifing to the calibration of the MEPDG software is described in *NCHRP Research Results Digest 283: Jackknife Testing—An Experimental Approach to Refine Model Calibration and Validation* (Transportation Research Board, 2003a).

The goal of NCHRP Project 9-30A was to build on the products from NCHRP Project 9-30 and other projects by using material properties measured in the laboratory in place of the default values that were used for calibration under NCHRP Projects 1-37A and 1-40D. Use of these measured mixture properties is expected to improve the goodness-of-fit and overall accuracy of the rut-depth transfer function included in the MEPDG software. (Note: *Transfer function* is used extensively in this report. A transfer function relates a pavement response parameter calculated with a mechanistic model to an observed distress. In other words, it transfers the pavement response parameter into an observed distress that can be measured along the roadway.)

1.2 Research Objective

The objective of this research effort was to propose revisions to the HMA rut-depth transfer function in the MEPDG software developed in NCHRP Project 1-37A for consideration by NCHRP and the AASHTO Joint Task Force on Pavements. The proposed revisions were based on the calibration and validation of multiple rut-depth transfer functions with measured material properties and performance data from roadways and other full-scale pavement sections that incorporate modified as well as unmodified asphalt binders.

1.3 Project Overview

NCHRP Project 9-30A was grouped into three phases, with multiple tasks in each phase. The following paragraphs provide an overview of the project.

- Phase I focused on enhancing the database [entitled Mechanistic–Empirical Distress Prediction Model (M-E_DPM)] that was developed under NCHRP Project 9-30 and populating the database with data from test sections and mixture tests used in this study. This first phase was basically a continuation of the work product developed under NCHRP Project 9-30 (Von Quintus et al., 2004; Von Quintus, Andrei, and Schwartz, 2005).
- Phase II focused on three areas: (1) hosting a facilitated workshop to identify the rut-depth transfer functions to be assessed under Phase III, (2) developing the experimental plan and sampling matrix for assessing the rut-depth transfer functions to be proposed for use in the MEPDG software, and (3) selecting test sections and projects for calibrating the rut-depth transfer functions proposed for use from the facilitated workshop. The facilitated workshop was considered an important activity within NCHRP Project 9-30A because of consensus reached between independent parties relative to M-E–based rut-depth transfer functions.
- Phase III included executing the experimental plan from Phase II. These activities under Phase III included testing HMA mixtures for measuring the plastic or permanent deformation coefficients, calibrating the rut-depth transfer functions, and assessing the results from each transfer function. The laboratory test program was divided into two parts. The first part was to determine the test conditions for measuring the plastic deformation coefficients, while the second part was the production test program for determining the field adjustment factors (calibration) of each rut-depth transfer function. This final phase of the project also included the calibration and validation of multiple rut-depth transfer functions programmed into the MEPDG software (Version 9-30A) and an assessment of each related to the use of repeated-load plastic deformation (RLPD) testing in support of the transfer functions.

1.4 Scope of Report and Project Documentation

This report is the documentation for NCHRP Project 9-30A and summarizes the research completed in the project. In addition to this introductory chapter, the other chapters of this research report are as discussed in the following:

- Chapter 2 is a summary of the findings from this study. The first section includes a review of the rut-depth transfer functions from the facilitated workshop. The next two sections summarize the improvements and enhancements that were made to Version 1.0 of the MEPDG software, and contain an overview of the database for retaining data used in the study. The fourth section presents the experimental sampling matrix and factors and lists the individual test sections used for assessing the rut-depth transfer functions. The fifth section includes a preliminary analysis of test sections included in the evaluation process. The next three sections include a review of the exploratory test program used to determine the laboratory test conditions, an analysis of the RLPD data, and an overview of the laboratory test plan for the test sections included in the experimental sampling template (including test specimen preparation). These sections also provide a summary of the instrumentation study for improving the laboratory tests for characterizing HMA mixtures and expanding the database used to store all field and laboratory test results. The final section

of Chapter 2 is a determination of the plastic deformation coefficients derived from laboratory repeated-load tests.
- Chapter 3 provides all data analyses, including interpretation and application of laboratory repeated-load tests, pavement response analyses, mixture physical properties, and measured rut depths. The first section provides the results from verifying the adequacy of the transfer functions using their global coefficients. The values for the global coefficients were found to be inadequate, so the second section discusses the recalibration process and important factors for improving on the accuracy and precision of the MEPDG rut-depth prediction model using different transfer functions. The calibration process includes determining the *m*-values (slope of secondary region), intercept, and stress coefficients from repeated load tests of appropriate transfer functions and determining the field-adjusted plastic strain parameters. The third section provides the relationships between the field-adjusted plastic strain parameters and volumetric properties of the HMA layers. These relationships are used to estimate the plastic strain parameters for Input Level 2. The fourth section assesses the effectiveness of each rut-depth transfer function, while the fifth proposes methods to incorporate the findings into current mixture design and construction acceptance procedures. The final section is an overview of the advanced mixture characterization tests and mechanistic-based rut-depth simulation model.
- Chapter 4 is a summary of the conclusions of the project, proposed actions, and proposals for future research.

The appendices provide more specific information on topics discussed in the body of the report. The following lists and briefly describes the information included in the appendices. (Note that Appendices G through K are available at the NCHRP Project 9-30A web page at http://apps.trb.org/cmsfeed/TRBNetProjectDisplay.asp?ProjectID=965.)

- Appendix A: Proposed Addendum to AASHTO Publication MEPDG-1: *Mechanistic–Empirical Pavement Design Guide, Interim Edition: A Manual of Practice*. This appendix provides a summary of the procedure to determine the HMA plastic deformation parameters to predict rutting.
- Appendix B: Software Modifications or Alterations to the MEPDG for Predicting Rut Depth. This appendix summarizes the enhancements and modifications that were made to the MEPDG Version 1.0 software to facilitate use of other rut-depth transfer functions.
- Appendix C: Step-by-Step Procedure for Adjusting the Global Calibration Coefficients of the MEPDG (Kaloush) Rut-Depth Transfer Functions. This appendix includes procedures proposed for use under NCHRP Project 1-40B for making adjustments to the global calibration coefficients to predict rutting.
- Appendix D: Dynamic Modulus Test Results. This appendix includes a summary of the dynamic modulus tests conducted in accordance with AASHTO TP 79 and the resulting master curves for the primary HMA mixtures included in the production test program.
- Appendix E: Repeated-Load Test Results. This appendix includes graphical summaries of the repeated-load plastic deformation tests conducted in accordance with AASHTO TP 79 and TP 332 for the core mixtures included in the production test program.
- Appendix F: Incremental Benefit–Cost Analysis: Comparison of Alternate Transfer Functions and Test Methods. This appendix explains the procedure used to compare the different transfer functions and test methods. It provides the background, reasoning, and assumptions used in the analyses.
- Appendix G: December 2005 Facilitated Workshop: Executive Summary and Minutes. This appendix is an overview and summary of the facilitated workshop. The purpose of the facilitated workshop was to select the M-E–based transfer functions and mechanistic-based models for predicting rut depths.
- Appendix H: User Manual for M-E_DPM Database. This appendix is the user manual for the M-E_DPM database that was populated with the laboratory and field test data used to calibrate and evaluate the rut-depth transfer functions included in this study.
- Appendix I: Simple Performance Test System Instrumentation. This appendix is the instrumentation study completed within NCHRP Project 9-30A for improving the measurement for materials characterization.
- Appendix J: Summary of Data from the Test Sections Used for the Calibration and Validation of MEPDG Version 9-30A. This appendix is a summary of the test sections (roadway segments and full-scale accelerated pavement tests) that were included in the calibration of the rut-depth transfer functions.
- Appendix K: Advanced Materials Characterization and Modeling. This appendix is an overview of the advanced model that was used to confirm and/or validate some of the simplifying assumptions included in the MEPDG rut-depth prediction and calculation methodology.

1.5 Lessons Learned

This section lists some lessons learned in accomplishing the objectives and goals of this project. These lessons learned do not necessarily represent the findings or conclusions from the research study. The findings and conclusions are summarized in Chapter 4.

1. You can never have enough material for use on future research projects. It is suggested that a minimum of 2,000 lbs of equivalent bulk mixture be retained and

stored for future validation efforts. Samples of both bulk mixture and component materials should be retained for use in future calibration and validation projects. The material samples should not be used to develop the prediction models—only to validate or calibrate (or both) the models to field-measured distress values.

The Materials Reference Library (MRL) (SHRP and Jones, 1993–1995) established under SHRP was important to this research plan, and support for the MRL should be continued. Many of the mixtures included in the study were obtained from the MRL. Some of the container labels, however, had incorrect information regarding the type of samples as well as the material inside the container. On a few of the projects, some containers had to be returned and the project dropped from the experiment or sampling matrix because sufficient materials were unavailable for preparing the test specimens. The type of material and samples need to be accurately identified on the container labels by using consistent terminology for the type of sample and material included in the container being shipped to the MRL. Accurate labels will reduce the effort prior to shipping the containers and reduce the shipping costs for returning any container with incorrect information on the label.

In addition, most of the more recent, non-LTPP projects identified as potential candidates in the NCHRP Project 9-30 experimental plan (Transportation Research Board, 2003b) had to be dropped because sufficient amounts of materials or bulk mixture were unavailable in the MRL.

2. Test methods for measuring the in-place properties are needed for determining the effect of aging on HMA mixtures. These methods should be applicable for testing field cores—an important component of any forensic investigation. More cores should have been taken along each project for judging and assessing the validity of the aging model included in the MEPDG as related to predicting rut depths and other distresses.

   The aging model included in the MEPDG software increases the stiffness of the asphalt over time. The stiffness increases but at a decreasing rate with time and depth. The MEPDG assumes that the coefficients of the transfer function are constant with time. For plastic deformation, that assumption was found to be reasonable but incorrect. For fracture-related distresses, that assumption is believed to be inaccurate. Although the fracture transfer functions were not investigated in NCHRP Project 9-30A, results from some of the earlier projects have suggested that one or more coefficients may need to be time dependent to accurately account for aging effects in predicting the evolution of distress (for example, thermal cracking).
3. The difference between the residual errors of runs made with measured (Input Level 1) and calculated (Input Level 3) dynamic modulus values from volumetric properties was small. This observation suggests that dynamic modulus, by itself, does not explain the effect of changing volumetric properties on rut depths. There were other reasons for the large differences between the predicted and measured values from different transfer functions.
4. Deviator stress in the plastic vertical strain transfer function (modified Leahy) and shear stress in the plastic shear strain transfer function (WesTrack) are important parameters in predicting incremental rut depth. The coefficients of the stress terms can be used with the depth functions to simulate the measured rut depths—eliminating bias and reducing the standard error. Although transfer functions with and without stress terms can be used, including stress in the transfer function is recommended. The key is in determining the coefficient of the stress term for the appropriate depth function.
5. The shear stress used in the repeated-load constant-height shear test is much lower than calculated using elastic layer theory near the edge of the tire. A larger shear stress is believed to be more representative of the in-place conditions. Larger shear stresses should have been used in the laboratory test program to determine the plastic deformation or shear strain coefficients. The higher shear stress is adjusted by lowering the shear stress term in the appropriate transfer function to simulate the measured rut depth. For consistency, the deviator stress used in the repeated-load axial-strain test is also lower than the deviator stresses computed with elastic layer theory.
6. The test temperature of 68°F (20°C) was found to be too low for the two repeated-load test methods (triaxial and shear) for some of the mixtures included in production testing. A value of 75°F to 85°F (24°C to 29°C) should have been used for determining laboratory-derived plastic deformation or strain coefficients. Similarly, the test temperature represented by the LTPP-bind high temperature at 50% reliability was found to be too high for some mixtures. The upper test temperature was lowered by 5°C during the production test program.
7. Do not underestimate the value and importance of facilitated workshops. The NCHRP Project 9-30A facilitated workshop was valuable in providing a diverse set of opinions related to test methods and models used to predict rutting and distortion of HMA mixtures. Appendix G (available to download from the NCHRP Project 9-30A web page at http://apps.trb.org/cmsfeed/TRBNetProjectDisplay.asp?ProjectID=965) is an overview and summary of the facilitated workshop. Even though there was a diverse set of opinions from the participants, consensus was reached on nearly all of the debated issues or

topics. The key to facilitation is having an independent facilitator supported by individuals that understand the different opinions for reaching consensus but do not voice their individual opinions.

8. The measurement error is the largest component of the standard error term for many of the distress transfer functions. Future studies should be planned for reducing the measurement error of different distresses. This measurement error must be taken into account or considered in developing, assessing, and comparing the accuracy of rut-depth transfer functions. This lesson learned also applies to other distresses predicted using M-E–based procedures.
9. The MEPDG outputs the predicted rut depth on a monthly basis. To evaluate the rutting evolution from accelerated pavement test (APT) sections with the MEPDG requires that the loads be applied over a longer time period; stretching the load cycles over a longer period of time results in more asphalt aging than actually occurs during the loading cycles for many APT sections. This will result in a negative bias between the predicted and measured rut depths. As a result, APT sections should only be used to calibrate or validate the transfer functions based on the final rut depth and not rut depth evolution unless the aging function is turned off. In other words, only the final rut depth can be used for those tests where the simulated truck loads are applied in less than one month.
10. The MEPDG assumes that each axle consists of dual tires. Previous versions of the MEPDG (Versions 1.1 and earlier) included a uniform distribution of truck loads related to traffic wander or the lateral distribution of wheel loads. Separating the dual tires by nearly 60 in. was used to simulate the loading of a single tire. MEPDG Version 9-30A revised the wander function to a normal distribution. Use of a normal distribution changed the computational methodology such that the HMA rutting from dual tires that are separated by the axle width was predicted to be very small to zero. An appropriate methodology is to assume that the spacing is zero between the duals and the weight of each tire is half of the single tire used in the simulated loading. This approach was used for simulating a single tire applied to the test pads at some of the APT facilities for use in this project.

CHAPTER 2

Summary of Findings

2.1 Mechanistic–Empirical Rut-Depth Transfer Functions

2.1.1 Facilitated Workshop on Rut-Depth Transfer Functions

A facilitated workshop was sponsored by NCHRP under this project to identify other rut-depth prediction models or transfer functions and mixture testing and characterization issues that should be considered in the production test program. The three objectives of the workshop were to:

1. Identify rut-depth transfer functions to be evaluated within NCHRP Project 9-30A. This objective was the primary focus of the workshop. The other two objectives were an outcome from this primary objective.
2. Develop guidance on two key issues affecting the use of rut-depth transfer functions included in the MEPDG software.
   a. The maximum prediction error allowable for the M-E–based rutting model.
   b. The design limit or failure criteria for rutting in HMA layers.
3. Identify problem statements for future requests for proposals.
   a. Identify short-term research efforts to evaluate the use of rutting models in HMA structural design, mixture design, and performance-based specifications.
   b. Identify key elements of a long-term research program to develop more fundamental mechanistic modeling systems for rutting based on work performed under NCHRP Project 9-19 (Tasks F and G) and other projects related to predicting rutting and/or distortion in HMA mixtures.

The following briefly defines those transfer functions recommended from the facilitated workshop and the focus of the research completed in NCHRP Project 9-30A. Appendix B describes the modifications and enhancements made to the MEPDG software in support of these additional transfer functions.

- It was planned that NCHRP Project 9-30A would consider both M-E–based and mechanistic-based prediction models. From the workshop presentations and discussions of the fully mechanistic-based prediction models, none were judged to be sufficiently developed to predict rutting along actual roadway segments. It was the consensus of the participants that development of fully mechanistic-based prediction models is a worthy pursuit, but one for the long-term given the time and cost of development and validation. This consensus item is being pursued by the Asphalt Research Consortium (ARC) through sponsorship of the FHWA.

  The consensus from the workshop participants regarding direction for the project was to focus on the enhancement of M-E–based rut-depth transfer functions that could replace the one included in the MEPDG software. It was also agreed that the NCHRP Project 9-30A team should identify a small subset of sections having the highest quality data in the M-E_DPM database that might serve as test cases for future mechanistic modeling of HMA rutting. Appendix H (available for download from the NCHRP Project 9-30A web page at http://apps.trb.org/cmsfeed/TRBNetProjectDisplay.asp?ProjectID=965) is a user's manual for the M-E_DPM database. The consensus of the workshop participants was that NCHRP Project 9-30A should characterize HMA mixtures (both neat and polymer modified) at selected sites using a series of advanced laboratory tests appropriate for providing material inputs to mechanistic-based prediction methods. These tests are described in Section 3.6 of this report and Appendix K. The results from these laboratory tests were entered in the M-E_DPM database for use in future research studies.
- As described in the NCHRP Project 9-30A statement of work, the primary focus of the project was to enhance the

MEPDG HMA rutting transfer function and the measurement of all associated material property inputs using Level 1 laboratory tests. There was debate during the facilitated workshop as to whether the current MEPDG rut-depth transfer function should be abandoned. A range of opinions were expressed, but the final consensus was that the current MEPDG transfer function should be included and mechanistic-based response methods should be used to confirm the underlying assumptions or devise a more rational basis for the assumptions and enhancement to the transfer function.

- The WesTrack rut-depth transfer function was the consensus selection for the alternate for comparison to the MEPDG transfer function. Material property inputs required for this transfer function were to be measured in the laboratory for the experimental sites, similar to the testing for the enhanced MEPDG model, if unavailable from other projects. The rutting predictions using the WesTrack transfer function should be compared against the predictions from the original and the enhanced MEPDG rutting model. If warranted, potential enhancements to the WesTrack rutting transfer function were to be explored.
- Three additional enhancements to the current MEPDG HMA rutting transfer function were identified for examination:
  - The mixture adjustment factors based on volumetric and gradation properties, as used in NCHRP Project 1-40B.
  - The addition of a stress term within the MEPDG rut-depth transfer function. This enhancement would be in addition to the resilient strain term already included in the rutting model. The two specific suggestions for further examination were the Verstraeten transfer function and Leahy's original plastic-to-elastic strain formulation that includes deviator stress. The consensus of the participants was to give priority to the Verstraeten transfer function and to evaluate the Leady transfer function, if time and funds permitted. These other rut-depth transfer functions are defined in the next section of this report.
  - The inclusion of mixture-specific plastic deformation coefficients measured in the laboratory, as HMA layer properties. Repeated-load plastic deformation tests should be included in the test program for each site. As part of NCHRP Project 1-40A, the independent review team also made this suggestion. Thus, revisions to the MEPDG software were to allow plastic deformation coefficients to be entered for individual HMA layers.
- It was the consensus of the participants that multiple rut-depth transfer functions, in addition to the original MEPDG transfer function (the baseline model), should be calibrated under the project. These transfer functions include:
  - The WesTrack shear strain, shear stress transfer function.
  - The Verstraeten deviator stress-based transfer function.
  - One or more enhanced versions of the MEPDG software.

  The rutting predictions from all of these transfer functions should be compared against each other. To the extent possible, any nearly mechanistic predictions using the advanced HMA material characterization for the select subset of experimental sites should also be compared against the M-E predictions.
- The important criteria to be considered in the model's evaluation process are listed in the following in order of importance, as established from consensus of the participants.
  - Model accuracy (consensus selection as the most important factor).
  - Sensitivity to HMA mixture volumetric properties (binder type, aggregate blend, etc.).
  - Sensitivity to temperature.
  - Robustness.

  Testing expense was one of the items discussed because it was included in the NCHRP Project 9-30A amplified work plan. It was the consensus of the group, however, that this was an unimportant issue.
- It was the consensus of the participants that the rut depth predictions should be as accurate as possible. The group did not reach consensus regarding any quantification of acceptable accuracy. In other words, a specific value determined as being good enough, in terms of accuracy, was not the consensus of the group.
- It was also the consensus of the participants that the rut depth model should have the capability to predict rut depths over the entire range of values. In other words, the participants agreed that the rutting comparisons should not be limited to values below some maximum rut depth.
- It was the consensus of the participants that both the evolution and maximum rut depth at the end of the design life were important. The consensus of the group was that one was not more important than the other.

2.1.2 Rut-Depth Transfer Functions

This section lists and defines the rut-depth transfer functions that were evaluated and compared for accuracy in this study. It first defines the transfer function included in the MEPDG Version 1.0 and then provides a brief discussion on the other transfer functions that were recommended for consideration from the facilitated workshop. Table 1 summarizes the statistical values for comparing predicted and measured rut depths using specific transfer functions, where available.

Table 1. Statistical values for rut-depth transfer functions.

Rut-Depth Transfer Function	R^2 Value[1]	Standard Error Value, S_e	Number of Data Points
MEPDG, vertical strain; Kaloush[2]	0.399	0.121	387
NCHRP Project 1-40 volumetric factor adjustments	0.65	0.105	425
Asphalt Institute; vertical strain and deviator stress	0.76[3]	NA	250 lab mixes
Modified Leahy; vertical strain and deviator stress[2]	0.58	0.135	225
Verstraeten; deviator stress[2]	0.55	0.143	225
WesTrack; shear strain and shear stress[4]	0.767	0.051	170

Notes:
1. The values in this column are for total measured rut depths. Thus, some of the error is probably from the plastic deformation in the unbound layers, where applicable.
2. Transfer function statistics are based on assuming that the dynamic modulus can explain the difference in rutting between projects and HMA mixtures.
3. This value is a comparison of the measured and predicted plastic strain values measured in the laboratory.
4. Transfer function statistics are based on actual RLPD tests for predicting rut depths.

NA = Not available or not applicable.

2.1.2.1 MEPDG Rut-Depth Transfer Function

The plastic strain relationship included in the MEPDG to predict rut depth in the HMA layer increments is shown as Equation 1 and represents the baseline condition for evaluating a mixture's susceptibility to distortion (ARA, Inc., ERES Consultants Division, 2004).

$$\varepsilon_p = \varepsilon_r K_Z \beta_{r1} 10^{k_{r1}} (T)^{k_{r2}\beta_{r2}} (N)^{k_{r3}\beta_{r3}} \quad (1)$$

where

ε_r = incremental plastic strain at the mid-depth of a thickness increment.
ε_p = resilient strain calculated at the mid-depth of a thickness increment.
T = temperature at the mid-depth of a thickness increment, °F.
N = number of axle load applications of a specific axle type and load interval within a specific time period.
$\beta_{r1}, \beta_{r2}, \beta_{r3}$, = local calibration coefficients; all equal to 1.0 for the global calibration effort completed in NCHRP Project 1-40D.
k_{r1} = plastic deformation factor and equal to −3.35412 based on the global calibration effort.
k_{r2} = plastic deformation factor related to the effect of temperature and equal to 1.5606 based on the global calibration effort.
k_{r3} = plastic deformation factor related to the effect of wheel loads and equal to 0.4791 based on the global calibration effort.
K_Z = depth function and equal to:

$$K_Z = (C_1 + C_2 D)(0.328196)^D \quad (2)$$

$$C_1 = -0.1039 H_{HMA}^2 + 2.4868 H_{HMA} - 17.342 \quad (3)$$

$$C_2 = 0.0172 H_{HMA}^2 - 1.7331 H_{HMA} + 27.428 \quad (4)$$

D = depth to the mid-depth of the thickness increment, in.
H_{HMA} = thickness of the HMA layers, in.

The rationale for the plastic to resilient strain ratio transfer functions is to consolidate the effects of stress level. Vertical stress affects the resilient elastic strain as well as plastic strain. Normalizing the plastic strain to the elastic strain is hypothesized to capture the stress effect without including it in the regression equation or transfer function (Kaloush and Witczak, 2000).

The regression coefficients or plastic deformation coefficients (k_{r1}, k_{r2}, k_{r3}) were determined from unconfined, uniaxial RLPD tests conducted in the laboratory and adjusted to field-measured values. The k_{r3} factor is the slope in the steady-state or secondary range, while k_{r1} is the intercept of the log–log relationship between the number of load applications and cumulative plastic strain. The k_{r2} factor is the effect of temperature on the intercept.

The MEPDG uses an incremental thickness and time approach in calculating total HMA rut depth. The depth function (refer to Equation 2) is included to consider the effect of confinement from the upper HMA thickness increments in calculating the incremental rut depths through all of the HMA layers. A time-hardening scheme is included to accumulate plastic deformation over multiple load levels and seasons (ARA, Inc., ERES Consultants Division, 2004). The depth function has received extensive criticism from industry regarding its applicability, while the time-hardening scheme has been used by others in calculating total HMA rutting with time.

2.1.2.2 MEPDG Default Plastic Deformation Coefficients Adjusted Based on Volumetric Properties

NCHRP Project 9-30 completed a brief evaluation of the MEPDG transfer function. A large bias was found between the predicted and measured rut depths, and this bias was related to HMA volumetric properties. The MEPDG adjusted rut-depth transfer function has the same mathematical equation; the only difference is that the global plastic deformation coefficients are adjusted based on the volumetric properties of the HMA mixture. The adjustments made to the plastic deformation coefficients are included as a comparison to the laboratory and field-calibrated values because of simplicity of use during the mixture design stage. Appendix C includes the portion extracted from the NCHRP Project 1-40B document for ready reference related to the rut-depth adjustment factors (Von Quintus, 2006).

2.1.2.3 Asphalt Institute Rut-Depth Transfer Function

The Asphalt Institute or original Leahy model formulation (Equation 5) originated from an extensive laboratory study completed in 1989 using uniaxial repeated-load plastic deformation responses measured on 250+ HMA test specimens (Leahy, 1989). This model has capabilities to consider temperature and seasonal effects. It is referred to in the MEPDG software modifications as the Asphalt Institute transfer function (refer to Appendix B).

$$Log\left(\frac{\varepsilon_p}{\varepsilon_r}\right) = -6.631 + 0.4354Log(N) + 2.767Log(T) + 0.110Log(\sigma_d) - 0.118Log(\eta) + 0.930Log(V_{beff}) + 0.501Log(V_a) \quad (5)$$

where

σ_d = deviator stress, psi.
η = viscosity of the asphalt binder at 70°F, $\times 10^6$ poise.
V_{beff} = effective asphalt content by volume, percent.
V_a = air void volume, percent.

The test program used to develop the transfer function or regression equation included two aggregate types, two asphalts, three amounts of asphalt, three deviator stress levels, and three test temperatures. This transfer function, however, was not calibrated to measured rut depths for confirming the applicability of the laboratory-generated regression coefficients of the material property parameters found to be important using uniaxial repeated load tests.

This transfer function was the basic methodology used in generating the MEPDG transfer function that was calibrated to field-measured rut depths (refer to Equation 1). Participants of the facilitated workshop requested that this equation form be used because of the deviator stress term that is believed to be important in evaluating the susceptibility of HMA mixtures to distortion or rutting.

2.1.2.4 Modified Leahy Rut-Depth Transfer Function

A modified form of the Asphalt Institute or original Leahy equation was used in NCHRP Project 1-40B in an attempt to explain the large bias between the predicted and measured rut depths (Von Quintus, Andrei, and Schwartz, 2005). This modified form of the original Leahy equation is shown in Equation 6, but it did not eliminate the bias or reduce the standard error using selected LTPP program's special pavement studies (SPS) SPS-1 and SPS-5 test sections.

$$Log\left(\frac{\varepsilon_p}{\varepsilon_r}\right) = -0.505 + 0.25Log(N) + 0.110Log(\sigma_d) + 0.930Log(V_{beff}) + 0.501Log(V_a) \quad (6)$$

The temperature and viscosity terms included in Equation 5 were removed because dynamic modulus is calculated on an incremental basis with HMA depth and time. It was hypothesized that the influences of temperature and viscosity on the intercept are adequately accounted for through their effect on dynamic modulus. The average intercept coefficient was determined at the equivalent temperature and calibrated to field-measured values. The effective asphalt content by volume and air void terms was left in the regression equation because of their significance found in NCHRP Project 1-40B [refer to Appendix C (Von Quintus, 2006)]. The other major difference between the original Asphalt Institute equation (Equation 5) and the modified Leahy equation (Equation 6) is that the modified Leahy equation was based on results from repeated-load confined, triaxial tests.

2.1.2.5 Verstraeten Rut-Depth Transfer Function

The Verstraeten deviator stress transfer function (refer to Equation 7) predicts plastic deformation as a function of deviator stress level, dynamic modulus of the mixture, and number of load applications (Verstraeten, Veverka, and Francken, 1982). Temperature is implicitly included in Equation 7 through its influence on dynamic modulus—similar to the modified Leahy transfer function (refer to Equation 6).

$$\varepsilon_p = A\frac{\sigma_1 - \sigma_3}{E^*}\left(\frac{N}{1000f}\right)^{b_{AC}} \quad (7)$$

where

ε_p = permanent or plastic strain.
σ_1 and σ_3 = vertical and radial stresses, psi.
E^* = dynamic modulus of asphalt mixture, psi.

N = number of load cycles.
f = frequency of load, Hz.
A and b_{AC} = regression coefficients.

The deviator stress ($\sigma_1 - \sigma_3$) divided by dynamic modulus (E^*) is a measure of the resilient strain in this model. For conventional mixtures, the recommended values for the plastic deformation or regression coefficients are $A = 57.5$ and $b_{AC} = 0.25$. These are considered the global default values for this transfer function, but they represent laboratory test conditions. The statistical terms from the original development are unavailable for this transfer function. The values included in Table 1 were determined from using this transfer function to predict the measured rut depth for some of the LTPP test sections included in NCHRP Project 9-30A prior to calibration.

The Verstraeten model was not developed for incremental rut-depth accumulation purposes, similar to the Witczak–Kaloush transfer function prior to calibrating the MEPDG. To correctly implement this transfer function within the MEPDG computational framework, some assumptions were made regarding strain hardening that takes place as the load cycles are applied to the pavement, which are discussed in Appendix B. The form of the equation included in the MEPDG Version 9-30A software uses the intercept measured at the equivalent temperature. In addition, the depth function included in the MEPDG (refer to Equation 2) is used with the Verstraeten transfer function for calculating incremental rut depth through the HMA layers.

2.1.2.6 WesTrack Rut-Depth Transfer Function

The WesTrack plastic shear strain transfer function was developed using data from the WesTrack field experiment (Epps et al., 2000). The mathematical formulation is M-E–based for predicting HMA rutting using shear strain and shear stress, and it is shown by Equation 8. This formulation was developed to provide a more realistic simulation through laboratory testing of the horizontal plastic deformations that can occur in the field (Sousa et al., 1994; Monismith, Popescu, and Harvey, 2006).

$$\gamma_p = ae^{b\tau}\gamma_e N^c \tag{8}$$

where

γ_p = permanent shear strain at a depth of 2 in. beneath the tire edge.
γ_e = corresponding resilient or elastic shear strain.
τ = corresponding elastic shear stress.
a,b,c = regression coefficients.

The resilient shear strain measured from the repeated-load simple shear tests conducted at constant height are required for calibration of the plastic deformation coefficients of the HMA mixture. The regression coefficients were determined at multiple temperatures. The c-exponent or term from all tests was averaged, and the average value was used to determine the a value or the effect of temperature on the intercept. For conventional HMA mixtures, the recommended values for the transfer function are $a = 2.114$, $b = 0.04$, and $c = 0.124$. The form of the equation included in the MEPDG Version 9-30A software uses the intercept measured at the equivalent annual temperature.

Table 2. Values of *K* as a function of HMA layer thickness for the WesTrack transfer function.

HMA Thickness, in.	*K*-Value
5 to 7	5.5
7 to 9	7.0
9 to 12	8.5
>12	10.0

The time-hardening principle included in the MEPDG is also used to estimate the accumulation of plastic shear strains in the HMA under varying site conditions. To implement this transfer function in the MEPDG computational framework, the N_{virt} expression in the software was changed as follows:

$$\ln(N_{virt}) = \left(\ln\left(\frac{\gamma_p}{\gamma_e}\right) - \ln(a) - b\tau\right)/c \tag{9}$$

The incremental plastic shear strain is computed for a given stress state, load frequency, modulus, and N computed in accordance with Equation 8. The rutting that is estimated in the HMA layer due to the plastic deformation is determined from the following equation, where K equals a coefficient related to the thickness of the HMA layer, as shown in Table 2. As a result, the depth function included in the MEPDG is turned off when using the WesTrack transfer function.

$$PD = K\gamma_p \tag{10}$$

where PD = permanent deformation.

The model was calibrated and validated for the WesTrack sections. The statistical terms summarized in Table 1 are from the original development and calibration work.

2.2 Improvements and Enhancements: MEPDG Software Version 9-30A

Multiple revisions were made to the MEPDG Version 1.0 under NCHRP Project 9-30A. This modified software is referred to as MEPDG Version 9-30A. The revisions to the software included adding the additional rut-depth transfer functions and revising some of the computational steps in support of those transfer functions. Other revisions to the MEPDG computational methodology, however, were identified to improve on the rutting predictions and were suggested

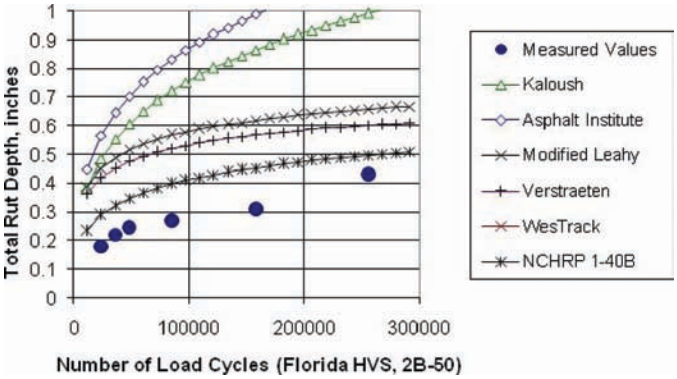

(a) Predicted rut depths for the FHWA HVS Test Pad 10-02, rutting experiment.

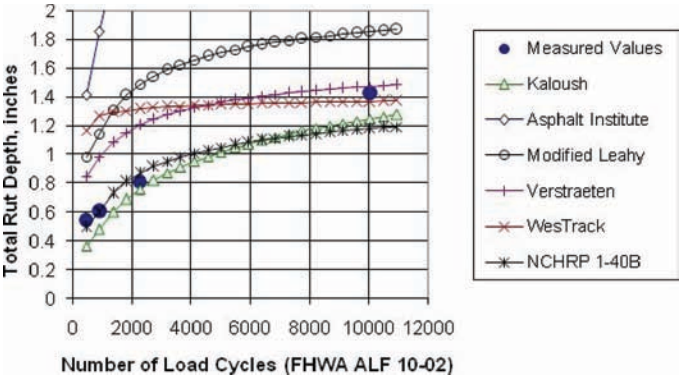

(b) Predicted rut depths for Florida HVS Test Pad 2B-50, modifier experiment.

Figure 1. Predicted rut depths using the different transfer functions for FHWA and Florida heavy vehicle simulator (HVS) sections, simulated truck loadings.

from the facilitated workshop. The revisions made to the software are listed in the following and discussed in more detail in Appendix B.

2.2.1 Additional Rut-Depth Transfer Functions

Three rut-depth transfer functions were added to the software: (1) the WesTrack shear strain and shear stress transfer function (Equation 8), (2) the Verstraeten deviator stress transfer function (Equation 7), and (3) the Asphalt Institute vertical elastic strain and deviator stress transfer function (Equation 5). Participants in the facilitated workshop recommended the inclusion of stress terms (deviator, shear, confinement) in addition to resilient strain. The other transfer functions used in the study are versions of these three or the MEPDG transfer function (referred to as the Kaloush transfer function in this report). Some coefficients of the transfer functions were zeroed out for the other rut-depth transfer functions that were identified in the previous section of this chapter. Appendix B includes screen shots for each of the transfer functions and explains the entry of the plastic deformation or strain coefficients for each transfer function.

Figures 1 through 4 include a comparison of the predicted rut depths for different transfer functions over a range of projects and pavement structures. These sites were selected because of anomalies reported by other projects and use of PMA mixtures on these sections. In addition, laboratory-measured dynamic modulus values were available for these HMA mixtures and were used to predict the measured rut depths.

Use of the different transfer functions resulted in a significant error in predicted rut depths for these examples; dynamic modulus by itself did not explain the rut depth in most cases. Likely reasons for the large difference between

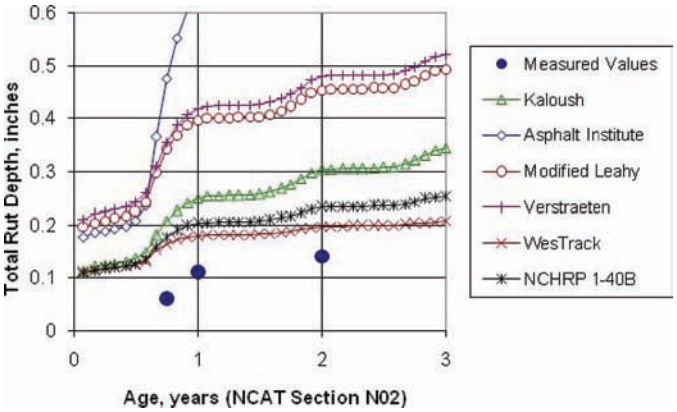

(a) Predicted rut depths for the NCAT Test Section N02.

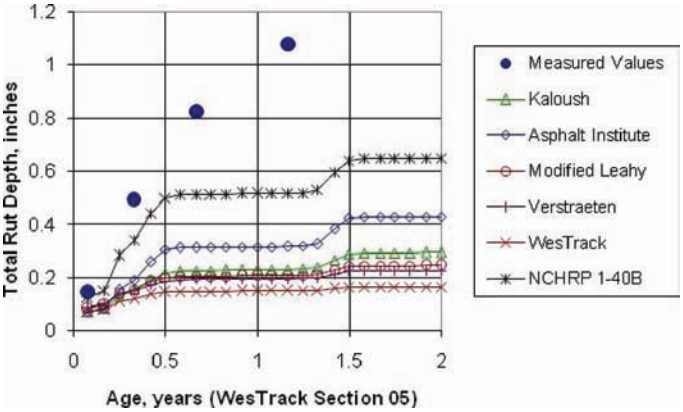

(b) Predicted rut depths for WesTrack Test Section 05.

Figure 2. Predicted rut depths using the different transfer functions for selected National Center for Asphalt Technology (NCAT) and WesTrack test sections.

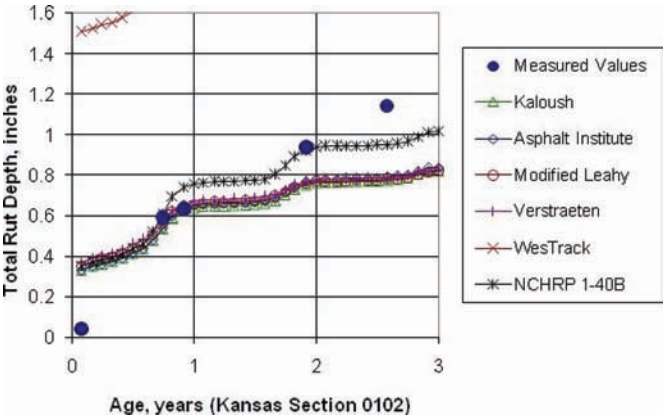

(a) Predicted rut depths for the Kansas SPS-0102, new construction, thin HMA.

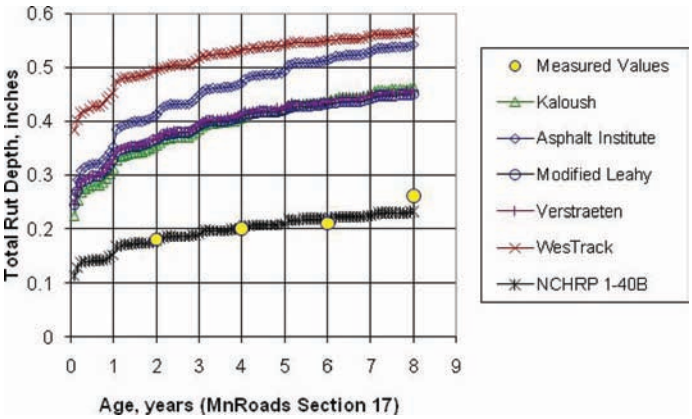

(b) Predicted rut depths for MnROADs Section 17, new construction, thick HMA.

Figure 3. Predicted rut depths using the different transfer functions for selected new construction test sections.

the predicted and measured values from different transfer functions are:

- The Asphalt Institute transfer function (Equation 5) predicts much higher rut depths than measured because it was never calibrated to field-measured values. The predicted values are based on laboratory-derived plastic deformation coefficients from unconfined, uniaxial repeated load tests without any adjustment to field-measured values.
- The Kaloush and Asphalt Institute transfer functions consistently result in higher rates of increasing rut depth over time compared to the measured values. The exponent for the number of load cycles is greater than for the other transfer functions, even though the Kaloush transfer function was calibrated to field-measured values. These transfer functions were derived from unconfined, uniaxial RLPD tests. Exhibit A lists the exponents for each transfer function.
- The WesTrack transfer function was calibrated using thicker HMA layers. For thin HMA layers [less than 4 in. (100 mm)], the WesTrack function was found to consistently and significantly predict rut depths higher than measured.
- The intercept is temperature dependent for the Kaloush, Asphalt Institute, and NCHRP Project 1-40B transfer functions, while the temperature term was excluded for the modified Leahy, Verstraeten, and WesTrack transfer functions. The intercepts for these three transfer functions are determined at the equivalent annual temperature and then adjusted based on dynamic modulus values. Applicability and use of the equivalent annual temperature concept in the MEPDG is discussed in Section 2.6.3.
- The Verstraeten transfer function (Equation 7) adjusts the number of load repetitions based on the frequency of loading used in laboratory repeated-load tests, while none of the other transfer functions consider frequency of loading

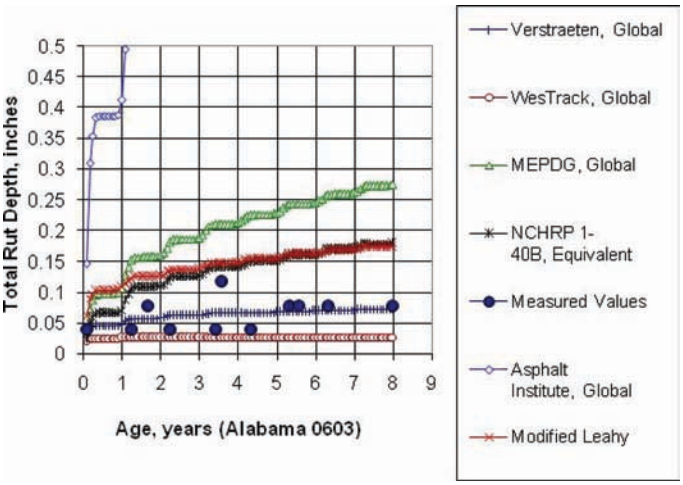

(a) Predicted rut depths for the Alabama SPS-0603, overlay of PCC pavement.

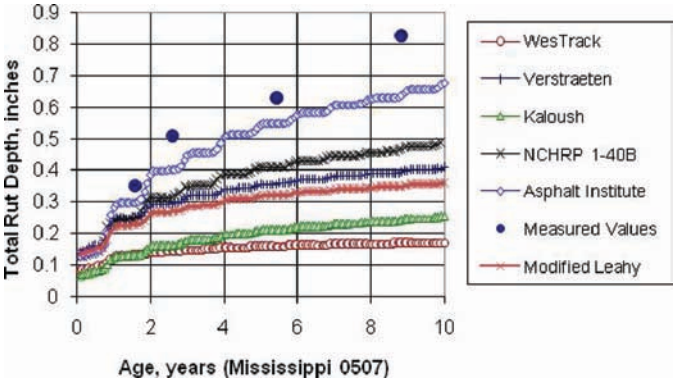

(b) Predicted rut depths for the Mississippi SPS-0507, overlay of HMA pavement.

Figure 4. Predicted rut depths using the different transfer functions for selected test sections in the LTPP SPS-5 and SPS-6 experiments, rehabilitated pavements.

Exhibit A

Unconfined, Uniaxial Based Values		Confined, Triaxial or Shear-Based Values	
Transfer Function	Exponent to the *N*-Term	Transfer Function	Exponent to the *N*-Term
Kaloush; Equation 1	0.4791	Modified Leahy, Equation 6	0.250
Asphalt Institute, Equation 5	0.435	Verstraeten, Equation 7	0.250
		WesTrack, Equation 8	0.124
The *N*-term exponent for the NCHRP Project 1-40B transfer function is dependent on the volumetric and aggregate properties of the HMA mixture.			

used in the laboratory. The MEPDG also considers speed of truck loadings, which is an input to the software.

An important observation and similarity between the transfer functions is that the *N*-term exponent is assumed to be independent of temperature, age, and dynamic modulus. Other similarities and differences between the transfer functions will be discussed in greater detail in Chapter 3 in relation to their effects on the standard error of the transfer function.

2.2.2 HMA Layer-Specific Plastic Deformation Coefficients

One set of plastic deformation coefficients is used for all HMA layers in the MEPDG versions (0.7, 0.9, 1.0, and 1.1) released through NCHRP. The MEPDG computational methodology assumes that the differences in HMA dynamic modulus will correctly account for differences in rutting susceptibility between different mixtures. This assumption has been found to result in a bias and increases the standard error of the predicted rut depths (Von Quintus, Andrei, and Schwartz, 2005; Von Quintus, 2005).

Work completed under NCHRP Project 1-40B recognized this limitation and suggested the use of layer-weighted plastic deformation coefficients. The procedure used to determine layer-specific plastic deformation coefficients for the Kaloush rut-depth transfer function is provided as Appendix C. This procedure was developed using test sections from the WesTrack and National Center for Asphalt Technology (NCAT) test roads and sections included in LTPP. Application of the procedure reduced the standard error, but the procedure does not consider layer location in the pavement structure (surface versus base mixtures) or the use of modified asphalts—both considered limitations for increasing the accuracy of the rut-depth transfer function.

The MEPDG software was revised to permit the user to enter layer-specific plastic deformation coefficients determined from laboratory repeated-load tests. Figures 5 and 6 provide a comparison of the total rut depths predicted over time for four conditions using the Wisconsin LTPP SPS-10116 test section: (1) global default plastic deformation coefficients that are layer independent, (2) the surface layer susceptible to plastic deformation, (3) the middle layer susceptible to plastic deformation, and (4) the lower HMA layer susceptible to plastic deformation.

As shown, the layer- or mixture-dependent plastic deformation coefficients can have a significant effect, which depends on the coefficients of the individual layers and location of the mixture. The deeper the distortion-susceptible layer, the lower the rutting for the Kaloush and WesTrack transfer functions. Conversely, the rutting predicted with the modified Leahy and Verstraeten functions increases the deeper the distortion-susceptible layer. This observation is inconsistent with experience from past forensic investigations and is

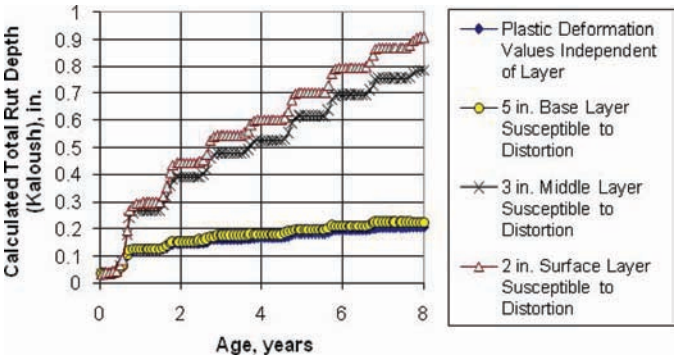

(a) Kaloush transfer function.

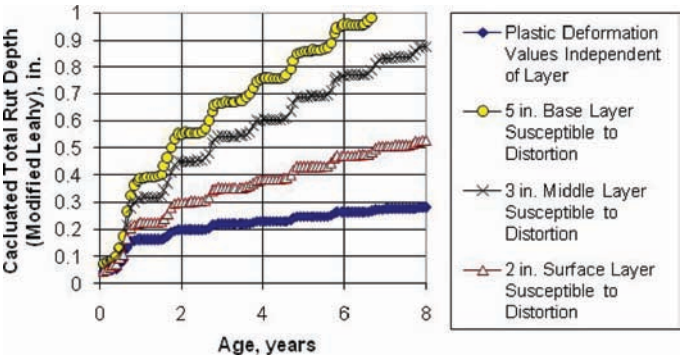

(b) Modified Leahy transfer function.

Figure 5. Predicted rut depths using layer-independent and mixture-dependent plastic deformation coefficients for the vertical-strain–based transfer functions.

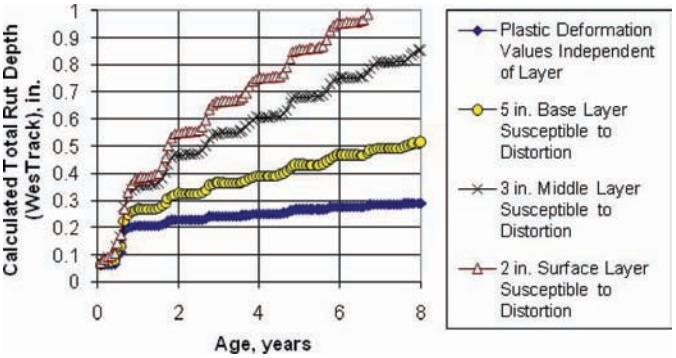

(a) WesTrack transfer function.

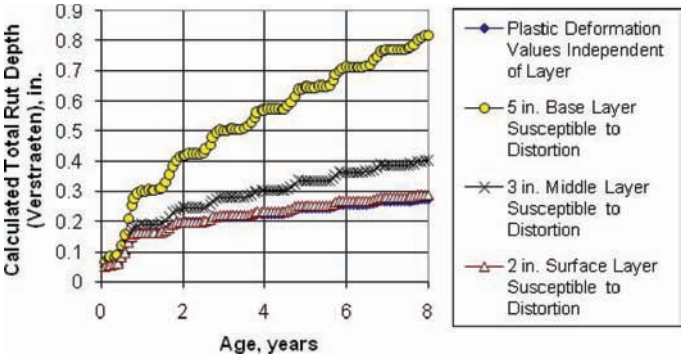

(b) Verstraeten transfer function.

Figure 6. Predicted rut depths using layer-independent and mixture-dependent plastic deformation coefficients for the shear strain and deviator-stress–based transfer functions.

believed to be related to the depth function in relation to the stress term in the modified Leahy and Verstraeten transfer functions, which is discussed next.

2.2.3 Depth Function Enhancement

Participants in the facilitated workshop recommended the development and inclusion of a less empirical formulation for the depth function embedded in the MEPDG.

Various formulations were considered using finite element analyses with the advanced materials characterization and rutting simulation. The depth function could not be explained through mechanistic analysis other than by the decrease in shear stress with depth. The advanced materials characterization and rutting simulations are discussed further in Chapter 3 and Appendix K.

Figures 7 and 8 show the effect of HMA thickness on the predicted HMA rut depth. These runs were completed using the typical pavement structure built at the NCAT test track (new construction) but with a constant temperature climate [40°C (104°F)]. As shown, the effect of increasing HMA thickness varies with transfer function, which is illustrated in Figure 9 in terms of the predicted total rut depth at 10 years for new construction and HMA overlays. The rut depth predicted with the deviator-stress–based transfer functions (Verstraeten and modified Leahy) continues to increase with increasing HMA thickness. Conversely, the rut depth decreases with increasing HMA thickness for the pure vertical strain–based function (Kaloush). The shear-strain and shear-stress–based transfer function (WesTrack) is different from all other transfer functions—the rut depth is relatively constant with increasing HMA thickness, with the exception for thin HMA layers (less than 5 in.). This result is more consistent with the authors' experience from forensic investigations.

2.2.3.1 HMA Layer Thickness Effect

Based on statistical analyses of rut depth data included in the LTPP database, rut depths were found to be dependent on HMA layer thickness groups—thin versus thick layers. The thicker HMA sections had lower rut depths (Rauhut, Eltahan, and Simpson, 1999). More importantly, some local calibration studies found the local calibration factors to be HMA-thickness–dependent [ARA, 2008 (Ohio)], while other

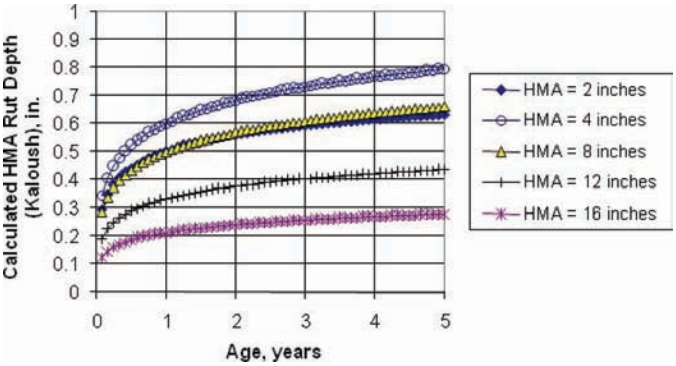

(a) Kaloush transfer function.

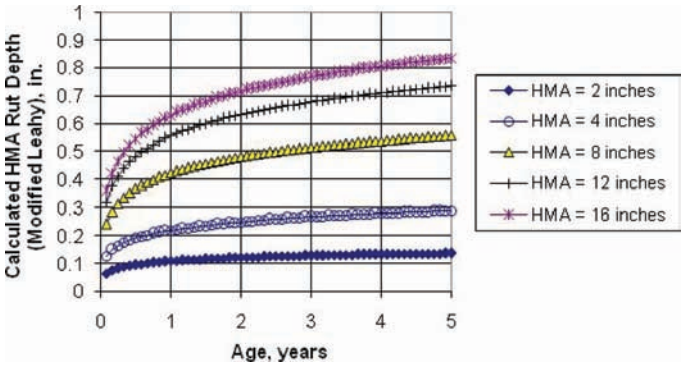

(b) Modified Leahy transfer function.

Figure 7. HMA layer thickness effect on rut depth for the vertical-strain–based transfer functions; new construction.

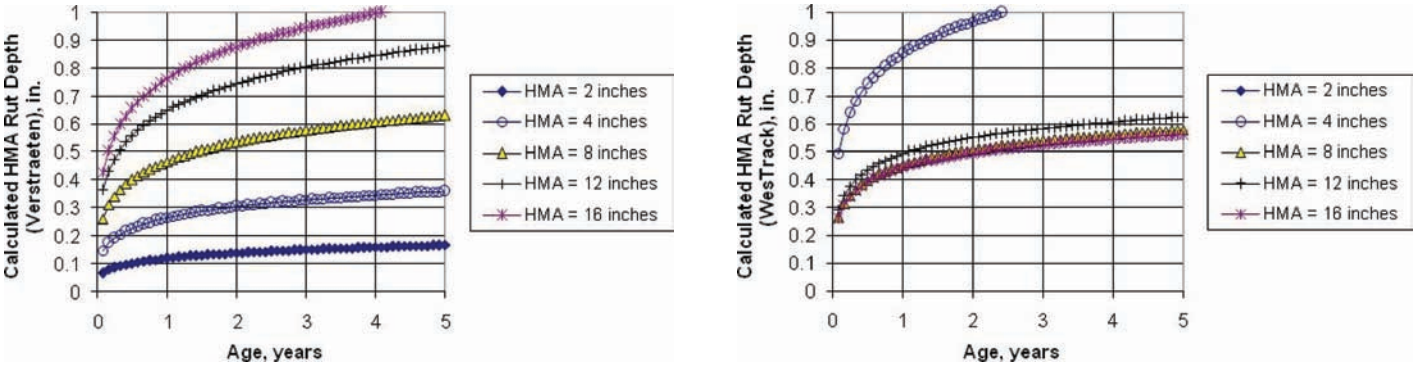

(a) Verstraeten transfer function.

(b) WesTrack transfer function.

Figure 8. HMA layer thickness effect on rut depth for the shear strain/stress and deviator-stress–based transfer functions; new construction.

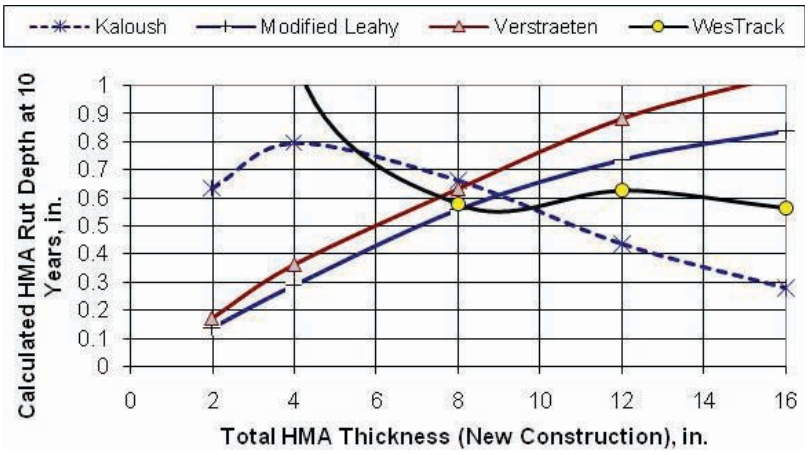

(a) New flexible pavement construction.

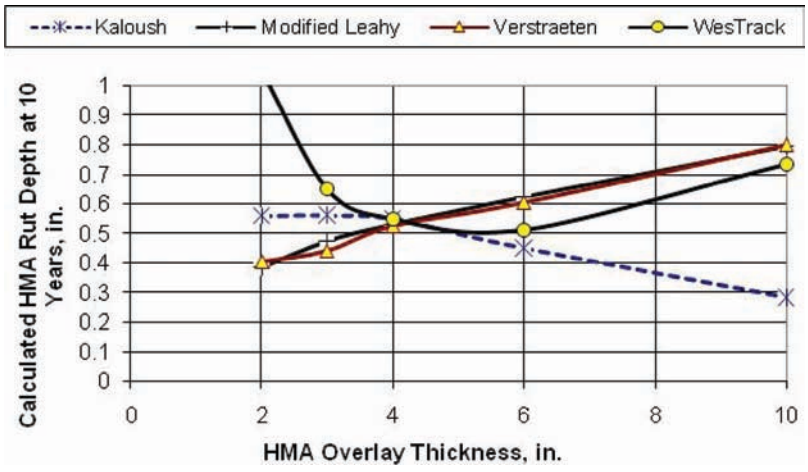

(b) HMA overlay of flexible pavements.

Figure 9. HMA layer thickness effect on calculated HMA rut depth for new construction and HMA overlays of flexible pavements.

studies found them to be independent of HMA thickness [ARA, 2009 (Missouri)].

One of the first local calibration studies completed found the coefficients of the transfer function to be consistent with those reported from NCHRP Project 1-40B [Von Quintus and Moulthrop, 2007 (Montana)]. As noted previously, using the HMA volumetric properties to adjust the coefficients of the Kaloush transfer function reduced the standard error (refer to Table 1) without taking HMA thickness into account.

Overall, increasing HMA thickness for deep-strength pavements should have minimal effect on HMA and total rutting, unless it is from structural rutting in the unbound layers. Thus, the depth function is believed to over-correct the incremental rutting based on vertical strain with layer depth since the calculated rut depth continually decreases with increasing HMA thickness. Conversely, the depth function is believed to under-correct the incremental rutting based on deviator stress with layer depth as the calculated rut depth continually increases with increasing HMA thickness. As such, the depth function used for the rut-depth transfer functions based on vertical resilient strain was found to be questionable, but there is insufficient data to suggest how it should be revised. This issue will be discussed further in Chapter 3.

The depth function in the MEPDG software was turned off when the WesTrack transfer function was used to predict rutting because that function uses a separate parameter for considering HMA thickness effects. The WesTrack transfer function is believed to be the more accurate in terms of simulating the findings from the LTPP studies, via higher rut depths for thin pavements and lower rut depths for thick HMA pavements (refer to Figure 9). This observation is consistent with the findings from the LTPP study (Rauhut, Eltahan, and Simpson, 1999), but the magnitude of the predicted rut depths for thin HMA layers (less than 4 in.) is believed to be high based on the authors' previous experience.

2.2.3.2 HMA Stress State Effect

The question is, why are there discrepancies between transfer functions and with LTPP findings and other experience? It is believed that the coefficient for the shear stress term (b) in the WesTrack transfer function and the deviator stress term (C_3) in the modified Leahy function are the reasons for the increased sensitivity of rutting to layer thickness. During the analyses completed during some earlier VESYS work, Florida's high tire pressure study (Florida Department of Transportation project "Flexible Pavement Failure Analysis—Impact of High Tire Pressures," Texas A&M Research Foundation, 1987–1990; all field work conducted under the supervision of Mr. Von Quintus), and Asphalt-Aggregate Mixture Analysis System (AAMAS), it was hypothesized that the shear or compressive strength of the mix and in-place shear stress (or octahedral shear stress) were important (Rauhut, Lytton, and Darter, 1984; Von Quintus et al., 1991). The strength of the mixture is not included as a parameter in any of the transfer functions, but stress is considered by all except for the Kaloush function.

Different values for the coefficients in the modified Leahy and WesTrack transfer functions were used to investigate the effect of shear stress and deviator stress terms on rut depth. The Verstraeten transfer function was not included in this evaluation because the exponent to the stress term is unity (refer to Equation 7), so no coefficient was programmed in the software.

Figure 10 shows the effect of shear stress on rut depth over a range of HMA layer thicknesses using the WesTrack transfer function, while Figure 11 shows the effect of deviator stress on rut depth for the modified Leahy function. A combination of values for the intercept and stress term can be used for which the rut depth becomes almost independent of HMA thickness. At about 6 in. to 8 in., the coefficients for both deviator stress and shear stress have little effect on rut depth with increasing HMA thickness. There is an effect, but the effect is small. This observation is consistent with the results from

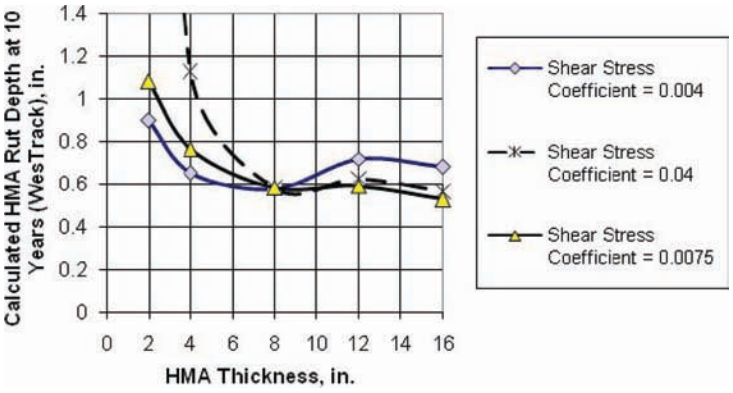

Figure 10. Effect of shear stress on rut depth; WesTrack transfer function.

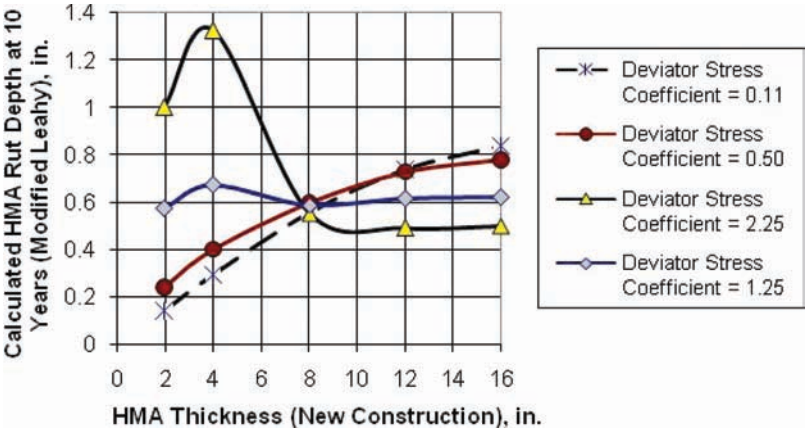

As the deviator stress term increases, the rut depth becomes less dependent on HMA thickness. At about a value of 1.0, the effect of thickness is similar to the WesTrack transfer function for shear stress (refer to Figures 9 and 10).

Figure 11. Effect of deviator stress on rut depth; modified Leahy transfer function.

many forensic investigations in measuring plastic deformation with depth in HMA layers.

In addition, there is a combination of deviator and shear stress terms for which the predicted rut depths from the WesTrack and modified Leahy transfer functions begin to converge, rather than diverge, for the thinner HMA pavements. The appropriate values from the preliminary study are $b = 0.01$ for the WesTrack transfer function and $C_3 = 1.0$ for the modified Leahy function.

The next question is, are the default values for the coefficients of the stress terms reasonable for the range in thickness where stress is important or has a significant effect on the calculated rut depth? Rather than just accept the numerical values that were defined during the development of the appropriate transfer function, the stress term values must be confirmed or redefined during calibration. In summary, the thicker sections should be used to determine the intercept coefficient of the transfer functions, where the predicted rut depth is almost independent of stress state (refer to Figures 10 and 11). After the thicker sections have been used to determine the value of the intercept coefficient for the appropriate transfer function, the thinner sections should be used to determine the coefficient of the stress term. This calibration process is discussed in greater detail in Chapter 3.

2.2.4 Plastic Deformation Coefficients for Unbound Layers

The local calibration factor for the unbound granular base and subbase layers cannot be entered for a specific cross section, while local calibration factors can be entered for fine- and coarse-grained subgrade soils. The MEPDG was revised so that the local calibration parameters could be entered for the unbound coarse-grained granular base and subbase layers. This revision did not result in significant changes to the total amount of rutting predicted with any of the transfer functions. Later versions of the MEPDG have included this revision.

2.2.5 Lateral Wander Effects

The standard deviation is used to define the practical limits of the width of the lateral distribution of wheel loads. A uniform distribution of wheel or axle loads is used between the limits defined by the standard deviation of wheel loads. A normal distribution is believed to provide a more realistic distribution of wheel loads for computing total rutting. Thus, the MEPDG was revised to include a normal distribution in the lateral location of the wheel loads for calculating the pavement responses in computing total rut depth. This revision is explained in more detail in Appendix B.

This change did not increase the magnitude of the predicted rut depths between MEPDG Versions 1.1 and 9-30A using the Kaloush transfer function, with the exception of the channelized truck traffic conditions shown in Figure 12(a). For channelized traffic, MEPDG Version 9-30A resulted in much less rutting with traffic wander values of less than 5 in. The modified Leahy transfer function also provided similar results, while the WesTrack and Verstraeten transfer functions resulted in higher rut depths for channelized traffic conditions [refer to Figure 12(b)].

The reason for the smaller rut depths for channelized traffic with the Kaloush and modified Leahy functions is believed to be related to the depth function, computational grid point locations, and other changes made to the software. The effect of traffic wander on the predicted rut depths using the WesTrack and Verstraeten transfer functions is similar to Version 1.1 using the Kaloush transfer function (refer to Figure 12). This discussion and results from Figure 12 make the point that the default values used are important relative to

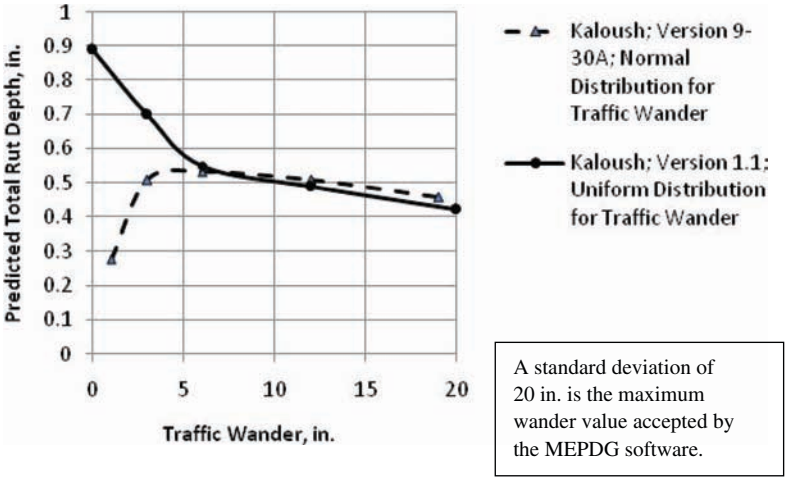

(a) Comparison of the predicted rut depth for the Kaloush transfer function using different traffic wander values in the MEPDG Versions 1.1 and 9-30A.

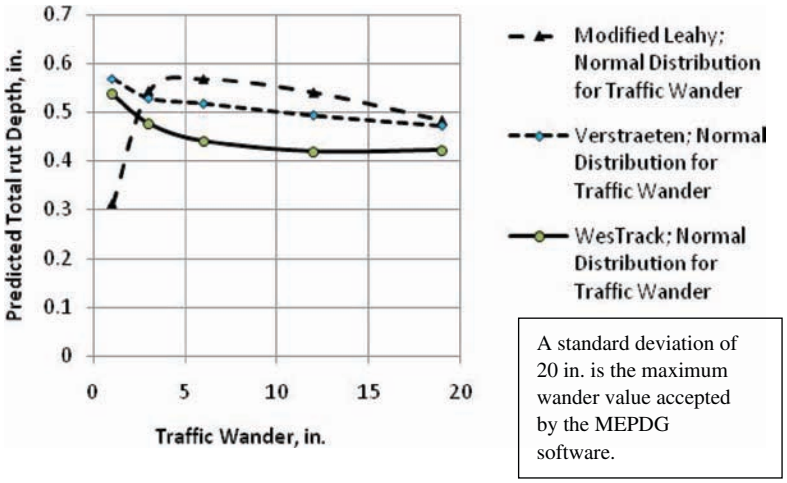

(b) Comparison of the predicted rut depth for the WesTrack, modified Leahy, and Verstraeten transfer functions using different traffic wander values in the MEPDG Version 9-30A.

Figure 12. Effect of traffic wander or standard deviator on rut depth.

the calibration process and should not be changed for some of the transfer functions in future use.

2.3 Data Storage

Model calibration and validation requires the assembly and analysis of large quantities of data for many field sites. A well-designed and easy-to-use relational database can greatly ease the management and access of this information. The global M-E database developed in NCHRP Project 9-30 was structured to focus on the calibration and validation of M-E–based distress transfer functions. The M-E_DPM database was developed to adapt to future research needs that will undoubtedly evolve over time. This database was explained in *NCHRP Research Results Digest 284* (Transportation Research Board, 2003b). Consequently, the design of an appropriate database structure was an important product in the overall development of the advanced validation refinement experimental plan developed under NCHRP Project 9-30 (Transportation Research Board, 2003a).

The purpose of this database is to provide an organized data storehouse for future use in improving M-E–based transfer functions for different distresses. Improvement is defined as the reduction of error between the distress observations and predictions. The following are important capabilities of the database.

1. M-E_DPM is able to address calibration and validation of both present and future M-E distress prediction models and mechanisms. In other words, the database is adaptable

to future research needs and allows the collective storage of test results (performance observations, material tests and properties, layer structure, traffic loads, etc.) from different agencies, projects, and data sources.
2. The database has the capability to store and maintain the data used for regional calibration studies. In this way, individual agencies can draw upon the results from other agencies to reduce potential duplication between agencies. More importantly, it promotes a coordinated effort between agencies in the use of regional data to enhance and refine model calibration factors or functions.

Consequently, M-E_DPM was designed and structured to be as dynamic as possible and to allow the collective storage of pavement data from a wide variety of data sources and tests (e.g., laboratory test methods). The M-E_DPM was built to include information and test data needed to support other distress transfer functions (top-down and bottom-up fatigue cracking, reflection cracking, transverse cracking, etc.), some of which may be revised with time. Specifically, the database was developed to maximize its potential use for implementing M-E–based distress transfer functions for use in design and analysis. Potential uses of M-E_DPM include, at a minimum:

- Regional calibration studies.
- Tying mixture design to structural design to performance-related specifications.
- Evaluating various hypotheses for distress mechanisms (for example, surface-initiated fatigue cracks, reflection cracks, M-E–based smoothness deterioration, and other transfer functions) as an essential step toward improved M-E–based performance models.

The NCHRP Project 9-30A effort focused only on population of those data elements related to HMA rutting. The M-E_DPM database was used to retain and store all field and laboratory test data from this project. Rather than creating another database that has similar functions and features, the existing database was used to store all data collected and measured during this project for both modified and neat HMA mixtures.

The M-E_DPM database is based on Microsoft Access 2000, similar to the standard data releases for the LTPP databases. The database has a text file editor and file format so that experimental features can be included in the database. The general features of the M-E_DPM database are described in Appendix H, which is a user manual for the database that documents the revisions and updates made to the structure and organization of the NCHRP Project 9-30 M-E_DPM database.

2.4 Experimental Plan for Calibration and Assessment of Rut-Depth Transfer Functions

As stated in the introduction, the ultimate goal of this research effort was to propose revisions to the HMA rut-depth transfer function in the MEPDG software for consideration by the AASHTO Joint Task Force on Pavements. The purpose of this section of Chapter 2 is to present the experimental plan, hypotheses, and sampling matrix that were prepared in NCHRP Project 9-30 and used to establish the coefficients of each transfer function to eliminate any bias and reduce the standard error (Transportation Research Board, 2003a).

2.4.1 Experimental Approach

Multiple participants voiced their concern at the facilitated workshop with using uniaxial, unconfined repeated load tests to determine the plastic deformation coefficients of the vertical-strain–based transfer functions. Many workshop participants were of the opinion that unconfined (uniaxial) repeated load tests would not capture the effect of the aggregate at higher stress levels and temperatures. As such, the experimental approach was grouped into two parts, A and B. The purposes of each part are described as follows.

- Part A: The purpose of this part of the experiment was to use results from accelerated loading facilities (ALF) with simulated truck loadings and test tracks with full-scale truck loadings to define details of the testing procedures to support the rut-depth transfer functions. As an example, what confinement pressure and vertical stress combinations are needed to define the effect of the stress state on plastic deformation throughout the HMA layers? The ALF programs for which rut depth data, mixture tests, and materials are available for testing include Caltrans heavy vehicle simulator (HVS), FHWA Turner–Fairbanks HVS, and the Florida Department of Transportation (DOT) HVS. In addition, test sections from the WesTrack and NCAT test tracks can be used. The reasons for using the ALF test pads and test tracks are that there are fewer unknowns and more controlled conditions. In addition, the materials placed along these test sections can be obtained for additional laboratory testing.
- Part B: The purpose of Part B was to use test track and full-scale roadway sections for determining the accuracy of the rut-depth transfer functions. This part of the experimental plan defines the standard error of the consensus transfer functions.

2.4.2 Hypotheses and Assumptions

The hypotheses and assumptions that were used in developing the experimental plan are listed in the following, some of which were based on expert opinions given at the workshop.

1. The measured rut depths from all projects represent the maximum difference between an actual or simulated wire line and the surface of the HMA. Thus, it was assumed that the rut-depth measurement error was the same for roadway segments, LTPP test sections, and test track sections. This assumption was probably incorrect where different methods were used to measure rutting, but it was expected to have minimal impact on the standard error and should not result in different biases or errors between the transfer functions.
2. The vertical and lateral stresses were computed with elastic layer theory and excluded the at-rest stress. Within the HMA layer, the at-rest stress has minimal effect on plastic deformation. Thus, it was assumed that the at-rest stress could be ignored for determining the plastic deformation coefficients of HMA mixtures at any test temperature or stress state.
3. The HMA layer was assumed to be isotropic. This assumption was incorrect and could be a critical error in predicting the HMA rut depths of some mixtures. Field measurements were made with the portable seismic pavement analyzer in NCHRP Project 10-65, "Nondestructive Testing Technology for Quality Control and Acceptance of Flexible Pavement Construction" (Phase 2, Part A—Interim Report, Task 6, March 2006, and Draft Final Report, July 2007), and the seismic modulus was found to be dependent on the direction of the rollers per the direction of testing (Von Quintus et al., 2009). To consider anisotropic conditions increases the complexity of the pavement response model. More importantly, assuming isotropic conditions should not result in a bias or standard error that is transfer function–dependent.
4. Aging of HMA mixtures can have a significant effect on rut depth. The aging model included in the MEPDG was assumed to be correct and to not result in a bias of the predicted rut depths between the transfer functions. The MEPDG aging simulation model increases the dynamic modulus of the HMA, and that increase was time and depth dependent. The plastic strain parameters were assumed to be independent of time. Thus, it was hypothesized that there would be no bias between roadway segments that included aging and the accelerated pavement tests and test tracks that excluded aging effects. If a significant bias was found between the two conditions for all transfer functions, this implied that the aging function needed to be revised or that aging should be applied to the plastic strain parameters of the transfer functions. To directly evaluate the in-place plastic deformation properties over time requires a test method with the capability to test cores. Cores were taken along some of the test sections to confirm or reject this hypothesis.
5. It was hypothesized that dynamic modulus by itself would not eliminate the bias or explain the plastic deformation of HMA mixtures, and that bias was dependent on mixture characteristics but was independent of design features and strategies. Mixture characteristics refer to volumetric properties, gradation, and mixture components. Results from NCHRP Projects 9-30(01) and 1-40B found a bias in the MEPDG rut depth predictions that was related to HMA volumetric properties and mixture types (Von Quintus, Andrei, and Schwartz, 2005; and Von Quintus, 2005). In addition, NCHRP 9-30(01) found that the residual errors of the MEPDG rut depth predictions were similar between different runs using dynamic modulus Input Levels 1 and 3. In other words, the difference between the residual errors of runs made with Input Levels 1 and 3 was small. This observation suggests that dynamic modulus, by itself, does not explain the effect of changing volumetric properties on rut depths. Figures 1 through 4 also support this hypothesis. Most of the error is from other sources (Von Quintus, Andrei, and Schwartz, 2005). Many of the facilitated workshop participants were also of the opinion that modulus by itself, although important, would not explain the plastic deformation measured on a wide range of HMA mixtures and climates.
6. It was hypothesized that the relative deviation or difference between measured and predicted rut depths for test sections in the same sampling cell was caused by material property differences and that difference can be captured by repeated-load triaxial or constant-height shear tests. Similarly, laboratory HMA repeated-load triaxial or constant-height shear tests will discriminate between the rutting resistance of modified and neat HMA mixtures. The relative deviations from using Input Level 1 laboratory-measured HMA mixture properties (dynamic modulus) with default plastic deformation coefficients can be compared to the relative deviations resulting from the use of repeated load tests to determine if repeated load tests in support of the transfer functions will explain these differences. The Asphalt Institute study identified systematic differences between the in-place plastic deformation coefficients of neat and modified HMA mixtures of companion projects (Von Quintus, Mallela, and Titus-Glover, 2007).
7. It was hypothesized that the depth correction or confinement function included in the MEPDG (refer to Equation 2) was a reasonable simulation of the effect of the upper HMA layers. Figure 9 demonstrated the effect of

HMA layer thickness on predicted rut depth for increasing layer thickness. The Kaloush transfer function results in significantly different thickness effects on predicted rut depth than the other transfer functions. However, as noted in the previous section, the depth function in combination with the different values for the stress terms of the WesTrack and modified Leahy transfer functions result in thickness effects of predicted rut depths that are consistent with previous observations. More importantly, simply increasing HMA layer thickness does not result in a consistent decrease in rut depth (refer to Figure 9). Most of the plastic deformation of HMA mixtures placed along the roadway occurs within the upper 6 in. of the mixture for well-designed mixtures. This observation is based on trenches and cores that have been taken on multiple forensic investigations to measure plastic deformation in different pavement layers. If this observation is correct, the hypothesis should be rejected. Many of the facilitated workshop participants were also of the opinion that this hypothesis would be rejected.

8. The rut-depth transfer function included in the MEPDG provided an accurate simulation of the evolution of rut depths measured on HMA-surfaced pavements over the design life of the pavement. Many of the participants that attended the facilitated workshop were of the opinion that this hypothesis would be rejected for uniaxial (unconfined) RLPD tests for HMA mixtures.
9. Laboratory HMA repeated-load triaxial or constant-height shear strain tests provide a simulation of HMA rutting evolution. Use of laboratory-derived values for the plastic strain coefficients, however, would result in a significant positive bias for the measured rut depths. The laboratory-derived values need to be adjusted to remove this bias to provide an accurate simulation of the entire evolution of rutting. In other words, the adjustment factors for the laboratory-derived plastic deformation or strain coefficients would not be equal to unity.
10. After calibration, the MEPDG plastic-to-elastic axial strain ratio rut-depth transfer function will have the same accuracy as the plastic shear strain and normal strain or stress-based transfer functions. Many of the workshop participants were of the opinion that this assumption or hypothesis would be rejected—a difference in precision would be found between the different transfer functions. Figures 1 through 4 also suggest that this hypothesis would be rejected after calibration because of the difference in predicted rut depths between the transfer functions.

2.4.3 Experimental Design

A detailed, statistically sound experimental plan (sampling template) was developed to refine the calibration of the different rut-depth transfer functions. The sampling template was designed to accomplish three objectives:

1. Determine whether there is bias in the rut-depth predictions or simulation model.
2. Establish the cause of any bias, if found through the validation process.
3. Determine the calibration coefficients or function to eliminate any bias, reduce the standard error of different rut-depth transfer functions, or both.

The sampling template was designed as a fractional factorial matrix because not all cells were expected to be filled with or without replicate roadway segments. Figure 13 shows the sampling matrix for the experimental plan to evaluate the different transfer functions over a range of HMA mixtures and layer thicknesses based on the results from NCHRP Projects 9-30(01) and 1-40B (Von Quintus, Andrei, and Schwartz, 2005 and Von Quintus, 2005). The following bullets provide an explanation and the reasoning for the primary tiers of the sampling template or matrix.

- Layer thickness was included as a primary tier in the sampling template to evaluate the depth correction function. Layer thickness was blocked into less than 5 in. and greater than 7 in. of HMA. Figures 7 through 9 illustrate the effect of HMA layer thickness on the predicted rut depth and suggest a potential bias effect from HMA thickness. For the rehabilitation cells, these thicknesses only apply to the HMA overlay.
- The Asphalt Institute sponsored study found that MEPDG Version 1.0 resulted in a significant bias in the predicted rut depth between neat and modified asphalts (Von Quintus, Mallela, and Titus-Glover, 2007). This potential bias is shown in Figure 14, rejecting hypothesis #5 (refer to Section 2.4.2) that dynamic modulus explains the difference in rut depth between neat and PMA mixtures. Mixture calibration coefficients were determined for the companion test sections (neat HMA and modified mixtures). A comparison of the plastic deformation intercept for the Kaloush transfer function (k_{r1}; refer to Equation 1) between neat and modified mixtures is also shown in Figure 14. Thus, neat HMA and modified mixtures were included in the sampling matrix to ensure that the repeated-load triaxial and constant-height shear tests in support of the transfer functions would discriminate the rutting potential of these mixtures that were identified from the Asphalt Institute study. Binder type was also a consensus parameter from the workshop for the sampling matrix.
- Mixture characteristics [aggregate gradation and voids filled with asphalt (VFA)] were included as a primary tier to ensure that the repeated load tests would discriminate

HMA Thickness	Mix Type	Grading	VFA	New Construction		Rehabilitation				Total No. of Sections
						HMA		PCC		
				Conv.	Deep Strength	Milled	Un-milled	Intact PCC; Crack/Break & Seat PCC	Rubb. PCC	
Thin	Neat	Fine	Low	N-1 (2)		N-2 (1)	N-3 (1)	N-4 (0)	N-5 (0)	4
		Fine	High	N-1 (2)		N-2 (0)	N-3 (0)	N-4 (0)	N-5 (0)	2
		Coarse	Low	N-1 (2)		N-2 (0)	N-3 (0)	N-4 (0)	N-5 (0)	2
		Coarse	High	N-1 (2)		N-2 (1)	N-3 (1)	N-4 (0)	N-5 (0)	4
	PMA	Fine	Low	M-1 (0)		M-2 (0)	M-3 (0)	M-4 (0)	M-5 (0)	0
		Fine	High	M-1 (0)		M-2 (0)	M-3 (0)	M-4 (0)	M-5 (0)	0
		Coarse	Low	M-1 (0)		M-2 (0)	M-3 (0)	M-4 (0)	M-5 (0)	0
		Coarse	High	M-1 (0)		M-2 (0)	M-3 (0)	M-4 (0)	M-5 (0)	0
Thick	Neat	Fine	Low		N-6 (1)	N-7 (0)	N-8 (1)	N-9 (1)	N-10 (0)	3
		Fine	High		N-6 (1)	N-7 (0)	N-8 (1)	N-9 (0)	N-10 (0)	2
		Coarse	Low		N-6 (2)	N-7 (1)	N-8 (0)	N-9 (1)	N-10 (1)	5
		Coarse	High		N-6 (2)	N-7 (1)	N-8 (0)	N-9 (0)	N-10 (1)	4
	PMA	Fine	Low		M-6 (1)	M-7 (1)	M-8 (0)	M-9 (0)	M-10 (0)	2
		Fine	High		M-6 (1)	M-7 (1)	M-8 (0)	M-9 (1)	M-10 (0)	3
		Coarse	Low		M-6 (2)	M-7 (0)	M-8 (1)	M-9 (0)	M-10 (1)	4
		Coarse	High		M-6 (2)	M-7 (0)	M-8 (1)	M-9 (1)	M-10 (1)	5
Total Sections				**8**	**12**	**6**	**6**	**4**	**4**	**40**

Notes:

1. The numbers included in the above cells identify the cell number and number of test sections planned for each cell; N-# is the cell identification, while the (#) is the number of test sections.
2. Thin surface: HMA layer less than 5 in. in thickness.
3. Thick surface: HMA layer more than 7 in. in thickness.
4. Conventional pavement, new construction: Flexible pavements with thin HMA surfaces and thick crushed aggregate base layers.
5. Deep-strength, new construction: Flexible pavements with thick HMA layers and relatively thin aggregate base layers and full-depth HMA pavements.
6. Neat asphalt mixtures: Unmodified asphalt binders.
7. PMA mixtures: Polymer-modified asphalt mixtures.
8. VFA: Voids filled with asphalt; "low" means higher air voids and low asphalt content mixtures, VFA < 50; "high" means low air voids and higher asphalt content mixtures, VFA > 60.
9. Grading: Fine and coarse as defined by the new Superpave grading definitions.
10. PCC = Portland cement concrete; Rubb. = rubblized; conv. = conventional

Figure 13. Sampling template for the experimental plan.

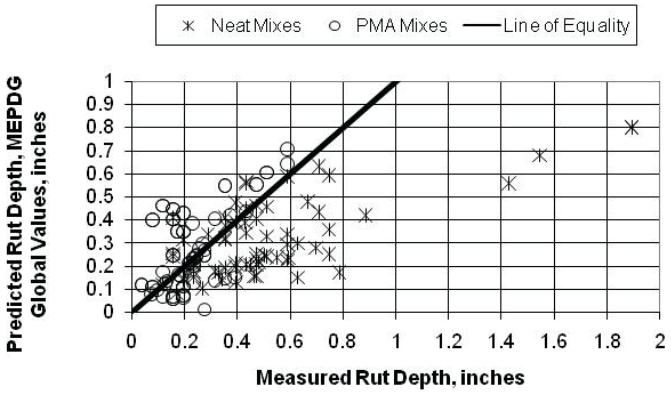

Rut depths were predicted using the global values for the Kaloush transfer function in the MEPDG Version 1.0. As shown, the MEPDG consistently overpredicted the rut depths of the PMA sections and underpredicted the rut depths of the companion, neat sections (Asphalt Institute, 2005).

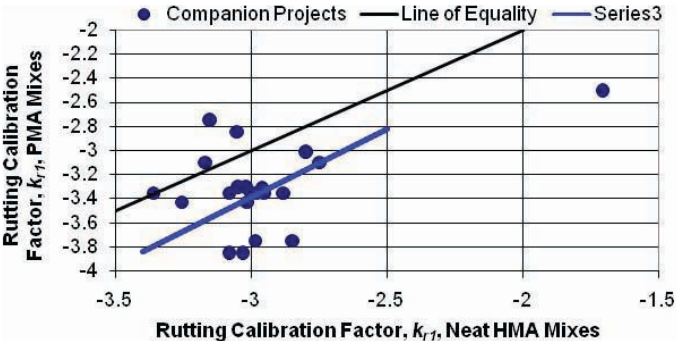

Comparison between the field-derived plastic deformation intercept of neat HMA and modified mixtures—companion projects; $k_{r1(PMA)} = 1.13\left(k_{r1(PMA)}\right)$ (Von Quintus, Mallela, and Titus-Glover, 2007).

Figure 14. Comparison of predicted and measured rut depths using global calibration factors included in the MEPDG for neat and PMA mixtures.

the rutting potential of mixtures over a diverse range of volumetric properties, as found in previous studies (Von Quintus, 2005 and 2006). Aggregate gradation and other volumetric properties were consensus parameters from the workshop for the sampling matrix.

- Different structures (from new construction to HMA overlays of PCC pavements) were included to compare the accuracy of the transfer functions based on vertical or compressive strains, shear strains and stresses, and normal stresses.

The sampling template is a balanced design that was blocked for specific design features for each type of pavement (new construction and rehabilitation). Blocking the fractional factorial was used to determine whether the bias and standard error of the transfer function were dependent on any of the primary tier parameters of the matrix. In other words, blocking is intended to answer the question: Is the bias and/or standard error of the transfer function dependent on type of mixture, mixtures' volumetric properties, pavement type, HMA thickness, and so forth?

A balanced incomplete blocking design was used to control variability in each block and allow more sensitive estimation of factor effects on the calibration coefficients and comparison between different rut-depth transfer functions. There are several methods that can be used to control or compensate for excessive variability in experimental measurements. The more common methods are repeat tests, replication, and local control of the experimental variables. Parts of all three methods were considered or combined into the sampling template for NCHRP Project 9-30A (refer to Figure 13).

1. Repeat rut depth measurements were used to determine the measurement error or variability. Most of the test sections included in the experimental plan have repeat measurements for the same site at the same time. Test sections were selected that have two to three repeat measurements or frequent rut depth measurements so that the measurement error or variability can be estimated for different ranges of rut depths.
2. Replication of sites was included for some cells. As noted previously, it is assumed that the statistics from the replicates in selected cells of the sampling template are applicable or equal to other cells within a specific block of the experimental design. Test sections were selected so that some cells in the sampling template contain two replicate projects or test sections to provide an estimate of the pure error of the transfer function.
3. Local control of variability was handled through the blocking design of the experiment. The factors used to block the experimental matrix for validating and comparing rut-depth prediction models included:
   a. Pavement family (e.g., new versus overlay), because of the influence on stress and strain distribution in the HMA layer.
   b. HMA thickness, because of the confinement effect (depth correction function) used in the MEPDG software.
   c. Modified and neat asphalt binders, because of their significantly different viscous behaviors (recovery differences) resulting in statistically different levels of rutting for the same conditions.
   d. Gradation type and volumetric properties, because of their effect on HMA plastic flow and their dependency on mixture confinement.

2.4.4 Pavement Types and Rehabilitation Strategies

Different pavement types and rehabilitation strategies were considered in calibrating the rut-depth transfer function in NCHRP Project 1-37A. The flexible pavement types included conventional (relatively thin HMA surface over thick crushed aggregate base), deep-strength, and full-depth HMA pavements. The rehabilitation strategies included HMA overlays of flexible pavements and intact and fractured PCC slabs. All of these rehabilitation and new construction strategies were also included as separate pavement families in the NCHRP Project 9-30 experimental sampling matrix (Von Quintus et al., 2004).

Results from the NCHRP Project 9-30(01) ancillary studies and the NCHRP Project 1-40B mixture calibration study found systematic differences in the magnitudes of the rut-depth residual error or bias that were mixture dependent but structure independent (Von Quintus, Andrei, and Schwartz, 2005 and Von Quintus, 2005). Figure 15 shows a comparison of the predicted HMA rut depths and residual errors (predicted minus measured values) for the NCAT, MnROAD, and WesTrack test tracks. The residual errors were related to the HMA volumetric properties and gradation.

Figure 16 shows the same residual errors after making adjustments for volumetric and gradation differences (refer to Appendix C). Thus, the original experimental plan from NCHRP Project 9-30 was revised to combine some of the HMA pavement families and rehabilitation strategies to reduce the number of test sections needed for calibrating multiple rut-depth transfer functions.

The combination of structural families was based on analyses of rut depths measured in LTPP and the NCHRP studies referenced. The LTPP data analysis study of the SPS and general pavement study (GPS) experiments found that the measured rut depths were dependent on HMA stiffness properties, base type (bound or unbound), whether the surfaced was milled, and traffic (Rauhut, Von Quintus, and Eltahan,

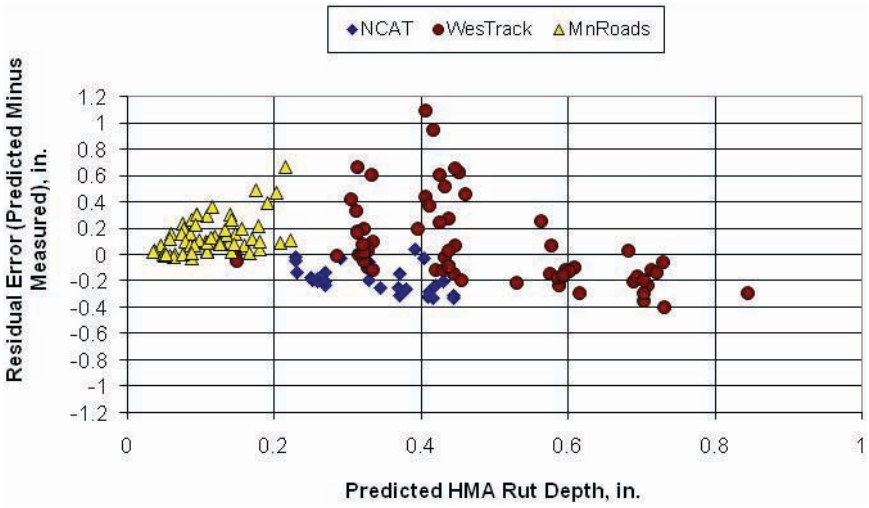

Figure 15. Residual error of predicted HMA rut depth for three experiments for the MEPDG transfer function using Level 1 inputs for the HMA layers (NCHRP Project 9-30; Von Quintus, Andrei, and Schwartz, 2005).

2000; Von Quintus and Simpson, 2000; and Von Quintus, Simpson, and Eltahan, 2000). Thickness, climate, subgrade soil type, and other factors were found to have a minor to no effect on rutting. The finding related to climate (no effect on rutting) contradicts previous experience—rutting should increase with warmer climates or higher temperatures. The explanation given for that finding is the asphalt grade is selected based on climate—harder asphalts are used in the warmer climates, so the binder effect cancels out the temperature effect. The other finding about rut depth being independent of HMA thickness contradicts the finding from the earlier LTPP study (Rauhut, Eltahan, and Simpson, 1999). The earlier study focused on the GPS test sections, while the latter studies included results from the SPS test sections.

The conventional pavements were also kept separate from the deep-strength and full-depth HMA pavements because of the thickness effect on rutting for the different rut-depth transfer functions for HMA and unbound pavement layers.

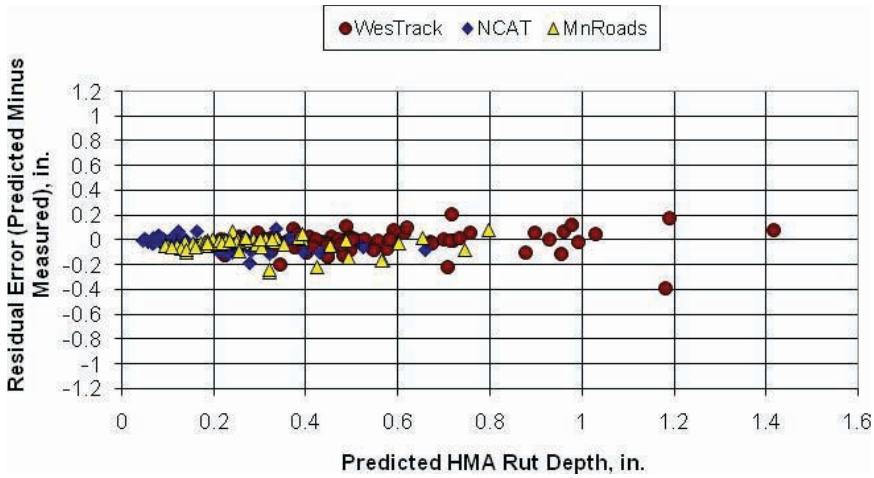

Figure 16. Residual error of predicted HMA rut depth for three experiments for the MEPDG transfer function using volumetric and material property adjustment factors from NCHRP Project 1-40B (Von Quintus, Andrei, and Schwartz, 2005).

NCHRP Project 1-40B found reasonable residual errors for the HMA rut-depth prediction model, but larger errors and a large bias for the unbound material's rut-depth transfer function. Although the focus of NCHRP Project 9-30A was on HMA rutting, incorporating the different influences of the unbound material rutting in the experimental plan had to be considered because the measured rut depths include this component. In addition, the LTPP study found base type to be a significant factor related to rutting (Rauhut, Eltahan, and Simpson, 1999).

2.4.5 Types of Test Sections

Three types of experimental test sections described in the following can be used in the calibration–validation refinement plan for the MEPDG rut-depth transfer function and its comparison to other transfer functions.

- APT experiments can be used for rapid verification of rut depth models and sensitivity of rutting to mixture properties. Results from this type of test section can be used to confirm the form of the transfer function and quantify the impact of dynamic modulus and other mixture properties for explaining the evolution of rutting. These test sections are basically independent of climatic factors and long-term aging of the asphalt binder. There are two issues, however, related to the use of APT facilities with simulated truck loading: (1) the effects of short-term load application and (2) the use of single tires. Both issues are discussed in more detail in the following.
- Short-term test track experiments can be used to calibrate and validate the effects of mixture type, HMA layer thickness, mixed-wheel loads, and wander on the distress predictions without the added complexity of long-term aging and extensive environmental variations. Results from this type of experiment are slightly dependent on the climatic factors and long-term aging of the asphalt binder.
- Long-term, full-scale field experiments or test sections can be used to fully calibrate and validate the rut-depth simulation model and confirm the combined influence of environmental, aging, and wheel load effects on these predictions. All test sections included in the NCHRP Project 1-37A calibration study came from this category (ARA, Inc., ERES Consultants Division, 2004).

All three types of experiments are valuable for evaluating different parts of the rut-depth transfer functions. As noted previously, there are two issues related to the use of APT facilities with simulated truck loading for predicting rut depth with the MEPDG.

1. Most of the simulated truck loadings are applied in a relatively short period of time. The MEPDG outputs the predicted rut depth on a monthly basis. To evaluate the rutting evolution from APT sections with the MEPDG requires that the loads be applied over a longer time period, so more asphalt aging is simulated than actually occurs during the loading cycles. This will result in a negative bias between the predicted and measured rut depths. As a result, APT sections should only be used to calibrate or validate the transfer functions based on the final rut depth and not rut depth evolution unless the aging function is turned off. In other words, only the final rut depth is used for those tests where the simulated truck loads are applied in less than one month.
2. Most APT facilities use a single tire for applying loads to the test pads. The MEPDG assumes that each axle consists of dual tires. Previous versions of the MEPDG (Version 1.1 and earlier) included a uniform distribution of truck loads related to traffic wander or the lateral distribution of wheel loads. Separating the dual tires by nearly 60 in. was used to simulate the loading of a single tire. Figure 17(a) illustrates that the rut depth is basically independent of spacing of the duals beyond about 30 in. (Version 1.0). MEPDG Version 9-30A revised the wander function to a normal distribution. Use of a normal distribution changed the computational methodology such that the HMA rutting was predicted to be very small to zero for a large spacing of the duals, as shown by Figure 17(b). An appropriate methodology is to assume that the spacing is zero between the duals and the weight of each tire is half of the single tire used in the simulated loading.

Figure 18 shows the effect of spacing of the duals on rut depth in accordance with the WesTrack, modified Leahy, and Verstraeten transfer functions. The Kaloush and modified Leahy transfer functions result in similar findings, while the WesTrack and Verstraeten functions provide similar results. Based on these results it was decided to simulate a single load by setting the spacing of the duals to 0 in. and the weight of one tire of the duals to be half of the total weight of the single tire used in the APT test program.

The project types that are suggested for use in the calibration–validation refinement plan and prediction model comparisons are listed in Table 3. These experiments and projects can be used to confirm the aging and climatic effects on rut depth by evaluating and comparing the calibration factors between each experiment. In fact, many of the test sections were used in the NCHRP Project 9-30(01) study [ancillary studies or pre-implementation studies using the MEPDG to determine the effect of

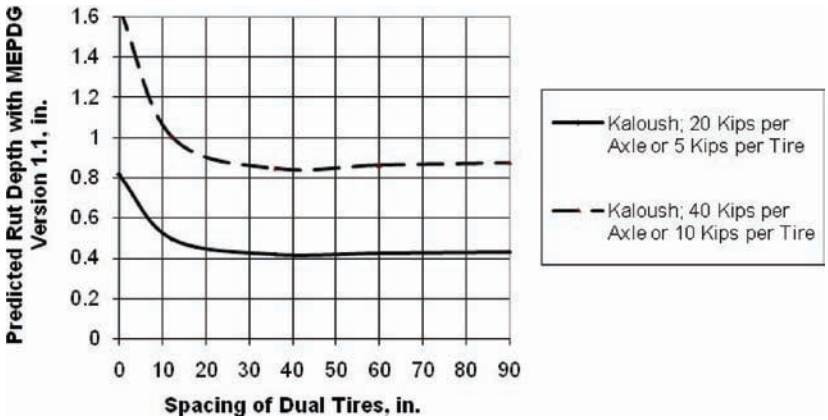

(a) Comparison of predicted rut depth using MEPDG Version 1.0 with a uniform distribution of traffic loads.

(b) Comparison of predicted rut depth using MEPDG Version 9-30A with a normal distribution of traffic loads.

Figure 17. Effect of spacing of dual tires on predicted rut depth using the Kaloush transfer function in MEPDG Versions 1.0 and 9-30A.

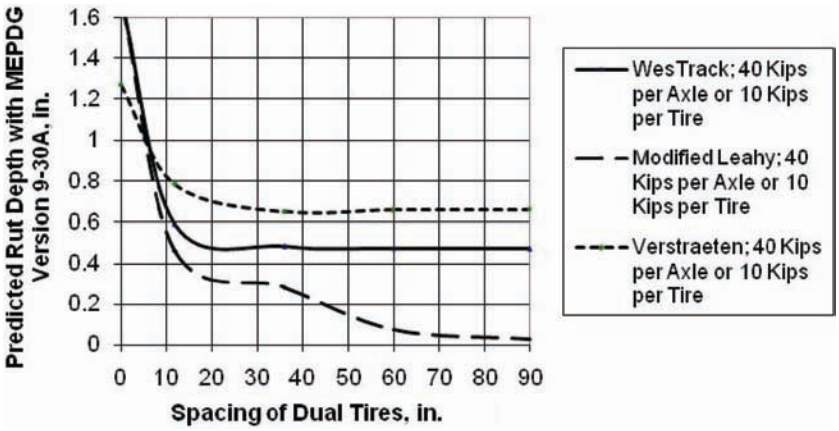

Figure 18. Effect of spacing of dual tires on predicted rut depth using the WesTrack, modified Leahy, and Verstraeten transfer functions in MEPDG Version 9-30A.

Table 3. Experiments and projects suggested for use in the calibration–validation refinement plan and evaluation of different rut-depth transfer functions.

Climate Independent or Climate Controlled				Climate Dependent, Plus Long-Term Aging of Asphalt	
Little to No Aging (Test Completed Within Months)		Some Aging (Test Completed in 3 Years or Less)			
FHWA HVS	Rounds 1 & 2	WesTrack	PRS study	MnROAD	Rounds 1 & 2
LSU HVS	CTB testing	NCAT	Rounds 1, 2, 3	LTPP	SPS-1
Caltrans HVS	HVS 1 & 2			LTPP	SPS-5
Florida HVS	Rounds 1 & 2			LTPP	SPS-6
				LTPP	SPS-9
				Nevada	I-80
				Mississippi	I-55
				Pennsylvania	Special study
				WRI	Binder study

PRS = Performance-related specification
WRI = Western Research Institute
LSU = Louisiana State University

volumetric properties on rut depths (Von Quintus, Andrei, and Schwartz, 2005)].

2.4.6 Number of Test Sections for Calibrating Rut-Depth Transfer Functions

The number of model evaluations (i.e., the sample size) to properly calibrate and validate the rut-depth transfer functions was evaluated for both bias and precision. The bias is the average residual error; therefore, the confidence interval on the mean can be used to relate sample size and bias. Letting e_t be the tolerable bias, the confidence interval on the mean yields the following expression:

$$N \geq \left(\frac{ts_y}{e_t} \right)^2 \tag{11}$$

Where s_y is the standard deviation of the true values of *Y*, and *t* is based on $n - 1$ degrees of freedom. For accuracy, the standard error of estimate is used. The tolerable bias was estimated from the precision of the rut depth measurements along the test section within the SPS-1 and SPS-5 experiments. This value was estimated to be 0.075 in. (1.9 mm).

Since the square of s_e is a variance, the confidence interval on the variance can be used to show the relationship between sample size and the relative error variance (s_e/s_y). The basic equation for the confidence interval is:

$$\sigma^2 \geq (n-1)\frac{s^2}{x_\alpha^2} \tag{12}$$

Where x_α^2 is the chi-square statistic for $n - 1$ degrees of freedom and level of significance, α. Inserting s_e and s_y yields:

$$\frac{s_e}{s_y} \geq \left[\frac{x_\alpha^2}{n-1} \right]^{0.5} \tag{13}$$

By selecting a level of significance, the relative deviation s_e/s_y can be determined for a selected sample size. Three levels of significance can be used in estimating the sample size for each distress: 75%, 90%, and 95%. A level of significance of 90% is suggested as a practical level in determining the sample size to be used in the experiment.

The original experimental matrix developed in NCHRP Project 9-30 was prepared for calibrating and validating all HMA distresses. Within this sampling template, traffic and climate were treated as secondary parameters because traffic is interrelated with HMA thickness and climate is interrelated with asphalt binder grade. The template was stratified or blocked by family of pavement for each distress. Each cell in the template represents the effect of changing structure and mixture. This type of matrix was selected because the experiment is focused on the benefits of Input Level 1 material characterization (measured laboratory values) on reducing the overall error as compared to Input Level 3 best-guessed material properties or Input Level 2 properties calculated from regression equations. The sampling template was also structured to determine the accuracy of the individual transfer functions.

The number of test sections within each cell for the primary tiers of the factorial was estimated so that the hypotheses could be accepted or rejected at a 90% confidence level. The coefficient of variation of the measured rut depths was assumed to be 10% in determining the number of test sections and individual observations. In summary, 40 test sections with different site and design features are needed for the experimental plan. This number is believed to be sufficient to cover a diverse set of mixtures and site conditions.

2.4.7 Criteria for Project Selection

The following lists the criteria and important considerations for selecting projects to calibrate and compare different M-E–based rut-depth transfer functions in the MEPDG. These criteria are listed in order of importance.

- **Material availability:** The controlling factor for test sections to be included in the experimental plan was the availability of materials for mixture testing for sections without Input Level 1 material properties. A minimum of 800 lbs of bulk mixture was required for each HMA layer. A sufficient amount of bulk HMA mixture was available for only a few projects or mixtures. Thus, a minimum of 1,000 lbs of aggregate and 100 lbs of the asphalt binder was obtained for each mixture. The HMA mixtures were reconstituted in the laboratory to the in-place properties reported in the construction records or LTPP database.
- **Time-series distress data:** Projects or test sections should have at least four rut depth measurements over time. Rut depths should be available for the first couple of years and then in 3-year intervals. It was important to capture the development of the rutting within the first 3 years or load cycles. The reason for these early measurements is to identify the initial or primary densification rate from the long-term or secondary (also referred to as the steady-state region) plastic deformation rate. It is also important that a consistent definition and measurement of the surface distresses be used throughout the calibration and validation process. The rut depths should be measured in accordance with the *Distress Identification Manual for the Long-Term Pavement Performance Project* (SHRP, 1993). All data used to establish the inputs for the models (including material test results, climatic data, and traffic data) and performance monitoring were collected or measured in accordance with standard procedures (for example, FHWA Publication Number SHRP-LTPP-OG-001: *Data Collection Guide for Long-Term Pavement Performance Studies*).
- **Nonconventional mixtures:** Test sections with nonconventional mixtures were targeted for inclusion in the experimental plan to ensure that the transfer functions and calibration factors were representative of these mixtures (refer to Figure 13). Nonconventional mixtures include stone matrix asphalt (SMA), PMA, and WMA. Most of the test sections included in the NCHRP Project 1-37A global calibration effort contained conventional, neat asphalt HMA mixtures.
- **HMA volumetric properties and mixture design:** The in-place air voids and other HMA volumetric properties immediately after construction must be available from construction or project records. Results from the mixture design process in selecting the target asphalt content are also needed for use in evaluating different mixtures using Input Level 2—estimating the plastic deformation coefficients from volumetric properties.
- **Number of layers:** Test sections were selected with the fewest number of structural layers and materials (e.g., one or two HMA layers, one unbound base layer, and one subbase layer) to reduce the amount of testing required for material characterizations and run time for the MEPDG Version 9-30A.
- **Other Level 1 input parameters:** The highest input level was used for the other input parameters in determining the standard error of each transfer function. This approach was used in the NCHRP Project 1-37A global calibration study. For the relative comparisons between the different prediction models, this requirement is not mandatory but is needed to define the standard error term for the transfer functions for different input levels. Input Levels 2, 3, or both can be used when just comparing the rut-depth transfer functions.

2.4.8 Projects Included in Sampling Template

As noted previously, NCHRP Projects 9-30 and 1-40B found that the standard error of the MEPDG rut-depth transfer function could be explained and reduced by adjusting the plastic deformation coefficients based on the HMA volumetric properties and gradation. Thus, the generalized sampling template was designed to consider these factors while combining some of the different pavement families (refer to Figure 13).

Projects were selected to accomplish two goals: (1) to calibrate and assess the rut-depth transfer functions, and (2) to develop Input Level 2 factors for estimating the plastic deformation coefficients from volumetric properties—similar to the procedure included in Appendix C for the

Table 4. New construction projects and number of test sections included in the experimental sampling template.

Section or Project	Experiment ID	Purpose	Mix Type	HMA Pavement		Comments
				Conventional	Deep Strength	
FHWA	WesTrack	Level 2 analysis	Neat	8	—	24 total sections
NCAT	Rutting	Level 2 analysis	Neat & modified	—	8	36 total sections
MnROADs	MnROADs	Level 2 analysis	Neat	4	4	14 total sections; forensic investigation
Caltrans	HVS	Level 2 analysis	Neat & modified	2	—	4 total sections
FHWA	HVS	Level 2 analysis	Neat & modified	2	2	8 total sections
Florida	HVS	Level 2 analysis	Neat & modified	2	2	8 total sections
Montana	SPS-9	Level 2 analysis	Neat & modified	—	2	3 total sections
Montana	SPS-1	Level 2 analysis	Neat	2	2	6 total sections
Nebraska	SPS-1	Level 2 analysis	Neat	2	2	8 total section; forensic investigation
Alabama	SPS-1	Level 2 analysis	Neat	2	2	8 total sections
TOTAL		**Level 2 Analysis**		**24**	**24**	
NCAT	Rutting	Calibration	Neat & modified	—	4	4 total sections; forensic investigation
Caltrans	HVS	Calibration	Modified	2	4*	10 total sections
FHWA	HVS	Calibration	Neat & modified	2	2	8 total test sections
Florida	HVS	Calibration	Neat & modified	2	2	8 total test sections
Arizona	SPS-1	Calibration	Neat & modified	2	2	8 total sections; forensic investigation
California	Perpetual	Calibration	Modified	—	2	2 total sections
Wisconsin	SPS-1	Calibration	Neat	2	4	8 total sections; forensic investigation
Wisconsin	SPS-9	Calibration	Neat & modified	1	1	4 total sections; forensic investigation
Kansas	SPS-1	Calibration	Neat	2	2	8 total sections; forensic investigation
Kansas	SPS-9	Calibration	Neat & modified	2	—	3 total sections; forensic investigation
TOTAL		**Calibration**		**15**	**23**	

*Composite or semirigid pavement structures; HMA over PCC or cement-treated base layers

Kaloush transfer function. Tables 4 and 5 identify the test sections that were used to accomplish these two goals. Table 4 lists the new construction projects, while Table 5 lists the HMA overlay projects.

The projects identified for a Level 2 analysis were used to identify and develop regression equations to estimate the plastic deformation coefficients from the HMA volumetric properties, and the projects identified for calibration were used to calibrate the transfer functions using laboratory-derived plastic deformation coefficients measured as part of this study or available from other research studies.

Table 6 lists the test sections that were initially identified as high priority sites in NCHRP Project 9-30 but were dropped from the NCHRP Project 9-30A sampling template because of missing data or insufficient component materials for preparing the test specimens. (Sample preparation procedures are discussed in the next section.)

2.5 Preliminary Analysis of Test Sections and HMA Mixtures

A preliminary analysis of the test sections and HMA mixtures recommended for calibration was conducted as part of the test section selection process.

2.5.1 Site Features and Layer Properties

Tables 4 and 5 list the projects that were used in the calibration process. Details of the project layer properties, measured rut depths, and other inputs to the MEPDG are included in

Table 5. HMA overlay projects and number of test sections included in the experimental sampling template.

Section or Project	Experiment ID	Purpose	Mix Type	Existing Pavement		Comments
				HMA	PCC	
Minnesota	SPS-5	Level 2 analysis	Neat	2	—	8 total sections
Minnesota	SPS-9	Level 2 analysis	Modified	2	—	3 total sections
NCAT	Rutting	Level 2 analysis	Modified	2	—	6 total sections
California	SPS-6	Level 2 analysis	Neat	—	4	6 total sections
California	SPS-5	Level 2 analysis	Neat & modified	4	—	8 total sections
Arizona	SPS-9	Level 2 analysis	Neat & modified	2	—	4 total sections
Maryland	SPS-9	Level 2 analysis	Neat & modified	2	—	5 total sections
TOTAL		**Level 2 Analysis**		**14**	**4**	
Nevada	I-80	Calibration	Neat & modified	2	—	4 total sections
NCAT	Rutting	Calibration	Neat & modified	2	—	4 total sections; forensic investigation
Montana	SPS-5	Calibration	Neat	2	—	8 total sections
Mississippi	SPS-5	Calibration	Neat	2	—	8 total sections; forensic investigation
Missouri	SPS-5	Calibration	Neat & modified	2	—	9 total sections
Missouri	SPS-9	Calibration	Neat & modified	—	2	4 total sections
Alabama	SPS-6	Calibration	Neat & modified	—	4	6 total sections
Texas	SPS-5	Calibration	Neat	2	—	8 total sections; forensic investigation
California	Perpetual	Calibration	Modified	—	2	2 total sections
California	HVS	Calibration	Modified	2	—	4 total sections
Colorado	SPS-5	Calibration	Neat	2	—	8 total sections
Arizona	SPS-5	Calibration	Neat	2	—	8 total sections; forensic investigation
TOTAL		**Calibration**		**18**	**8**	

Appendix J. Table 7 provides a summary of key data elements and the range of maximum rut depths, while Figure 19(a) compares the maximum rut depth recorded at each test section with HMA layer thickness. As shown, HMA overlay thickness (excluding the thickness of the existing HMA layers for overlays) does not have an effect on rut depth. There are other factors affecting the total rut depth. For new construction, the maximum rut depth is slightly greater for the thinner HMA layers (0.456 in. for sections less than 8 in. and 0.355 in. for sections 8 in. or greater). Using the *t*-test, however, the mean rut depths for the two data sets (less than 8 in. and greater than or equal to 8 in.) were found to not be significantly different.

The effect of thickness is mixture dependent for the individual projects. For example, Figure 19(b) shows the effect of HMA overlay thickness for test sections included in the Mississippi SPS-5 project. As shown, the maximum rut depth increases with increasing overlay thickness. This observation is different from Figure 19(a) and previous findings reported in other LTPP studies. Figure 19(c) shows the effect of HMA total thickness on rut depth for the test sections included in the Wisconsin SPS-1 project. As shown, rut depth also increases with increasing layer thickness. This observation is also different from Figure 19(a) and previous findings reported from other LTPP studies. From the forensic investigation of the Wisconsin SPS-1 project, the rutting was found to be a result of instability in the lower HMA layers rather than additional densification of the HMA layers (refer to Section 2.5.3).

The point of these comparisons and discussions is that the mixture distortion properties for the individual mixtures or test sections are the more important parameter. Those sites that exhibit anomalies or rut depth characteristics that deviate from previous studies were selected for forensic investigations to explain the rut depth trends. These projects were also selected for the calibration study to confirm that the plastic strain coefficients can explain those anomalies. The forensic investigations are discussed in Section 2.5.3.

Field evaluation activities were also performed to collect data for refining the calibration and validation of the transfer functions. These field evaluation activities consist of sampling and testing the pavement materials and structure and collecting truck traffic and climate data. Most of this data for determining the inputs to the MEPDG was available from DataPave, the LTPP database. For non-LTPP projects, all data were extracted from existing reports, construction files, or

Table 6. Projects dropped or eliminated from the experimental sampling template because of missing data or insufficient materials availability.

Project or Section	Experiment ID	Reason for Dropping Project
Western Research Institute	Binder study	Insufficient materials sampled during construction.
Pennsylvania DOT	Pavement instrumentation study	Insufficient materials sampled during construction.
California	LTPP SPS-5	Missing air void and other volumetric data after construction.
Nebraska	LTPP SPS-1	Insufficient materials available in MRL.
Alabama	LTPP SPS-1	Includes RAP in mixture—insufficient RAP stored in MRL.
Alabama	LTPP SPS-5	Decided not to include this project because polymer-modified asphalt was not included in experiment.
Arkansas	LTPP SPS-1	Insufficient materials included in MRL.
Arizona	LTPP SPS-6	Insufficient aggregate in MRL.
Florida	LTPP SPS-1	Insufficient aggregate in MRL; quarry was closed; additional aggregate unavailable.
Florida	LTPP SPS-5	Insufficient aggregate in MRL.
Florida	LTPP SPS-9	Insufficient aggregate in MRL.
Indiana	LTPP SPS-6	Asphalt containers were not properly sealed—insufficient asphalt in remaining containers.
Indiana	LTPP SPS-9	Asphalt containers not properly marked; not sure which asphalt container has the neat and which has modified asphalt.
Maine	LTPP SPS-5	Insufficient asphalt in MRL.
Missouri	LTPP SPS-6	Asphalt used in mixture not identified.
Missouri	LTPP SPS-9	Insufficient aggregate in MRL.
Montana	LTPP SPS-1	Insufficient aggregate in MRL.
North Carolina	LTPP SPS-5	No asphalt samples in MRL.
North Carolina	LTPP SPS-9A	No aggregate samples in MRL.
North Carolina	LTPP SPS-9	No aggregate samples in MRL.
Nebraska	LTPP SPS-9	No materials in MRL.
Nebraska	LTPP SPS-1	Insufficient aggregate in MRL; unsure about quarry used or source of aggregate.
New Mexico	LTPP SPS-5	Insufficient asphalt and containers not labeled.
Nevada	LTPP SPS-1	Aggregate containers not labeled in MRL.
Ohio	LTPP SPS-1	Aggregate containers not labeled in MRL.
Pennsylvania	LTPP SPS-6	Did not include a polymer-modified asphalt.

testing documents. The following summarizes the data elements that were obtained for each test section or project to establish the MEPDG inputs. A more in-depth analysis of these data elements is included in Appendix J.

- **Traffic:** For test sections located on the highway network, weigh-in-motion (WIM) and automated vehicle classifiers (AVC) were used to estimate the actual truck traffic, both for axle weight distributions and number of load applications. The historical truck traffic data were based on actual measurements over the analysis period. Tire pressures were unavailable for most of the highway segments, so the tire pressure was assumed to be 120 psi, the value assumed in the NCHRP Project 1-37A calibration effort. Measured tire pressures were available for the APT facilities and test tracks. Annual average daily truck traffic (AADTT) and truck counts were available for all sections, while WIM data was available on most but not all LTPP test sections. For sites where WIM data were unavailable, the default normalized axle load distributions from NCHRP Project 1-37A were used in the calibration process.
- **Nondestructive deflection tests:** Falling weight deflectometer (FWD) deflection basin tests were periodically measured for most test sections listed in Tables 4 and 5. Deflection basin tests were used to back-calculate the in-place modulus values of the unbound layers and subgrade to confirm the resilient modulus value used in the calibration process. A minimum of two time periods was used in estimating the in-place elastic modulus values for all unbound layers and subgrade: (1) immediately after construction (to establish the baseline values) and (2) prior to sampling and testing the pavement structure. *Immediately after construction* is defined as being within the same season that the wearing surface was placed. Back-calculated elastic layer modulus values for the unbound layers were adjusted to laboratory-equivalent values, which are explained in the next bullet item.
- **Pavement layer and materials information:** The layer thickness and material properties of each pavement layer

Table 7. Range of maximum measured rut depths for projects included in the calibration–validation process.

Project	Experiment	Purpose	Pavement Type and Thickness	Max. Rut Depth, in.
Florida	HVS, PMA, 2B-50	Level 2 analysis	Conv.; 4 in.	0.386
Florida	HVS, neat, 3B-50	Level 2 analysis	Conv.; 4 in.	0.919
FHWA	HVS, PMA, 7/2	Level 2 analysis	Deep strength, 8 in.	.472
FHWA	HVS, neat, 10/2	Level 2 analysis	Deep strength, 8 in.	1.429
FHWA	WesTrack, 5, coarse	Level 2 analysis	Conv.; 6 in.	1.077
FHWA	WesTrack, 3, fine	Level 2 analysis	Conv.; 6 in.	0.552
FHWA	WesTrack, 11, fine-plus	Level 2 analysis	Conv.; 6 in.	0.354
NCAT	Rut, PMA, N02	Level 2 analysis	Full depth; 19.2 in.	0.14
NCAT	Rut, PMA, N13	Level 2 analysis	Full depth; 19.2 in.	0.23
NCAT	Rut, neat, N03	Level 2 analysis	Full depth; 19.2 in.	0.29
NCAT	Rut, neat, E03	Level 2 analysis	Full depth; 19.2 in.	0.43
MnROADs	Initial, 01	Level 2 analysis	Conv.; 5.7 in.	0.306
MnROADs	Initial, 21	Level 2 analysis	Conv.; 6.7 in.	0.58
MnROADs	Initial, 04	Level 2 analysis	Deep strength, 8.3 in.	0.48
MnROADs	Initial, 15	Level 2 analysis	Deep strength, 10.4 in.	0.316
Wisconsin	SPS-1, 113	Calibration	Conv.; 5.5 in.	0.226
Wisconsin	SPS-1, 117	Calibration	Deep strength; 11.0 in.	0.394
Kansas	SPS-1, 102	Calibration	Conv.; 4.3 in.	1.14
Kansas	SPS-1, 101	Calibration	Conv.; 7.2 in.	0.63
Kansas	SPS-1, 104	Calibration	Full depth, 19.2 in.	0.24
Kansas	SPS-1, 106	Calibration	Full depth, 14.6 in.	0.39
Oklahoma	SPS-1, 113	Level 2 analysis	Conv.; 4.5 in.	0.591
Oklahoma	SPS-1, 114	Level 2 analysis	Deep strength, 8.1 in.	0.197
Oklahoma	SPS-1, 115	Level 2 analysis	Deep strength, 16.5 in.	0.354
Arizona	SPS-5, RAP, 502	Calibration	Overlay, 2.7 in.	0.433
Arizona	SPS-5, virgin, 504	Calibration	Overlay, 4.8 in.	0.197
Arizona	SPS-5, virgin, 507	Calibration	Overlay, 6.8 in.	0.354
Arizona	SPS-5, RAP, 508	Calibration	Overlay, 6.5 in.	0.433
Montana	SPS-5, RAP, 502	Calibration	Overlay, 2.6 in.	0.472
Montana	SPS-5, virgin, 507	Calibration	Overlay, 7.2 in.	0.354
Missouri	SPS-5, RAP, 502	Calibration	Overlay, 2.1 in.	0.236
Missouri	SPS-5, RAP, 508	Calibration	Overlay, 7.6 in.	0.354
Texas	SPS-5, neat, 505	Calibration	Overlay, 2.0 in.	0.354
Texas	SPS-5, RAP, 508	Calibration	Overlay, 7.3 in.	0.315
Mississippi	SPS-5, virgin, 505	Calibration	Overlay, 2.0 in.	0.433
Mississippi	SPS-5, virgin, 507	Calibration	Overlay, 5.0 in.	0.827
Alabama	SPS-6, intact, 603	Calibration	Overlay, 3.6 in.	0.118
Alabama	SPS-6, B&S, 607	Calibration	Overlay, 4.3 in.	0.236

Conv. = conventional

were extracted from construction files or DataPave. The layer thickness, HMA volumetric properties, and material properties of each unbound layer of each test section are included in Appendix J. Laboratory repeated-load resilient modulus tests were used to estimate the in-place modulus for each unbound layer using the procedure summarized in FHWA Design Pamphlet No. FHWA-RD-97-077 and described in more detail in Report No. FHWA-RD-97-085 (Von Quintus and Killingsworth, 1997a and 1998). The HMA in-place volumetric properties and aggregate blend for each HMA layer were extracted from construction files or DataPave. The back-calculated elastic layer modulus

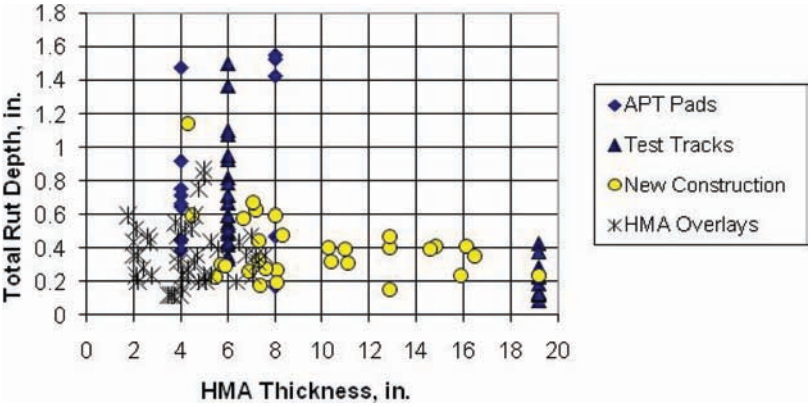

(a) Combined data for many test sections included in Table 7.

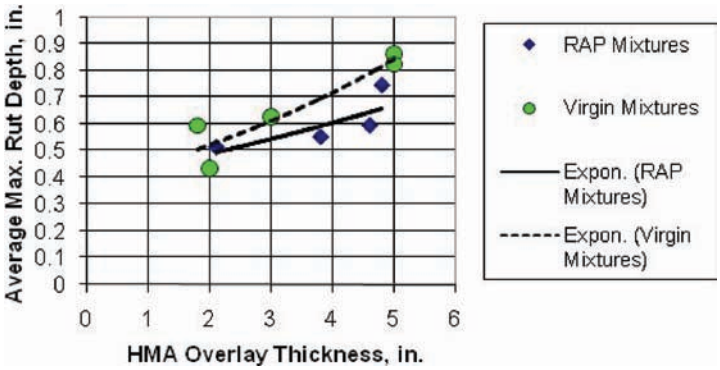

(b) Mississippi SPS-5 project data.

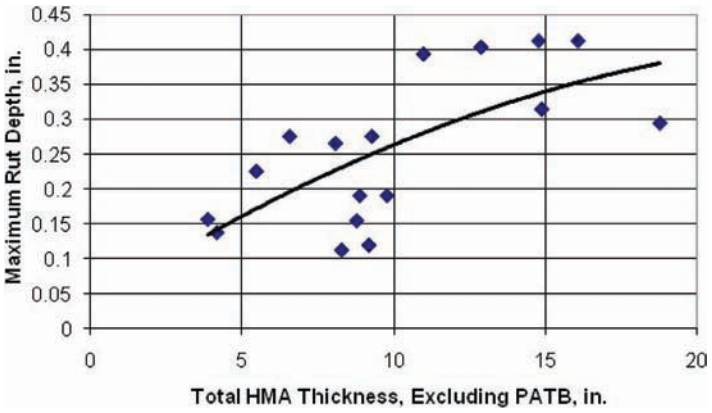

(c) Wisconsin SPS-1 project data.

PATB = permeable asphalt treated base

Figure 19. Comparison of maximum rut depth and HMA layer thickness.

values for all unbound layers and subgrade were adjusted to laboratory-equivalent conditions using the *C*-factors determined and recommended for use from the 1995 LTPP data analysis study (Von Quintus and Killingsworth, 1997b and 1998). The resilient modulus, dry density, and water content entered in the MEPDG for all unbound layers represented equivalent conditions. In other words, the maximum dry density and optimum water content were not used when the resilient modulus was measured at a different dry density and water content.

- **Distress surveys:** Rut depth measurements have been made on all test sections included in Tables 4 and 5 in accordance with the *Distress Identification Manual for the Long-Term Pavement Performance Project* (SHRP, 1993). The rut depths that populate the M-E_DPM database represent the average maximum vertical displacement

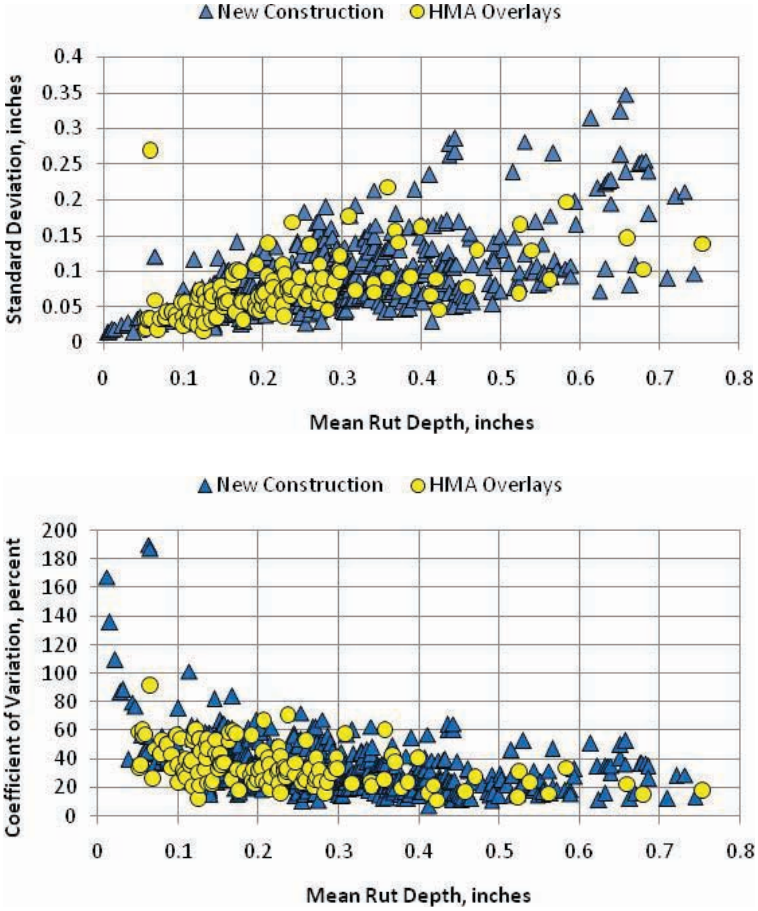

Figure 20. Standard deviation and coefficient of variation as a function of the average measured values; LTPP data.

between a string or wire line and the pavement surface over the entire lane width along the test section. Rut depths were measured every year for the first 3 years after construction, with a minimum of one average reading over time. Figure 20 shows the relationship between the mean measured rut depth and coefficient of variation and standard deviation of the measured values for the LTPP sites. The LTPP sites were used to estimate the standard deviation of measured values because of the consistency in the method and equipment used to measure rut depths over time. As shown, the precision of the field-measured values can be low.

- **Climate:** Automated weather stations (AWSs) are used to collect the climate data that is needed to predict moisture and temperature histories with the MEPDG. The MEPDG software contains many weather stations. The test section location was checked against the AWS sites included in the software to ensure that a site or a combination of sites (to develop a virtual weather station) have sufficient weather data for the subject calibration site. The virtual weather stations were established based on the latitude, longitude, and elevation of each test section.

2.5.2 Field-Derived Plastic Deformation Coefficients

Field-derived plastic deformation coefficients were determined for selected test sections included in Tables 4 and 5 that minimize the difference between the predicted and measured rut depths. This analysis was completed to determine the intercept coefficient, *N*-term exponent, and stress-term coefficient, if applicable, of each transfer function that provide an accurate simulation of the rut depths measured over time. These field-derived coefficients were also used to determine the transfer functions that would or would not accurately predict the evolution of rutting over a diverse range of mixtures and pavement structures.

Figures 21 through 24 compare the predicted and measured rut depths for each transfer function for the same test sections included in Figures 1 through 4. As shown, all of the transfer functions were found to provide an accurate simulation of the measured rut depths (ranging from very low to high rut depths) over a diverse range of mixtures, conditions, and pavement structures. Figures 21 through 24 suggest that hypothesis #8 in Section 2.4.2 will be accepted.

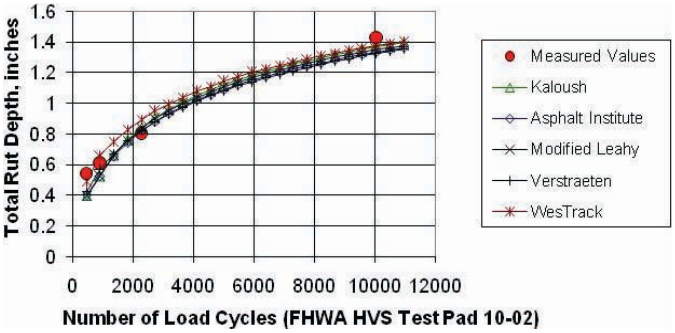

(a) Predicted rut depths for the FHWA HVS test pad 10-02, rutting experiment.

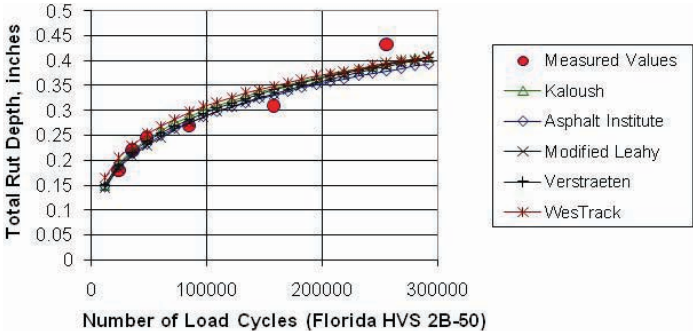

(b) Predicted rut depths for Florida HVS pad 2B-50; modifier experiment.

Figure 21. Field-matched plastic deformation coefficients using the different transfer functions for FHWA and Florida HVS sections, simulated truck loadings.

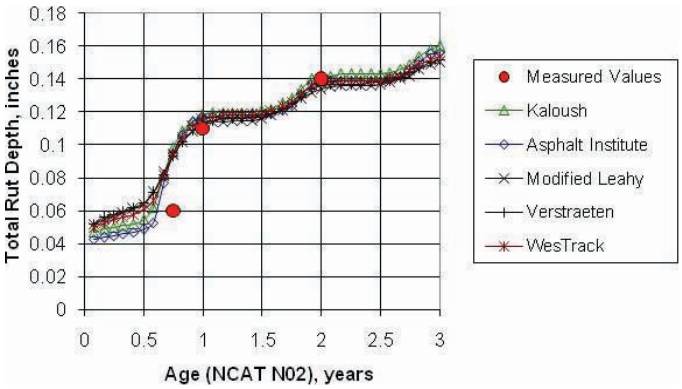

(a) Predicted rut depths for NCAT test section N02.

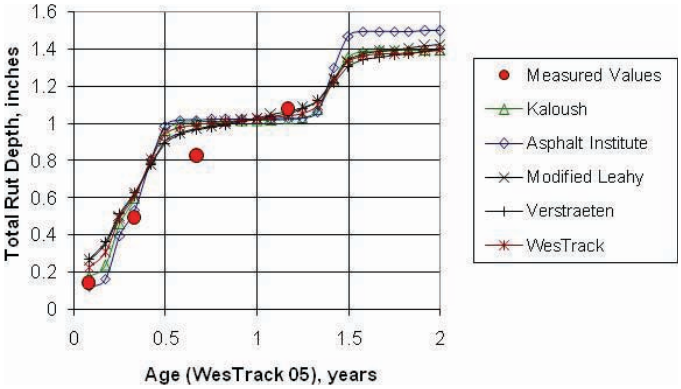

(b) Predicted rut depths for WesTrack test section 05.

Figure 22. Field-matched plastic deformation coefficients using the different transfer functions for selected NCAT and WesTrack test sections.

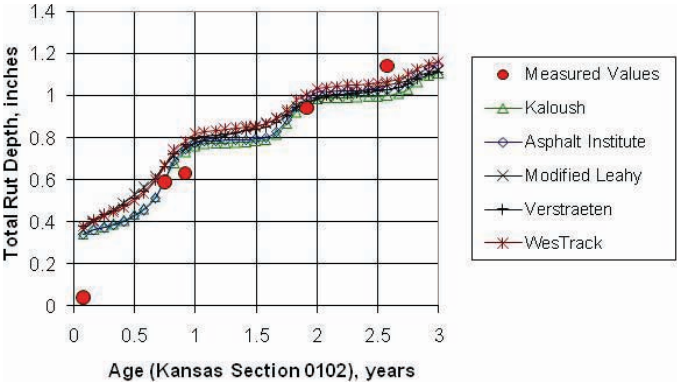

(a) Predicted rut depths for the Kansas SPS-0102, new construction, thin HMA.

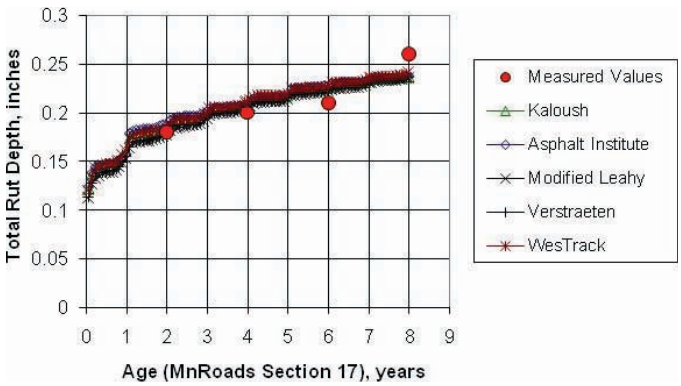

(b) Predicted rut depths for MnROADs section 17, new construction, thick HMA.

Figure 23. Field-matched plastic deformation coefficients using the different transfer functions for selected new construction test sections.

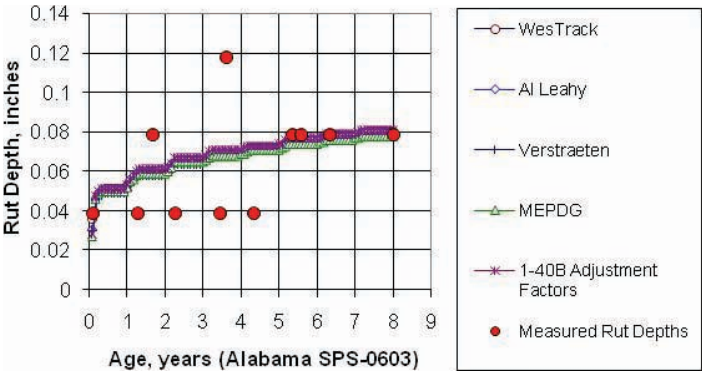

(a) Predicted rut depths for the Alabama SPS-0603, overlay of PCC pavement.

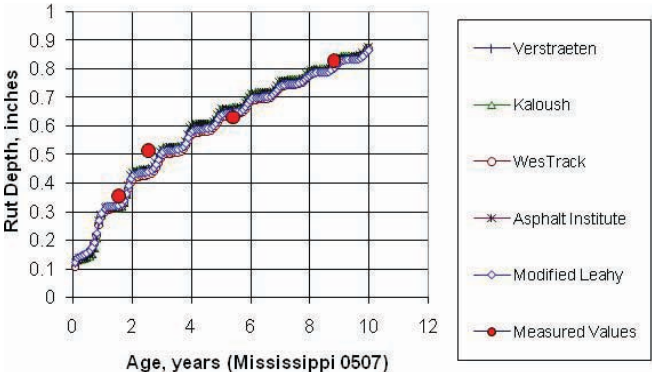

(b) Predicted rut depths for Mississippi SPS-0507, overlay of HMA pavements.

Figure 24. Field-matched plastic deformation coefficients using the different transfer functions for selected test sections in the LTPP SPS-5 and SPS-6 experiments, rehabilitated pavements.

Tables 8 and 9 include the plastic strain coefficients for each transfer function from selected sites (new construction and HMA overlay projects, respectively). The field-derived values were used to determine the relationship between the HMA volumetric properties and the plastic deformation coefficients, similar to the procedure used to determine the relationships presented in Appendix C. The development of the relationships to estimate the plastic strain coefficients from volumetric properties is discussed in Chapter 3 as part of the calibration process.

The test sections with coefficients, exponents, or both that deviated significantly from the Kaloush global values were selected for forensic investigations to determine the reason for the large difference. The forensic investigations are discussed in the next section and in Appendix J.

The other important observation from these field-derived values is that the *N*-term exponent was found to be the same among all of the transfer functions (refer to Tables 8 and 9). This observation suggests that hypotheses #8 and #10 (refer to Section 2.4.2) will be accepted after calibration and will be independent of test condition (i.e., confined versus unconfined tests). The question then is, will laboratory repeated-load tests provide the plastic deformation coefficients of the transfer functions that are directly correlated to the field-derived values? That question is addressed in Chapter 3.

2.5.3 Forensic Investigations

The plastic deformation in different pavement layers was not measured as part of the NCHRP Project 1-37A calibration process. One area of improvement would be to measure the plastic deformation in each pavement layer and subgrade so that the HMA plastic deformation coefficients of different transfer functions can be assessed. Based on the follow-up study in NCHRP Project 9-30, Von Quintus, Andrei, and Schwartz (2005) found that the total rut depth error was more affected by rutting in the unbound layers than in the HMA layers. Thus, trenches were excavated to measure the rut depths in the individual HMA layers to more clearly define the error by material or layer type.

Forensic investigations were conducted on the test sections with high levels of rutting [exceeding 0.5 in. (12.7 mm) on average] and those with large differences between the predicted and measured rut depths using the default plastic deformation coefficients. In other words, forensic investigations were conducted on projects where the predicted rut depths were believed to be outliers or to deviate significantly from the measured values. The purposes of the field investigations were to (1) measure the plastic deformation in each pavement layer and (2) determine whether a construction or material defect would explain the difference between the predicted and measured rut depths. The forensic investigations included trenches and cores for test sections where the predicted rut depths were found to be significantly less than the measured rut depth.

- Trenches were excavated to measure the amount of rutting in each paving layer and subgrade. For those sections that exhibit cracking, the trenches can also be used to determine the direction of crack propagation for use in future studies.
- Cores were recovered for measuring the volumetric and plastic deformation properties of the HMA layers after traffic or over time. The plastic deformation tests performed included the repeated-load constant-height shear test. The cores were also used to visually inspect the mixtures and identify any debonding, moisture damage, or stripping.

Field investigations were not performed on any project with very low rut depths or HMA overlays of Portland cement

Table 8. Field-derived plastic strain coefficients for selected new construction test sections.

Test Section	Intercept Coefficient					*N*-Term Exponent
	Kaloush	Asphalt Institute	Modified Leahy	Verstraeten	WesTrack	
FHWA ALF; neat, 10-2	-2.55	-6.63	-0.80	70.2	2.78	0.317
FHWA ALF; Styrelf, 7-2	-2.63	-6.60	-0.91	35.0	2.20	0.245
FHWA ALF; Novophalt 8-2	-3.00	-6.95	-1.36	10.0	0.76	0.180
California, modified, 609HB	-2.761	-6.375	-2.163	98.7	3.619	0.35
California, RHMA, 611HB	-2.20	-5.903	-1.735	155.1	13.30	0.25
Florida; modified, 1B-50	-3.03	-6.60	-0.919	42.6	0.753	0.335
Florida; neat, 5B-50	-3.32	-6.865	-0.834	57.2	0.427	0.45
WesTrack 05; coarse grading	-2.28	—	-0.45	75	3.46	0.31
WesTrack 03; fine grading	-2.53		-0.58	66	2.56	0.28
NCAT S02; SBS, PG 76-22	-2.85	-6.75	-1.39	15.0	0.38	0.35
NCAT E06; neat, PG 67-22	-3.00	-6.15	-1.68	17.5	0.482	0.45
NCAT; Florida, neat	-2.55	-6.29	-0.82	21.7	1.36	0.23
NCAT; Florida, modified	-2.55	-6.3	-0.802	10.2	1.12	0.20
NCAT; Florida, base	-2.85	-6.55	-1.25	45.0	0.85	0.275
Indiana, 7A	-0.55	-4.69	0.795	1250	65	0.29
Indiana 7B	-0.65	-4.73	0.67	1280	52.5	0.25
Indiana 8A	-0.70	-4.70	0.71	1450	50	0.255
Indiana 8B	-0.50	-4.5	1.025	1750	75	0.23
Missouri N-10, surface	-1.94	-5.71	-0.28	127	5.08	0.235
Missouri N-10, base	-2.14	-5.76	-0.30	110	4.36	0.245
Oklahoma N-9, surface	-2.85	-6.95	-1.75	10.0	0.20	.31
Oklahoma N-9, base	-2.51	-6.85	-1.45	12.0	0.80	0.36
Oklahoma N-9, rich layer	-2.25	-6.10	-0.75	42.0	0.87	0.40
MnROADs 04; AC 120/150	-2.42	—	-0.422	44.4	1.225	0.35
MnROADs 17; AC-20	-2.363	—	-0.385	48.5	0.826	0.335
Arizona SPS-0116; surface	-2.38	-6.44	-1.101	31.7	1.95	0.31
Arizona SPS-0116; binder	-2.38	-6.44	-1.101	31.7	1.95	0.31
Arizona SPS-0116; ATB	-2.18	-6.64	-0.851	24.4	2.34	0.23
Montana SPS-0116; surface	-2.08	-6.2	-0.82	54.5	3.25	0.32
Montana SPS-0116; binder	-2.08	-6.2	-0.82	54.5	3.25	0.32
Montana SPS-0116; ATB	-1.83	-5.9	-1.01	42.5	2.89	0.23
Kansas SPS-0116; surface	-2.88	-6.58	-1.19	32	0.97	0.37
Kansas SPS-0116; binder	-2.88	-6.58	-1.19	32	0.97	0.37
Kansas SPS-0116; ATB	-2.58	-6.68	-1.00	45	1.03	0.31
Wisconsin SPS-0116; surface	-1.85	-6.6	-1.534	34.3	0.85	0.25
Wisconsin SPS-0116; binder layer	-1.93	-6.01	-1.32	30.0	1.25	0.30
Wisconsin SPS-0116; ATB layer	-1.85	-6.86	-1.55	27.5	0.538	0.50

Note: Values for the plastic strain coefficients for the LTPP SPS-1 projects with multiple HMA layers were defined using a specific procedure. The sections with a wearing surface and binder layer were first determined, then those parameters were used for the test sections with an ATB layer to determine the values for the plastic strain coefficients for the asphalt-treated base (ATB) layer.

concrete (PCC) pavements. It was assumed that the plastic deformation in any unbound layer and subgrade beneath the PCC slabs would be immeasurable and that the plastic deformation in the HMA layers, unbound layers, and subgrade would also be immeasurable for test sections with less than 0.25 in. (6 mm) of total rutting measured at the surface.

The test sections where a forensic investigation was conducted are identified in Tables 4 and 5, and the details of these investigations are provided in Appendix J. Examples from the trenches and cores recovered from three of the sites are given in Figures 25 through 30. Field investigations for some full-scale roadways and test track sections included in the calibration–validation plan had already been performed. The following bullets explain the construction and material anomalies that were found from the field investigations that have an impact on the measured rut depths.

- **Construction anomalies:** Wisconsin SPS-1 project, test section 0113—The aggregate base layer was stabilized. Test sections with the asphalt-treated base layer exhibited much greater rut depths than the sections without the asphalt-stabilized base. Forensic investigation confirmed that most of the rutting occurred in the asphalt-stabilized base of the Wisconsin SPS-1 project.

Table 9. Field-derived plastic strain coefficients for selected HMA overlay test sections.

Test Section	Kaloush	Asphalt Institute	Modified Leahy	Verstraeten	WesTrack	*N*-Term Exponent
Arizona SPS-0506	-1.809	-5.85	-0.272	200	1.670	0.30
Arizona SPS-0507	-1.427	-5.75	-0.534	340	3.460	0.30
Arizona SPS-0503	-1.708	-5.73	-0.498	255	1.253	0.28
Arizona SPS-0508	-1.687	-5.79	-0.164	178	1.340	0.28
Montana SPS-0504	-2.278	—	-0.286	—	1.28	0.31
Montana SPS-0507	-2.300	—	-0.335	—	1.115	0.31
Montana SPS-0508	-2.8	-6.22	-0.63	100	1.2	0.31
Colorado, no RAP	-1.935	-5.88	-0.872	87.5	7.14	0.25
Colorado, with RAP	-1.912	—	-0.943	—	5.31	0.25
Texas SPS-0504	-2.290	—	-0.344	244	1.179	0.35
Texas SPS-0507	-2.000	-6.35	-0.459	145	1.150	0.35
Texas SPS-0503	-1.785	-5.95	-0.151	137	1.800	0.25
Texas SPS-0508	-1.651	—	-0.144	135	1.850	0.25
Mississippi SPS-0507	-3.107	-6.05	-1.640	90.2	0.169	0.55
Mississippi SPS-0504	-3.090	—	-1.676	83.8	0.609	0.55
Missouri SPS-0504	-1.582	—	-0.755	—	0.888	0.175
Missouri SPS-0507	-1.649	-6.45	-0.691	63.3	0.912	0.175
Missouri SPS-0509	-2.257	—	-0.711	—	0.832	0.23
Missouri SPS-0508	-1.705	-6.12	-0.612	95.5	1.477	0.23
Alabama SPS-0607	-2.280	-6.38	-0.332	85.0	1.091	0.29
Alabama SPS-0608	-2.530	—	-0.704	43.0	0.500	0.29
Alabama SPS-0662	-2.450	-6.17	-0.650	46.0	0.569	0.29
Alabama SPS-0663	-2.389	—	-0.750	38.0	0.400	0.29

Note: The Asphalt Institute transfer function was only used for a limited number of sections with HMA overlays because of its similarities to the modified Leahy function and large value for the temperature exponent.

Trench excavated along the LTPP Wisconsin test section 55-0113. The HMA layer was supposed to be about 5-in. in thickness. It was found to be over 14-in. in thickness. The thinner test sections had the lower rut depths without the asphalt-treated base layer.

Figure 25. Forensic investigation of the Wisconsin SPS-1 project, test section 55-0113.

Trench excavated from Wisconsin test section 55-0116. This test section had the greater measured rut depth and included the asphalt-treated base layer.

Figure 26. Forensic investigation of the Wisconsin SPS-1 project, test section 55-0116.

- **Construction anomalies:** Kansas and Iowa SPS-1 projects—For the sections exhibiting the greater rut depths, most of the rutting occurred in the aggregate base layer, which was documented during the forensic investigations of these projects. The aggregate base layer became wet from heavy rainfall during construction of selected test sections.

Figure 27. Forensic investigation of the Arizona SPS-5 project.

- **Material defects:** Arizona SPS-1, Kansas SPS-1, Mississippi SPS-5, and Texas SPS-5 projects—Stripping, moisture damage, debonding, or combinations of these were exhibited at different levels along these projects.

The MEPDG assumes that the aging function for the dynamic modulus of the HMA mixtures will correctly account for the reduction in plastic deformation over time. Many of the sections used in the initial comparisons of the predicted and measured rut depths were found to have a significant bias that was dependent on the predicted rut depth. One of the potential reasons for this difference is the aging effect on the plastic deformation coefficients of these mixtures. The testing of the specific layers where the rutting occurred can be used to evaluate that assumption and determine whether aging should be considered for the plastic deformation coefficients.

Six 6-in. diameter cores were drilled and recovered for testing using the repeated-load constant-height shear test because of its ability to test field cores with layer thicknesses of less than 4 in. Two cores were tested at the same three test temperatures for production testing, as discussed in Section 2.9.5.

Figure 28. HMA cores recovered from the Arizona SPS-5 project.

2.6 Exploratory Test Program

Participants at the facilitated workshop voiced concern regarding the use of uniaxial and triaxial tests and questioned the conditions of the test for measuring the properties of HMA mixtures in support of the rut-depth transfer functions. The debate and concerns are included in Appendix G. The key question raised and debated during the facilitated workshop was, what confining pressure, deviator stress, and temperature should be used to determine the plastic deformation coefficients? Previous laboratory studies have been conducted to quantify the effect of stress state (confining pressure and deviator stress) and temperature on plastic deformation. The major gap is relating laboratory-derived values to conditions that exist along the roadway.

Two studies were initiated prior to the production test program: (1) an instrumentation study for HMA testing and characterization to identify specimen preparation and measurement issues in measuring HMA plastic deformation properties, and (2) an exploratory test program for defining test conditions. These are discussed in the following sections.

2.6.1 Instrumentation Study

The Simple Performance Test System (SPT, now termed the Asphalt Mixture Performance Tester, AMPT) developed under NCHRP Project 9-29 was proposed for use to measure the dynamic modulus and plastic deformation data for verifying or recalibrating the MEPDG HMA rut-depth transfer function and other similar models. The NCHRP Project 9-30A panel requested data supporting the use of the SPT prior to starting the production test program. In addition, the NCHRP Project 9-30A panel requested recommendations on the instrumentation to be used in collecting uniaxial and triaxial compression data.

Left: Trench excavated within section 48-0507 (virgin mixture)

Right: trench excavated within section 48-0508 (RAP mixture)

Figure 29. Forensic investigation of the Texas SPS-5 project.

Advanced Asphalt Technologies, LLC (AAT) was the prime contractor for NCHRP Project 9-29 and was a subcontractor on NCHRP Project 9-30A. As such, AAT directed the effort for preparing the report and proposals in response to NCHRP's request. Appendix I of this report documents the results from the instrumentation study for improving on the measurement of HMA mixture responses that are needed for characterizing or determining the HMA properties for predicting rut depths over time. This section of the research report provides a summary of the findings included in Appendix I.

The key finding from the plastic deformation experiment was that spring-loaded linear voltage displacement transducers (LVDTs) cannot be used with specimen-mounted instrumentation for plastic deformation testing. At the high temperatures used in plastic deformation testing, the spring force causes significant creep of the gauge points and substantial error in the resulting plastic strain measurements. Miniature, loose-core LVDTs must be used to make these measurements. The following summarizes the recommendations from the instrumentation study.

1. The 70-mm gauge length used in the SPT for dynamic modulus testing is acceptable for use in NCHRP Project 9-30A. A paired *t*-test analysis of dynamic modulus and phase angle data found no significant difference between

Left: Cores recovered from test section 48-A0507 (virgin mixture)

Below: Cores that show stripping and moisture damage in localized areas in the existing HMA layer

Figure 30. HMA cores recovered from the Texas SPS-5 project.

data collected using gauge lengths of 70 mm and 100 mm. The difference in quality between the 70-mm and 100-mm gauge length data was insignificant.

2. The plastic strains obtained from the actuator displacement were generally greater than those obtained with a 100-mm gauge length. The actuator displacement, however, is recommended for use in NCHRP Project 9-30A. The paired *t*-test analysis of the plastic strain curves found significant differences, but a similar analysis assuming independent tests did not. The use of the actuator displacement to collect plastic strain data results in a substantially simpler instrumentation system and has similar precision to the specimen-mounted system. If specimen-mounted instrumentation is used, it must incorporate lightweight, loose-core LVDTs, which are very difficult to properly position on the test specimen, particularly in confined tests, which was considered potentially important for the production test program for NCHRP Project 9-30A. The actuator displacement is clearly able to detect differences in the plastic strain response of different mixtures and has the potential to make the RLPD test a routine test for agency laboratories.
3. The differences found in this study appear to be the result of the non-uniform distribution of air voids in gyratory-compacted specimens, not the instrumentation. Further refinement of the test specimen preparation procedures is needed to minimize air void gradients and to eliminate areas of relatively high air voids that might be present at the ends of the test specimens.

Recommendations #2 and #3 had a significant impact on the NCHRP Project 9-30A test plan—specifically, the need to use a rolling wheel compactor for preparing the test specimens and to better define the laboratory test conditions. Specimen preparation for some of the laboratory tests and test conditions is defined in Section 2.8.4.

2.6.2 Stress State for Plastic Deformation Testing

An important point in evaluating HMA mixtures in the laboratory is to use realistic stress states for measuring the pertinent engineering properties. Historically, most HMA properties are determined from measurements made in the low stress range. This is adequate if only relative comparisons of different HMA mixtures are made. For mixture evaluation and predicting distress, however, relative comparisons can be inadequate. Thus, a question is, are the stress states that have

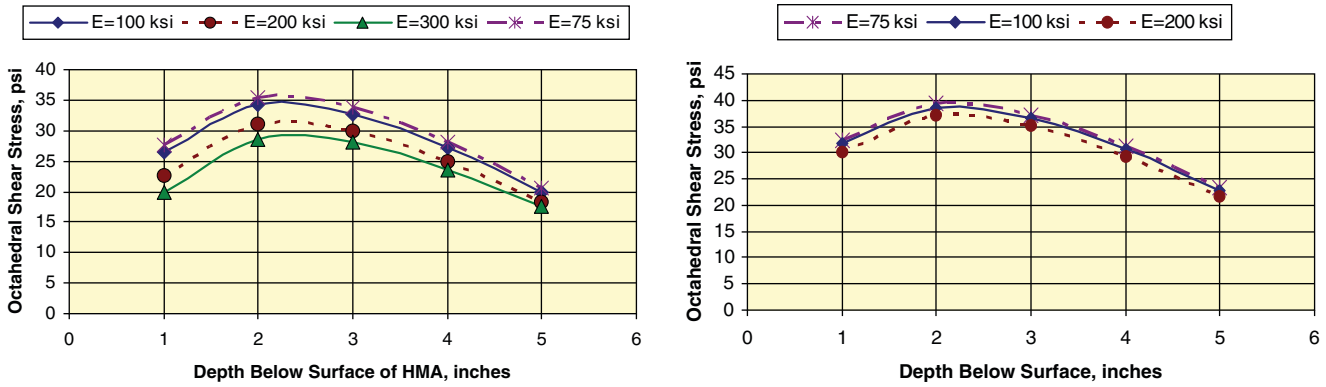

(a) HMA overlay of flexible pavement.

(b) HMA overlay of rigid pavement.

Figure 31. Octahedral shear stress through an HMA 6-in. overlay.

been used in the laboratory close to those that occur on the roadway under trucks and environmental loads? Stress state depends on tire pressure, tire type, axle load, temperature, layer thicknesses, pavement type, and so on.

To estimate the roadway conditions to be simulated in the laboratory and to be consistent with the structural evaluation procedures, elastic layer theory or other response models can be used to calculate the stresses and strains in an HMA layer under different loading, environmental, and structural conditions. Of course, all assumptions used with elastic layer theory apply to these recommendations, and the normal and principal stresses calculated on an element in an HMA layer will not necessarily be the same as those in a triaxial test specimen. Thus, it has been recommended that the octahedral shear stress theory (distortion energy theory) be used to calculate the confining stress and vertical stress in the laboratory test specimen to result in an equivalent maximum octahedral shear stress calculated in the HMA layer itself. The octahedral shear stress is given by:

$$\tau_{OCT} = \frac{1}{3}\left[(\sigma_1 - \sigma_2)^2 + (\sigma_2 - \sigma_3)^2 + (\sigma_3 - \sigma_1)^2\right]^{0.5} \qquad (14)$$

The octahedral shear stress at failure represents the critical shearing stress at yielding or disorientation. For an analysis of stress, elastic layer theory has been used to calculate the normal and principal stresses that exist in an element in the HMA layer for determining the appropriate laboratory loading conditions. This allows factors such as contact pressures, tire types, and total loads to be considered in the laboratory during mixture design and analysis to ensure that the HMA mixture can sustain the imposed stresses. The stress predicted using the octahedral shear stress theory is used in triaxial compression tests.

Figures 31 and 32 illustrate some examples of the change in the octahedral shear stress throughout the depth of the HMA overlay and throughout an HMA layer of a flexible pavement. The HMA overlay thickness used in this example is 6 in.

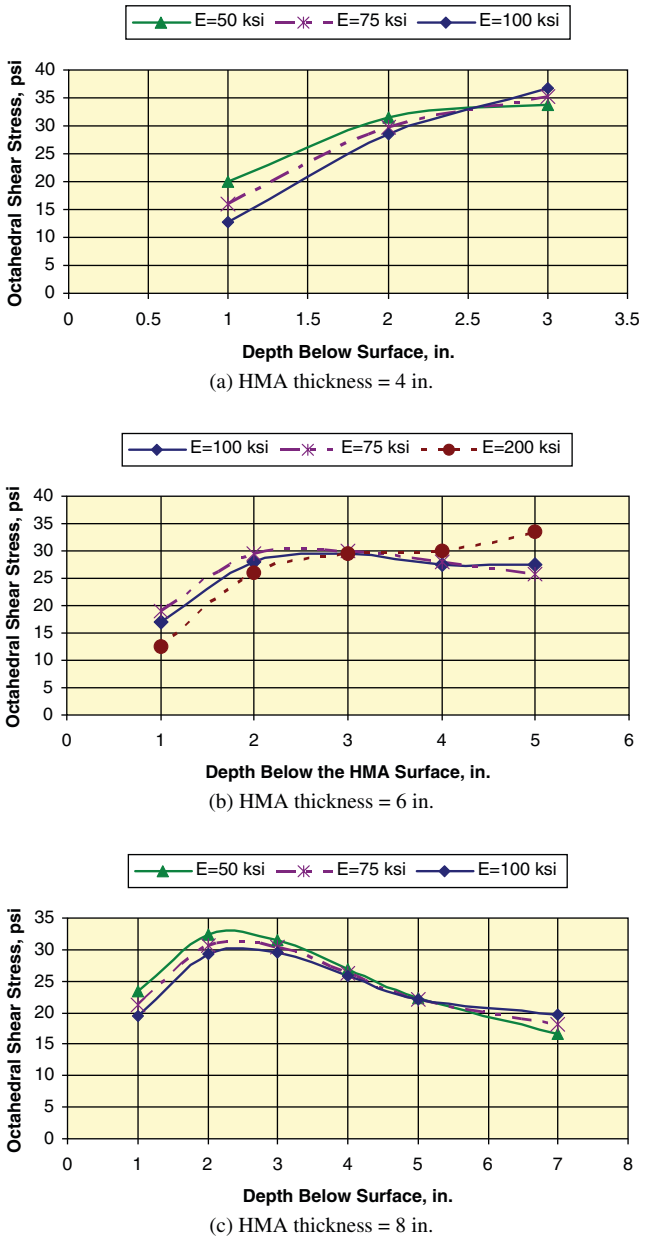

(a) HMA thickness = 4 in.

(b) HMA thickness = 6 in.

(c) HMA thickness = 8 in.

Figure 32. Octahedral shear stress through an HMA layer; flexible pavement with aggregate base layer.

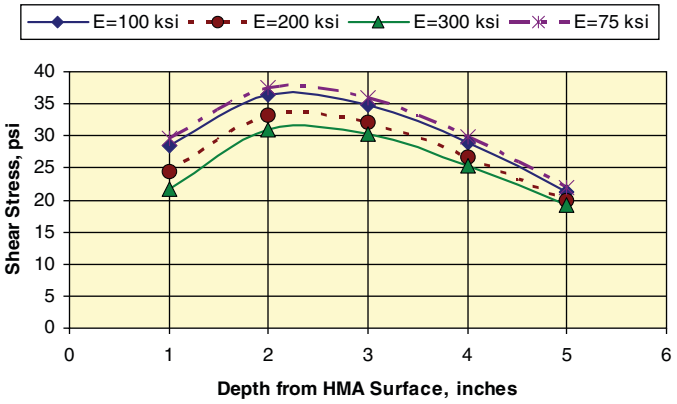

(a) HMA overlay of flexible pavement.

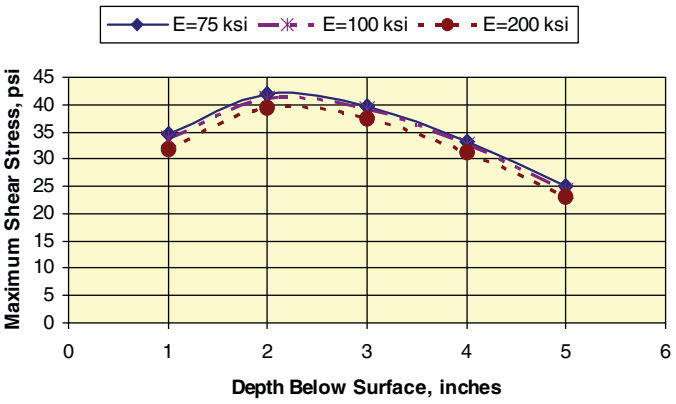

(b) HMA overlay of flexible pavement.

Figure 33. Maximum shear stress through an HMA 6-in. overlay.

for the existing flexible and PCC pavements. Figures 33 and 34 were also prepared for the maximum shear stress in the HMA overlay and new HMA layer. All of these example computations assumed full friction between each of the paving layers and used an 18-kip single-axle load with tire pressures of 120 psi.

The maximum octahedral shear stress generally occurs under the wheel load at a depth of 2 in. to 4 in. below the surface, while the maximum shear stress occurs near the outside edge of the tire nearer the surface to values within the inside edge of the tire at depths of 2 in. to 4 in. below the surface. As reported by many others, the lateral and vertical stresses computed with elastic layer theory vary with structure, depth, and radius from the center of the wheel loads. The following lists the octahedral shear stresses for different deviator stresses used in laboratory repeated-load tests.

Deviator stress, psi	20	40	60	80	100
Octahedral stress, psi	28.3	56.6	84.9	113.1	141.4

An exploratory test program was implemented to determine the range of confining pressures and vertical stresses that should be used in the laboratory test program using compression-type tests.

2.6.3 Temperature for Plastic Deformation Testing

As noted in Section 2.2.1, two types of transfer functions were programmed in the MEPDG Version 9-30A: (1) those with temperature included as a dependent variable (Kaloush, Asphalt Institute, and NCHRP Project 1-40B) and (2) those without temperature (modified Leahy, Verstraeten, and WesTrack). For the transfer functions that exclude temperature, it is assumed that the variation in dynamic modulus with temperature accurately accounts for the accumulation of plastic strain.

The HMA mixtures are tested at the equivalent annual temperature for determining the plastic deformation coefficients. It was initially envisioned that the test program could be reduced to one temperature per mixture and that test temperature would be defined by Equation 15 or a similar procedure, via the effective pavement temperature (T_{Eff}) at a 50% reliability level (Monismith et al., 1994).

$$T_{Eff}\left(RutDepth\right) = 30.8 - 0.12\left(D_{cr}\right) + 0.92\left(MAAT_{Design}\right) \qquad (15)$$

where

D_{cr} = critical depth from pavement surface, mm.
$MAAT_{Design}$ = mean annual air temperature, °C.

$$MAAT_{Design} = MAAT_{Avg} + K_{\alpha}\left(\sigma_{MAAT}\right) \qquad (16)$$

where

$MAAT_{Avg}$ = mean annual air temperature, °C.
K_{α} = value at the designated reliability level.
σ_{MAAT} = standard deviation of distribution of MAAT for site location from LTPPBind.

Different locations were used to evaluate the applicability and use of the effective pavement temperature concept with the MEPDG computational methodology. The four locations were the Montana SPS-1 site, the Arizona SPS-5 site, the Alabama SPS-6 site, and the Wisconsin SPS-1 site. The effective pavement temperatures for these sites were determined in accordance with Equation 15 and are listed in Exhibit B.

The Kaloush, modified Leahy, and WesTrack transfer functions were used to compute the HMA rut depths over time for these sites using the actual climate data and effective pavement temperatures listed in Exhibit B. Figures 35 through 37 compare the predicted rut depths using the actual climate data and effective temperatures. As shown, use of the effective temperature overpredicts the rut depth using the Kaloush and modified Leahy transfer functions (refer to Figures 35 and 36). Use of the effective temperatures for the WesTrack transfer function more closely esti-

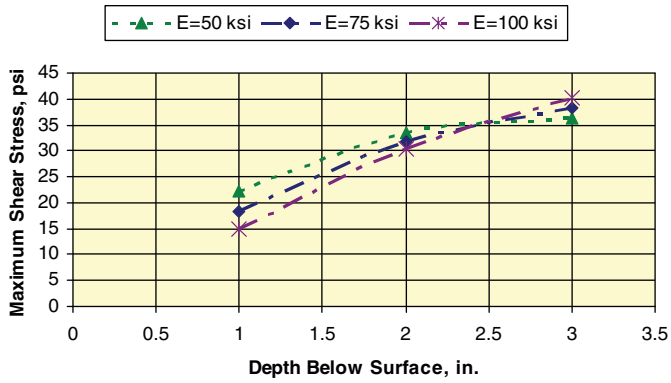

(a) HMA surface thickness = 4 in.

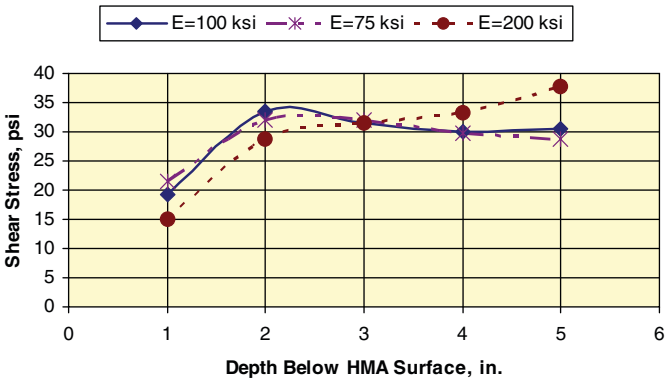

(b) HMA surface thickness = 6 in.

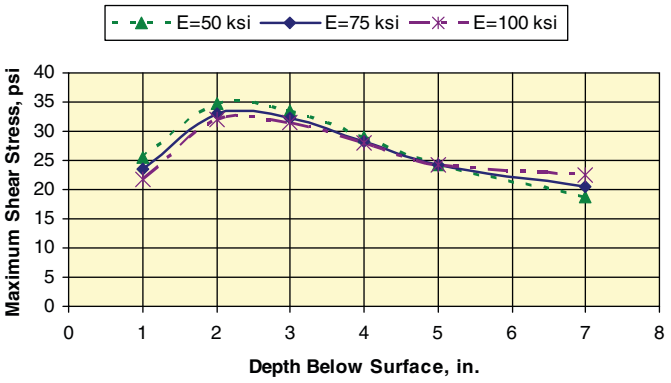

(c) HMA surface thickness = 8 in.

Figure 34. Maximum shear stress through an HMA layer; flexible pavement with an aggregate base layer.

Exhibit B

Site	Effective or Equivalent Annual Temperature, °C			
	Equation 15	MEPDG		
		Kaloush	WesTrack	Modified Leahy
Arizona SPS-5	44.9	42.0	45.8	42.6
Alabama SPS -6	38.7	28.3	41.2	34.6
Montana SPS-1	30.5	24.3	27.0	25.1
Wisconsin SPS-1	28.6	28.1	35.0	20.5

mates the predicted rut depth for the actual climate data (refer to Figure 37).

The equivalent annual temperature is defined as the constant temperature entered in the MEPDG that results in the same amount of rut depth as for the actual climate data. The equivalent annual temperatures were determined for the same four sites listed previously. Figure 38 compares the effective pavement and equivalent annual temperature determined through the MEPDG for multiple sites included in Tables 4 and 5. As shown, there can be a difference between the two temperatures used to characterize the HMA mixtures and predict total rut depth. In summary, the equivalent annual temperature for determining the plastic deformation coefficients for the transfer functions needs to be determined through the MEPDG to reduce bias and the standard error. The use of Equation 15 will increase the standard error and may also result in a bias for some of the transfer functions.

2.6.4 Exploratory Test Program: Defining Test Conditions

Stress state or deviator stress is important and does affect the rutting of HMA mixtures. Selected HMA mixtures can also be stress sensitive under some higher temperature conditions. The objective of the exploratory RLPD test program was to provide a consistent evaluation of the effects of temperature and stress state (deviator and confining stress) on HMA plastic deformation. These results provide fundamental insights into HMA mixture response to temperature and stress state variables and for defining test conditions for the broader set of mixtures included in the production test program. The results also provide some guidance for proposing enhancements to the MEPDG rut-depth transfer functions and prediction model.

2.6.4.1 Hypotheses for Exploratory Test Program

The following lists the hypotheses for the plastic deformation law using procedures based on elastic layer theory and laboratory repeated-load uniaxial or triaxial testing to measure critical mixture properties (plastic deformation coefficients: slope and intercept in the steady-state or secondary region of the plastic deformation relationship), similar to the Kaloush rut-depth transfer function. These hypotheses and assumptions were used to develop the mixture adjustment factors under NCHRP Project 1-40B (Von Quintus, 2006) and to develop the exploratory experimental test program.

1. The total plastic strain increases with increasing deviator stress (or wheel load) and decreases with increasing confining pressure. In other words, as the confining pressure increases and the repeated vertical stress remains the same,

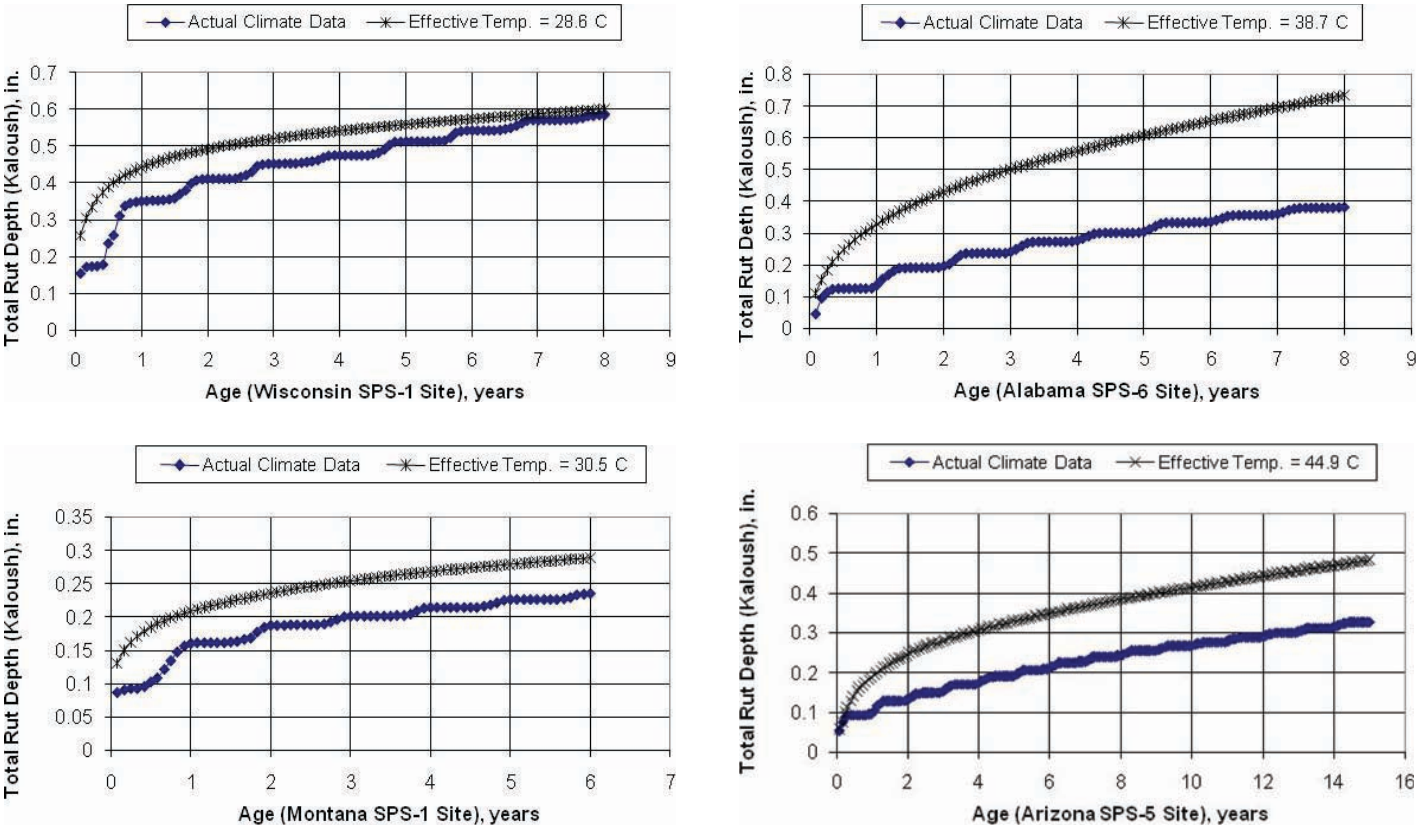

Figure 35. Comparison of predicted total rut depths based on actual climate data and effective pavement temperature using the Kaloush transfer function.

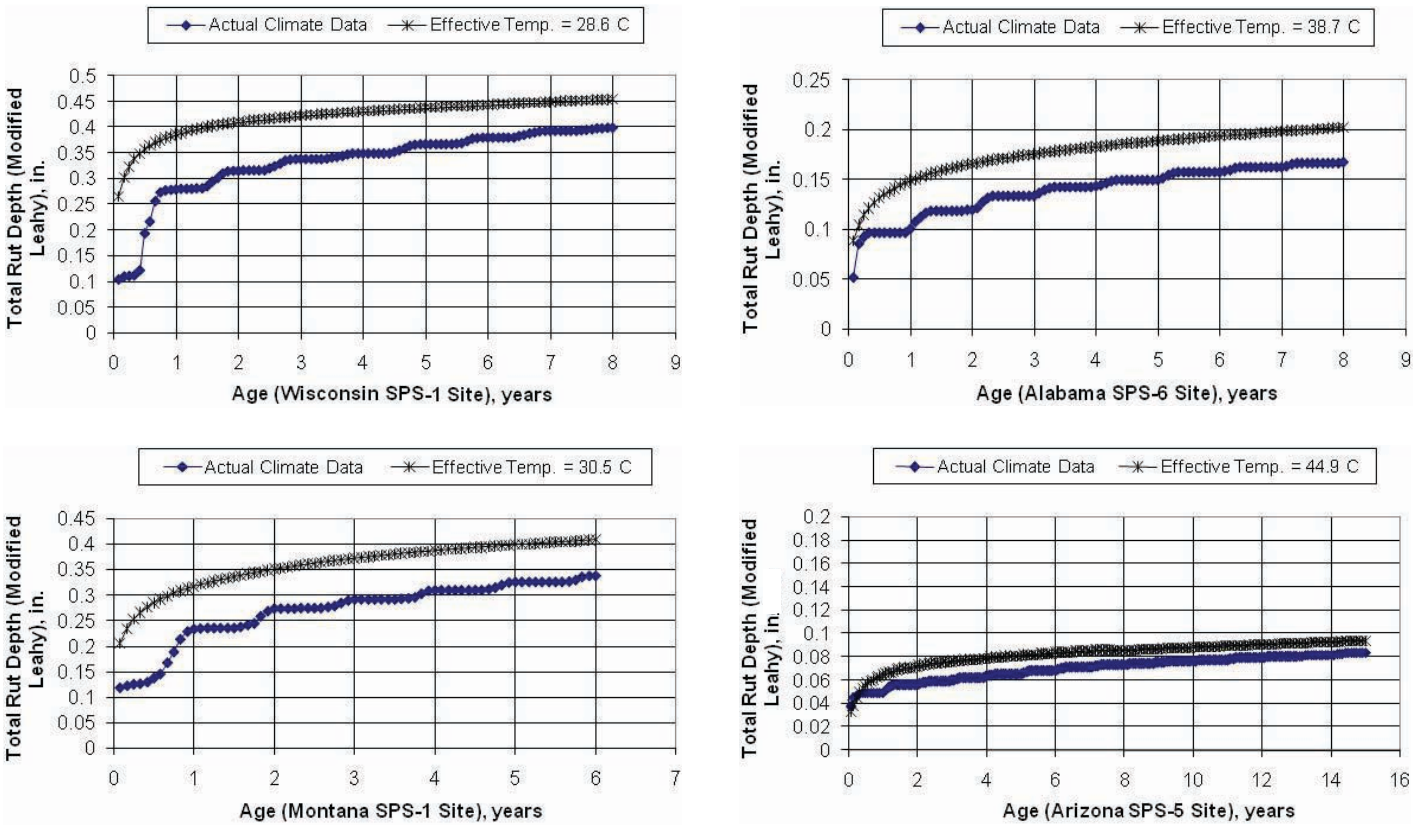

Figure 36. Comparison of predicted total rut depths based on actual climate data and effective pavement temperature using the modified Leahy transfer function.

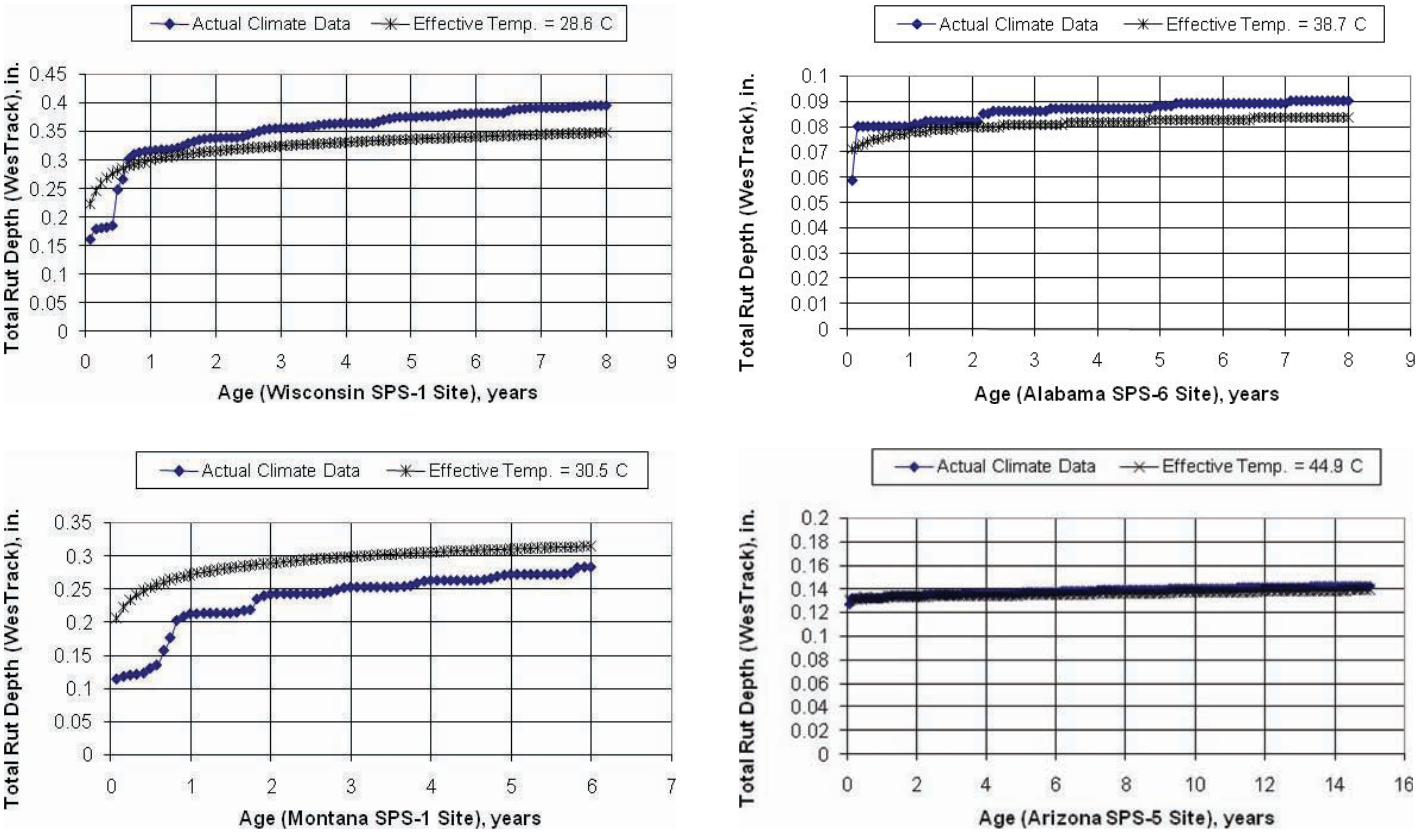

Figure 37. Comparison of predicted total rut depths based on actual climate data and effective pavement temperature using the WesTrack transfer function.

the plastic deformation decreases per load application for repeated-load triaxial tests. The effects of confining pressure and deviator stress are temperature dependent—the higher the temperature, the greater the effects of confining pressure and deviator stress. It is hypothesized that temperature is the more important parameter in determining the plastic deformation coefficients for HMA mixtures.

2. For dense, well-graded HMA mixtures, deviator stress has little effect on the resilient and dynamic modulus. However, as the confining pressure increases, the resilient and dynamic modulus of gap-graded or more open-graded HMA mixtures will increase above some temperature. (For most mixtures this high temperature is 70°F to 100°F.)
3. For dense-graded HMA mixtures, the total plastic strain versus temperature relationship is inversely proportional to the dynamic modulus versus temperature relationship. Thus, the modulus–temperature relationship can be used to estimate the plastic-strain–temperature relationship, decreasing

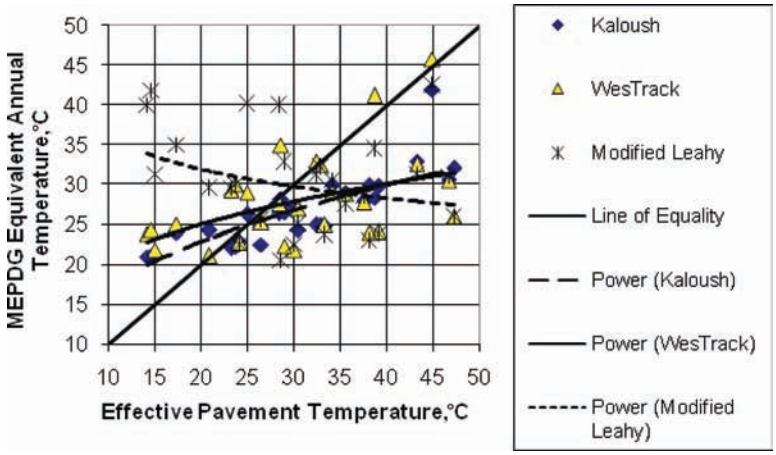

Figure 38. Comparison of effective pavement and equivalent annual temperatures.

Table 10. Test matrix for the exploratory repeated-load plastic deformation test program.

Deviator Stress, psi	Confining Pressure, psi								
	0 psi, Unconfined			10-psi Confinement			20-psi Confinement		
	Test Temperature, °F								
	100	120	140	100	120	140	100	120	140
30					X				
50		X		X	X	X		X	
70					X				

the number of test temperatures that need to be used in the laboratory for mixture characterization purposes.

4. The slope and intercept are determined within the steady-state region of the test. As temperature increases, the total plastic deformation increases. At temperatures above about 70°F, the slope decreases with increasing temperature, but the intercept increases when plotting the results from a repeated-load plastic deformation test.

2.6.4.2 Experimental Test Program and Materials Included in Exploratory Test Program

Table 10 summarizes the systematic partial factorial variations of temperature and confining and deviator stress, with three different scenarios for each parameter. Five replicates were tested for each combination of temperature and stress state. Some additional test specimens were prepared and tested for those cells where the specimens failed early or had unique characteristics. The additional tests were used for confirmation and did not change any of the conclusions or results.

One ALF mixture was selected for the exploratory study to define the testing conditions for the production test program, the control mix with the unmodified PG 70-22 binder. This HMA mixture has the advantage of being well characterized in the laboratory. In addition, comprehensive sets of performance data are available from the ALF field testing. Results of the exploratory testing program augment the existing set of test results for this mixture from FHWA (Stuart and Mogawer, 2002; FHWA, 2004).

Table 11 summarizes the binder properties for the PG 70-22. Table 12 summarizes the aggregate properties for this

Table 11. Asphalt binder properties.

Binder Type	PG 70-22	Air Blown	SBS LG	CR-TB	Ter-Polymer	SBS 64-40
Lane	1-bottom, 2 and 8	3 and 10	4 and 11	5	6 and 12	9
Asphalt PG	70-22	70-28	70-28	76-28	70-28	70-34
Continuous PG	72-23	74-28	71-29	79-28	74-31	71-38
Original Binder						
Temp. when G*/sinδ = 1.00 kPa	73.4	75.5	72.4	79.5	78.0	71.7
Temp. when MVR = 50 c^3 at 10 min	73.6	74.8	77.2	80.6	81.2	77.0
Rolling Thin Film Oven Residue						
Temp. when G*/sinδ = 2.2 kPa	72.9	74.1	71.6	81.4	74.5	71.8
Pressure Aging Vessel Residue						
Temp. when G*(sinδ) = 5000 kPa	26.0	22.6	18.1	17.9	14.3	8.6
Temp. when S at 60 s = 0.30 (+10°C)	-23.6	-28.9	-30.6	-32.9	-31.3	-38.5
Temp. when m at 60 s = 0.30 (+10°C)	-23.5	-28.3	-29.8	-27.6	-34.1	-39.5
Critical cracking temp. using BBR and DT	-21.9	-26.8	-28.9	-31.6	-33.1	-41.0
Cracking temp. using BBR alone	-22.1	-27.1	-33.7	-32.9	-31.1	-36.0

Note: The asphalt binder properties are provided for the other binders used in the FHWA ALF experiment for comparison to the PG 70-22.
G* = Complex shear modulus
δ = Phase angle
MVR = Material volumetric-flow rate
S = Creep stiffness
m = Creep slope

Table 12. Aggregate properties.

Aggregate Property		Value
Gradation, sieve size (mm); percent passing	19.0	100
	12.5	93.6
	9.5	84.6
	6.3	—
	4.75	56.7
	2.36	34.9
	2.00	—
	1.18	24.8
	0.600	18.2
	0.425	—
	0.300	13.1
	0.150	9.3
	0.075	6.7
Bulk dry SG		2.947
Bulk SSD SG		2.952
Apparent		3.001
Water abs., %		0.6

mixture, and Table 13 identifies the sources of the aggregates used in the mixture. Figure 39 shows the gradation for this 12.5-mm mixture used in the exploratory RLPD test program. Table 14 includes the job mix formula for the mixture, while Table 15 provides the mixture design properties.

2.6.4.3 Effect of Confinement

Figure 40 summarizes the influences of confining stress on the plastic strain after 1,000 and 2,000 load cycles at a deviator stress of 50 psi and a temperature of 120°F. Higher loading cycles were not included in Figure 40 because tertiary flow occurred at around 2,000 cycles without confinement. At 10 psi all of the test specimens continued throughout the 10,000 loading cycles, while most of the unconfined tests were stopped shortly after 2,000 loading cycles. These test results clearly indicate that a small confining pressure of 10 psi substantially reduces the plastic strains throughout the test program. Increasing the confining pressure to 20 psi only caused a slight additional reduction in plastic strains.

Similar results were observed during the testing completed within the cost allocation project sponsored by FHWA and the AAMAS study sponsored by NCHRP (Rauhut, Lytton, and Darter, 1984 and Von Quintus et al., 1991). In fact, the testing completed with the cost allocation project suggested that 5 psi confinement was sufficient to measure the plastic deformation properties of HMA mixtures using repeated-load triaxial tests.

Figure 41 shows the influence of confinement on the average slope of those test specimens that continued throughout the total number of loading cycles. As shown, the slope of the plastic strain relationship between the different decades of loading cycles was substantially lower for both confining pressures at the higher number of loading cycles. At the lower number of loading cycles, the slopes were within the same range. As the number of loading cycles increased, the slope continued to decrease with confinement, while it consistently increased for the case without confinement.

The experimental plan did not address the question of determining the threshold confinement at which plastic strains are substantially reduced. Based on the testing completed within the AAMAS study and the FHWA cost allocation study completed in the 1980s, confining pressures of 5 psi and greater substantially reduce the plastic strains and deformations in HMA mixtures (Rauhut, Lytton, and Darter, 1984 and Von Quintus et al., 1991). Thus, these test results suggest that production tests be run with confinement to eliminate premature tertiary flow. A confining pressure of 10 psi was the value recommended for the production test program.

2.6.4.4 Effect of Deviator Stress

The plastic strain relationship or transfer function in the MEPDG (refer to Equation 1) implicitly assumes a linear relationship between plastic strain and deviator stress for a given pavement structure. Figure 42 summarizes the influence of deviator stress on the plastic strain at a confining pressure of 10 psi and a temperature of 120°F. These results suggest that linearity is only roughly approximated at the lower number of loading cycles. The higher the number of loading cycles, the more nonlinear the relationship becomes. A power law trend line of the form shown in Equation 17 can be fit to each of the curves between deviator stress and total plastic strain

Table 13. Aggregate sources.

FHWA Material Control Number	Material Designation	Source	Sample Size
B-6262	No. 10 diabase screening with hydrated lime	Loudoun Quarry; Herndon, VA	10 tons
B -6263	Grade F and G diabase (sand size)	Luck Stone; Leesburg, VA	10 tons
B-6264	No. 78 diabase	Loudoun Quarry; Herndon, VA	10 tons
B-6265	No. 68 diabase	Loudoun Quarry; Herndon, VA	10 tons

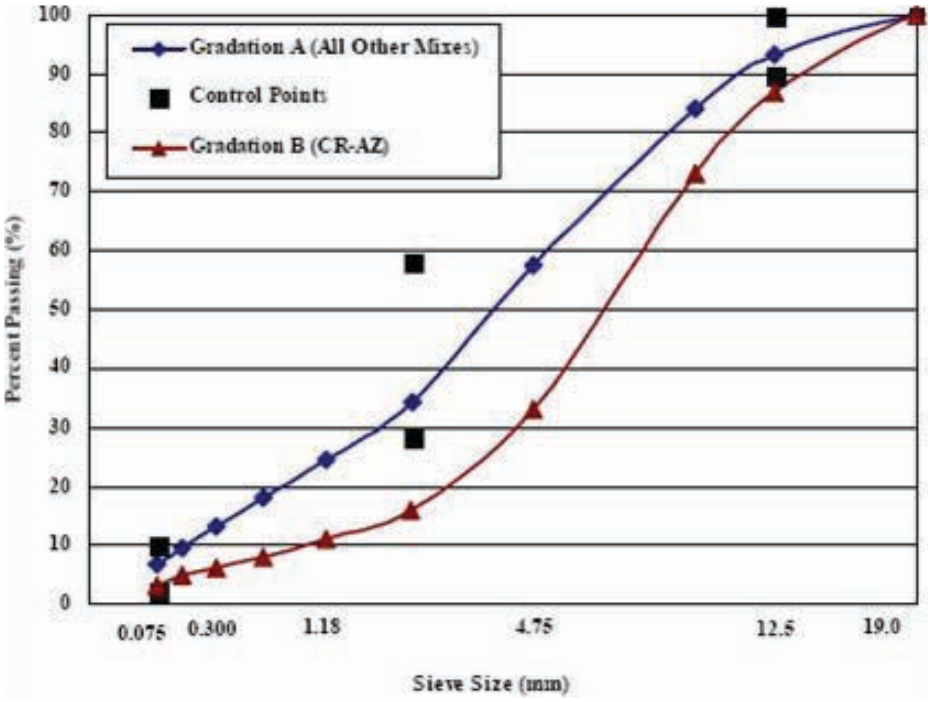

Figure 39. Aggregate gradations.

Table 14. HMA job mix formula.

Binder content (% total weight)	5
Air voids (%)	7
Aggregate composition (%)	
No. 68 (FHWA 6265)	16.5
No. 78 (FHWA 6264)	36.5
Grade F and G (FHWA 6263)	27
No. 10 (FHWA 6262)	20

Table 15. HMA mixture design properties.

Asphalt binder type	PG 70-22
Lane	1 (bottom), 2, and 8
Total binder content, % by mass	5.3
Effective binder content, % by mass	5.0
Asphalt binder absorption, % by mass	0.3
Effective binder content, % by total volume	12.5
Dust, % passing the #200 (75-µm) sieve	6.3
Dust to effective binder content	1.26
Design air voids, %	5.0
Void in mineral aggregate at design air voids, %	17.5
Voids filled with asphalt at design air voids, %	71.2
Specific gravity of binder	1.030
Maximum specific gravity	2.704
Effective specific gravity of aggregate	2.975
Bulk dry specific gravity of aggregate	2.947

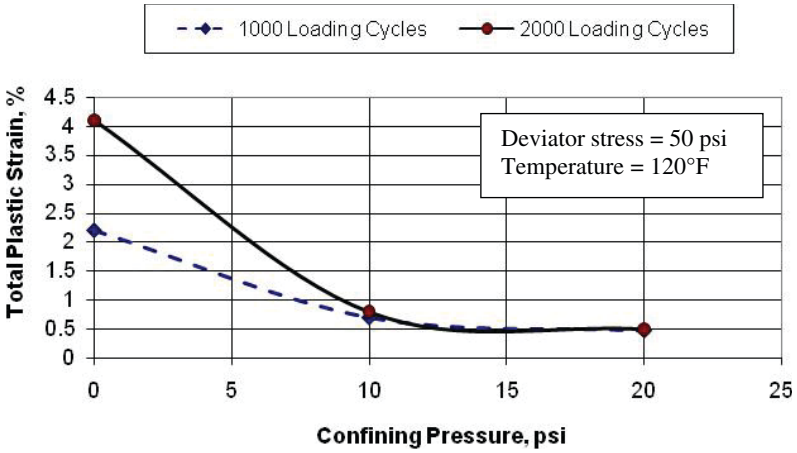

Figure 40. Influence of confining pressure on total plastic strain.

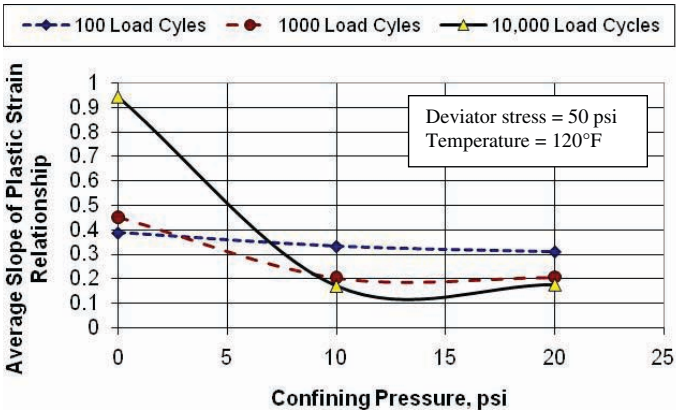

Figure 41. Influence of confining pressure on slope of steady-state or secondary region from repeated-load triaxial tests.

to quantify the degree of linearity. The *c* and *m*-values are summarized in Table 16.

$$\varepsilon_p = c(\sigma_d)^m \quad (17)$$

where

σ_d = deviator stress, psi.

c, m = regression constants between deviator stress and plastic strain.

A value for *m* equal to 1.0 corresponds to linear proportionality between plastic strain and deviator stress. The computed values for *m* range from about 1.2 to 1.5, indicating some stress nonlinearity. This nonlinearity was also found in the AAMAS and cost allocation studies (Von Quintus et al., 1991; Rauhut, Lytton, and Darter, 1984).

More importantly, the slope of the plastic strain relationship also appears to be influenced by deviator stress level at the higher number of loading cycles. For the lower number of loading cycles, the average slopes were approximately equal

Table 16. Power law deviator stress trend line coefficients (refer to Equation 17) from the exploratory test data.

N	*C*	*m*
1000	5.87E-05	1.23
2000	5.15E-05	1.30
5000	4.36E-05	1.39
10000	3.25E-05	1.50

for the different deviator stresses. Figure 43 summarizes the influence of deviator stress on the slope of the plastic strain relationship at the same conditions as from Figure 42 within different decades of loading cycles. As shown, the average slope of the plastic strain relationship begins to increase at an increasing rate with increasing deviator stress. Inclusion of this effect into the MEPDG HMA rutting model should be considered.

The use of nonlinearity has been recommended for consideration in rut-depth prediction models (Monismith and Wallace, 1982). This suggestion, however, has largely been ignored in most test programs but is grounded in reality. The key question is, does nonlinearity have a significant effect or impact on the plastic deformation coefficients of the different transfer functions? This question is addressed later in this chapter and in Chapter 3.

The data summarized in Figures 42 and 43 do not indicate a clear choice for the deviator stress to be used for production RLPD testing. At the low 30-psi deviator stress, the maximum plastic strains were all low and the average slopes continued to decrease with increasing load cycles. At a 50-psi deviator stress, no significant differences of the slopes were noted in comparison to the 30-psi deviator stress. At the higher deviator stress value with confinement, however, the slopes started to increase for the higher number of load cycles. The 70-psi deviator stress was selected as the most appropriate level for

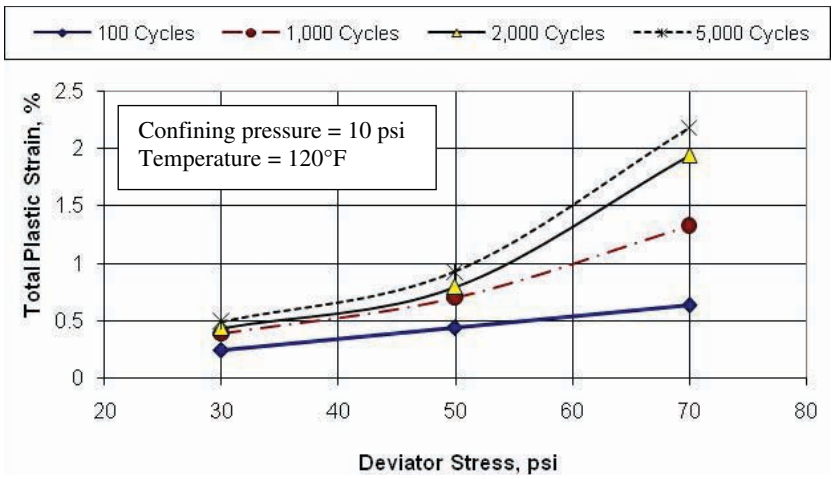

Figure 42. Influence of deviator stress on total plastic strain.

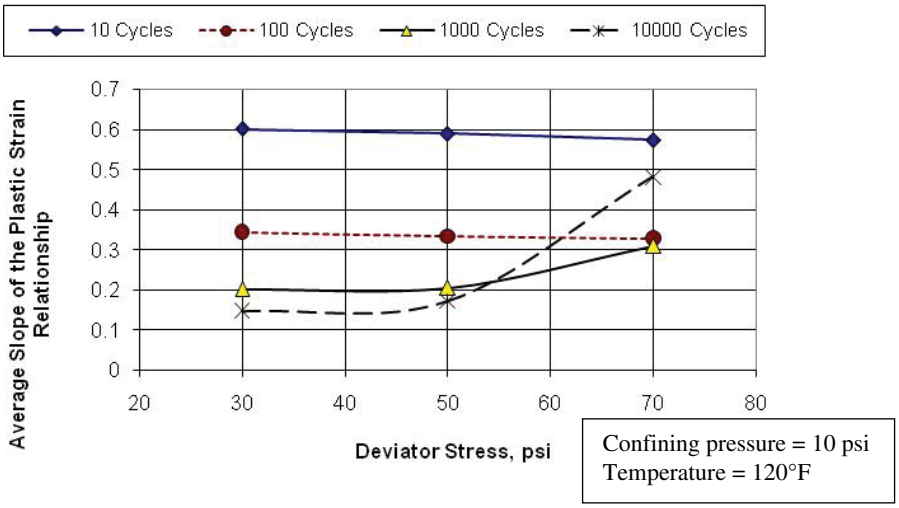

Figure 43. Influence of deviator stress on slope of steady-state or secondary region from repeated-load triaxial tests.

production testing because of the higher vertical or normal stress near the pavement surface. The higher level of deviator stress will likely better discriminate between mixtures with different strengths.

2.6.4.5 Effect of Temperature

Figure 44 summarizes the influence of temperature on plastic strain at a confining pressure of 10 psi and a deviator stress of 50 psi. There is one anomalous trend in the data in Figure 44, in particular for the high cycle results at 100°F. Examination of the individual replicates at 100°F indicates that some specimens began to enter tertiary flow at the end of the test and therefore had high plastic strain values at large values for loading cycles. The specimens tested at 100°F exhibited more of a tendency to reach tertiary flow than did the specimens tested at 120°F. The specimens at the highest temperature of 140°F exhibited the lowest tendency to reach tertiary flow. This observation, however, is not unique and is not considered to be an anomaly. Similar observations have been noted from testing many different mixtures, including the VESYS preliminary work in explaining alpha and gnu (refer to Section 2.7.1), the FHWA cost allocation project, and the NCHRP AAMAS study.

Tertiary flow or accelerated plastic strains with continued loading cycles within a repeated-load triaxial test are used to define the flow number and are supposed to represent the flow related to distortion. The tertiary flow or the sudden increase in measured plastic vertical deformation, however, is not from traditional distortion but from internal damage

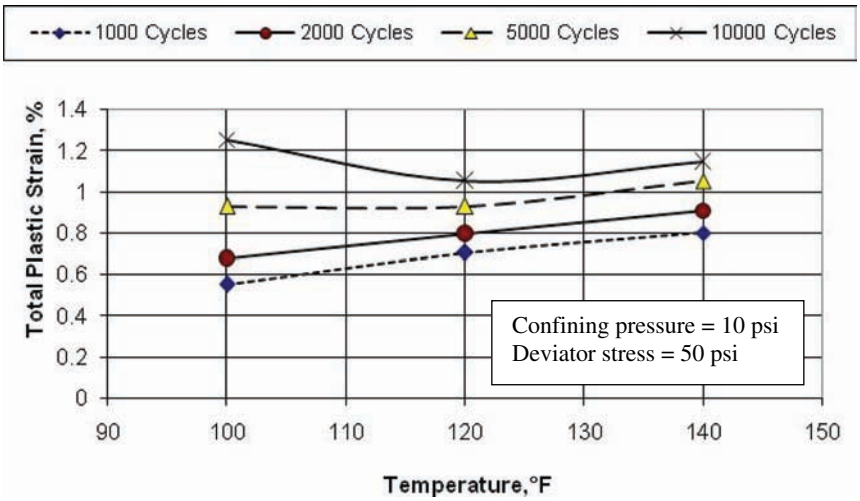

Figure 44. Influence of temperature on total plastic strain.

that occurs in the test specimen at lower temperatures and higher stiffness values, in comparison to higher temperatures and lower stiffness values.

The damage is related to the development of micro-cracks in the triaxial test specimen that can result in bulging of the test specimen (increase in the diameter). This condition was first observed during the VESYS laboratory work in the mid to late 1970s. The repeated-load triaxial tests were taken to 100,000 load cycles with tertiary flow occurring at some of the lower test temperatures and not being observed at higher test temperatures. This becomes a critical issue with repeated-load triaxial tests in terms of data analysis for all of the traditional rut-depth transfer functions. The key point is to recognize the existence of this effect. In the AAMAS procedure, this point was estimated from the vertical strain at which failure occurs from a confined or unconfined compressive strength test. This point is more related to distortion damage rather than the pure definition of rutting.

Healing or elastic recovery is another important property of the HMA mixtures that can lead to differences between field and laboratory test results because temperatures along the roadway are not constant as they are in the laboratory. ARC is investigating the effect of healing on both distortion and fracture as related to aging differential in the asphalt binder. (Products and software being developed by the Asphalt Research Consortium under sponsorship by the FHWA; products and software have yet to be released but have been presented at various FHWA Expert Task Group meetings of the Asphalt Fundamental Properties and Advanced Modeling, 2009 through 2011.)

Considering only the curves at 1,000 and 2,000 loading cycles in Figure 44, the overall temperature dependence can be quantified by power law trend lines in accordance with Equation 18. The trend line values for d and n are summarized in Table 17. The value for d is around 1.0, which is substantially less than the temperature exponent value of 1.5606 in the globally calibrated Version 1.0 of the MEPDG. In other words, the results in Figure 44 suggest that the MEPDG may overstate the sensitivity of HMA rutting to temperature. This observation was a reason why temperature was excluded from the modified Leahy transfer function.

$$\varepsilon_p = d(T)^n \tag{18}$$

Table 17. Power law temperature trend line coefficients (refer to Equation 18) from the exploratory test data.

N	*d*	*n*
1,000	3.36E-05	1.11
2,000	1.32E-05	0.857
5,000*	1.71E-05	0.363

*Probably unreliable because of tertiary flow.

On the other hand, Figure 45 shows a summary of the influence of temperature on the average slope of the plastic strain relationship. As shown, the slope decreases with increasing temperature. This observation is not unique. Others have reported similar findings when using compression type tests (uniaxial and triaxial) in predicting rutting of HMA mixtures. Although the slope decreases with increasing temperature, the intercept from the secondary or steady-state region of the plastic strain relationship increases with increasing temperature.

The slope m and the intercept I within the steady-state region are related for a specific type of mix, but no universal relationship has been reported between the two parameters across all mixtures. This was observed in the initial VESYS work in terms of the alpha versus gnu relationship reported by Rauhut et al. (1976 and 1980). A reason for this observation is end effects or boundary conditions of the uniaxial and triaxial tests if test specimens are not properly conditioned to eliminate these effects or conditions. The difficult point is to determine an adequate number of conditioning cycles for each test specimen.

I is inversely proportional to m. This implies that k_{r1} (intercept factor) is related to k_{r3} (slope). This observation was also found in the testing completed in the earlier VESYS work and in the AAMAS study. Figures 44 and 45 were investigated together to ensure that the results made practical sense; rut depth increases with temperature. The more important finding from this study is that the slope of the plastic strain relationship is dependent on temperature. This temperature influence needs to be considered to enhance or make future improvements to the rut-depth transfer function.

In summary, test temperature is a dominant factor of HMA behavior and does have an impact on the HMA plastic deformation coefficients. No one single value of the steady-state slope or intercept should be initially assumed for rut depth predictions. To define the effect of temperature, more testing is required to determine the effective temperature for a specific mixture and climate. Thus, it is believed to be appropriate to characterize HMA behavior by running production RLPD tests at a minimum of three temperatures, even for the transfer functions that exclude temperature.

2.6.4.6 Summary

All analyses point toward the use of a 10-psi confining pressure and a 70-psi deviator stress for production RLPD testing using multiple test temperatures. The following bullets provide more detail for the test conditions recommended.

- Multiple confining stresses do not seem warranted at this time for making improvements to the prediction model. Confining stress has a major impact on the RLPD response

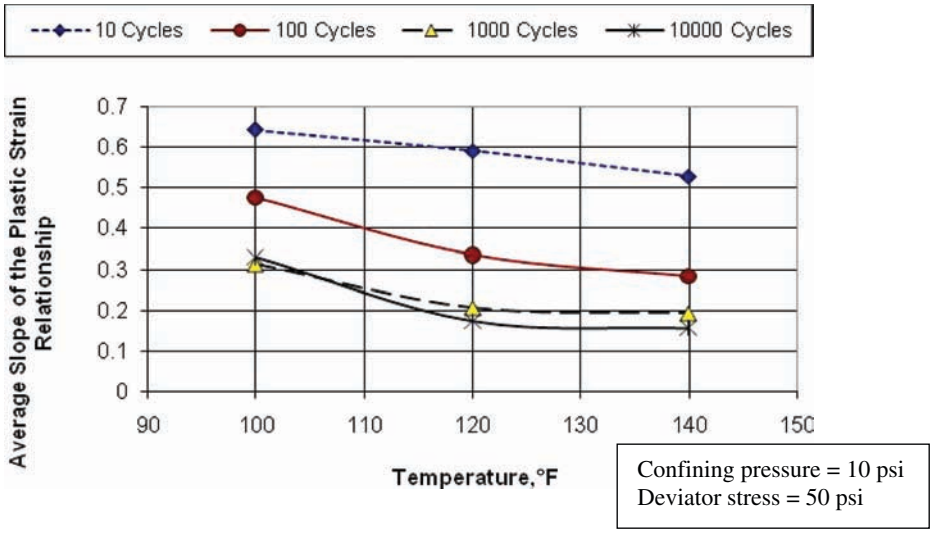

Figure 45. Influence of temperature on slope of steady-state or secondary region from repeated-load triaxial tests.

as compared to unconfined (or near-unconfined) conditions. The average slope of the steady-state portion of the plastic strain relationships for the unconfined condition are close to the globally calibrated value in Version 1.0 of the MEPDG: 0.4791 (refer to Figure 41), while the average slope of the steady-state portion for the confined tests is substantially less with values ranging from 0.17 to 0.25. Slopes measured in the steady-state region in confined tests are consistent with the values included in the modified Leahy and Verstraeten transfer functions. Confinement is needed to accurately predict the time–history rut depth data found on many of the LTPP test sections, as reported from NCHRP Project 9-30(01) (Von Quintus, Andrei, and Schwartz, 2005). Thus, an enhancement of the current model is to define the plastic deformation coefficients using repeated-load confined, triaxial tests.

- Multiple deviator stresses also are not warranted. Although the assumption in the MEPDG of linear proportionality between plastic strain and deviator stress is probably not justified, the degree of nonlinearity is not great and can be approximated without extensive testing. A deviator stress of 70 psi is suggested based on the exploratory test program; however, 50 psi could also be used without reducing the quality of the data.
- Testing at multiple temperatures is believed to be justified to more specifically define the exponent of the plastic deformation relationship and the intercept used. The globally calibrated MEPDG HMA rutting model assumes that this exponent is 1.5606. NCHRP Project 1-40B, however, reported that the temperature exponent was dependent on the volumetric and aggregate properties of the mixtures as well as the two other *k*-values (refer to Equation 1) to reduce the standard error term of the rut-depth prediction equation. The results presented here suggest that this value is also too high and may be closer to 1.0 or less for good quality HMA mixtures. Given that temperature is the dominant factor influencing HMA behavior and that the details of this influence will be mixture specific, it seems appropriate to determine this aspect of the behavior more completely and accurately. The temperature effect will be evaluated relative to the standard error term after calibration of the different transfer functions to determine its effect.

The following summarizes the triaxial test conditions recommended for the production test program.

- Deviator stress = 70 psi
- Confining pressure = 10 psi
- Temperature, three values = 20°C, LTPP-bind high temperature at 50% reliability, and the midrange temperature between those two temperatures.

2.6.5 Repeated-Load Constant-Height Shear Test Program

The repeated-load constant-height shear test was conducted in accordance with AASHTO T 320. The shear stress for the repeated-load constant-height shear test was based on the analyses completed as part of this study and under the SHRP asphalt research program (SHRP et al., 1994; Monismith, Deacon, and Harvey, 2000; and Monismith, Popescu, and Harvey 2006). A total of 5,000 loading cycles were used to estimate the plastic deformation coefficients of the WesTrack transfer function. A shear stress of 10 psi was used in the test

program. The shear stress is much lower than the shear stress computed near the surface of HMA layers (refer to Figure 34). The lower shear stress value was used to ensure that the maximum strain value would not be exceeded within the test.

2.7 Analysis of Repeated-Load Plastic Deformation Test Data

The analysis of repeated-load plastic deformation data was completed to determine if other forms of the laboratory-derived plastic strain or deformation transfer functions would provide greater accuracy in predicting HMA rutting. The analysis consisted of (1) determination of the model or transfer function coefficients from laboratory tests, (2) exploration of more sophisticated mechanistic analysis tools to provide insight into appropriate formulations for model revisions and enhancements, and (3) establishment of an analysis approach for the production test program.

2.7.1 Repeated-Load Triaxial/ Flow Number Test

2.7.1.1 Plastic Axial Strain Accumulation Patterns

Repeated-load triaxial plastic deformation test results typically follow the pattern shown in Figure 46. During the primary stage, the plastic axial strain accumulates rapidly but at a decreasing rate. In the secondary stage, plastic axial strain accumulates at a constant rate (in log–log space), while it accumulates at an increasing rate in the tertiary stage. This pattern will be referred to as Pattern A in this report. Most rut-depth transfer functions are based on the secondary or steady-state stage. In other words, the slope and intercept from the steady-state stage are used to determine the coefficients of the transfer functions.

Two points need to be defined or identified in Figure 46: the beginning and ending cycle values for the secondary stage, defined as N_{si} and N_{sf}, respectively. The N_{sf} limit is similar but not identical to the flow number. The flow number concept has been proposed for use to characterize a mixture's resistance to plastic deformation (Witczak et al., 2002). The flow number is the number of load cycles at which the plastic strain starts to increase at an increasing rate. In order for the flow number concept to be used to evaluate and compare HMA mixtures, the mixtures need to exhibit tertiary flow at some point in the loading process.

This concept is similar to laboratory wheel tracking tests where the vertical distortion or displacement of the test specimens is used to judge the acceptability of the mixture. Mixtures are considered acceptable as long as the test specimens can inhibit a specified vertical displacement for a specified number of loading cycles. The acceptability of the flow number test has been questioned because mixtures can go into tertiary flow at a lower temperature and not exhibit that characteristic at higher test temperatures (refer to Section 2.6.4.5). More importantly, none of the HMA mixtures included in this study actually exhibited this characteristic in terms of field performance (accelerated rut depths measured after some level of traffic).

Two other plastic axial strain patterns, however, are common and are illustrated in Figure 47. Pattern B [refer to Figure 47(a)] is the condition where the secondary stage continues to the end of the test. In other words, there is no tertiary stage. Pattern C [refer to Figure 47(b)] is the condition where the slope outside the primary stage continues to decrease but at a decreasing rate. In other words, there are no steady-state and tertiary stages. This pattern is referred to in this report as the plastic-strain-hardening region. Pattern A is more representative of unconfined or uniaxial repeated load tests, while Patterns B and C are more representative of confined or triaxial repeated load tests.

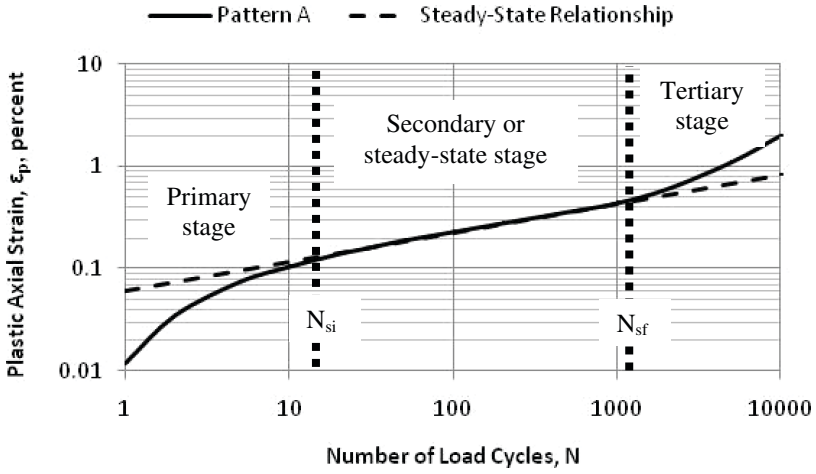

Figure 46. Typical accumulation of plastic axial strain measured in the laboratory—Pattern A.

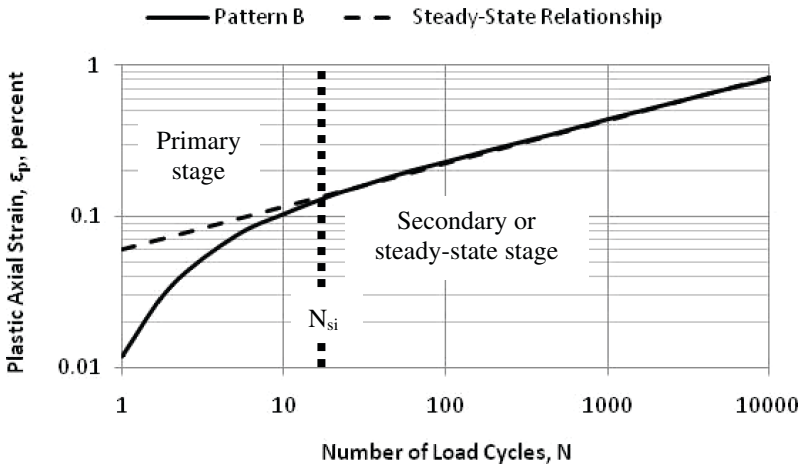

(a) Plastic axial strain accumulation; Pattern B.

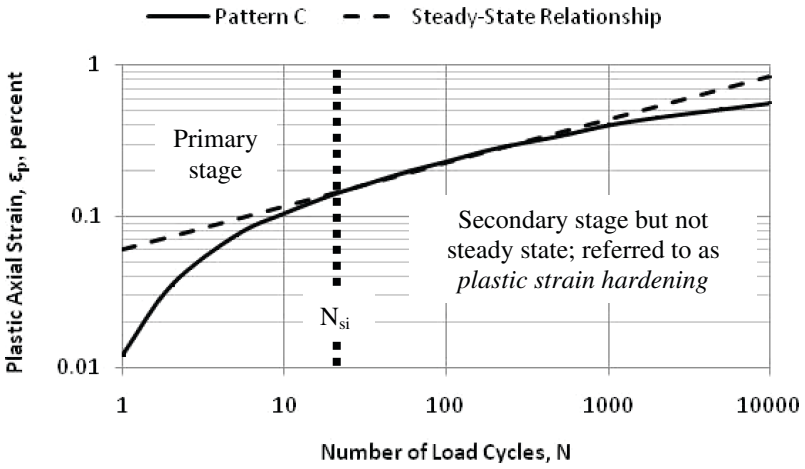

(b) Plastic axial strain accumulation; Pattern C.

Figure 47. Accumulation of plastic axial strain Patterns B and C.

2.7.1.2 Simple Power Law Simulation

Typical plastic strain coefficients are obtained from fitting a power model, as shown by Equation 19, to the secondary stage of the number of load cycles versus plastic axial strain relationship:

$$\varepsilon_p = aN^b \tag{19}$$

For which, *a* and *b* are the intercept and slope of the curve in log–log space, respectively. The intercept *a* represents the plastic strain at $N = 1$, and the slope *b* represents the rate of change in plastic strain in the secondary stage. The two basic parameters that have been used in comparing the results from repeated-load triaxial test results are alpha and gnu. These two parameters are inputs to the VESYS program that was developed under FHWA sponsorship many years ago, and are defined in the following equations (Rauhut et al., 1976; Rauhut, 1980; Kenis, Sherwood, and McMahon, 1982; and Kenis, 1977).

Mu, μ:

$$\mu = \frac{I(m)}{\varepsilon_r} \tag{20}$$

Alpha, α:

$$\alpha = 1 - m \tag{21}$$

where

I = intercept with the plastic strain axis of the relationship between the log of the number of load repetitions versus plastic strain.

m = slope of the linear portion or steady-state region of the relationship between the log of the number of load repetitions versus log of the plastic strain.

ε_r = resilient strain of the repeated-load plastic deformation test. The resilient strain is assumed to remain constant throughout the test, after the initial load applications.

Table 18. Power law model parameters (Equation 19).

Temperature T (°F)	Conf. Stress σ_c (psi)	Dev. Stress $\Delta\sigma$ (psi)	Intercept a	Slope b	R^2	N_{si}	ε_{psi}
120	0	50	0.0013	0.3933	0.9980	61	0.006345
120	10	50	0.0020	0.1781	0.9986	82	0.004472
120	20	50	0.0013	0.1772	0.9992	82	0.002874
120	10	30	0.0012	0.1643	0.9941	83	0.002529
120	10	50	0.0020	0.1781	0.9986	82	0.004472
120	10	70	0.0019	0.2558	0.9994	75	0.005605
100	10	50	0.0005	0.3606	0.9928	66	0.002248
120	10	50	0.0020	0.1781	0.9986	82	0.004472
140	10	50	0.0026	0.1642	0.9937	82	0.005307

The plastic deformation coefficients are identical to the laboratory-derived values used to determine the VESYS rut depth parameters: $a = I$ and $b = m$. The VESYS rut-depth prediction model was considered and debated at the facilitated workshop but was not one of the consensus transfer functions. The extensive amount of testing and analysis of repeated-load triaxial data for that model was reviewed and used to improve on the determination of the plastic deformation coefficients.

The process of fitting Equation 19 to the laboratory-measured data has not been standardized, even though these parameters have been reported for many mixtures over the past decades. Several procedures have been proposed and used in recent years (Rauhut, Lytton, and Darter, 1984; Leahy, 1989; Zang et al., 2002; Biligiri, 2007; Archilla, Kobayashi, and Diaz, 2008). These procedures differ primarily in their determination of where the primary stage ends and the tertiary stage begins, so these data can be trimmed before fitting Equation 19 to the secondary stage data only.

Many alternatives for extracting just the secondary stage response were investigated as part of this research. Each alternative yielded different—often significantly different—estimates for the a and b parameters (Equation 19). The procedure used for this part of the study consists of two steps.

1. The first step is to determine the start of the tertiary stage, if one exists. Adapting an approach originally proposed by Zang et al. (2002), a power model is fit to a successively smaller subset of the data points ($I = 1 \ldots N$) and the predicted plastic strain at the N^{th} cycle is compared to the corresponding measured value. Specifically, the N_{sf} value corresponding to the end of the secondary stage is determined using the following iterative algorithm:
   (a) Set the initial number N of data points to be analyzed equal to N_{MAX}.
   (b) Determine the regression parameters a and b (refer to Equation 19).
   (c) Compare the predicted cumulative plastic strain at N to the respective measured value. If the calculated value is less than 2% from the measured value, N is defined as N_{sf}. Otherwise, set $N = N - 1$ and repeat steps (b) and (c).
2. The next step is to identify the initial point of the secondary stage, N_{si}. This is done by examining the derivative of the power law model using the last regression parameters found from the previous algorithm and determining the point where the derivative becomes essentially constant. This point is defined as N_{si}.

After the N_{si} and N_{sf} points have been identified, the data corresponding to the primary and tertiary (if present) stages can be trimmed and the power law model fit to the secondary stage data points only. The final power model regression parameters for the secondary stage, the goodness of fit, and the N_{si} and its respective plastic strain magnitude ε_{psi} are summarized in Table 18 for all test conditions for the ALF2 control mixture.

Figure 48 shows the variation of the estimated a and b values as functions of confining stress. The magnitudes of the a and b values are consistent with those from other studies (e.g., Leahy, 1989). The trend observed in Figure 48(a) for the slope b is consistent with the overall results observed in the RLPD tests. Small amounts of confinement greatly suppress the accumulation of plastic strain. Larger amounts of confinement have a diminishingly smaller effect. Based on the trends in Figure 48, the majority of the plastic strain suppression occurs at a confining stress of somewhere between 0 (i.e., unconfined) and 10 psi. Figure 48(b) indicates that confining stress delays the beginning of the secondary stage and reduces the plastic strain level at which it occurs.

The variation of the intercept a with confining stress shown in Figure 48 is more complicated. The a value counterintuitively increases as confinement increases from 0 to 10 psi and then shows the expected decrease as confinement is increased still further to 20 psi. The lack of a consistent trend in the intercept is likely due to the interactions between a and b and the greater weight that the slope b has on the fitting process. The intercept a is extrapolated from the

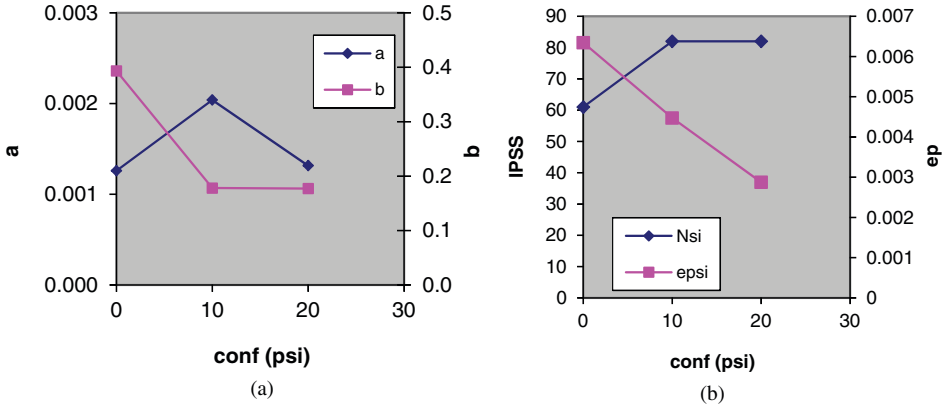

Figure 48. Influence of confining stress on power model parameters.

secondary stage response and thus is very sensitive to the value of *b*, particularly in log–log space.

Figure 49 summarizes the variations in *a* and *b* with deviator stress. The rate of plastic strain (slope *b*) increases with increasing deviator stress [Figure 49(a)], as expected. Once again, though, the intercept *a* exhibits irrational behavior; *a* increases as expected as $\Delta\sigma$ increases from 30 to 50 psi, but it then inexplicably decreases as $\Delta\sigma$ increases further to 70 psi. The interactions between *a* and *b* and the fact that *a* is an implicitly extrapolated parameter are the probable causes of this behavior, as described previously. The number of cycles to reach the secondary stage reduces slightly and the respective plastic strain level increases significantly with increasing deviator stress [Figure 49(b)].

Figure 50 summarizes the variations in *a* and *b* with temperature. Both trends agree with expectations. While the slope *b* decreases with increasing temperature, the intercept *a* increases substantially. At high temperatures the binder is less viscous and the mixture relies more on the underlying aggregate friction to resist plastic deformation, which is consistent with the trends in both *a* and *b*. The mixture also reaches the secondary stage at higher strains as temperature increases.

2.7.1.3 Enhanced Power Law Simulations

Although the power law model captures the secondary stage repeated load behavior, it does not realistically capture the primary-stage deformations. This may be another partial explanation for the irrational trends observed for the intercept *a*, since this in effect is an extrapolated measure of the early (i.e., $N = 1$) primary state response. The tertiary stage observed in the unconfined tests also cannot be captured by the simple power law model. The Francken model augments the simple power law with an exponential function to capture the tertiary stage response (Biligiri, 2007):

$$\varepsilon_p = aN^b + c\left(e^{dN} - 1\right) \tag{22}$$

For which, the additional parameters *c* and *d* are nonnegative quantities. The exponential term in Equation 22 increases the plastic strains with increasing *N* into the tertiary range. Figure 51 shows the Francken model and the power law model fitted to an unconfined RLPD test. The plot is in log–log space to provide better visualization of all three stages of plastic deformation. The Francken model provides a more realistic representation of tertiary stage response as compared to the power law. For the confined RLPD tests in which ter-

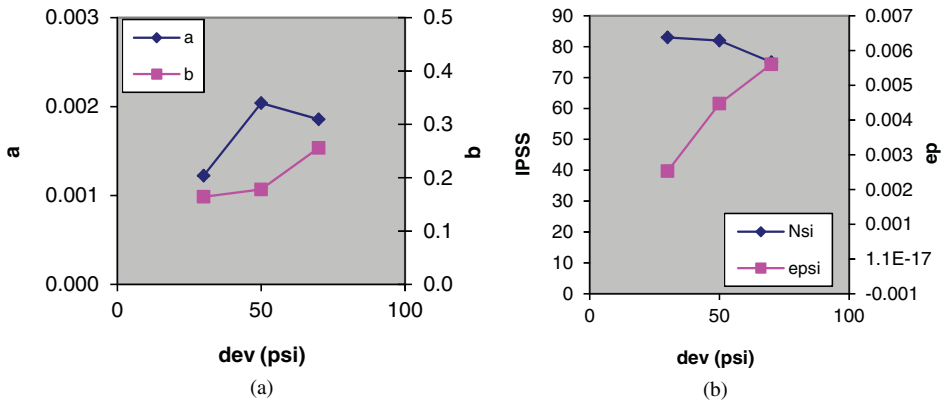

Figure 49. Influence of deviator stress on power model parameters.

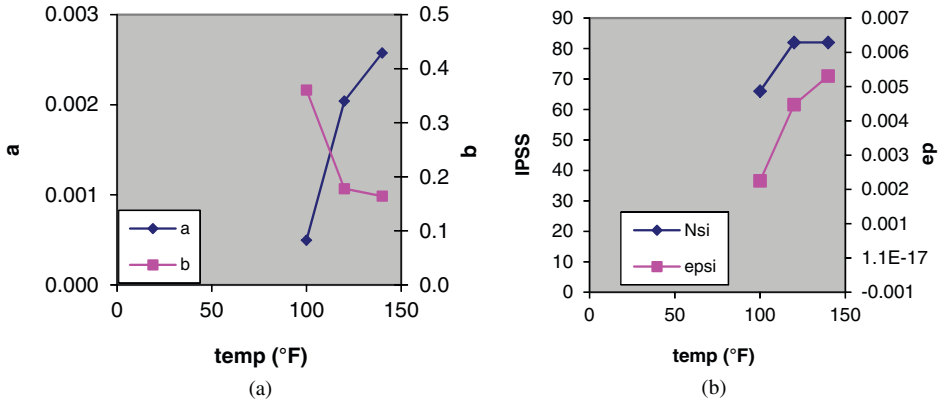

(a) (b)

Figure 50. Influence of temperature on power model parameters.

tiary flow does not occur, the parameters *c* and *d* are sensibly equal to zero.

The Francken model *a* and *b* parameters are equivalent to their counterparts in the power law model. The trends described in Figure 48 to 50 apply also to these parameters in the Francken model.

The structure of the Francken model suggests another enhancement to better capture the primary-stage RLPD response. The motivation for this enhancement comes from examination of the residuals from the power law model for the first 100 cycles, which usually spans most of the primary stage. The variation of the residuals with *N* has the form of an exponential function, which can be captured by including a second exponential function as part of the intercept term. This modified Francken model has the following form:

$$\varepsilon_p = \left(k_1 e^{k_2 N} + a\right) N^b + c\left(e^{dN} - 1\right) \quad (23)$$

This modified model can fit all three stages of the RLPD response with one continuous model. Figure 52 compares the modified Francken model with the original form and the power law model. The residuals from the primary stage in the modified Francken model are minimized without compromising the accuracy in the secondary and tertiary stages. Table 19 summarizes the modified Francken model parameters for all of the RLPD tests on the ALF2 control mixture.

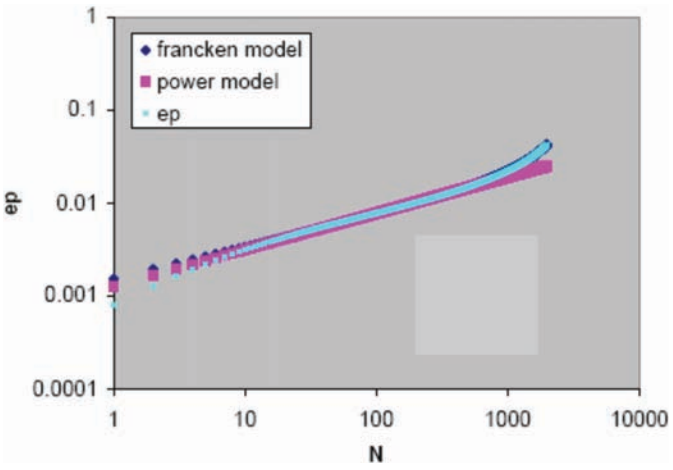

Figure 51. Comparison between Francken model and power law model for unconfined* RLPD *triaxial test.

2.7.2 Repeated-Load Constant-Height Shear Tests

The repeated-load constant-height shear test exhibits slightly different patterns in contrast to the repeated-load axial test. Figure 53 shows the two patterns that are typical with the repeated-load shear test data and that are based on the review of test results from this study, as well as from SHRP and other projects. The intercept and slope from the steady-state region were used to determine the inputs to the transfer function (refer to Equation 8).

2.7.3 Summary

Pattern A (refer to Figure 46) is not typical of rut depths measured along a roadway or test section. Rut depths increase shortly after construction but increase at a decreasing rate. Based on the review of rut depths on most of the test sections in the LTPP program and from monitoring HMA test sections for decades, the authors have not observed an increasing rate in rut depth over time after the first 2 to 3 years of performance without a significant or abrupt increase in traffic or some defect, like stripping or debonding between two HMA layers. Pattern A is believed to be characteristic of a laboratory-false condition—tertiary flow does not occur years after the mixture has been placed unless some site feature changes, like an increase in truck traffic.

The pattern measured in the laboratory is dependent on the mixture's resistance to deformation and its ability to recover deformation, as well as on the testing conditions (temperature, confining pressure, and deviator stress). The

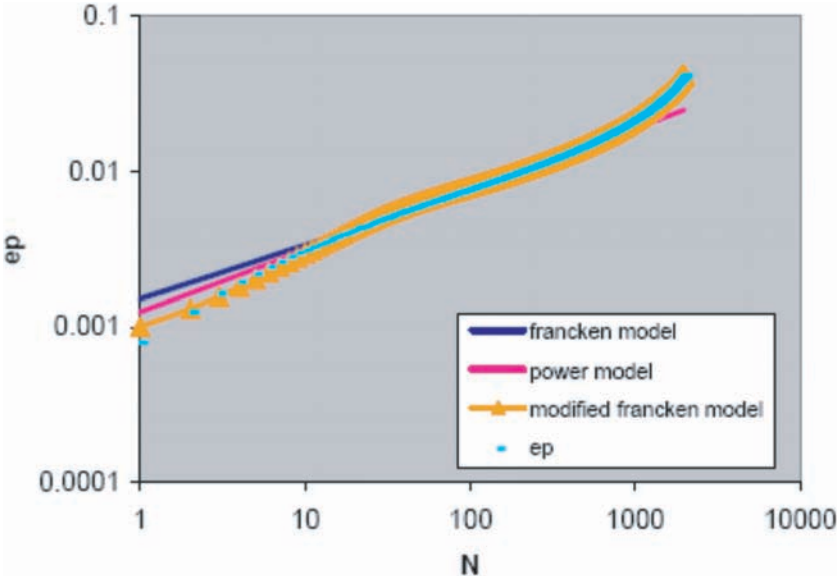

Figure 52. Modified Francken model fitted to unconfined RLPD triaxial test data.

key for all patterns is identifying the breakpoints between the different stages. Pattern A is more characteristic of coarse and gap-graded mixtures when using uniaxial or unconfined repeated-load tests. Pattern C (plastic-strain-hardening region) was observed on many of the testing projects completed for the VESYS program using confined tests, especially for dense, fine-graded mixtures. The slope and intercept were determined using the higher number of load cycles to minimize the residual error and bias between the measured and predicted rut depths.

One observation to be pointed out is that few pavements exhibit the tertiary stage or Pattern A (refer to Figure 46). This observation is based on the experience of the authors with observing the accumulation of rut depths on many LTPP test sections, as well as from forensic investigations. Another observation is that the plastic shear strain coefficients [secondary slope (b) and intercept (a) in Equation 8] are determined on a more consistent basis because the general pattern consists of two basic stages (refer to Figure 53), both of which are more steady state than for the plastic axial strain accumulation (refer to Figures 46 and 47).

The major difference between the plastic axial and plastic shear strain accumulation is in the primary stage or region. The plastic shear strain accumulates at a much lower rate than the plastic axial strain. It is difficult to determine which is more representative of field conditions. Chapter 3 addresses this difference in patterns relative to the field-measured values.

2.8 Laboratory Production Test Program

Two repeated-load plastic deformation tests are required in support of the rut-depth transfer functions recommended from the facilitated workshop. These two tests include the repeated-load triaxial or uniaxial test (referred to in current literature as the flow number test) and the repeated-load constant-height shear test. Repeated-load plastic deformation tests were included to permit enhancements to the MEPDG rut-depth prediction methodology to account for different types of mixtures and site conditions.

As noted previously, the measured rut depths could not be solely explained by the difference in dynamic modulus

Table 19. Modified Francken model parameters (Equation 23).

Temperature T (°F)	Conf. Stress σ_c (psi)	Dev. Stress $\Delta\sigma$ (psi)	a	b	c	d	k_1	k_2	R^2
120	0	50	0.0023	0.2578	0.0076	0.0007	-0.0014	-0.0721	0.9998
120	10	50	0.0021	0.1751	0	0	-0.0008	-0.0177	0.9995
120	20	50	0.0013	0.1785	0	0	-0.0006	-0.0435	0.9993
120	10	30	0.0013	0.1576	0	0	-0.0005	-0.0136	0.9970
120	10	50	0.0021	0.1751	0	0	-0.0008	-0.0177	0.9995
120	10	70	0.0018	0.2565	0	0	-0.0008	-0.0898	0.9994
100	10	50	0.0004	0.3892	0	0	-0.0001	-0.1535	0.9941
120	10	50	0.0021	0.1751	0	0	-0.0008	-0.0177	0.9995
140	10	50	0.0030	0.1447	0	0	-0.0005	-0.0017	0.9972

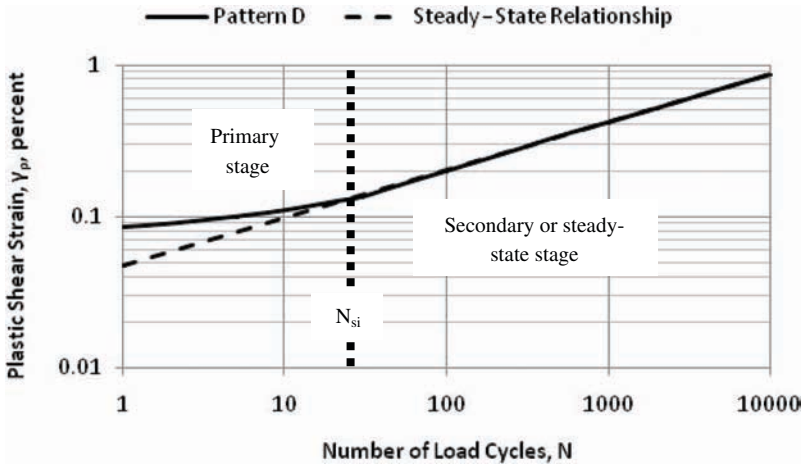

(a) Plastic shear strain accumulation; Pattern D.

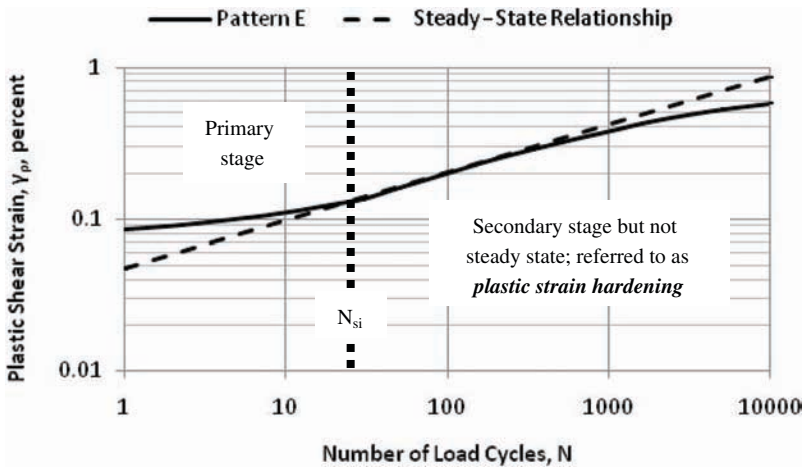

(b) Plastic axial strain accumulation; Pattern E.

Figure 53. Accumulation of plastic shear strain, Patterns D and E.

between the different test sections; gradation and volumetric properties had a significant effect. It is hypothesized that the repeated-load plastic deformation tests will adequately capture these effects in predicting rut depth (refer to hypothesis #6 in Section 2.4.2). These factors must be accounted for to reduce the standard error and decrease the level of uncertainty in the predictions. The other tests needed to enter MEPDG Level 1 inputs include dynamic modulus and asphalt physical property tests. The asphalt physical property tests are required when using Level 1 inputs (dynamic modulus for the HMA mixture).

The type and number of tests generally follow the recommendations from NCHRP Project 9-30. It should be understood that this does not include all material mechanical properties needed for model execution, only those that were unavailable within the LTPP and M-E_DPM databases.

2.8.1 Types of Samples for Testing

During NCHRP Project 9-30, different types of samples for production testing were investigated for use in the MEPDG calibration–validation process. The experimental plan recommended that the same type of samples be used between all projects or test sections to minimize differences caused by different preparation methods. The following lists and briefly discusses the different options that were considered, as well as the one selected for use in the production testing program.

- **Bulk mixture sampled during production.**

  Bulk mixture was the preferred type of sample to be used for testing the HMA mixture and determining the inputs for rut-depth transfer functions. Two reasons for this type of sample being the preferred method are (1) it does not require simulated short-term aging in the laboratory and (2) all test specimens in the NCHRP Project 9-19 test program were prepared using bulk mixture. Thus, there would be no difference between simulated aging performed in the laboratory and the actual aging during mix production, so the results from NCHRP Project 9-19 would be directly applicable to this study. Differences between actual and

simulated aging could increase the standard error of the rut-depth transfer functions.

The disadvantage of this type of sample is that the mixture must be reheated for compaction, and therefore the reheating will result in additional aging of the HMA mixture. This disadvantage, however, was not believed to be significant because all of the test specimens would be compacted to the in-place air voids. The effects of reheating bulk mixture were investigated in the AAMAS study, and it was found that about 5% of additional compaction effort was needed to simulate the in-place air voids of the HMA mixture (Von Quintus et al., 1991).

The use of bulk mixture was excluded because few LTPP and other project test sections had sufficient bulk mixture stored in the MRL.

- **Field cores drilled immediately after construction or gyratory specimens compacted during construction.**

  Both cores and gyrator-compacted test samples are available in the MRL for most of the LTPP projects. The use of field cores was excluded from consideration for use in the production test program because the repeated-load triaxial test requires different test specimen geometry. In addition, air voids are variable along a project, even with a uniform rolling pattern. The higher variance in air voids between cores, as compared to test specimens compacted in the laboratory, increases the variability in the plastic deformation coefficients needed as inputs to the rut-depth transfer functions. An increase in variance of the test results means that more test specimens are needed for the same confidence level.

  The use of gyratory-compacted samples prepared during construction was also excluded from consideration because all of the samples stored in the MRL were compacted to an air void level of about 4%. The rut-depth transfer functions require the test specimens to be compacted to the in-place air voids measured after construction. In addition, the triaxial repeated-load plastic deformation test requires different test specimen geometry from those compacted with the gyratory compactor. The gyratory-compacted specimens stored in the MRL are 2 to 3 in. in height.

- **Component materials (aggregate, asphalt, filler, etc.) used to produce the HMA mixture.**

  The use of component materials to reconstitute the HMA mixture in the laboratory was the preferred and recommended type of sample for testing the HMA mixtures. This method was selected because many more of the LTPP and other projects had sufficient amounts of component materials stored in the MRL. Multiple projects and test sections were identified for this effort based on the availability of producing 500 lbs to 800 lbs of HMA mixture using reconstituted materials from the MRL.

  The disadvantage of this method is that the mixture must be mixed and short-term aged in the laboratory using aggregates that are typically dried to a constant weight, removing most of the moisture in the aggregate. This type of sample preparation method also takes much more time to produce the samples than the use of bulk mixture. The use of a small-scale laboratory batch-type plant helps to reduce the sampling variance found between smaller individual batches of the mix. Thus, this method was considered acceptable and was selected for preparing the test specimens for the production test program.

  On a few of the projects selected for the production test program, it was found that there were sufficient amounts of asphalt available but insufficient amounts of aggregate in the MRL. For these cases, additional aggregate was sampled from the quarries used to produce the HMA mixture. The additional aggregate was blended with the aggregate stored in the MRL to minimize any potential bias in the aggregate properties between the two time periods.

2.8.2 Asphalt Physical Property Tests

Asphalt binder physical properties were available in the LTPP database and from other studies documenting the properties of the materials used to produce the HMA. When the physical properties were unavailable from other records and databases, the asphalt binder properties were measured in the laboratory. Table 20 summarizes the asphalt binder properties for the projects.

2.8.3 HMA Mixture Design

HMA mixture designs were recovered from construction records and files for most of the projects included in the study. The HMA mixture design records are needed to determine the sensitivity of density and air voids to variations in asphalt content and to estimate the saturation asphalt content. The saturation asphalt content is one of the parameters used to estimate the plastic deformation coefficients for the Kaloush transfer coefficient (refer to Appendix C). The mixture designs and data are included in the test section reports in Appendix J.

2.8.4 Test Specimen Preparation

2.8.4.1 Sample and Test Specimen Preparation and Fabrication

Specimens for triaxial testing were fabricated in accordance with AASHTO PP 60. This is the specimen fabrication standard developed in NCHRP Project 9-29 for making specimens for the AMPT.

Fabrication of specimens for simple shear testing used rolling wheel compaction and generally followed AASHTO PP 3.

Table 20. Asphalt binder properties for selected projects used to assess the different transfer functions.

Project Identification	Specific Gravity	Softening Point, °F	Penetration at 77°F, 1/10 mm	Viscosity	
				Absolute, 140°F, Poise	Kinematic, 275°F, cSt
Alabama SPS-6 mix	1.035	161.0	27	116,600	4,245
Arizona, SPS-5 virgin mix	1.025	134.0	18	8,890	589
Caltrans, PBA-6A	1.006	142.3	115	26,690	1,272
Caltrans, Valero AR-8000	1.032	136.0	26	9,912	778
Mississippi, SPS-5 virgin mix	1.038	137.0	32	11,910	988
Missouri, SPS-5 RAP binder	1.033	145.2	30	29,310	1,254
Missouri, SPS-5 virgin binder	1.026	128.8	47	7,280	754
Missouri, SPS-5 virgin, surface	1.012	119.1	73	2,190	416
Montana, SPS-5 virgin mix	1.034	125.5	49	4,030	492
Wisconsin SPS-1 mix, ATB	1.033	124.9	56	4,060	533
Wisconsin SPS-9	—	—	70	—	449
NCAT, 64-22, NuStar	1.034	129.7	42	7,190	697
NCAT, 67-22 mix	1.039	135.7	40	11,680	971
NCAT, 76-22 mix	1.036	160.3	29	130,100	3,735

This standard was developed during SHRP but was deleted from the AASHTO provisional standards in 2003. The setup or compaction mold allowed preparation of a variable-length slab that was 30-in. wide and 4-in. thick. The variable length was needed because the amount of materials available from the MRL for some of the projects was insufficient for compacting the full-size, 30-in. by 30-in. HMA slab specified in AASHTO PP 3. Figure 54 shows the variable-length rolling wheel compaction mold.

2.8.4.2 Reconstitution of Mixtures

Aggregates were extracted from the barrel samples shipped from the MRL and sieved to blend the aggregates

Figure 54. Fabricated rolling wheel mold used to compact HMA for the repeated-load constant-height shear test and the HMA pad from the rolling operation.

to the average gradation reported during construction. The average or target gradation for the samples is included in the test section reports in Appendix J. In some cases, the target gradation reported during construction deviated from the job mix formula established and reported from the mixture design records.

The HMA slabs required between 250 lbs and 300 lbs of mixture, depending on size. Mixture batches were prepared using a large pugmill mixer. Figure 55 shows the pugmill mixer used on this project. This mixer can produce approximately 100-lb batches. The larger batches were used to reduce potential differences between batches of the same mixture.

(a) Pugmill mixer or device used to mix and produce the HMA mixtures.

(b) Close-up of the paddles inside the pugmill mixer for mixing the HMA.

Figure 55. Large pugmill mixer used to produce the HMA samples for the production test program.

2.8.4.3 Short-Term Aging of Mixtures

After mixing, the HMA was removed from the pugmill mixer and short-term-oven–aged for 4 hours at 135°C in accordance with AASHTO R 30 prior to compaction.

2.8.4.4 Compaction of Mixture Samples

Two types of devices were used to compact the HMA mixture samples for the repeated-load triaxial and shear tests. The triaxial mixture samples were compacted in an Interlaken gyratory compactor to a height of 170 mm. This height provides a relatively uniform air void distribution from top to bottom of the test specimen using this compactor. Figure 56 shows the gyratory compactor used for compacting the HMA mix samples.

The mixture for the repeated shear test specimens was compacted in the fabricated compaction mold (refer to Figure 54) using a small self-propelled roller with a static steel drum weight of 3,000 lbs. Figure 57 shows the roller being used to compact

Figure 56. Interlaken gyratory compactor for compacting the HMA samples.

Figure 57. Self-propelled roller with a static steel drum weight of 3,000 lbs used to compact the shear test specimens.

one of the HMA pad samples. The rolling wheel compactor was used to reduce the potential impact of the detrimental boundary conditions of the gyratory-compacted 6-in. diameter specimens for shear testing. Such gyratory-compacted specimens exhibit much higher air voids around the edges and ends of the test specimens that remain in place for shear testing.

2.8.4.5 Coring and Trimming of Test Specimens for Testing

Two types of test specimens were drilled from the gyratory- and roller-compacted HMA samples. A 100-mm-diameter by 170-mm-high core was cut from the middle of the gyratory-compacted sample using a standard diamond-bit coring drill attached to a stand to allow proper alignment. The ends of the core were sawed smooth and parallel using a double-bladed saw for creating the test specimen used for dynamic modulus and repeated-load triaxial tests. Figure 58 shows the coring and sawing equipment, the core drilled from the gyratory-compacted sample, and the test specimen after sawing both ends of the test specimen.

Full depth samples were cored from the HMA slab using a standard core drill with a nominal 150-mm-diameter coring bit, as shown in Figure 59. For the full-size, 30-in. by 30-in. HMA slab, 12 cores were drilled, while nine cores were removed from the smaller, 30-in. by 12-in. HMA slab.

The 50-mm-thick shear test specimens were sawed from the middle of the full depth cores using a double-bladed saw to ensure that the ends were parallel. Specimens for testing were selected based on their air void content. With some mixtures, the average air void content reported by LTPP could not be achieved.

2.8.5 Testing of HMA Mixtures

2.8.5.1 Dynamic Modulus Testing

Dynamic modulus testing was performed with an Interlaken AMPT in accordance with AASHTO TP 79. This is the standard developed in NCHRP Project 9-29 for testing dynamic modulus and flow number of mixtures with the AMPT.

On-sample LVDTs were used to measure strains, and the data were processed using a regression technique for fitting sinusoidal data (refer to Appendix D). Several indicators were used to determine the quality of the data. The most important ones are:

- Load standard error—ensures sinusoidal loading.
- Deformation standard error—ensures sinusoidal strain measurements.
- Uniformity of the deformation measurements—minimizes variation between specimen-mounted LVDTs.
- Uniformity of the phase angle measurement—minimizes variation between specimen-mounted LVDTs.
- AASHTO TP 79—provides limits for the data quality indicators for good quality data.

Dynamic modulus master curves were developed by testing at three temperatures and four loading frequencies in accordance with AASHTO PP 61. This is the standard developed in NCHRP Project 9-29 for using the AMPT to construct dynamic modulus master curves for pavement structural design. It includes:

- Recommended temperatures and loading frequencies.
- Fitting of the master curve using the MEPDG dynamic modulus equation.

Figure 58. Coring equipment and operation for preparing the dynamic modulus and repeated-load triaxial test specimens.

- Computation of the modulus at the temperatures used in the MEPDG from the fitted master curve.

The procedure estimates the master curve for the colder temperatures because the equipment developed in NCHRP Project 9-29 cannot test at temperatures below about 0°C. The three test temperatures used in the test program are the upper-level temperatures where all of the plastic deformation occurs in HMA mixtures. Typical fitted master curves for each of the mixtures included in the production testing program using AASHTO PP 61 are included in Appendix D. Equation 24 is the MEPDG master curve equation used to develop the master curves included in Appendix D, while Figure 60 shows an example of the fitted modulus data in developing the master curve.

$$Log(E^*) = \delta + \frac{\alpha}{1 + e^{\beta + \gamma(Log(\omega_r))}} \quad (24)$$

Table 21 summarizes the dynamic modulus measured at selected test temperatures and loading frequencies for comparing the different HMA mixtures for the projects used to assess the different rut-depth transfer functions. As shown, there is a wide range of dynamic modulus values for these mixtures.

2.8.5.2 Repeated-Load Plastic Deformation Test

Repeated-load plastic deformation data were collected with an Interlaken AMPT in accordance with AASHTO TP 79. This is the standard that was developed in NCHRP Project 9-29 for testing dynamic modulus and flow number of mixtures with the AMPT. Figure 61 shows the test specimen with the LVDTs mounted to the specimen. Appendix E provides graphical representations of results from the repeated-load plastic deformation tests.

The AMPT repeated load test used a pulse duration of 0.1 s and a dwell time of 0.9 s. The plastic strain in the test

(a) Twelve cores being drilled from the HMA pad that was compacted with the rolling wheel compactor.

(b) and (c): A 50-mm-thick shear test specimen being sawed from the middle of the full depth core using a double-bladed saw to ensure that the ends were parallel.

Figure 59. Coring equipment and operation for preparing the repeated-load constant-height shear test specimens.

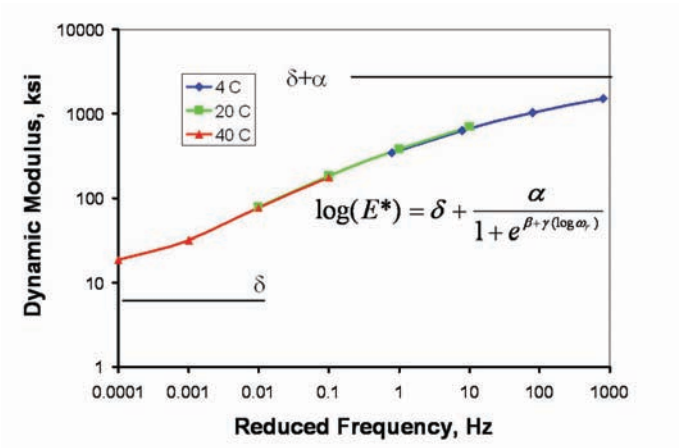

Figure 60. Example of fitting dynamic modulus data for developing the master curve.

specimen is monitored with an actuator-mounted LVDT. This testing was conducted at multiple temperatures using 10-psi confinement with a deviator stress of 70 psi. The tests were run to the lesser of 10,000 cycles or a plastic axial strain of 5%.

The repeated shear testing was conducted using an Interlaken Simple Shear Tester in accordance with AASHTO T 320. In this test, a repeated shear stress of 10 psi is applied to the specimen while applying sufficient axial stress to keep the height of the specimen constant. LVDTs on the specimen monitor the shear and the axial deformations. A shear pulse duration of 0.1 s and a 0.6-s rest period or dwell time were used. The test was continued to 5000 cycles or a plastic shear strain of 5%. Figure 62 shows the shear test specimen with the LVDTs mounted to the specimen.

Table 21. Dynamic modulus measured at selected temperatures for a loading frequency of 10 Hz for selected HMA mixtures included in production test program.

Project Identification	Mixture Type	Dynamic Modulus, ksi			
		40°F	70°F	100°F	130°F
Alabama, SPS-6	Overlay binder	2050.2	915.9	277.5	94.1
Arizona, SPS-5	Overlay binder	3012.2	2103.1	777.2	148.0
California I-710	CA47	2593.9	1432.6	400.3	86.2
California I-710	CA47M	870.8	282.8	99.6	49.6
California I-710	CA52	2840.5	1623.3	457.9	108.3
Florida, NCAT	HMA base	2149.8	1097.6	384.4	135.5
Colorado, SPS-5	Binder, RAP	2219.8	1127.3	349.5	92.8
Colorado, SPS-5	Binder, virgin	2008.4	838.7	215.3	60.9
Florida, NCAT	HMA N1	1587.0	717.9	222.5	59.8
Florida, NCAT	HMA N2	1841.8	918.0	344.0	127.3
Indiana, NCAT	HMA 7A	2056.7	874.2	224.4	65.2
Indiana, NCAT	HMA 7B	1829.3	758.2	187.2	43.2
Indiana, NCAT	HMA 8B	2018.3	922.0	252.0	59.6
Mississippi, SPS-5	Overlay binder	2116.1	888.4	224.2	62.4
Missouri, SPS-5	Binder, RAP	1939.8	874.1	246.1	66.5
Missouri, SPS-5	Binder, virgin	2089.4	959.7	274.4	90.0
Missouri, SPS-5	Surface	1617.9	585.1	147.0	48.6
Montana, SPS-5	Binder, virgin	2172.3	939.8	232.3	57.8
Wisconsin, SPS-1	HMA base, ATB	1727.0	634.9	158.8	48.7
Wisconsin, SPS-1	HMA binder	1758.6	566.1	112.9	33.0
Wisconsin, SPS-1	HMA surface	1498.4	522.9	130.4	41.4

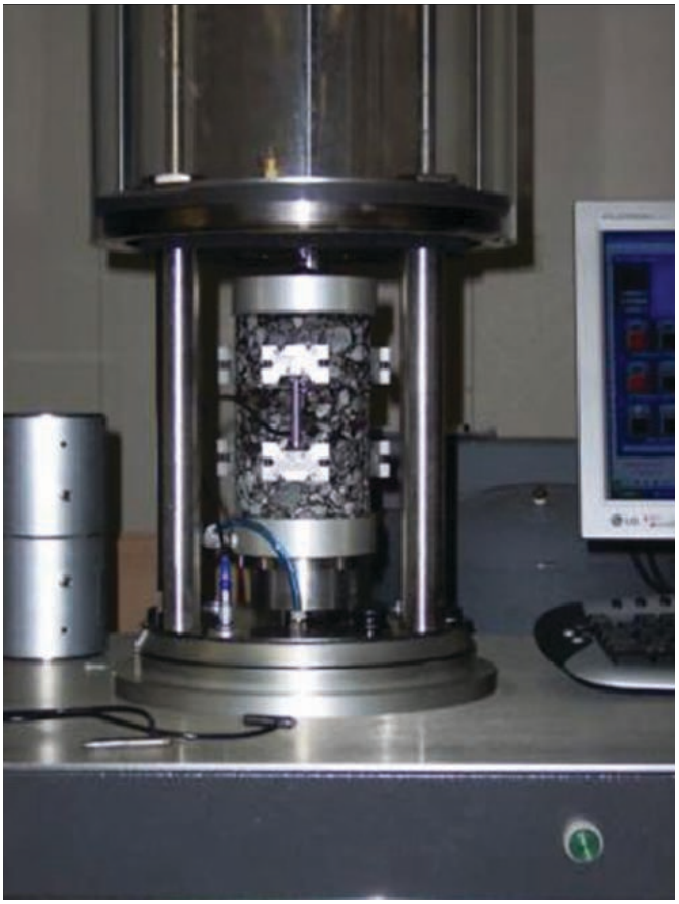

Figure 61. Test specimen setup for the triaxial repeated-load plastic deformation test.

Figure 62. Test specimen setup for the repeated-load constant-height shear plastic deformation test.

2.9 Determination of Laboratory-Measured Plastic Strain Coefficients

This section demonstrates and explains determination of the plastic strain coefficients from repeated-load triaxial and constant-height shear tests, similar to the discussion included in Section 2.7. Mixtures selected for the demonstration were based on those exhibiting different plastic strain accumulation patterns shown in Figures 46, 47, and 53, as well as mixtures that exhibit different responses between triaxial and constant-height shear test results.

The three mixtures selected for the demonstration were the Missouri SPS-5 binder mixture with RAP, the Montana SPS-5 binder mixture without RAP (virgin mixture), and the Wisconsin SPS-1 wearing surface. Figure 63 displays the results from the repeated-load triaxial test, while Figure 64 displays repeated-load constant-height shear test results.

The three test temperatures initially used in the production test program were defined as (1) 50% reliability performance-grade (PG) high temperature, (2) 20°C (68°F), and (3) the middle-range temperature between the first two. The upper temperature was lowered during the production test program because the 50% reliability PG high temperature was found to be too high for some of the mixtures. Similarly, 20°C was found to be too low for some mixtures. The temperatures proposed for future testing are discussed in Chapter 3.

All transfer functions in MEPDG Version 9-30A represent the steady-state or secondary region from repeated-load plastic deformation tests. The laboratory test results from the secondary region of the repeated-load confined, triaxial and constant-height shear tests can be represented by Equation 25.

$$\varepsilon_p(Lab) \text{ or } \gamma_p(Lab) = I_s(N)^m \quad (25)$$

where

$\varepsilon_p(Lab)$ = plastic axial strain accumulated in repeated-load triaxial tests, in./in.

$\gamma_p(Lab)$ = plastic shear strain accumulated in repeated-load shear tests, in./in.

m = average slope in secondary region of repeated load tests.

I_s = intercept from secondary region of repeated load tests (similar to Equation 18), in./in.

$$Log(I_s) = d + nLog(T) \quad (26)$$

where

T = test temperature, °F.

d, n = regression constants from secondary region of repeated load tests.

The following subsections demonstrate determination of the coefficients from laboratory repeated-load tests (refer to Equations 25 and 26) and identify some of the differences and similarities between results from the two repeated load tests for use in determining inputs to the appropriate rut-depth transfer functions.

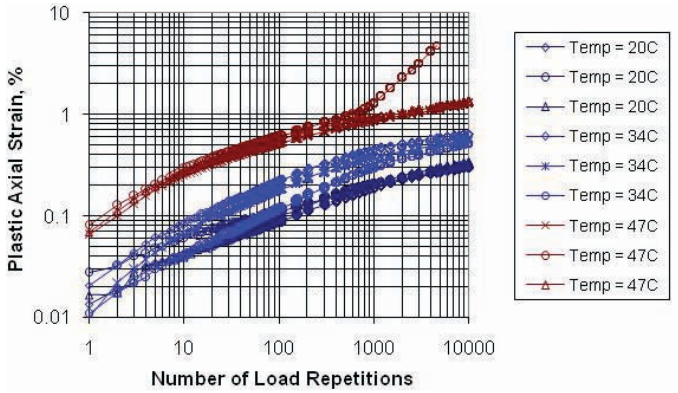

(a) Missouri SPS-5 binder layer with RAP mixture.

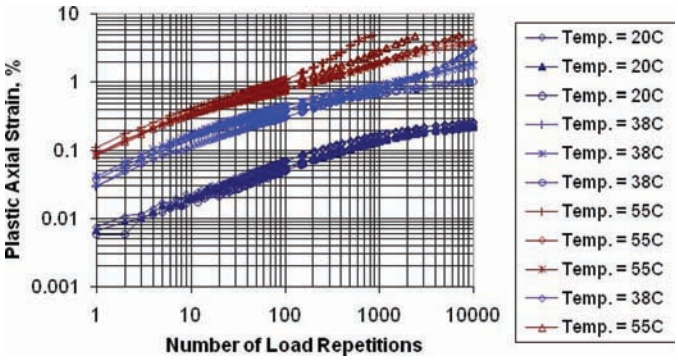

(b) Montana SPS-5 binder layer without RAP mixture.

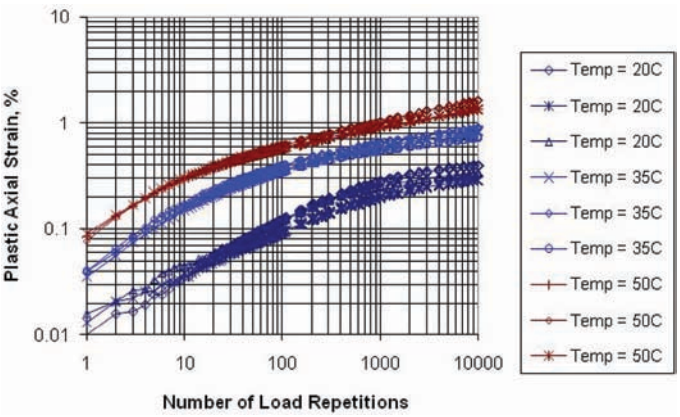

(c) Wisconsin SPS-1 wearing surface mixture.

Figure 63. Repeated-load triaxial test results for three of the mixtures.

2.9.1 Slope of Secondary Region: Exponent for Number of Load Cycles

This section explains determination of the m-values or slopes for individual test specimens and determination of the representative m-value for a specific mixture across all temperatures.

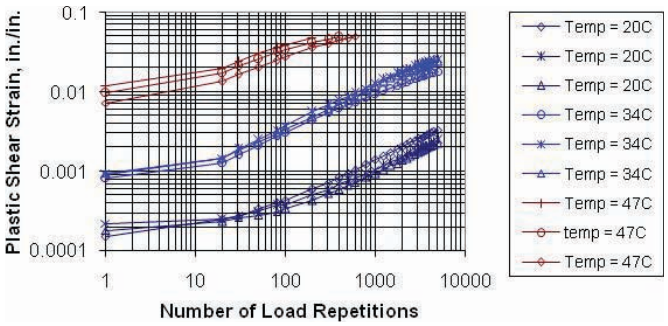

(a) Missouri SPS-5 binder layer with RAP mixture.

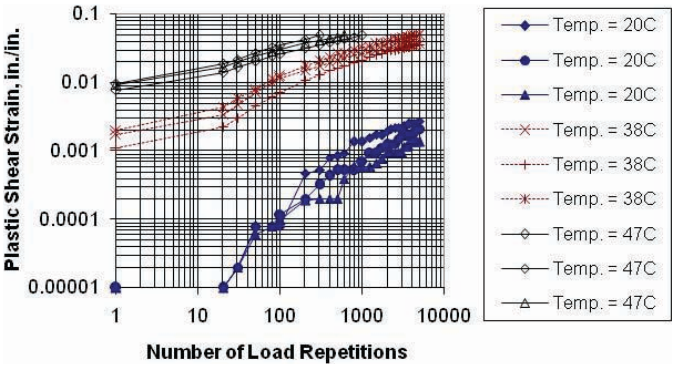

(b) Montana SPS-5 binder layer without RAP mixture.

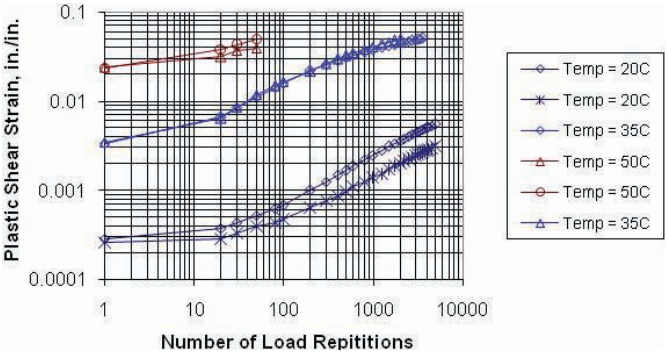

(c) Wisconsin SPS-1 wearing surface mixture.

Figure 64. Repeated-load constant-height shear test results for three of the mixtures.

2.9.1.1 Determination of m*-Values for Individual Test Specimens*

Systematic differences exist between the repeated-load triaxial and constant-height shear tests (refer to Figures 63 and 64). The accumulated plastic axial strain increases at the beginning of the repeated load triaxial, but at a decreasing rate until the rate of change becomes relatively constant (compare Figures 46 and 47 to Figure 63). Conversely, the rate of increase of the accumulated plastic shear strain is small at the beginning of the repeated-load shear test and then increases until the rate of change becomes relatively constant (compare Figure 53 to Figure 64). The initial areas for both tests should be excluded from determining the slope of the secondary region or *m*-value.

The average slope of the secondary region for laboratory repeated-load tests is determined in accordance with the procedure summarized in Section 2.7.1.2 and based on a moving range of loading cycles. (For example: 1 to 10, 2 to 20, 3 to 30, . . . ; 10 to 100, 20 to 200, 30 to 300, . . . ; 100 to 1000, 200 to 2000, 300 to 3000, ...) The secondary region is the area where the slope or increase in accumulated plastic strain becomes relatively constant with number of loading cycles (refer to Figures 46, 47, and 53). The moving range procedure is relatively easy to use to illustrate the accumulated plastic strain pattern for a particular test specimen. The range, however, is dependent on the data or test results (similar to preparing a histogram); a range of load cycles that is too small will exhibit high variation in the computed slopes from point to point, while a range that is too large will not exhibit much change in the computed slopes over the number of load cycles. The typical range of loading cycles varies between some constant number of load cycles (10 to 200) and a decade, as noted previously. A range of 10 to 200 load cycles was used for most of the tests.

Two opposite possibilities exist over the entire number of loading cycles or beyond the secondary region of repeated load tests: (1) the slope continues to decrease with number of loading cycles [refer to Figure 47(b) (Pattern C) and Figure 53(b) (Pattern E)], and (2) the slope starts to increase at an increasing rate (refer to Figure 46). Determining the slope or *m*-value for these conditions is discussed in the following.

- When a test specimen starts to exhibit continual decrease in plastic strains with continued loading cycles (referred to in this report as *plastic strain hardening*), the average slope should be determined for the plastic-strain-hardening region. In some cases, it is difficult to determine whether the slope ever becomes constant or continually decreases. For these cases, the average slope in the plastic-strain-hardening region or outside the primary region should be used.
- When a test specimen exhibits accelerated plastic deformation [slopes start to continually increase at an increasing rate; typically referred to as tertiary flow and characteristic of repeated-load confined, triaxial tests (refer to Figure 46, Pattern A)], that part of the test should be excluded from determining the slope in the secondary region of the test. In other words, the average slope is determined between the primary and tertiary flow regions.

Figures 65 through 67 illustrate the average change in slope for the entire load cycles for the confined, triaxial tests, while Figures 68 through 70 illustrate the same

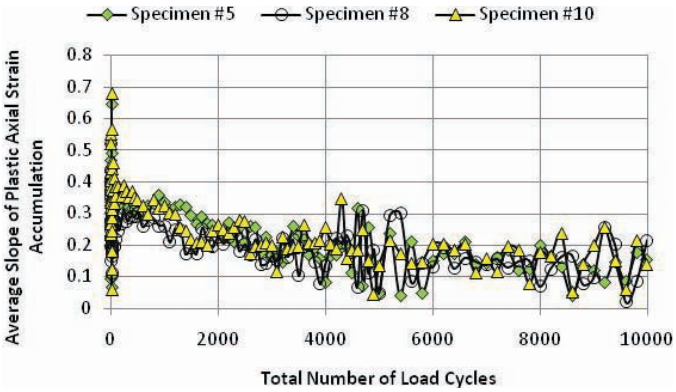

(a) Test temperature equals 68°F [refer to Figure 62(a)].

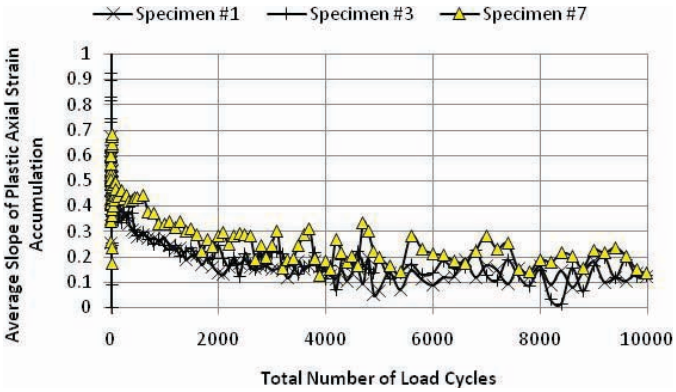

(b) Test temperature equals 95°F [refer to Figure 62(a)].

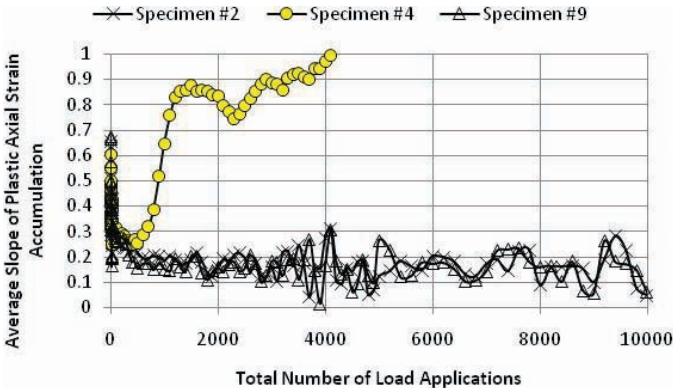

(c) Test temperature equals 117°F [refer to Figure 62(a)].

Figure 65. Change in slope from repeated-load triaxial test results for the Missouri SPS-5 binder layer with RAP mixture.

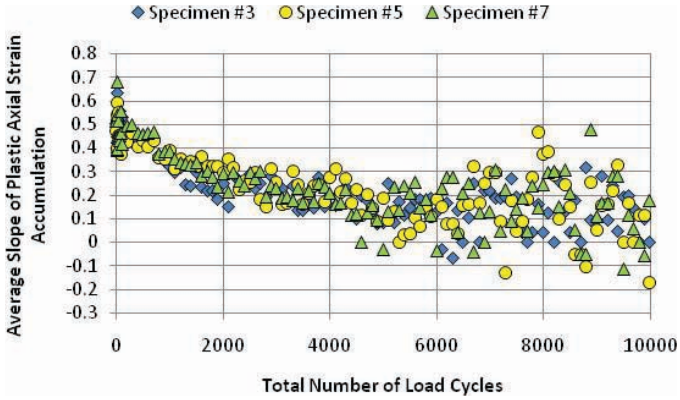

(a) Test temperature equals 68°F [refer to Figure 62(a)].

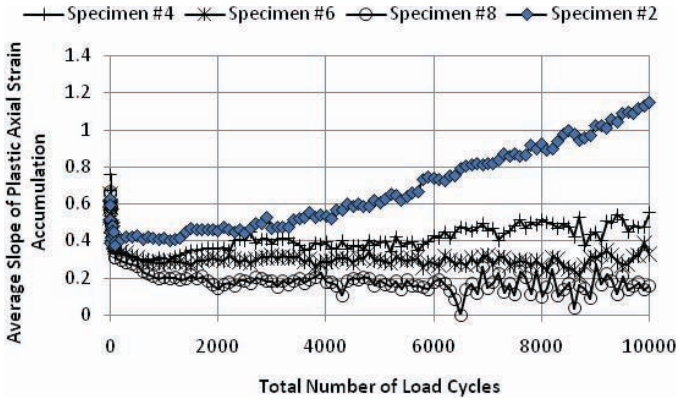

(b) Test temperature equals 100°F [refer to Figure 62(a)].

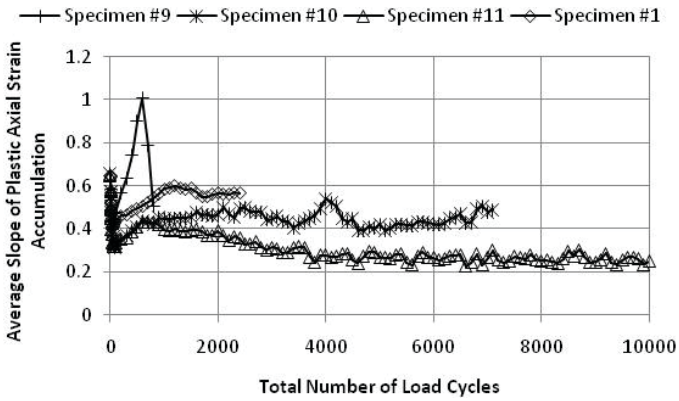

(c) Test temperature equals 131°F [refer to Figure 62(a)].

Figure 66. Change in slope from repeated-load triaxial test results for the Montana SPS-5 binder layer without RAP mixture.

results but for constant-height shear tests. When the slope becomes relatively constant (defined as the secondary region), that value should be used as the exponent for the load cycle term (N) or m-value in the simulation of laboratory test results (refer to Equation 25). Tables 22 and 23 summarize the plastic strain pattern for each test specimen and m-values for the three mixtures from the repeated-load triaxial and shear tests, respectively. The following points should be noted in determining the m-value for individual test specimens.

1. The secondary region begins with a higher number of load cycles for the lower test temperatures of both repeated load tests.
2. The secondary region for specimens that exhibit tertiary flow (Pattern A; refer to Figure 46) can be short, as shown

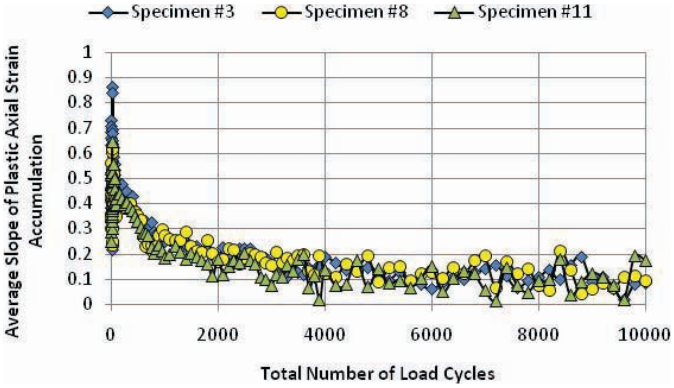

(a) Test temperature equals 68°F [refer to Figure 62(a)].

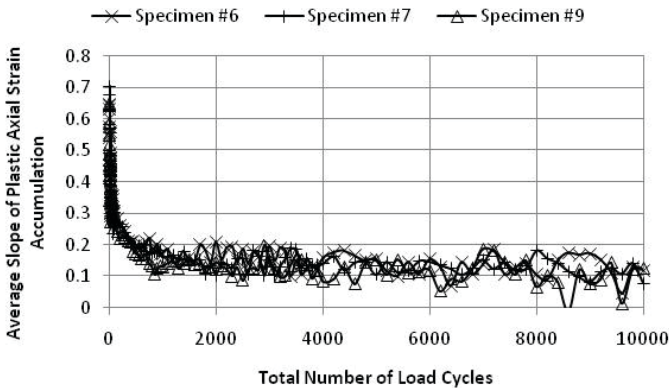

(b) Test temperature equals 95°F [refer to Figure 62(a)].

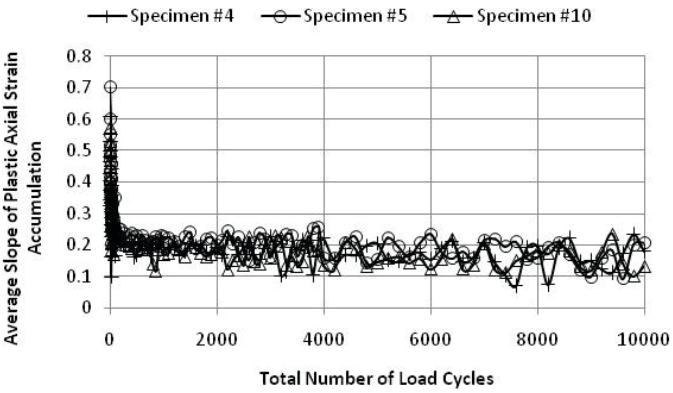

(c) Test temperature equals 122°F [refer to Figure 62(a)].

Figure 67. Change in slope from repeated-load triaxial test results for the Wisconsin SPS-1 wearing surface mixture.

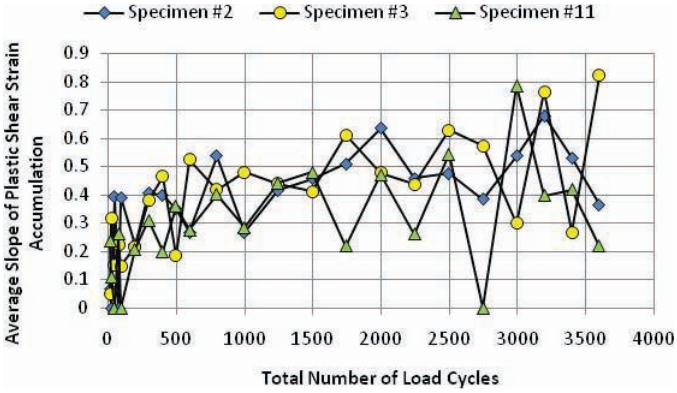

(a) Test temperature equals 68°F [refer to Figure 62(a)].

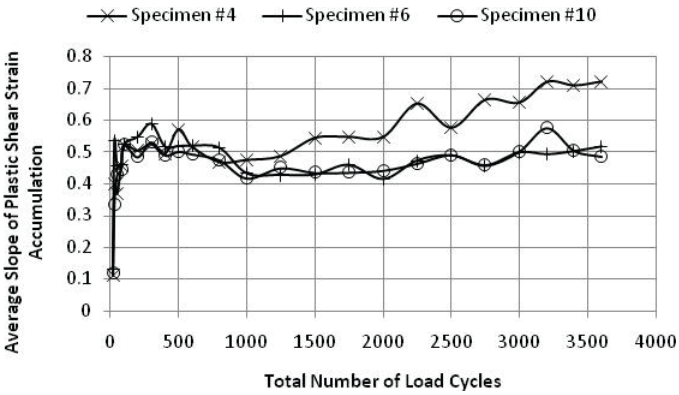

(b) Test temperature equals 95°F [refer to Figure 62(a)].

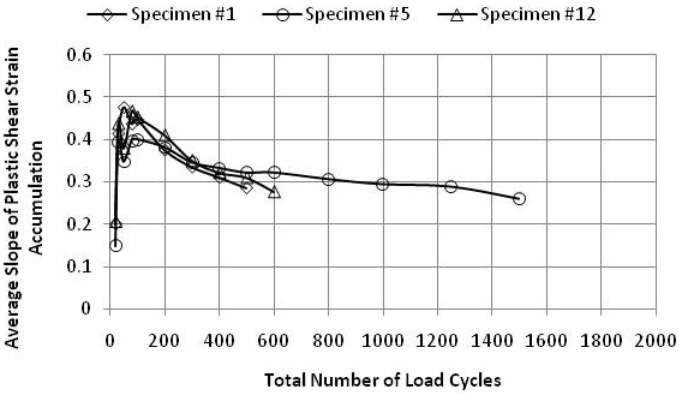

(c) Test temperature equals 117°F [refer to Figure 62(a)].

Figure 68. Change in slope from repeated-load constant-height shear test results for the Missouri SPS-5 binder layer with RAP mixture.

by the test results for specimen #4 of the Missouri SPS-5 mixture [refer to Figure 65(c)]. The reason only one of the three triaxial specimens exhibited tertiary flow is unknown but is not considered an anomaly.

3. The constant-height shear specimens exhibited large plastic strains for the initial load cycle for the higher test temperatures. Some of the plastic shear strains were so large that the specimen reached its maximum shear strain in relatively few load cycles, as exhibited by the Wisconsin SPS-1 wearing surface mixture [refer to Figure 70(c)]. The test temperature was reduced by 5°C to ensure an adequate number of load cycles to determine the *m*-value. Test results from these specimens were generally excluded from determination of the *m*-values and other plastic strain coefficients.
4. Some specimens exhibited erratic behavior in terms of the rate of plastic strain accumulation for the higher test temperatures of both repeated load tests [refer to Figures 66(c) and 70(c)]. The reason for this erratic behavior

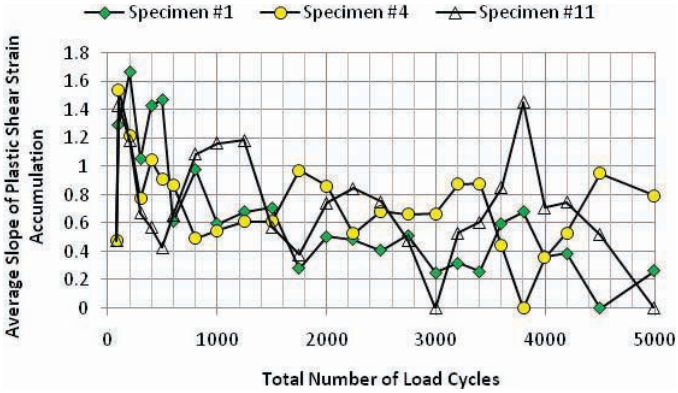

(a) Test temperature equals 68°F [refer to Figure 62(a)].

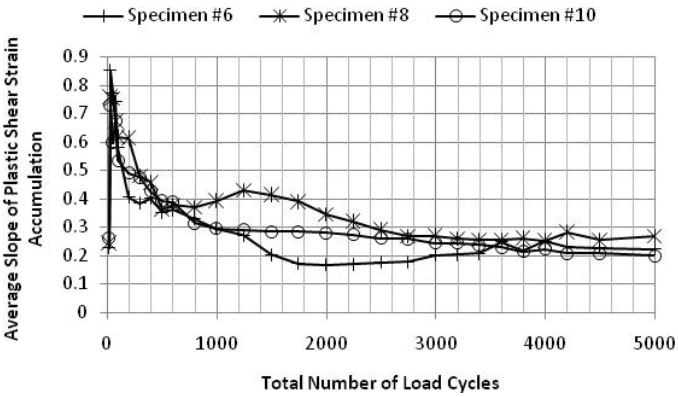

(b) Test temperature equals 100°F [refer to Figure 62(a)].

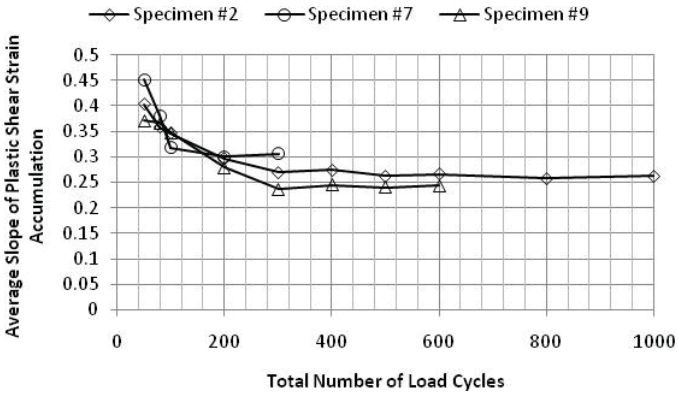

(c) Test temperature equals 117°F [refer to Figure 62(a)].

Figure 69. Change in slope from repeated-load constant-height shear test results for the Montana SPS-5 binder layer without RAP mixture.

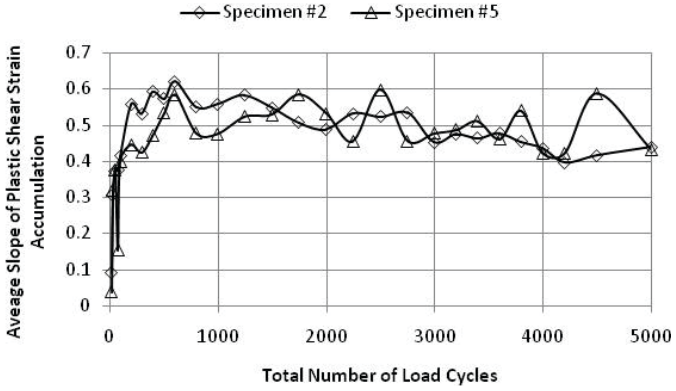

(a) Test temperature equals 68°F [refer to Figure 62(a)].

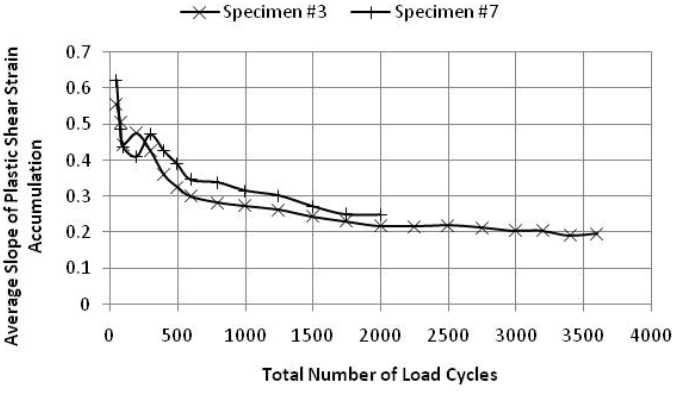

(b) Test temperature equals 95°F [refer to Figure 62(a)].

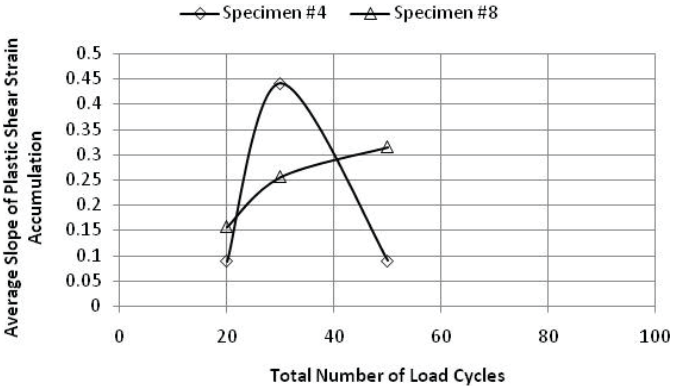

(c) Test temperature equals 122°F [refer to Figure 62(a)].

Figure 70. Change in slope from repeated-load constant-height shear test results for the Wisconsin SPS-1 wearing surface mixture.

is unknown, so the higher test temperature was reduced by 5°C, as noted previously.

2.9.1.2 *Determination of Representative* m*-Value for a Mixture*

The methodology included in the MEPDG Version 9-30A assumes that the slope or *m*-value of the secondary region is independent of test temperature for all of the rut-depth transfer functions. Any change in temperature is accounted for through the temperature term for some rut-depth transfer functions, which only affects the intercept of the transfer function. The exploratory test program (refer to Section 2.6) found that the average slope between the selected test temperatures from the repeated-load triaxial test were approximately equal, supporting that hypothesis. The representative *m*-value for each mixture was determined by the following decision criteria:

Table 22. Repeated-load triaxial test results for the three mixtures included in the demonstration.

Mixture	Test Temp., °F	Test Specimen	Plastic Strain Pattern	Slope, *m*-Value	Intercept Coefficients	
					d	*n*
Missouri; SPS-5 binder mix with RAP	68	5	B	0.17	-11.163	4.0
	68	8	B	0.17		
	68	10	B	0.18		
	95	1	B	0.25		
	95	3	B	0.24		
	95	7	B	0.21		
	117	2	B	0.16		
	117	4	A	0.24		
	117	9	B	0.13		
Montana; SPS-5 binder mix without RAP	68	3	B, but variable	0.10	-11.054	3.0
	68	5	B, but variable	0.08		
	68	7	B, but variable	0.11		
	100	4	B	0.39		
	100	6	B	0.32		
	100	8	C	0.19		
	100	2	A	0.40		
	131	9	A, but variable	0.48		
	131	10	B, but variable	0.43		
	131	11	C	0.25		
	131	1	A	0.44		
Wisconsin; SPS-1 wearing surface mix	68	3	B	0.14	-8.233	2.8
	68	8	C	0.15		
	68	11	B	0.12		
	95	6	B	0.17		
	95	7	B	0.13		
	95	9	B	0.09		
	122	4	B	0.15		
	122	5	B	0.19		
	122	10	B	0.16		

Notes:
The highlighted cells visually separate the results from the three temperatures used in the test program.
The intercept coefficients of *d* and *n* listed above are for Equation 26.

Table 23. Repeated-load constant-height shear test results for the three mixtures included in the demonstration.

Mixture	Test Temp., °F	Test Specimen	Plastic Strain Pattern	Slope, *m*-Value	Intercept Coefficients	
					d	*n*
Missouri; SPS-5 binder mix with RAP	68	2	D, but variable	0.43	-19.448	8.0
	68	3	D, but variable	0.45		
	68	11	D, but variable	0.35		
	95	4	A	0.48		
	95	6	D	0.43		
	95	10	D	0.45		
	117	1	E	0.29		
	117	5	E	0.30		
	117	12	E	0.28		
Montana; SPS-5 binder mix without RAP	68	1	D, but variable	0.41	-22.387	9.8
	68	4	D, but variable	0.61		
	68	11	D, but variable	0.42		
	100	6	D	0.22		
	100	8	D	0.27		
	100	10	E	0.25		
	117	2	D	0.26		
	117	7	D	0.31		
	117	9	D	0.24		
Wisconsin; SPS-1 wearing surface mix	68	2	D	0.47	-14.718	6.2
	68	5	D	0.48		
	95	3	E	0.21		
	95	7	E	0.23		
	122	4	E, but variable	0.24		
	122	8	D, but variable	0.21		

Notes:
The highlighted cells visually separate the results from the three temperatures used in the test program.
The intercept coefficients of *d* and *n* listed above are for Equation 26.

- If the *m*-value (average slope in secondary or plastic-strain-hardening region) does not consistently change with test temperature and the values are statistically the same, average all *m*-values. The average *m*-values determined at the lower test temperature (68°F), however, will probably be different from those measured at the higher test temperatures.
- If the *m*-value for 68°F is statistically different from the higher test temperatures but the values are similar for the higher test temperatures, average the *m*-values at the higher test temperatures.
- If the *m*-value consistently changes with test temperature (increasing or decreasing with test temperature) and all values are statistically different, determine the representative *m*-value at the equivalent annual temperature (refer to Section 2.6.3).

Figures 71 and 72 illustrate the impact of test temperature on the *m*-value for the three mixtures. The next section provides a brief discussion of the test results for each mixture and identifies the more important differences and similarities between the test procedures for deriving that *m*-value. These differences are discussed in Chapter 3 for all mixtures included in the calibration of the different transfer functions.

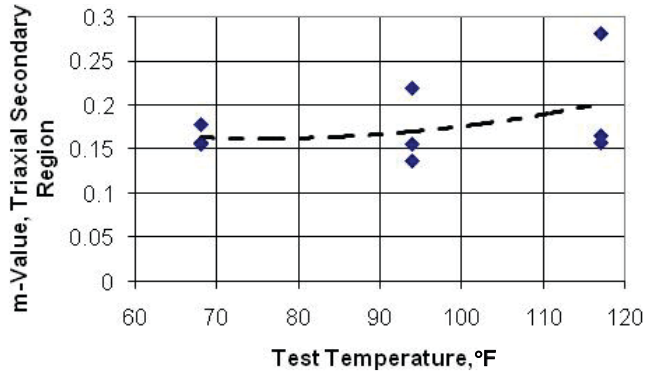

(a) Missouri SPS-5 binder layer with RAP mixture.

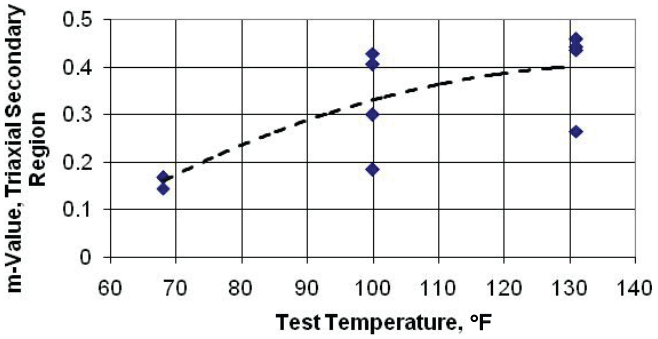

(b) Montana SPS-5 binder layer without RAP mixture.

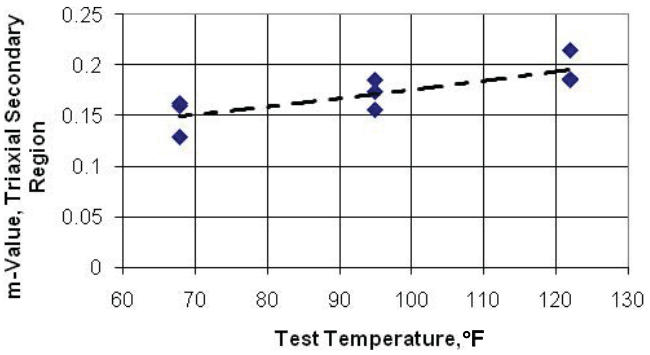

(c) Wisconsin SPS-1 wearing surface mixture.

Figure 71. Average slope in secondary region from repeated-load triaxial tests for three of the mixtures included in the demonstration.

2.9.2 Temperature Exponent: Effect on Intercept from Secondary Region

The temperature exponent was determined from the three test temperatures in accordance with the procedure outlined in Section 2.6.4.5 using Equation 26. Tables 22 and 23 list the laboratory-derived average temperature exponent (*n*) for the repeated-load triaxial and constant-height shear tests, respectively, for the three mixtures used in the demonstration.

The global temperature exponent for the Kaloush transfer function (k_{r2}) is 1.5606 (refer to Equation 1) and 2.767 for the original Asphalt Institute function (refer to Equation 5). For the confined triaxial test, the temperature exponent *n* was found to be significantly greater than the global values for those transfer functions, while it was found to be significantly less for the mixtures included in the exploratory test program (see Section 2.6). The temperature exponent for the repeated-load constant-height shear test results was found to be much greater than for the triaxial test, even though temperature is not included in the WesTrack transfer function.

2.9.3 Intercept from Secondary Region: Equivalent Annual Temperature

Two values are reported for the intercept from repeated load tests and are defined as (1) the primary intercept and (2) the secondary region intercept (also called the steady-state region). The primary intercept is the plastic strain recorded after the first load cycle, while the secondary region intercept is the value determined by extrapolating the secondary region back to the plastic strain for the first load cycle (refer to Figures 46, 47, and 53).

Figures 73 and 74 illustrate the two intercepts from the repeated-load triaxial and constant-height shear tests, respectively, for the three mixtures used in the demonstration. As shown, the intercept from both tests is highly temperature dependent. In addition, the primary intercept from the triaxial tests is consistently and significantly lower than the

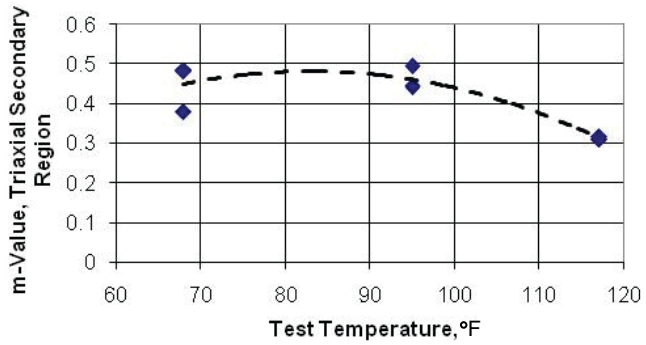

(a) Missouri SPS-5 binder layer with RAP mixture.

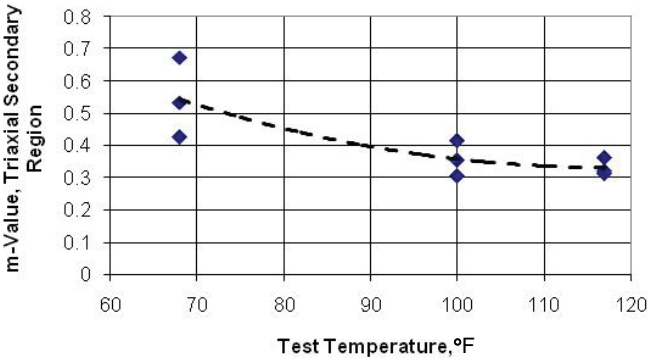

(b) Montana SPS-5 binder layer with virgin mixture.

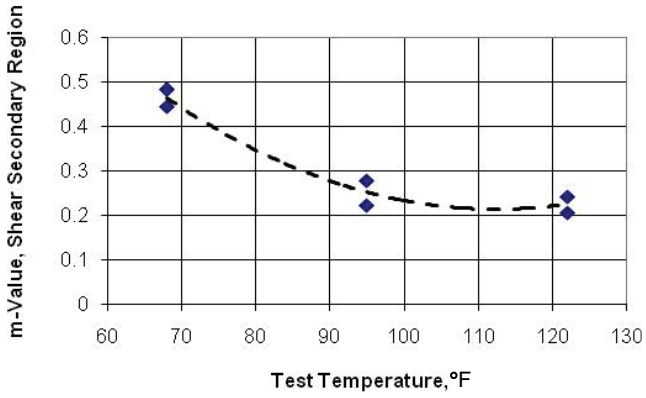

(c) Wisconsin SPS-1 wearing surface mixture.

Figure 72. Average slope in secondary region from repeated-load shear tests for three of the mixtures included in the demonstration.

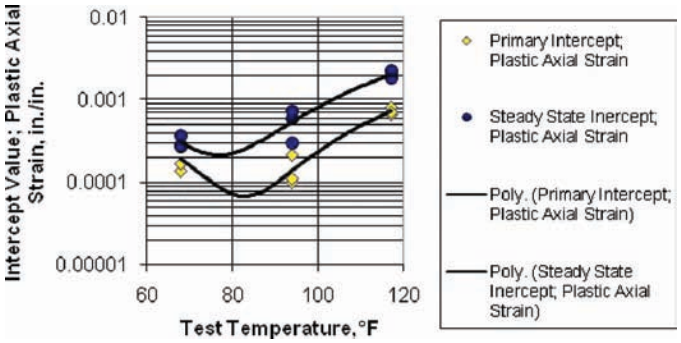

(a) Missouri SPS-5 binder layer with RAP mixture.

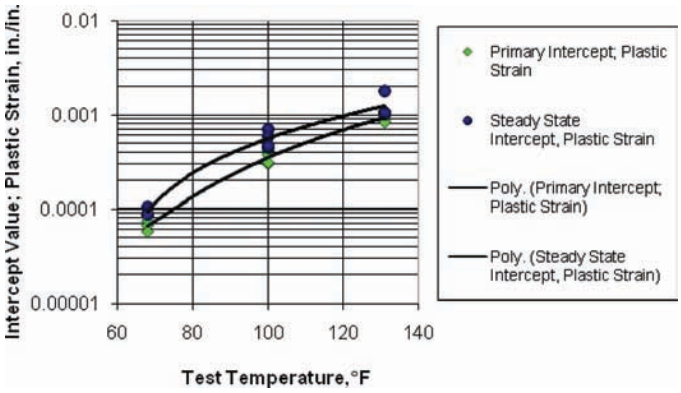

(b) Montana SPS-5 binder layer without RAP mixture.

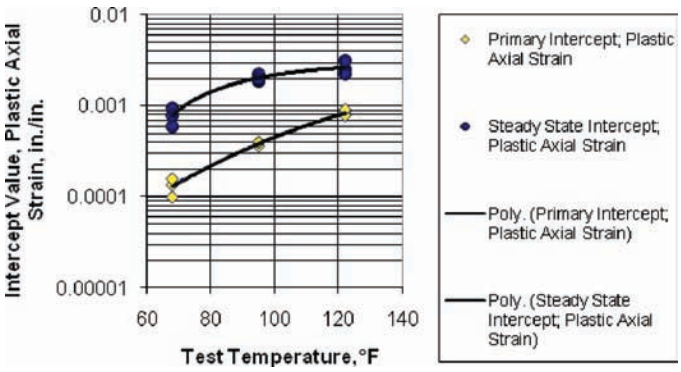

(c) Wisconsin SPS-1 wearing surface mixture.

Figure 73. Average intercept from the secondary region from repeated-load triaxial tests for the three mixtures included in the demonstration.

secondary or steady-state intercept. This observation is consistent with previous experience and can be explained by Figures 46 and 47. Conversely, the primary intercept value from the constant-height shear tests is similar to but can be greater than the secondary intercept. This observation from the test results can be explained by Figure 53.

Another important observation from comparing Figures 73 and 74 is the impact of test temperature on the secondary intercept. The impact of test temperature is much greater for the constant-height shear test than for the triaxial test. Figure 73 illustrates that there is less than a decade difference in the primary or secondary intercepts over the test temperatures for the triaxial tests, while Figure 74 shows that there can more than two decades of difference in the intercepts across the test temperatures for the constant-height shear test. This is the reason why the *n*-value is greater from the constant-height shear tests than the *n*-value from the triaxial tests.

2.9.4 Reconstituted Mixture Test Specimens

Tables 24 and 25 summarize the plastic deformation or strain coefficients determined from the repeated load tests

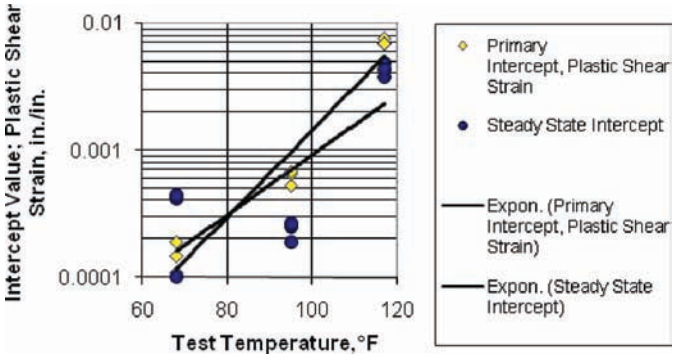

(a) Missouri SPS-5 binder layer with RAP mixture.

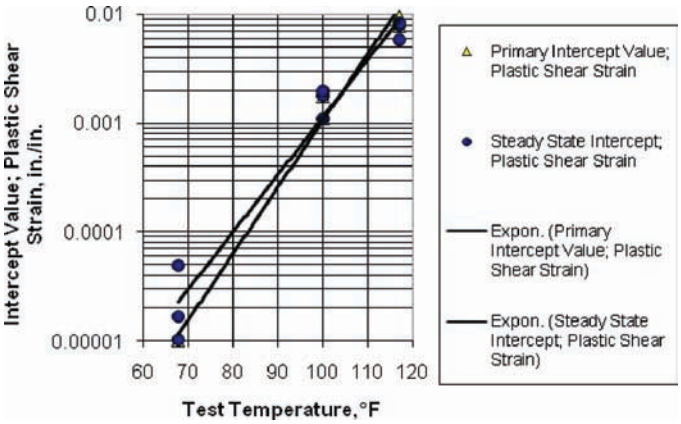

(b) Montana SPS-5 binder layer without RAP mixture.

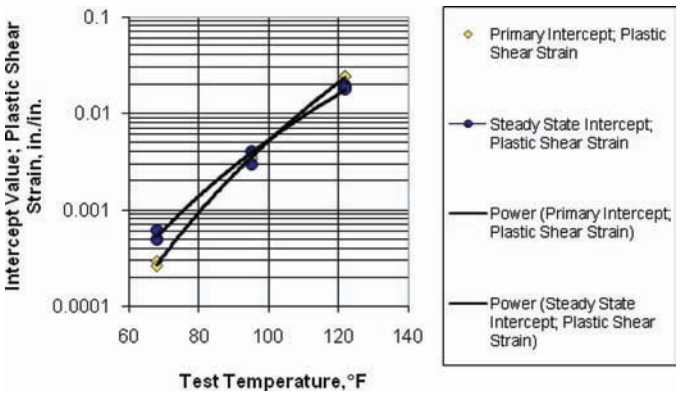

(c) Wisconsin SPS-1 wearing surface mixture.

Figure 74. Average intercept for the secondary region from repeated-load shear tests for the three mixtures included in the demonstration.

for which both tests were used to derive the coefficients. Table 24 lists the plastic strain coefficients from repeated-load triaxial test specimens, while Table 25 lists the values from repeated-load constant-height shear tests. As shown, most of the laboratory-derived values are significantly different from those used in the global calibration process. The following identifies some of the more important findings between the two repeated load tests.

- The variability of *m*-values for the same test temperature increased with increasing temperature for the triaxial tests, while the variability of *m*-values decreased with increasing temperature for the shear tests. This finding was also observed in testing the mixtures used in the exploratory test program (refer to Section 2.6). This is considered an important finding relative to the number of test specimens needed to determine the *m*-value at the same level of confidence—increasing variability requires more test specimens for the same confidence level or interval.
- The *m*-values from the 68°F (20°C) triaxial tests were found to be significantly less than the *m*-values from the shear tests at 68°F. More importantly, the *m*-values from the triaxial tests generally increased with increasing test temperature, while the *m*-values from the shear test consistently decreased with increasing test temperature. Thus, the *m*-values from both tests approach one another at the higher test temperature.
- The average *m*-values determined for the midrange and high test temperatures were found to not be statistically different for all mixtures except for the Missouri mixture tested with the shear test and the Wisconsin mixture tested with the triaxial test.
- The exponent of the *N*-term in the Kaloush transfer function was 0.4761 (refer to Equation 1) and was derived from unconfined, uniaxial repeated load tests. The Missouri and Wisconsin mixtures were found to have *m*-values from the triaxial test that were significantly less than that global value, while only the Montana mixture had values that were slightly less than the global value. Conversely, the exponent of the *N*-term in the WesTrack transfer function was 0.124 (refer to Equation 8), which is significantly less than the measured values. The *m*-values derived from both laboratory tests (triaxial and shear) were found to be similar to or within the same range as the *N*-term exponent of the modified Leahy and Verstraeten transfer functions (a global value of 0.25; refer to Equations 6 and 7). The *m*-value for the modified Leahy transfer function was derived from actual field-measured rut depths.

The laboratory-derived average temperature exponent from the repeated-load triaxial and constant-height shear tests is significantly greater than the global default values for the Kaloush and modified Leahy transfer functions (refer to Equations 1 and 6). The temperature-related intercept was determined based on whether temperature was included as an independent parameter in the transfer function.

- For those rut-depth transfer functions that include temperature as a parameter, the temperature dependency of the intercept is defined through the exponent of the temperature term that is determined from repeated-load test

Table 24. Laboratory-derived plastic strain coefficients from repeated-load triaxial tests of reconstituted specimens (refer to Equations 25 and 26).

Test Section and Mixture Identification	Repeated-Load Confined, Triaxial Tests		
	N-Term Exponent, *m*-Value	Intercept, *d*	Temp. Exponent, *n*
Alabama SPS-6 polymer-modified mix	0.251	-8.28	2.53
Arizona SPS-5, without RAP	0.281	-9.740	3.15
Arizona SPS-5, with RAP	0.265	-6.12	1.74
California, perpetual pavement, CA-47	0.211	-8.885	2.85
California, perpetual pavement, CA-47M	0.185	-7.150	2.10
California, perpetual pavement, CA-52	0.260	-8.898	2.89
Colorado, binder layer with RAP	0.201	-6.633	1.94
Colorado, binder layer without RAP	0.126	-6.799	2.05
Florida PMA mix (NCAT N1 section)	0.251	-8.672	3.0
Florida Neat mix (NCAT N2 section)	0.182	-7.476	2.30
Florida base mix	0.139	-9.195	3.30
Indiana low void mix (NCAT Section 7A)	0.237	-7.311	2.20
Indiana low void mix (NCAT Section 7B)	0.238	-5.48	1.30
Indiana wearing surface mix (Section 8B)	0.207	-5.879	1.50
Mississippi SPS-5, without RAP	0.343	-9.097	3.00
Missouri; SPS-5 binder mix with RAP	0.178	-11.163	4.00
Missouri; SPS-5 binder mix without RAP	0.183	-9.934	3.50
Missouri; SPS-5 wearing surface	0.216	-11.455	4.25
Montana SPS-5 without RAP	0.365	-11.054	3.90
Montana SPS-5 with RAP	0.288	-9.911	3.40
Wisconsin; SPS-1 wearing surface	0.159	-8.233	2.80
Wisconsin SPS-1 ATB mix	0.159	-7.622	2.40
Wisconsin SPS-1 binder mix	0.264	-5.110	1.20

Table 25. Laboratory-derived plastic strain coefficients from repeated-load shear tests of reconstituted specimens (refer to Equations 25 and 26).

Test Section and Mixture Identification	Repeated-Load Constant-Height Shear Tests		
	N-Term Exponent, *m*-Value	Intercept, *d*	Temp. Exponent, *n*
Alabama SPS-6 polymer-modified mix	0.380	-13.619	5.2
Arizona SPS-5, without RAP	0.390	-20.670	8.5
Arizona SPS-5, with RAP	0.334	-12.501	4.65
California, perpetual pavement, CA-47	0.160	-14.955	5.8
California, perpetual pavement, CA-47M	0.221	-10.882	3.6
California, perpetual pavement, CA-52	0.181	-15.102	6.1
Colorado, binder layer with RAP	0.285	-12.852	4.9
Colorado, binder layer without RAP	0.313	-15.111	6.0
Florida PMA mix (NCAT N1 section)	0.242	-23.592	10.1
Florida neat mix (NCAT N2 section)	0.245	-22.856	9.5
Florida base mix	0.262	-23.242	9.8
Indiana low void mix (NCAT Section 7A)	0.280	-18.110	7.50
Indiana low void mix (NCAT Section 7B)	0.245	-17.480	7.30
Indiana wearing surface mix (Section 8B)	0.216	-16.276	6.80
Mississippi SPS-5, without RAP	0.433	-22.523	9.70
Missouri; SPS-5 binder mix with RAP	0.407	-19.448	8.0
Missouri; SPS-5 binder mix without RAP	0.333	-20.811	8.8
Missouri; SPS-5 wearing surface	0.370	-20.308	9.0
Montana SPS-5 without RAP	0.259	-22.387	9.8
Montana SPS-5 with RAP	0.236	-21.400	9.3
Wisconsin; SPS-1 wearing surface	0.237	-14.718	6.2
Wisconsin SPS-1 ATB mix	0.510	-23.913	10.7
Wisconsin SPS-1 binder mix	0.334	-23.070	10.3

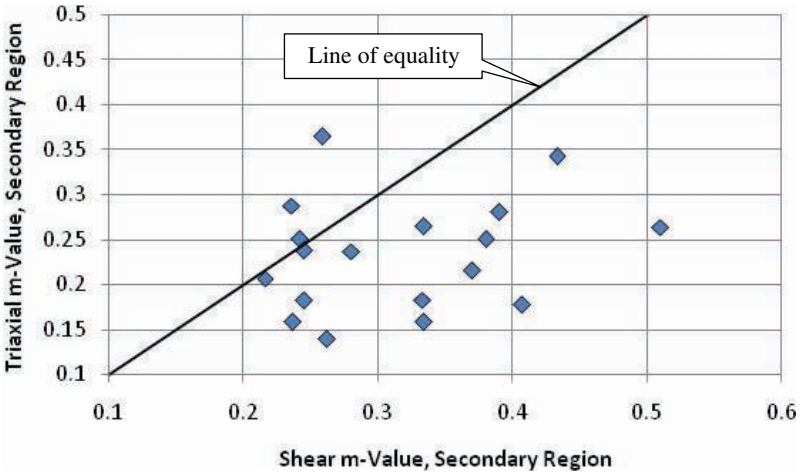

Figure 75. The m-values (refer to Equation 25) derived from different repeated load tests.

results. This determination is part of the calibration procedure explained in Chapter 3.

- For those rut-depth transfer functions that exclude the temperature term, the intercept is determined at the equivalent annual temperature (refer to Section 2.6.3).

It was hypothesized that the two tests would be different, but the relative change in laboratory-derived plastic strain coefficients (refer to Equations 25 and 26) between different mixtures would be the same for the two tests. In other words, a trend or correlation exists between the same plastic strain coefficient measured from the repeated-load triaxial and shear tests (refer to hypothesis #10 in Section 2.4.2). Figures 75 through 78 compare the plastic strain coefficients (refer to Equations 25 and 26) determined from the repeated-load triaxial and constant-height shear tests. As shown, the correspondence between the same coefficients determined from the two tests is poor or nonexistent. This observation implies that the two tests are measuring different mixture responses, which was unexpected. Based on this observation, it was expected that the tenth hypothesis listed in Section 2.4.2 would be rejected—there would be a difference in the error terms of the transfer function used in the calibration process. The coefficients derived from the two test procedures do deviate from one another. The impact of this finding is discussed in Chapter 3.

Figure 79 compares the primary and secondary intercepts for both repeated load tests. As shown, the two intercept values derived from repeated-load shear tests are distributed or fall around the line of equality, while the secondary intercept is consistently and significantly greater than the primary intercept derived from the repeated-load triaxial tests. It is also important to note that there is a large amount of variability between the two intercepts from both tests.

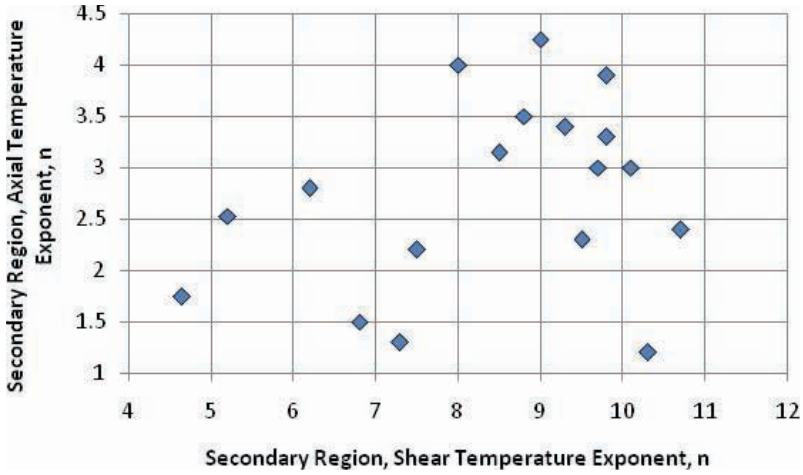

Figure 76. Temperature exponent (n-value; refer to Equation 26) derived from different repeated load tests.

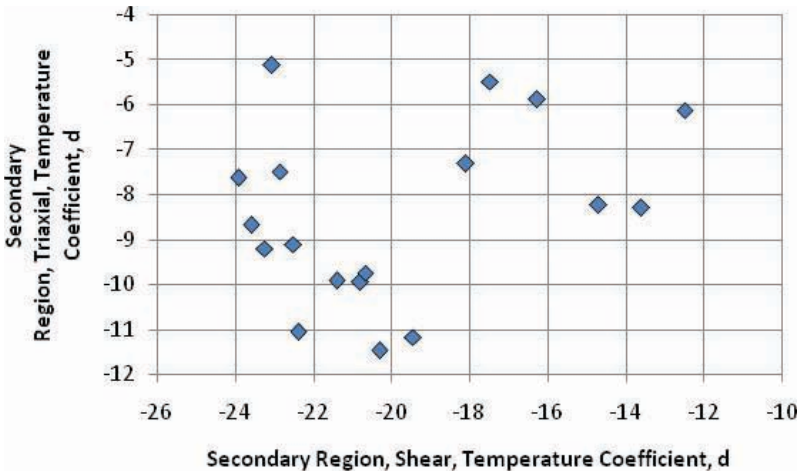

Figure 77. Temperature coefficient (d-value; refer to Equation 26) derived from different repeated load tests.

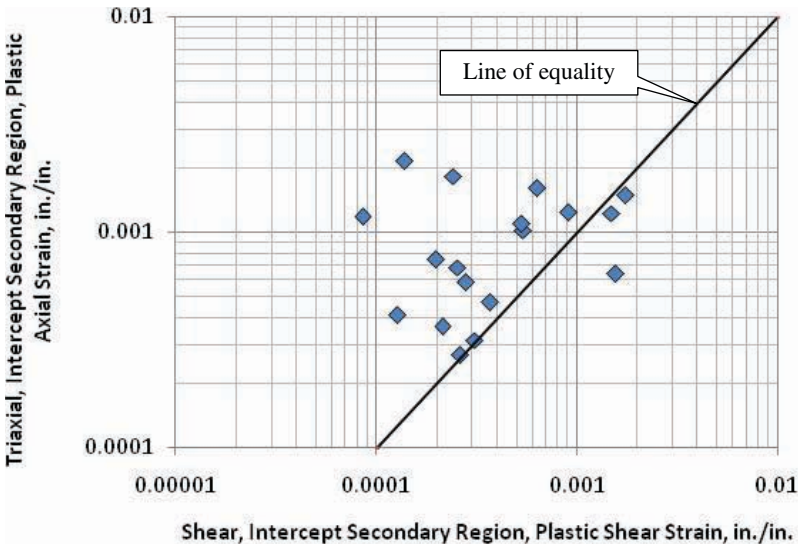

Figure 78. Plastic strain intercept (I_s value; refer to Equation 26) derived from different repeated load tests.

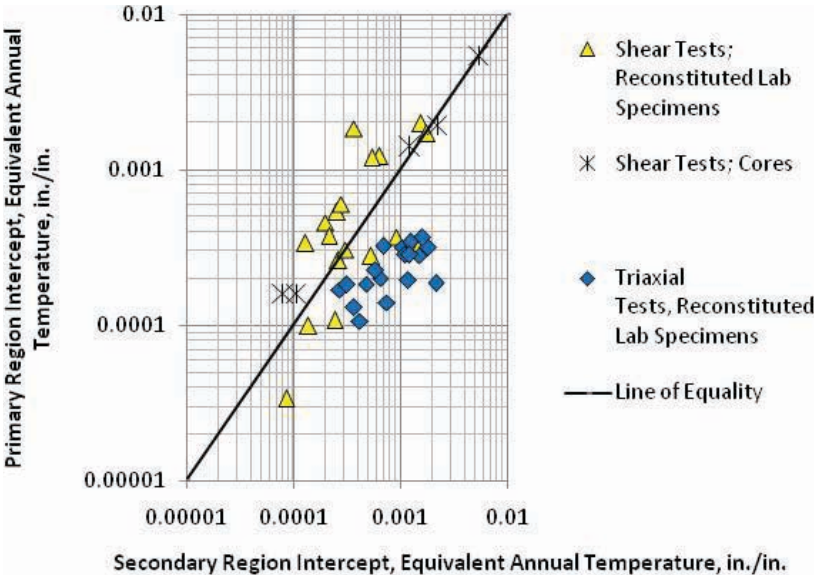

Figure 79. Relationship of intercept values from the secondary and primary regions for both repeated load tests.

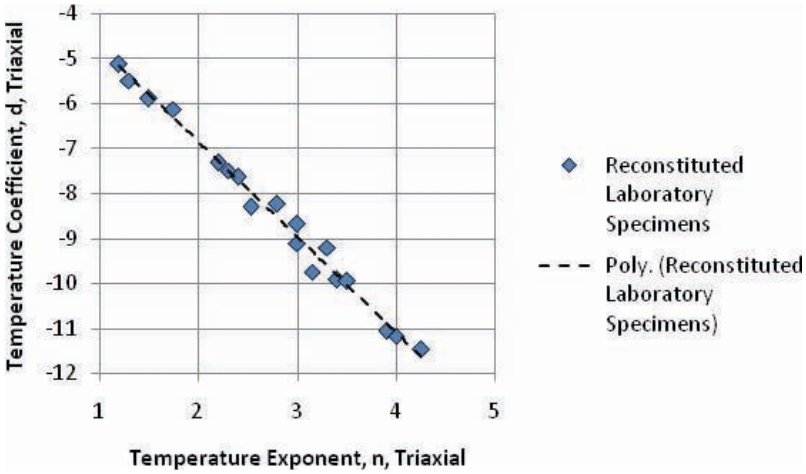

Figure 80. Relationship of temperature exponent (n-value) and coefficient (d-value) from repeated-load triaxial tests (refer to Equation 26).

The more important observation from the laboratory-derived coefficients for the intercept (refer to Equations 25 and 26) from both tests is illustrated in Figures 80 and 81. Figure 80 shows the relationship between the *n*-value and *d*-value from the triaxial tests, while Figure 81 shows the relationship derived from the shear tests. As shown, *d* is related to *n* from both tests.

2.9.5 Field Cores

Cores were recovered and tested from three of the test sections (Arizona, Texas, and Wisconsin), as noted in Section 2.5.3. Some of the cores from the Texas and Wisconsin projects could not be tested. Cracking, disintegration, or both were observed in the wearing surface of the Texas project and in the asphalt-treated base (ATB) mixture for the Wisconsin project. Moisture damage was also present in the lower layers of the Texas project.

Table 26 summarizes the average *m*-values and other plastic strain coefficients derived from field cores with the repeated-load constant-height shear test. Although there are few data points, the intercepts are consistently lower for the field cores in comparison to the reconstituted test specimens, while the *m*-values are similar. This observation supports the hypothesis that the *m*-value does not change over time or with different levels of aging, and supports hypothesis #4 in Section 2.4.2.

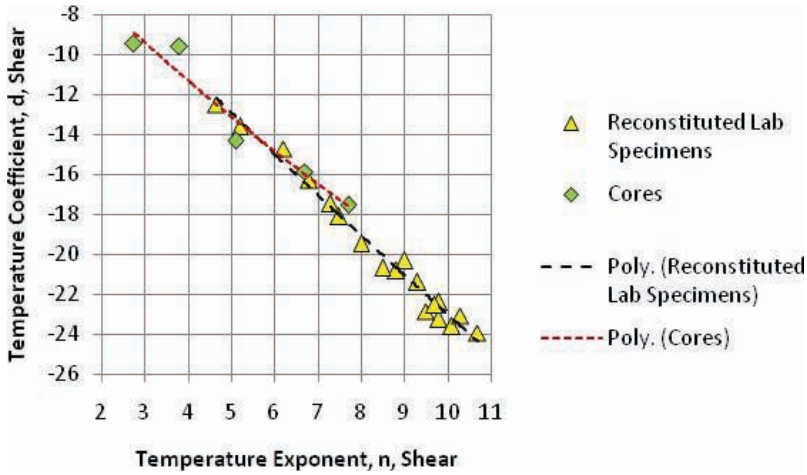

Figure 81. Relationship of temperature exponent (n-value) and coefficient (d-value) from repeated-load shear tests (refer to Equation 26).

Table 26. Laboratory-derived plastic strain coefficients from field cores: repeated-load shear tests (refer to Equations 25 and 26).

Test Section and Mixture Identification	Repeated-Load Constant-Height Shear Tests		
	N-Term Exponent, *m*-Value	Intercept, *d*	Temp. Exponent, *n*
Arizona SPS-5 mixture with RAP	0.261	-9.477	2.75
Arizona SPS-5 mixture without RAP	0.260	-14.302	5.1
Wisconsin SPS-1 wearing surface	0.272	-9.601	3.8
Wisconsin SPS-1 binder mixture	0.227	-17.512	7.7
Wisconsin SPS-1 ATB mixture	0.307	-15.840	6.7

The relationship or correlation between the intercept from the secondary and primary regions for the field cores is compared to the reconstituted, short-term aged, laboratory-compacted specimens in Figure 79. As shown, the field cores resulted in a similar relationship around the line of equality. This finding supports hypothesis #4 in Section 2.4.2 in that the test results from short-term, laboratory-compacted specimens can be used to predict the long-term rut depths or the rutting evolution for a wide range of mixtures.

Another important observation is that the *n* versus *d* relationship (refer to Equation 26) derived from the field cores is the same as the relationship derived from reconstituted, short-term aged, laboratory-compacted specimens (refer to Figure 81). These comparisons illustrate the value of being able to test field cores after construction and at different time periods to determine the effect of aging on the plastic strain coefficients—a benefit and advantage of the repeated-load constant-height shear test.

CHAPTER 3

Data Interpretation and Application

3.1 Verification of Transfer Functions with Global Calibration Coefficients

The MEPDG Version 9-30A was executed using each transfer function to predict the rut depths for the test sections listed in Tables 4 and 5 and verify the values of the global coefficients. The verification of the transfer functions was completed in accordance with the AASHTO *Manual of Practice for Local Calibration of the Mechanistic–Empirical Pavement Design Guide* to judge whether the transfer functions and global coefficients were a reasonable simulation of the measured rut depths (AASHTO, 2010). Two parameters were used in determining whether the transfer function was adequate or needed to be recalibrated to the specific features under evaluation: the slope and intercept between the predicted and measured values.

The verification/calibration/validation sampling template was designed to accomplish three objectives (refer to Figure 13):

1. Determine whether there is bias in the rut depth predictions or simulation model.
2. Establish the cause of any bias, if found through the validation process.
3. Determine the calibration coefficients or function to eliminate any bias, reduce the standard error of different rut-depth transfer functions, or both.

This part of Chapter 3 evaluates the transfer functions included in the MEPDG Version 9-30A to determine whether any are considered appropriate for use without modification.

3.1.1 Global Default Values: Input Level 3

The transfer functions and their global coefficients included in Section 2.1.2 were used to predict the rut depths measured on the test sections included in Tables 4 and 5. Figures 1 through 4 include comparisons of the predicted and measured time-series rut depths for a range of mixtures, pavement structures, and test sections using the global transfer functions. Figures 82 and 83 provide some additional comparisons of the predicted and measured time-series rut depths to illustrate the variation in the time-series data between the measured and predicted rut depths.

Figures 84 through 88 compare the predicted and measured rut depths and the residual error from the transfer functions versus HMA thickness, while Table 27 summarizes the statistical terms from these comparisons. As shown, the magnitudes and increases in rut depth over time are different—none of the transfer functions consistently predicted the magnitude and change in magnitude of rut depths over time. One reason for the extensive scatter is the selection process for many of the test sections, which included anomalous projects identified from other studies, projects with both modified and neat HMA mixtures, and projects with a wide range of HMA thickness and support conditions.

Use of the NCHRP Project 1-40B procedure to adjust the coefficients of the Kaloush transfer function is included in Section 3.3.

In summary, none of the rut-depth transfer functions using their global coefficients are believed to provide an accurate simulation of the measured rut depths, confirming that one set of plastic strain values is insufficient for use over a diverse set of dense-graded HMA and pavement structures. [Note: Results from the statistical analysis or *p*-values from the Student's *t*-test for the line of equality and origin are not provided because of the extensive variability shown in Figures 84 through 88. It is rather obvious that the hypothesis (that the global transfer function provides a reasonable simulation of the measured rut depths) is rejected and that the standard error terms are large, suggesting a poor correlation.] As such, the rut-depth transfer functions need to be recalibrated, redefined, or laboratory repeated-load plastic deformation tests used to improve on the accuracy and precision of the transfer functions.

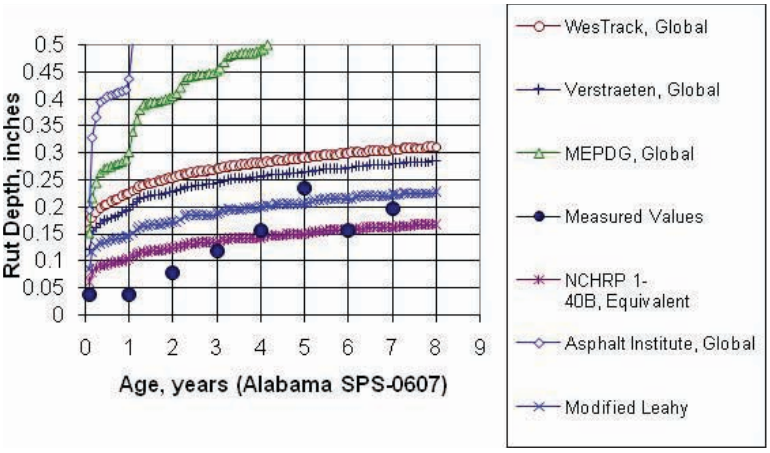

(a) HMA overlay of PCC pavement, crack and seat section; Alabama SPS-6, Section 0607.

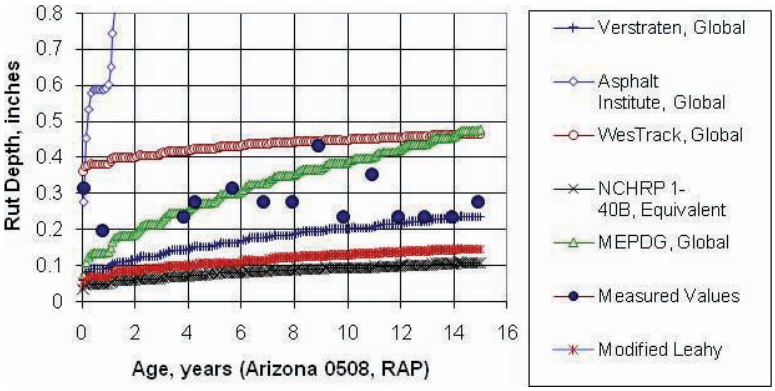

(b) HMA overlay of HMA pavement; Arizona SPS-5, Section 0508.

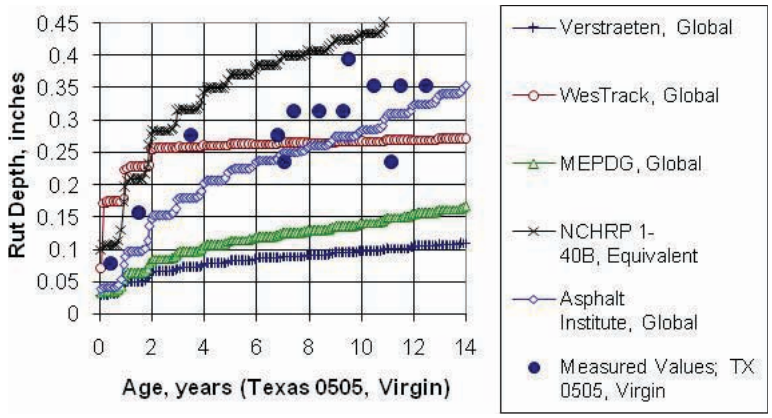

(c) HMA overlay of HMA pavement; Texas SPS-5, Section 0505.

Figure 82. Comparison of predicted and measured time-series rut depths for HMA overlay projects.

Prior to starting the recalibration process, an analysis of the residual errors (refer to Figures 84 to 88) was completed relative to the sampling template (refer to Figure 13). The following identifies observations from the analysis.

- **Large standard errors:** The standard errors resulting from these comparisons are large in relation to values that have been previously reported for all transfer functions, with the exception of those reported in the AASHTO *Local Calibration Guide* using the global values for the plastic strain coefficients; values from 0.10 in. to 0.20 in. were reported for the LTPP sites in the demonstration (AASHTO, 2010). One reason for these high error terms is the diversity of conditions and mixtures for the projects selected for

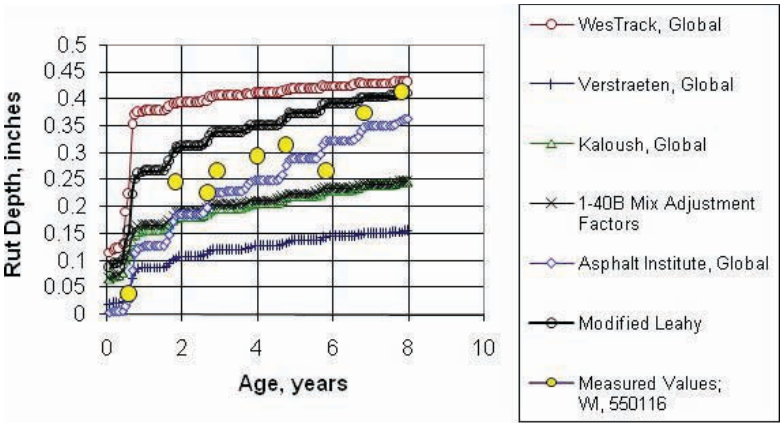

(a) Wisconsin SPS-1 site, section 55-0116, with deep strength HMA.

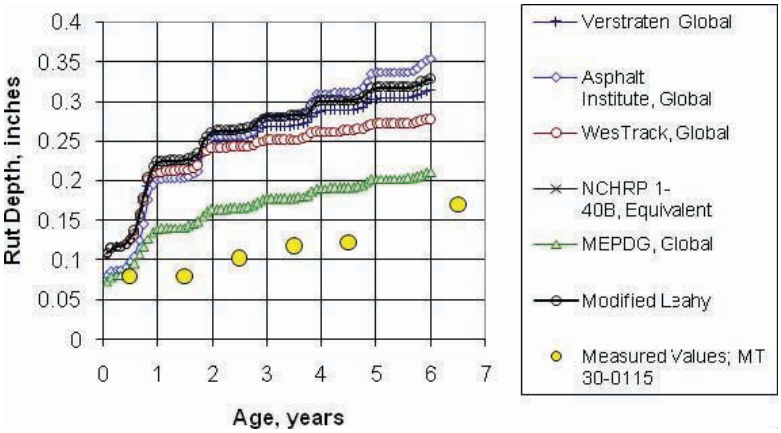

(b) Montana SPS-1 site, Section 30-0115, with asphalt treated base.

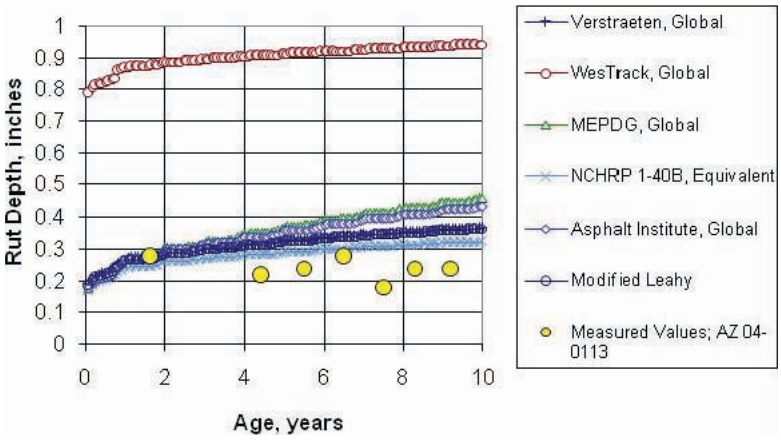

(c) Arizona SPS-1 site, Section 30-0113, with crushed stone base.
Note: The WesTrack function overpredicts the measured values because of the thin HMA layer and lower modulus aggregate base.

Figure 83. Comparison of predicted and measured time-series rut depths for new construction projects.

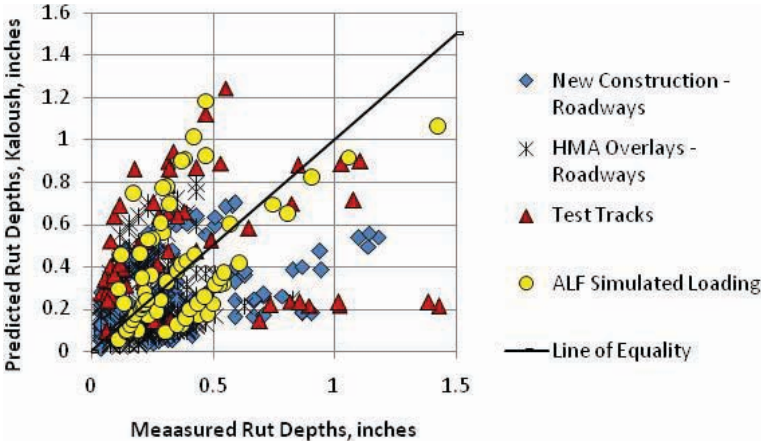

(a) Comparison of measured and predicted rut depths for different pavement structures.

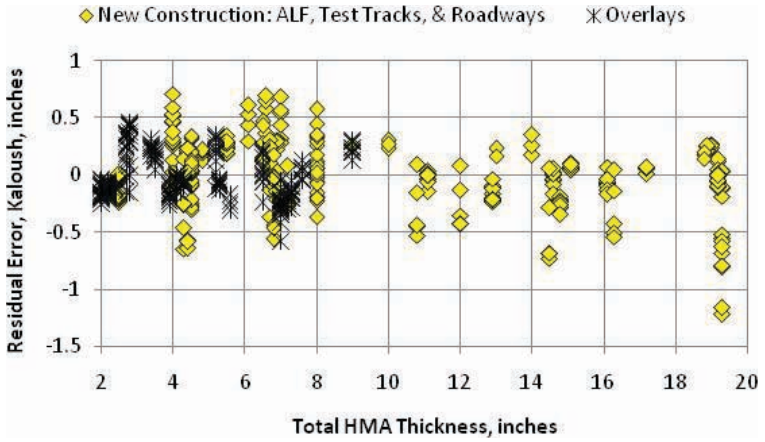

(b) Residual error as a function of total HMA thickness (new mixtures) for new construction and overlays.

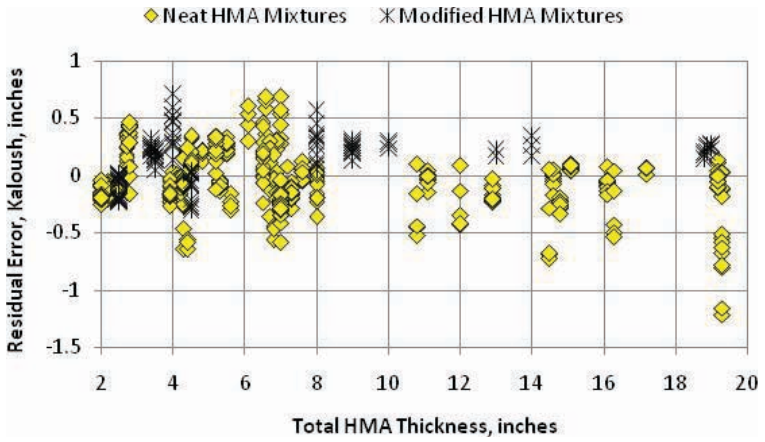

(c) Residual error as a function of total HMA thickness (new construction) for neat and modified HMA mixtures.

Figure 84. Comparison of predicted and measured rut depths for the Kaloush transfer function.

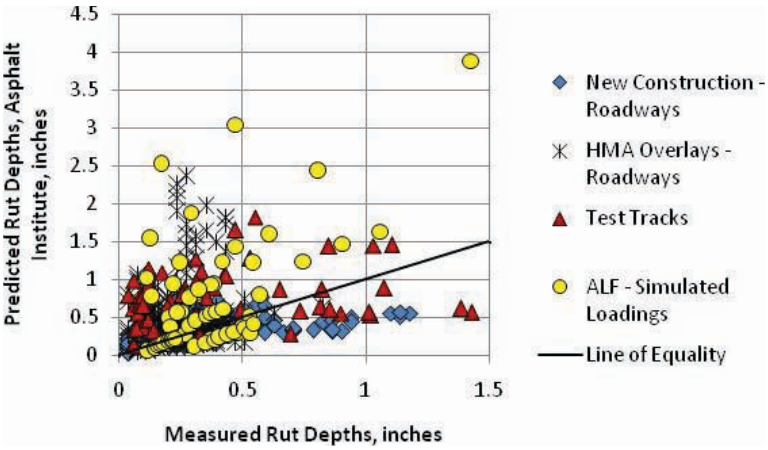

(a) Comparison of measured and predicted rut depths for different pavement structures.

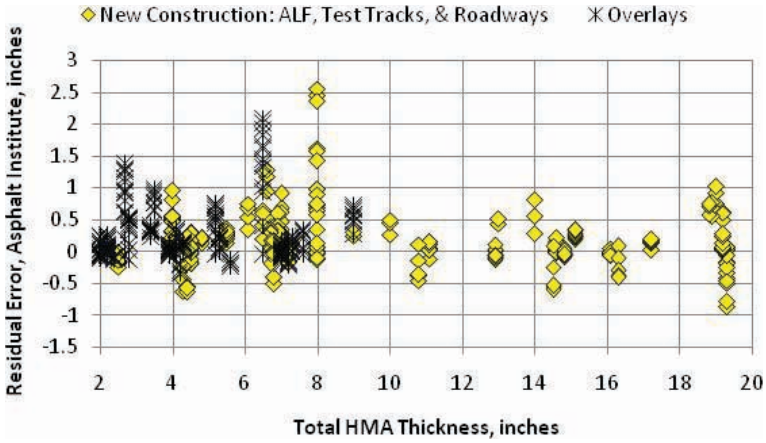

(b) Residual error as a function of total HMA thickness (new mixtures) for new construction and overlays.

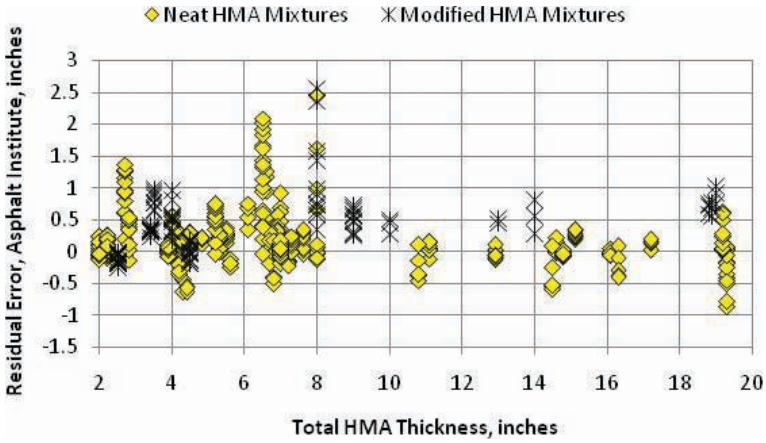

(c) Residual error as a function of total HMA thickness (new construction) for neat and modified HMA mixtures.

Figure 85. Comparison of predicted and measured rut depths for the Asphalt Institute transfer function.

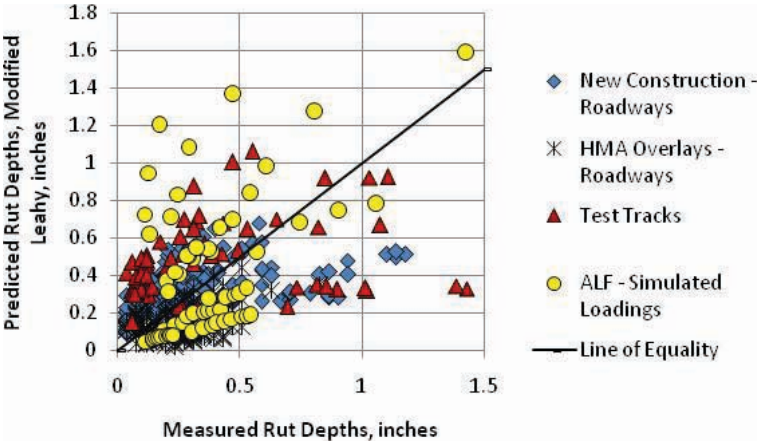

(a) Comparison of measured and predicted rut depths for different pavement structures.

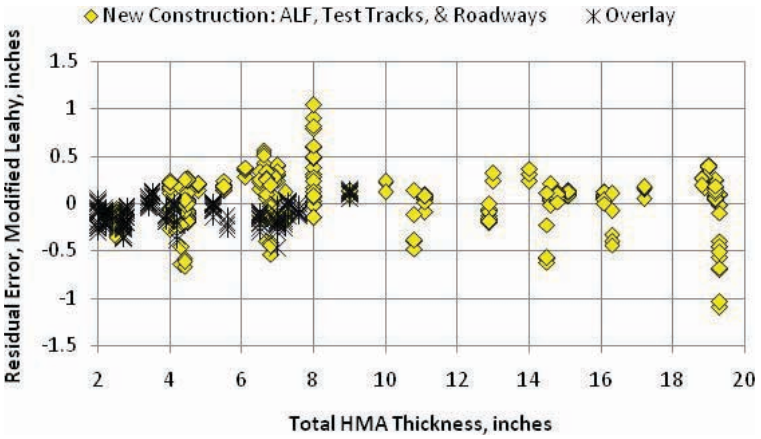

(b) Residual error as a function of total HMA thickness (new mixtures) for new construction and overlays.

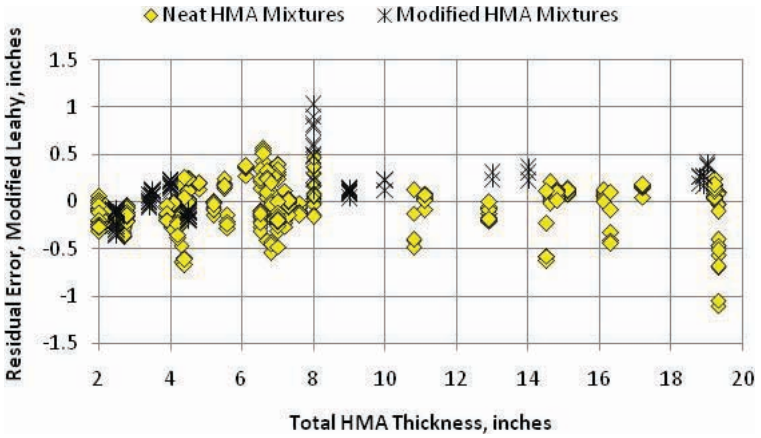

(c) Residual error as a function of total HMA thickness (new construction) for neat and modified HMA mixtures.

Figure 86. Comparison of predicted and measured rut depths for the modified Leahy transfer function.

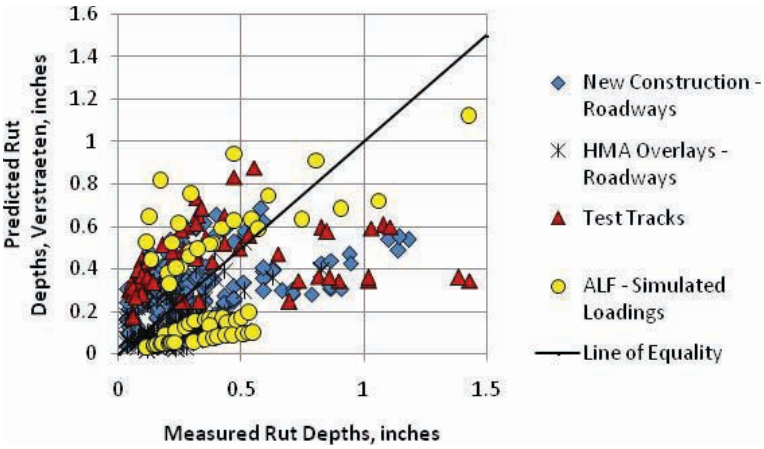

(a) Comparison of measured and predicted rut depths for different pavement structures.

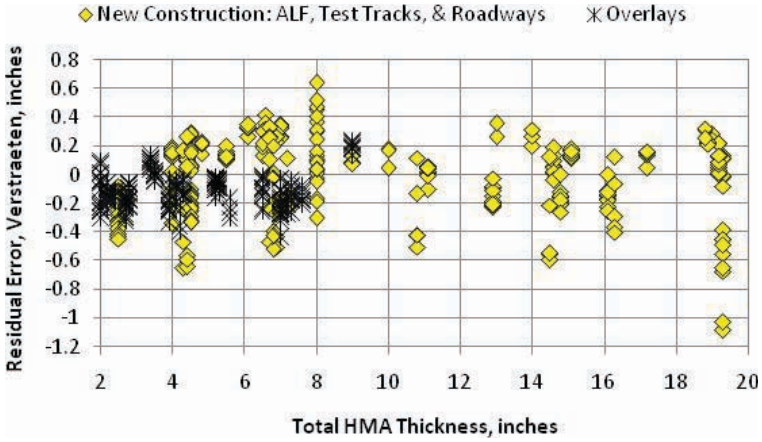

(b) Residual error as a function of total HMA thickness (new mixtures) for new construction and overlays.

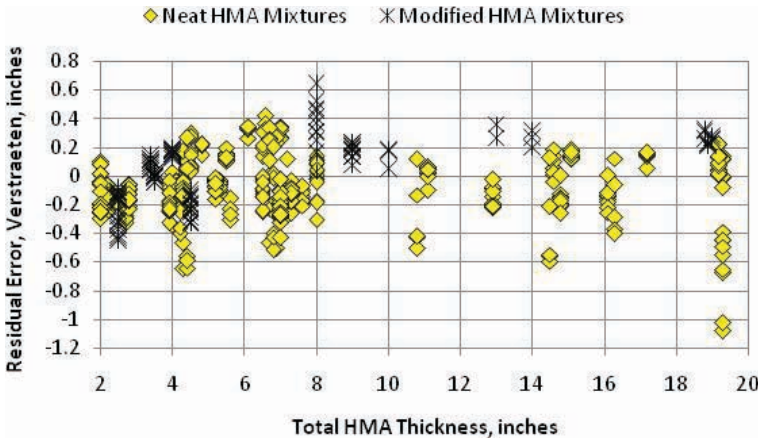

(c) Residual error as a function of total HMA thickness (new construction) for neat and modified HMA mixtures.

Figure 87. Comparison of predicted and measured rut depths for the Verstraeten transfer function.

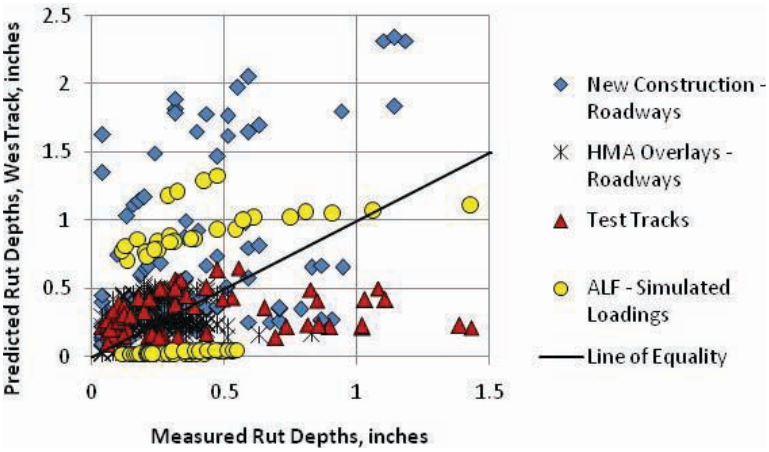

(a) Comparison of measured and predicted rut depths for different pavement structures.

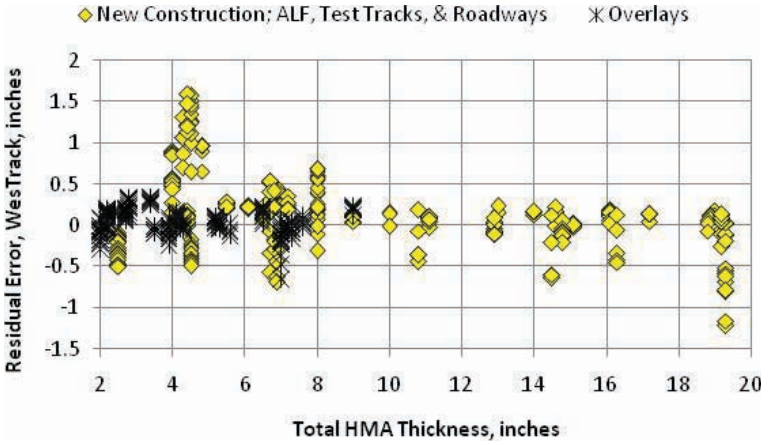

(b) Residual error as a function of total HMA thickness (new mixtures) for new construction and overlays.

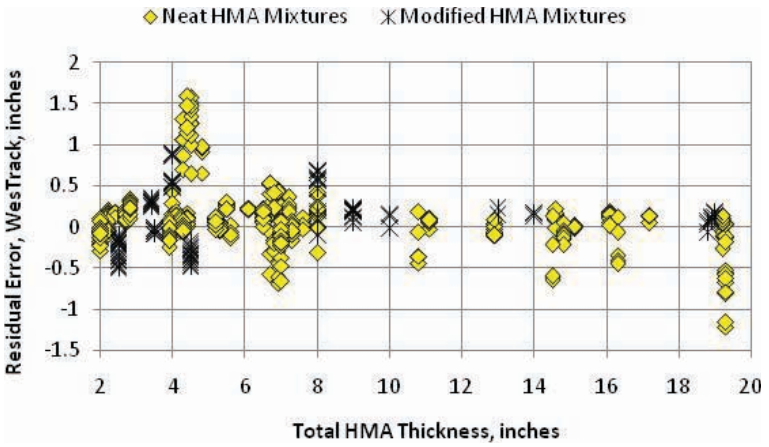

(c) Residual error as a function of total HMA thickness (new construction) for neat and modified HMA mixtures.

Figure 88. Comparison of predicted and measured rut depths for the WesTrack transfer function.

Table 27. Statistical parameters of comparison between predicted and measured rut depths for each rut-depth transfer function using the global coefficients—Input Level 3.

Transfer Function	Statistical Parameters for the Global Plastic Deformation Values				
	Number of Data Points	Bias, in.	Standard Error, s_e	s_e/s_y	R^2
Kaloush (Equation 1)	451	-0.0077	0.2610	1.201	Very low
Asphalt Institute (Equation 5)	451	0.2231	0.4424	2.036	Very low
Modified Leahy (Equation 6)	433	-0.0247	0.2406	1.107	Very low
Verstraeten (Equation 7)	451	-0.0588	0.2197	1.0119	Very low
WesTrack (Equation 8)	451	0.0908	0.3574	1.6448	Very low

Notes:
1. See text for an explanation for the poor statistical parameters included in this table.
2. Includes test sections used for Input Levels 1 and 2; refer to Tables 4 and 5.
3. Use of the NCHRP Project 1-40B mixture adjustment relationships is included in Section 3.4.

verifying the global calibration values. These projects include a wide range of HMA thicknesses, support conditions, structures, mixture types, and volumetric properties. None of the global values for the transfer function take into account the difference between modified and neat HMA mixtures without testing, as well as other mixture properties. It was assumed that dynamic modulus would explain any difference between the mixtures in terms of rutting resistance, which is an incorrect assumption.

- **Transfer function bias:** The Kaloush and modified Leahy transfer functions were the only ones with a bias below the tolerable level of 0.05 in. Potential reasons for the higher bias are noted in the following bullets.
- **Rutting in the unbound layers:** An observation for all transfer functions is that predicted rut depths in the unbound layers are higher than observed or reported from forensic investigations for most of the test sections that were constructed in accordance with the specifications. The predicted rut depths were found to be lower than in those sections where rainfall or construction-related issues caused an increase in the water content of the granular base and/or embankment soils (for example, the Nebraska and Kansas SPS-1 projects). Rutting in the unbound layers is discussed further in Section 3.2.2.
- **Total HMA thickness:** As the total HMA thickness decreases for new construction projects, the residual error of the Kaloush and WesTrack transfer functions becomes positive; the MEPDG overpredicts the measured rut depths for thin HMA layers. This observation has been reported from other local calibration studies of the MEPDG for the Kaloush transfer function (for example, Arizona, Missouri, Utah, and Wisconsin).
- **Neat versus modified HMA mixtures:** There is a consistent difference in the residual errors between the neat and modified HMA mixtures. All transfer functions in the MEPDG overpredict the rut depths for the thicker HMA modified layers in comparison to neat HMA layers (refer to Figures 84 through 88). In other words, dynamic modulus does not accurately account for the benefit from PMA mixtures. The Asphalt Institute also reported this observation (Asphalt Institute, 2005). For the WesTrack transfer function, HMA thickness effects overshadow the effect of mixture type.
- The Asphalt Institute transfer function has the larger standard error and positive bias (refer to Table 27). The reason for the large positive bias and high error term is that the temperature coefficient (a value of 2.767; refer to Equation 5) and viscosity are indirectly considered twice. The lower-viscosity asphalt reduces the dynamic modulus and also increases the predicted rut depth, independent of its effect on dynamic modulus.
- The modified Leahy transfer function has a standard error similar to the Kaloush equation without directly considering temperature and viscosity, but it includes deviator stress, effective asphalt content by volume, and air void content for predicting rutting (refer to Equation 6).
- The WesTrack transfer function has a higher bias than the other transfer function based on triaxial tests, except for the Asphalt Institute function. The reason for the higher positive bias is that the rut depths for relatively thin HMA layers were significantly overpredicted (refer to Figure 88).

In summary, HMA thickness, mixture type, and rutting in the unbound layers are the reasons for the poor correlation between the measured and predicted rut depths.

3.1.2 Dynamic Modulus

The AASHTO *Manual of Practice for the Mechanistic–Empirical Pavement Design Guide* requires measurement of HMA dynamic modulus values for Input Level 1 (AASHTO, 2008). Dynamic modulus values were measured for all HMA

mixtures included in the laboratory production test program, as well as for other HMA mixtures included in Tables 4 and 5. Table 21 and Appendix D provide the dynamic modulus values for the mixtures included in the production test program for this project. These values were used to predict the rut depths using the global default values for the plastic strain coefficients of each transfer function.

Figures 89 and 90 compare the predicted and measured rut depths for some of these sites in comparison to the use of the global default values. As shown, use of dynamic modulus values did not improve the rut depth predictions through reductions in bias and standard error. This observation suggests that hypothesis #5 (see Section 2.4.7) is accepted or confirmed—dynamic modulus by itself will not adequately account for the rutting resistance of HMA mixtures. It also suggests, however, that the Witczak dynamic modulus regression equation provides a reasonable prediction of the measured dynamic modulus values; there is little difference in predicted rut depths between the use of the regression equation or the laboratory-measured dynamic modulus for the core test sections. As such, dynamic modulus measured in the laboratory in accordance with AASHTO T 79 by itself did not improve on the accuracy and precision of the transfer functions.

3.1.3 Summary: Redefining the Input Levels

Results of the comparison of the measured and predicted values using the global plastic strain coefficients with and without laboratory-measured dynamic modulus values suggest that all of the transfer functions need to be recalibrated or repeated load tests used to determine values for the mixture-specific plastic strain coefficients. In other words, repeated-load plastic deformation tests need to be

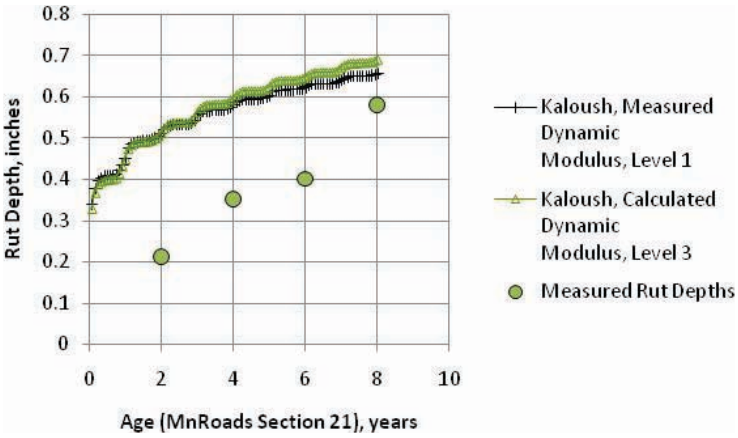

(a) New construction HMA pavement; MnROAD Section 21.

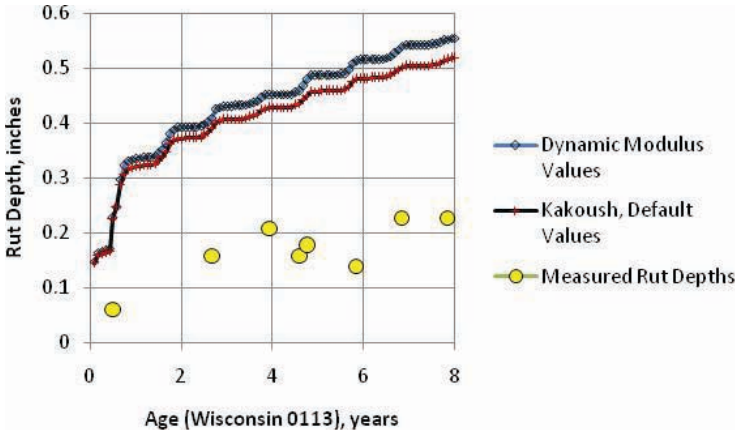

(b) New construction HMA pavement; Wisconsin SPS-1, Section 0113.
(Note: The accumulation of the predicted rut depths over time is different from the time-series–measured rut depths.)

Figure 89. Predicted and measured time-series rut depths comparing use of laboratory-measured dynamic modulus values and default values for new construction projects.

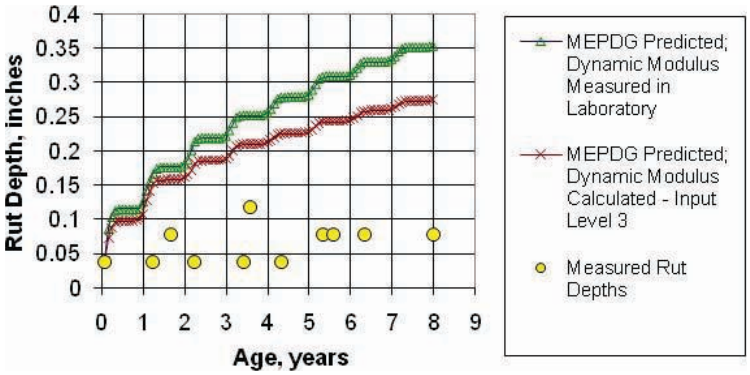

(a) HMA overlay of PCC pavement; Alabama SPS-6, Section 0603. (Note: The accumulation of the predicted rut depths over time is different from the time-series measured rut depths.)

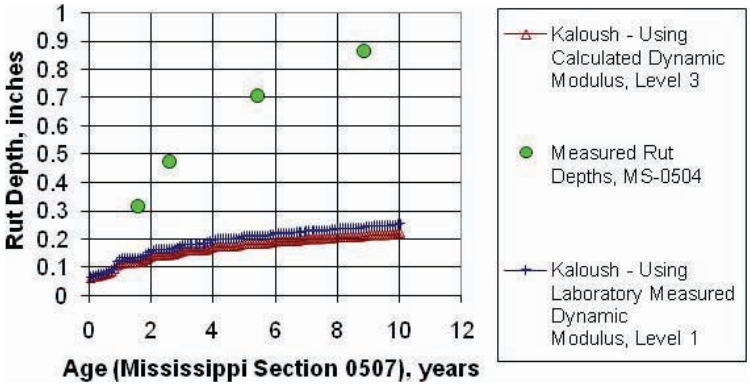

(b) HMA overlay of HMA pavement; Mississippi SPS-5, Section 0503. (Note: The accumulation of the predicted rut depths over time is different from the time-series measured rut depths.)

Figure 90. Predicted and measured time-series rut depths comparing use of laboratory-measured dynamic modulus values and default values for HMA overlay projects.

completed to reduce the bias and decrease the standard error of the transfer functions. The following redefinitions of the input levels in the 2008 MEPDG *Manual of Practice* are proposed.

- **Input Level 1:** Use of repeated-load plastic deformation tests to determine the values for the plastic strain coefficients.
- **Input Level 2:** Use of HMA volumetric properties for each layer to estimate the values of the plastic strain coefficients to eliminate bias and reduce the standard error.
- **Input Level 3:** Use of recalibrated global values for the plastic strain coefficients. However, the overall median value to reduce bias between the measured and predicted maximum rut depths will have little effect on the precision of the transfer functions. This level is not recommended for use because of the large standard errors reported in Table 27. An assessment and comparison of the different input levels is provided in Section 3.4.

3.2 Calibration and Validation of Laboratory-Derived Transfer Functions: Input Level 1

Even though mechanistic concepts provide a more rational and realistic methodology than empirical design procedures, all prediction models have errors. These errors explain the scatter in the data about the line of equality between the predicted and observed values of distress. Calibration is the mathematical process through which the residual error and the bias or systematic difference between observed and predicted values of rutting is minimized. Validation is the process for confirming that the calibrated model and transfer function can produce robust and accurate predictions for cases other than those used for transfer function calibration. Successful validation requires that the bias and precision statistics of the transfer function for the validation data set be similar to those obtained during calibration. Validation is discussed in Section 3.2.5.

The results from previous calibration studies (including NCHRP Projects 9-30 and 1-40B, and individual agency calibration projects) were used in determining the coefficients for the rut-depth transfer functions. The parameters that have been reported to reduce model bias and the standard error of the predicted rut depths include HMA thickness, volumetric properties of the HMA layers (air voids, asphalt content, and gradation), and the density and moisture content of unbound layers. In addition, the coefficient of the stress term was identified as an important parameter related to the effect of HMA thickness on the predicted rut depths, as discussed in Section 2.2.3.2. This part of Chapter 3 discusses the factors related to calibration and validation of the transfer functions.

3.2.1 Rut-Depth Measurement Error

Poor correlation was found between the predicted and measured rut depths using the global calibration values. Von Quintus, Andrei, and Schwartz (2005) reported that one possible reason for the poor correlation is the rut-depth measurement error. In other words, there is more variability in the measured rut depths within a segment than between all segments. As an example, the standard deviation of the average maximum rut depth between all of the segments included in the demonstration projects for the AASHTO *Local Calibration Guide* was reported to be 0.0754 in., while the standard deviation of the average rut depths within the monitoring period for a specific section was reported to be as high as 0.085 in.

Figure 91 illustrates the dispersion in rut depth measurements for two SPS-5 projects. As shown, the measurement error can be relatively large in some cases, and as the measurement error increases, the standard error increases. Varying the local calibration values to represent different site conditions and materials will not reduce the data measurement error. The measurement error, however, does not explain the poor correlations summarized in Table 27.

3.2.2 Unbound Layers

It has been reported that the β_{s1} coefficient of unbound layers in the MEPDG is related to the in-place water content and density of the unbound layer at construction (AASHTO, 2010; Von Quintus and Moulthrop, 2007). The sections with the highest measured rut depths were those with the higher water contents and lower densities in comparison to the

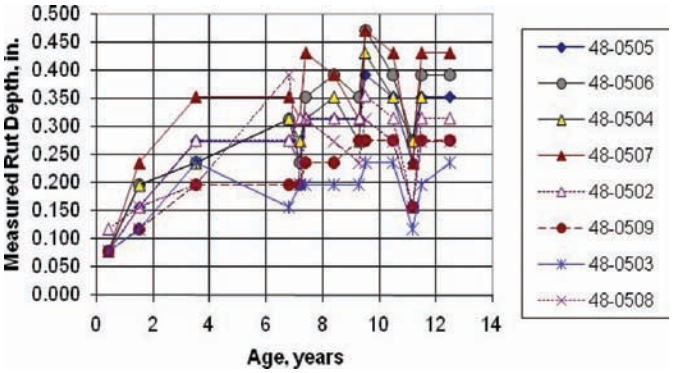

(a) Texas SPS-5 test sections.

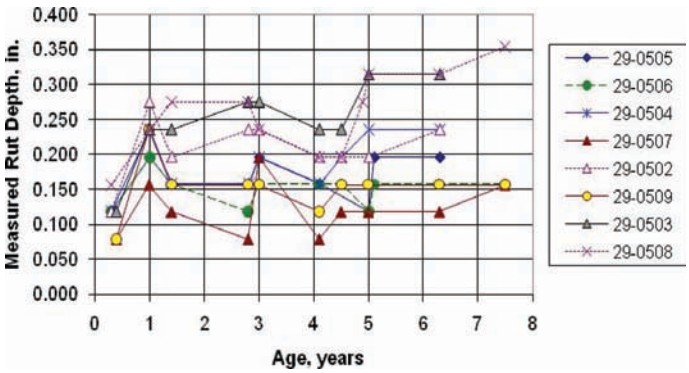

(b) Missouri SPS-5 test sections.

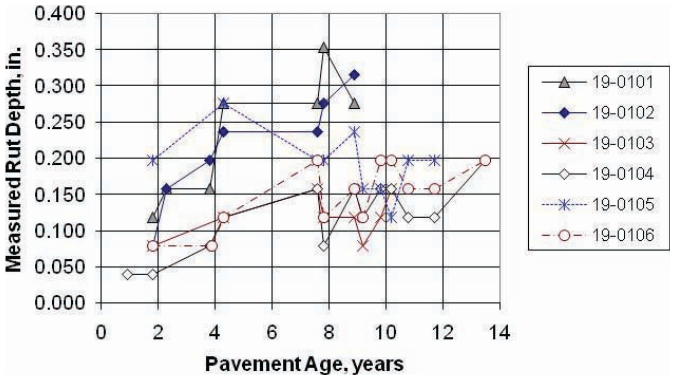

(c) Iowa SPS-1 test sections.

(d) Oklahoma SPS-1 test sections.

Figure 91. Rut depths measured over time for two LTPP SPS-1 and two SPS-5 projects.

maximum dry unit weight and optimum water content (the thinner Kansas and Nebraska SPS-1 sections).

Forensic investigations were performed for most of the test sections exhibiting excessive rutting, either within this project or by the individual state highway agency. Some agencies conducted forensic investigations to determine the rutting in individual layers. This information was used to estimate material-dependent calibration factors for the unbound layers.

The maximum predicted rutting in the unbound layers of individual sections varied from 0.1 in. to over 0.5 in. This level of rutting in the unbound layers and foundation was found to be consistent with some of the forensic investigations, but not all. The MEPDG both underpredicted and overpredicted the rutting measured in the unbound layers where forensic investigations had been completed.

For the sections with optimum or below-optimum water contents of the unbound layers, measured rutting was consistently overpredicted, while those with higher levels of saturation were underpredicted. The local calibration value for the unbound layers (β_{s1}) was estimated by making repeat runs of the MEPDG Version 9-30A with varying values for a limited number of segments to reduce the bias within each segment. The β_{s1} local calibration parameters of the unbound layers estimated based on water content and density in relation to the maximum dry density and optimum water content of the unbound materials and soils are provided in Table 28. These values are consistent with the results reported by AASHTO and the Montana DOT (AASHTO, 2010; Von Quintus and Moulthrop, 2007).

An average value was estimated for both fine- and coarse-grained soils for new construction and HMA overlay projects. An insufficient number of segments with different soils were available to determine whether the unbound layer calibration value is soil- or material-type dependent. The values in Table 28 were used for all test sections included in the local calibration effort for the rut-depth transfer functions.

3.2.3 HMA Transfer Function Parameters

Table 29 lists the variables included in the transfer functions (see Section 2.1.2). These parameters were investigated as to their impacts on the predicted rut depth.

3.2.3.1 HMA Thickness

HMA thickness is indirectly considered by all transfer functions because of the depth function. The depth functions for the different transfer functions were discussed in Section 2.1.2. As discussed in Chapter 2, the MEPDG Version 9-30A was used to predict the maximum rutting for varying HMA layer thicknesses for conventional, deep-strength, and HMA overlay projects. These computational results for the effect of HMA thickness on rut depth identified potential discrepancies with results from forensic investigations and other studies.

Figure 92 shows the effect of increasing HMA thickness on rut depth with the different transfer functions for the different types of pavement structures included in Tables 4 and 5. The rut depth predicted with the deviator-stress–based transfer functions (modified Leahy and Verstraeten) continue to increase with increasing HMA thickness for new construction and HMA overlays of flexible pavements. Conversely, the rut depth decreases with increasing HMA thickness for the pure vertical-strain–based functions (Kaloush function). Some local calibration studies completed by individual state agencies have included an HMA thickness adjustment factor for the Kaloush transfer function. The shear strain- and stress-based transfer function (WesTrack) is different—the rut depth is relatively constant with increasing HMA thickness, with the exception of thin HMA layers (less than 5 in.).

For composite pavement structures or HMA overlays of PCC pavements, the effect of thickness is significantly different than for new construction or HMA overlays of flexible pavements. The maximum rut depth calculated with

Table 28. Calibration values recommended for use for the unbound layers.

Condition of Unbound Layers	Unbound Base or Coarse-Grained Soils	Fine-Grained Subgrade Soil
Near maximum unit weight and optimum or equilibrium water content; modified Proctor-test-based values	0.3	0.3
Near maximum unit weight and optimum or equilibrium water content; standard Proctor-test-based values	0.5	0.5
Near maximum unit weight but higher water contents above optimum	0.75	0.75
Lower densities (below maximum unit weight) and higher water contents (above optimum)	3.0	1.25

Table 29. Parameters considered in the different rut-depth transfer functions in the MEPDG Version 9-30A.

Transfer Function	Parameters Directly Included in Transfer Function					
	Depth Function	Stress	Pav't. Temp.	Mix Properties		
				Air Voids	Asphalt Content	Asphalt Viscosity
Kaloush, Equation 1	Continuous function based on HMA thickness	No	Yes	No	No	No
NCHRP Project 1-40B, Appendix C	Continuous function based on HMA thickness	No	Yes	Yes	Yes	No
Asphalt Institute, Equation 5	Continuous function based on HMA thickness	Deviator stress	Yes	Yes	Yes	Yes
Modified Leahy, Equation 6	Continuous function based on HMA thickness	Deviator stress	No	Yes	Yes	No
Verstraeten, Equation 7	Continuous function based on HMA thickness	Deviator stress	No	No	No	No
WesTrack, Equation 8	Stepped function based on HMA thickness	Shear stress	No	No	No	No

the Kaloush and modified Leahy transfer functions for increasing HMA layer thickness is similar to that for flexible pavements—rut depth increases with increasing HMA layer thickness for the modified Leahy function, and rut depth increases with HMA thickness to about 4 in., at which point rutting starts to decrease, with the Kaloush function. Conversely, the maximum rut depth slightly increases with increasing HMA layer thickness for the WesTrack transfer function.

In summary, HMA thickness does affect the computed rut depth. The question becomes, is it a correct or accurate simulation of the field-measured values? Based on previous studies and forensic investigations of measured rut depths with pavement depth, it is believed that the WesTrack shear strain- and stress-based transfer function is more consistent with the field-measured values based on measured rut depths versus HMA thickness from the SPS-1, SPS-5, and SPS-6 experiments (Von Quintus and Yau, 2001; Rauhut, Eltahan, and Simpson, 1999).

3.2.3.2 Stress Term

Four of the six rut-depth transfer functions include a stress term (refer to Table 29): the Asphalt Institute (refer to Equation 5), modified Leahy (refer to Equation 6), Verstraeten (refer to Equation 7), and WesTrack (refer to Equation 8) functions. Figures 10 and 11 in Chapter 2 identify the importance of the stress term in relation to simulating the measured rut depth for varying HMA thicknesses.

As noted in Chapter 2, a combination of values for the intercept and stress term can be used for which the rut depth becomes less dependent on HMA thickness. In other words, there is a combination of deviator and shear stress terms for which the predicted rut depths from the WesTrack and modified Leahy transfer functions begin to converge, rather than diverge for the thinner HMA pavements. This observation is consistent with the results from many forensic investigations in measuring plastic deformation of individual HMA and unbound layers.

To investigate the impact of the stress term, multiple runs of MEPDG Version 9-30A were made for multiple test sections to determine the value of the coefficient to minimize any thickness adjustment factor for predicting rut depths of thin and thick HMA layers for the same mixture. Pavements with thick HMA layers were used to determine the transfer function coefficients for varying stress coefficient values to simulate the time-series rut depth measurements. The test sections used in this evaluation were the LTPP SPS-1 and SPS-5 projects because the same HMA mixture was used with varying HMA layer thickness to determine the effect of HMA thickness on rut depths.

Figure 93 shows the relationship between the stress-term coefficient and intercept value for the WesTrack and modified Leahy transfer functions. These combined values resulted in minimal bias between the predicted and measured rut depths. Those model coefficients determined from the thick HMA sections were used to predict the rut depths of thin HMA layers for the same mixture. In other words, the value of the stress term was varied to determine its effect (if any) on model bias between thin and thick HMA layers.

Figure 94 shows the effect of shear stress on rut depth over a range of HMA layer thicknesses using the WesTrack

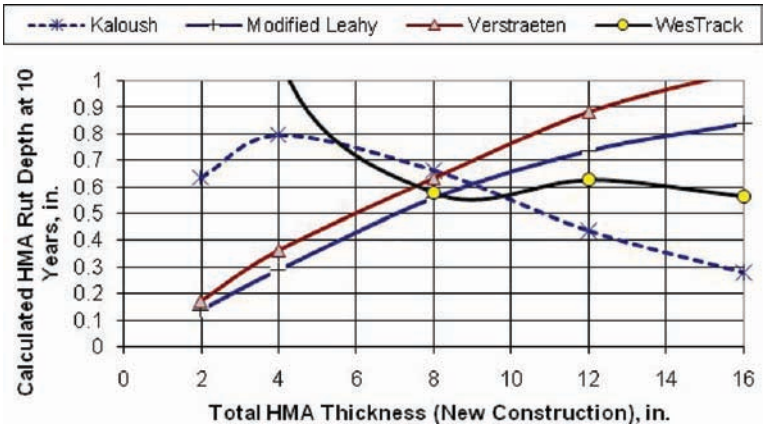

(a) New conventional and deep strength flexible pavement construction.

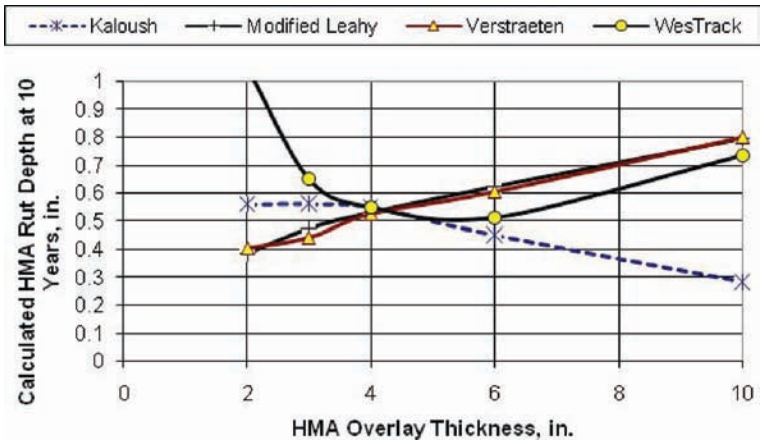

(b) HMA overlay of flexible pavements.

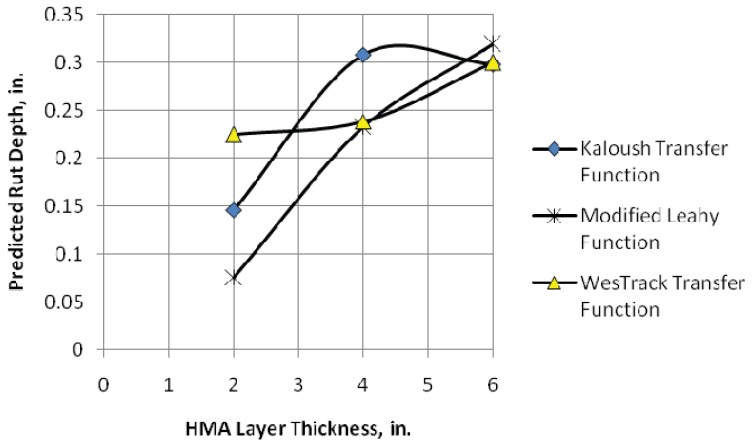

(c) Composite pavements.

Figure 92. HMA layer thickness effect on calculated HMA rut depth for new construction—conventional and deep-strength flexible and composite pavements.

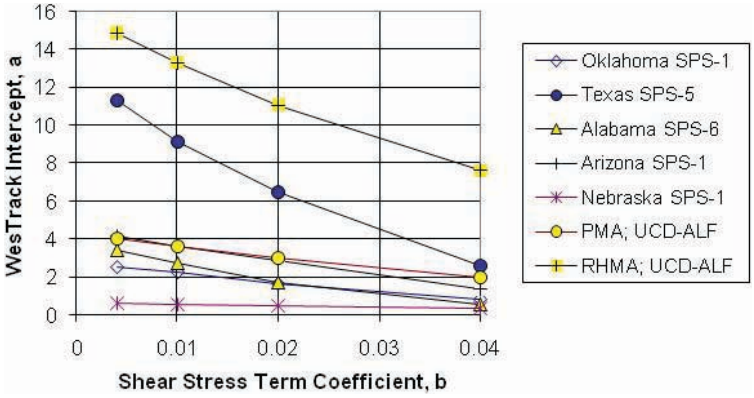

(a) Shear stress effect on the intercept of the WesTrack transfer function.

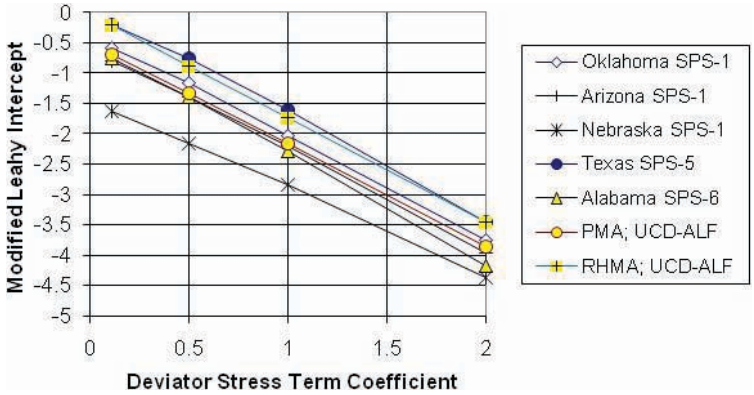

(b) Deviator stress effect on the intercept of the modified Leahy transfer function.

Figure 93. Effect of stress term to eliminate the thickness adjustment factor for the transfer functions with a stress term.

transfer function for flexible pavements and HMA overlays, while Figure 95 shows the effect of deviator stress on rut depth for the modified Leahy function. Figure 96 provides a similar comparison but for composite pavement structures. The following summarizes the results for the two transfer functions.

- **WesTrack transfer function:** The default value for the coefficient of the stress term is 0.04 (refer to Equation 8). Use of that value resulted in a positive bias—the predicted rut depths are much higher than the measured values (a positive residual error for thin HMA layers—see Figure 88). The use of lower values for the stress-term coefficient consistently reduced the bias or residual error between the predicted and measured rut depths (refer to Figure 94). For conventional HMA pavements and HMA overlays of flexible pavements, a value for the stress coefficient of about 0.01 reduces the need for any thickness adjustment factor between thin and thick HMA pavements. For composite pavement structures [refer to Figure 96(a)] or HMA overlays of intact PCC pavements, however, the bias or average residual error between thick and thin HMA layers does not converge to zero. This observation suggests a thickness adjustment will be needed for predicting the HMA rut depth of HMA surfaces over PCC bases or extremely stiff bases. The lower value for the shear stress coefficient was used for the LTPP SPS-1 project because of the range in HMA thickness—all other factors are generally the same. Figure 97 provides a comparison of the predicted and measured rut depths using values for the shear stress parameter of 0.04 and 0.01. As shown, the value of 0.01 significantly reduced the difference between the predicted and measured values. Thus, this value was used for the final calibration using all other test sections.
- **Modified Leahy transfer function:** The default value for the coefficient of the stress term is 0.11 (refer to Equations 6 and 7). Use of that value resulted in a positive bias for thin HMA layers—the predicted rut depths are greater than measured values (see Figure 86). The use of higher values for the stress-term coefficient reduced the bias or residual error between the predicted and measured rut depths for the initial test sections used in the preliminary evaluation. For conventional HMA pavements, a value for

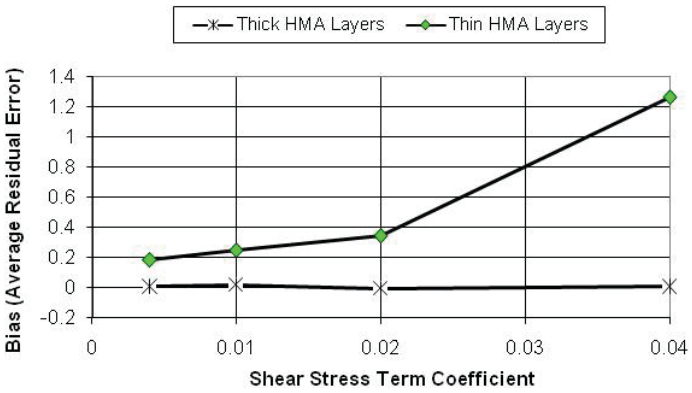

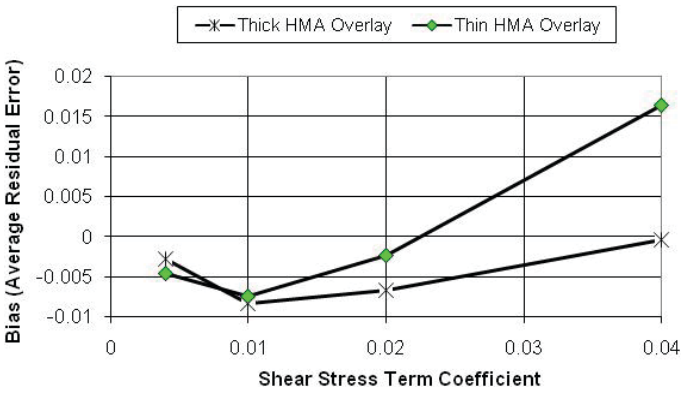

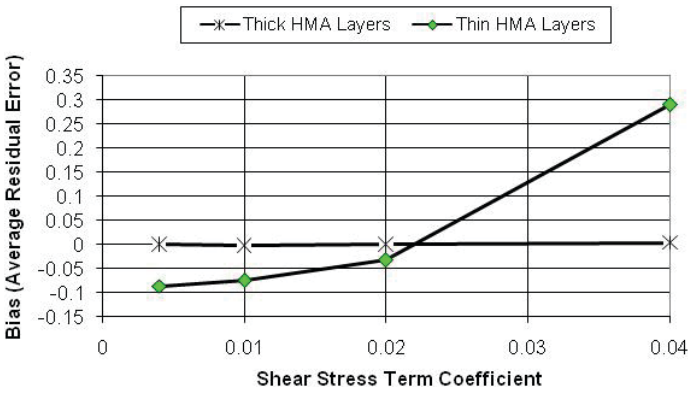

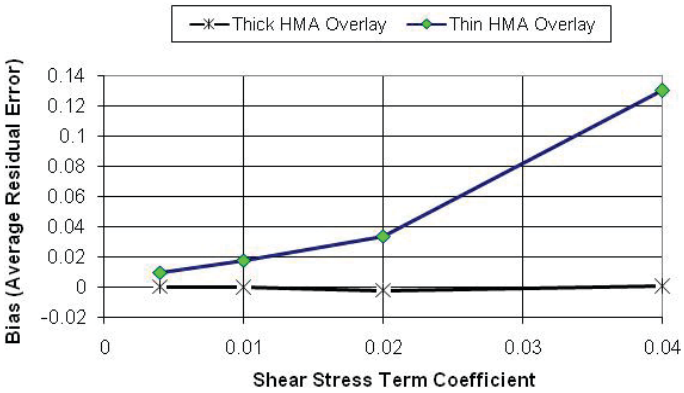

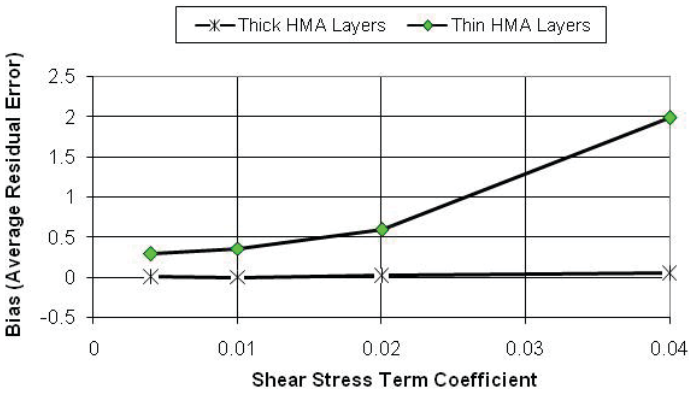

Nebraska, Arizona, Oklahoma SPS-1 projects, Texas SPS-5 project, and Alabama SPS-6 project

(a) New construction projects.

(b) HMA overlay projects.

Figure 94. Effect of shear stress term on the difference between the predicted and measured rut depths using the WesTrack transfer function.

the stress coefficient of about 1.0 eliminates the need for any thickness adjustment factor between thin and thick HMA pavements on the average. For HMA overlays and composite pavements [refer to Figures 95 and 96(b)], however, the bias or average residual error between thick and thin HMA layers does not converge to zero. This observation suggests that a thickness adjustment will be needed for predicting the HMA rut depth of HMA surfaces over very stiff supporting layers. The higher value for the deviator stress coefficient was used for the LTPP SPS-1 project, similar to that for the WesTrack function. Figure 98 provides a comparison of the predicted and measured rut depths using values for the deviator stress parameter of 0.11 and 1.0. As shown, the value of 0.11 results in less difference between the predicted and measured rut depths. The reason for this difference from the initial runs is related to the depth function. In any case, the original value recommended for use by Leahy was used in the final calibration of the modified Leahy transfer function for all other test sections.

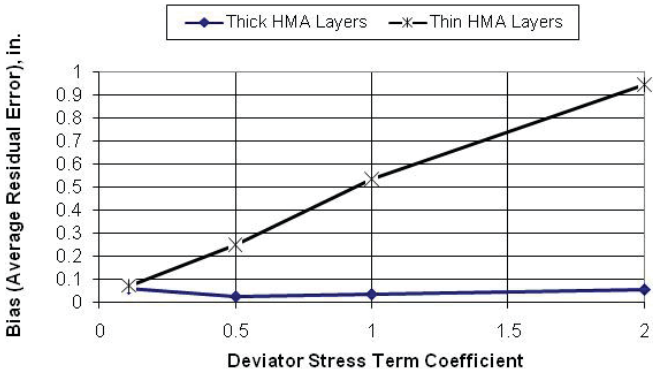

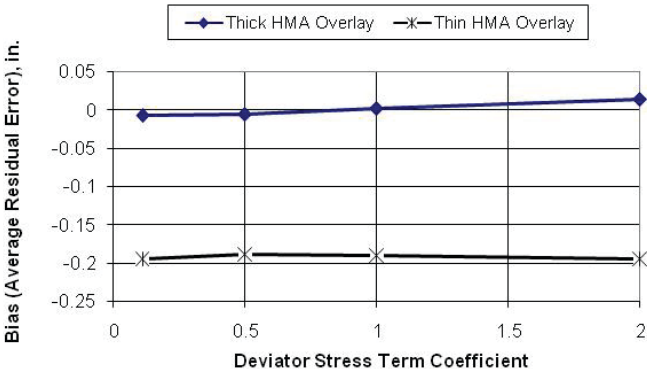

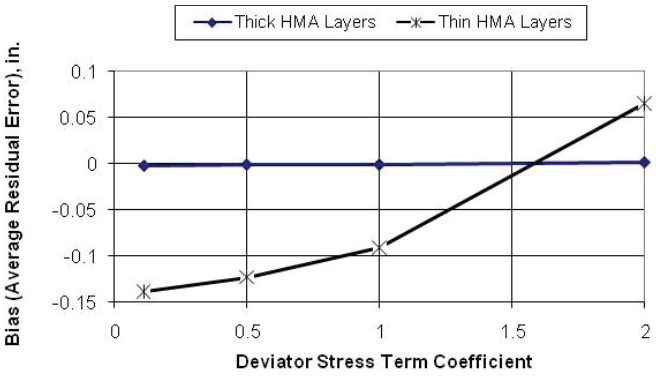

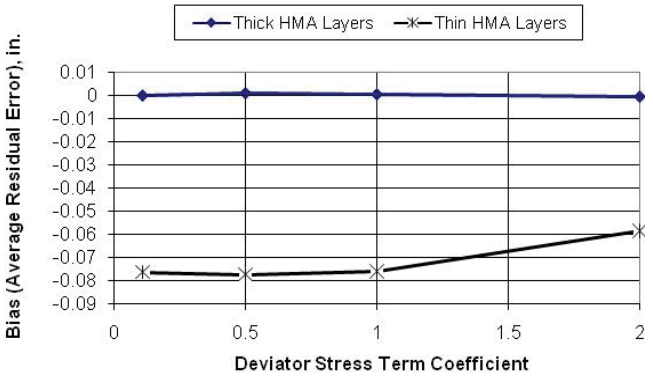

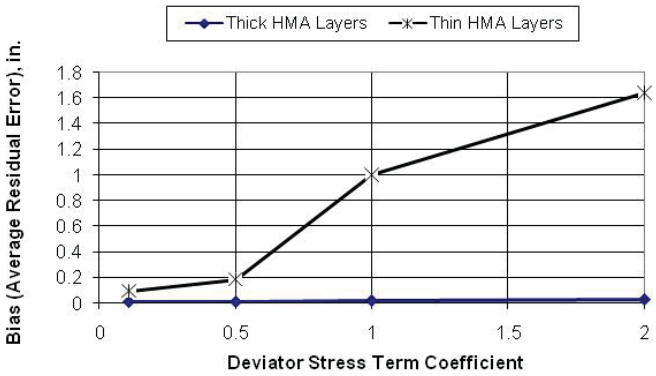

Nebraska, Arizona, Oklahoma SPS-projects, Texas SPS-5 project, and Alabama SPS-6 project

(a) New construction projects.

(b) HMA overlay projects.

Figure 95. Effect of deviator stress term on the difference between the predicted and measured rut depths using the modified Leahy transfer function.

In summary, specific values for the stress terms were found to minimize model bias for conventional flexible and deep-strength flexible pavements. The appropriate values recommended for use are $b = 0.01$ for the WesTrack transfer function (refer to Equation 8) and $C_3 = 0.11$ for the modified Leahy and Asphalt Institute transfer functions (refer to Equations 6 and 7). For composite pavements, however, the bias does not approach zero. This implies that the stress term value has little impact on the model bias for composite pavements or HMA layers supported by stiff layers. Thus, the values of the stress coefficient determined for conventional HMA pavements were used for composite pavements and HMA overlays of intact PCC slabs, and a thickness adjustment factor is needed to reduce the bias between thin and thick overlays for both transfer functions.

3.2.3.3 Temperature

Three of the transfer functions include a temperature term (refer to Table 29): Kaloush, NCHRP Project 1-40B adjustments, and the Asphalt Institute (refer to Table 29). Repeated load tests were performed at three test temperatures ($T_{\text{eff rut}}$). Figure 99 shows the effect of test temperature on the m-value and intercept from the secondary region of

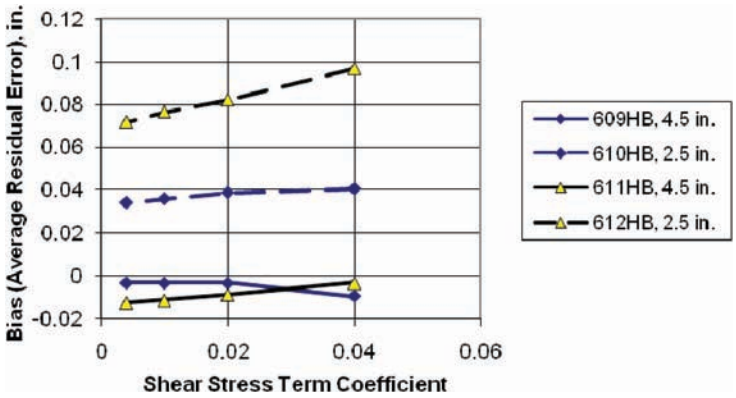

(a) WesTrack transfer function; shear stress.

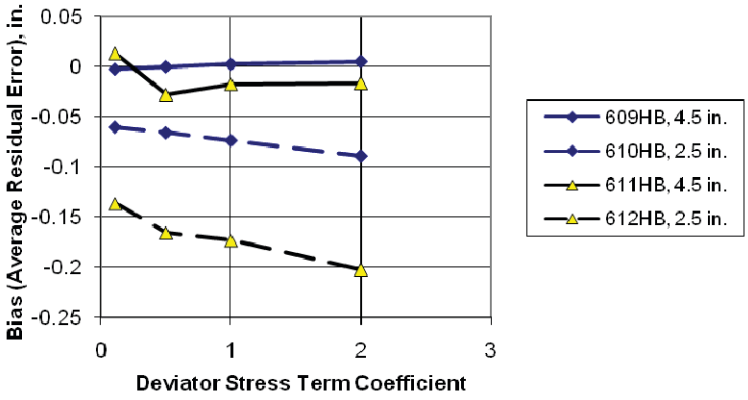

(b) Modified Leahy transfer function; deviator stress.

Figure 96. Effect of stress term on the difference between the predicted and measured rut depths using UCD-ALF test pads; composite pavements.

the plastic deformation tests. There are trends in the data, but the *m*-value and intercept from both repeated load tests are mixture sensitive and are not highly correlated.

The *d* and *n* parameters of Equation 26 were determined for all repeated load tests (refer to Tables 22 through 25 in Chapter 2). Figure 100 shows the relationship between the *d* and *n* values for all tests. As shown, the effect of temperature on plastic deformation appears to be the same for repeated-load shear testing of laboratory-prepared and field cores as well as for laboratory-prepared repeated-load triaxial tests. More importantly, the relationship between *n* and *d* is the same from both triaxial and shear tests.

This observation between the *d* and *n* values is the reason for excluding temperature from many of the rut-depth transfer functions. There is a consistent impact from temperature on the rutting resistance of HMA mixtures that can be adequately accounted for by the dynamic modulus/temperature relationship or master curve. This was one of the reasons why the temperature term was excluded from the modified Leahy function.

In summary, the k_2 parameter or exponent for the temperature term of the Kaloush and NCHRP Project 1-40B transfer functions was set at 1.5606 and not varied between the different mixtures (refer to Equation 1 and Appendix C). The reason for setting this value as a constant was based on the findings for which the impact of temperature was found to be similar between significantly different mixtures and pavement structures. Thus, the *k2* parameter recommended for use was simply assumed for all mixtures and conditions.

For those transfer functions that exclude temperature, the laboratory-derived intercept is defined at the equivalent pavement temperature. The equivalent pavement temperature for each test section was calculated using Equations 5 and 6. The equivalent annual temperature is defined as the constant temperature entered in the MEPDG that results in the same amount of rut depth as for the actual climate data. The laboratory-derived *m*-value and intercept from the secondary region of the repeated load tests were determined at the equivalent annual temperature for the reconstituted

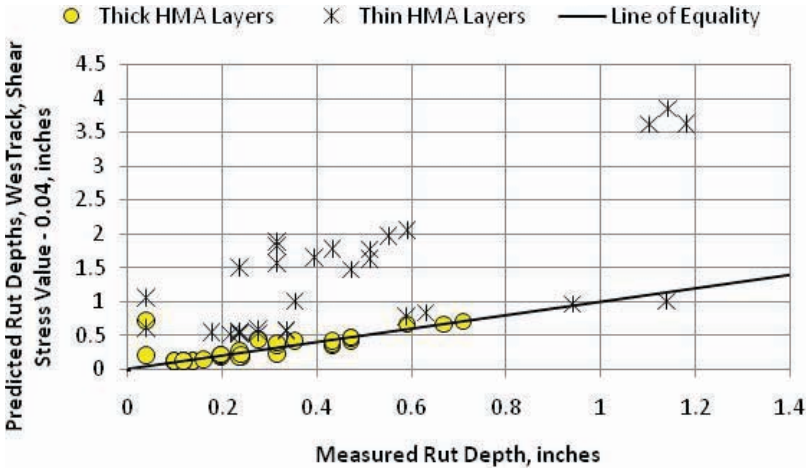

(a) Shear stress parameter value of 0.04.

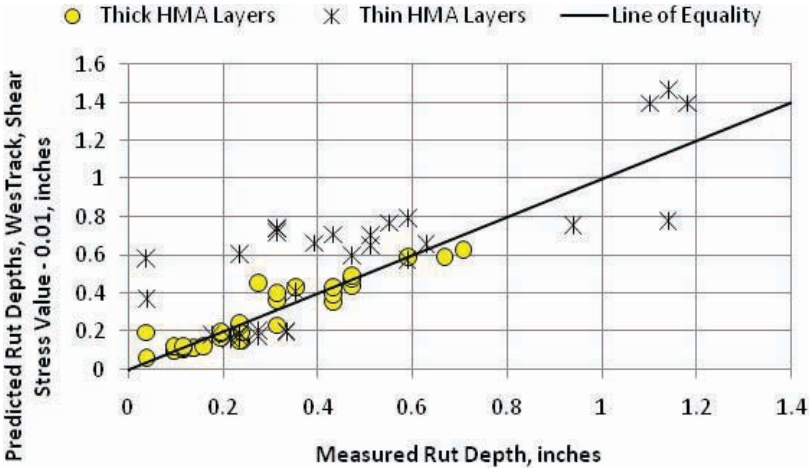

(b) Shear stress parameter value of 0.01.

Figure 97. Effect of the shear stress term in the WesTrack function on reducing the difference between the predicted and measured rut depths.

specimens for transfer functions that exclude temperature as a dependent variable.

The relationship between the *m*-value and intercept is provided in Figure 101. As shown, the correspondence between the two plastic deformation parameters is poor, confirming the initial results presented in Chapter 2 (refer to Figure 38). As the *m*-value increases, however, there is a general decrease in the intercept. This observation between the intercept and slope from the secondary region was also reported by Rauhut et al., in the VESYS work completed for FHWA, in terms of alpha and mu—refer to Equations 20 and 21 (Rauhut et al., 1976 and Rauhut et al., 1984). There is poor correspondence between the two, but trends do exist.

3.2.3.4 Volumetric Properties

Three of the rut-depth transfer functions consider the volumetric properties in estimating the intercept of the plastic deformation coefficients: NCHRP Project 1-40B, Asphalt Institute, and modified Leahy. Under NCHRP Projects 9-30 and 1-40B, the volumetric properties of the in-place mixtures were found to have a significant impact on reducing the standard error and bias of the Kaloush transfer function using the global values of the plastic strain coefficients. Previous results found that increasing air voids and increasing asphalt contents will result in higher measured rut depths.

The modified Leahy and Asphalt Institute transfer functions include air voids and asphalt content, which have been found to be reasonable in accounting for the effect of the volumetric properties on the plastic deformation coefficients. In addition, it is believed that considering the effect of air voids and asphalt content as part of the NCHRP Project 1-40B volumetric adjustment factors for estimating the plastic strain coefficients is the reason why there was a reduction in the standard error in comparison to using the Kaloush default transfer function (Von Quintus et al., 2009). Use of

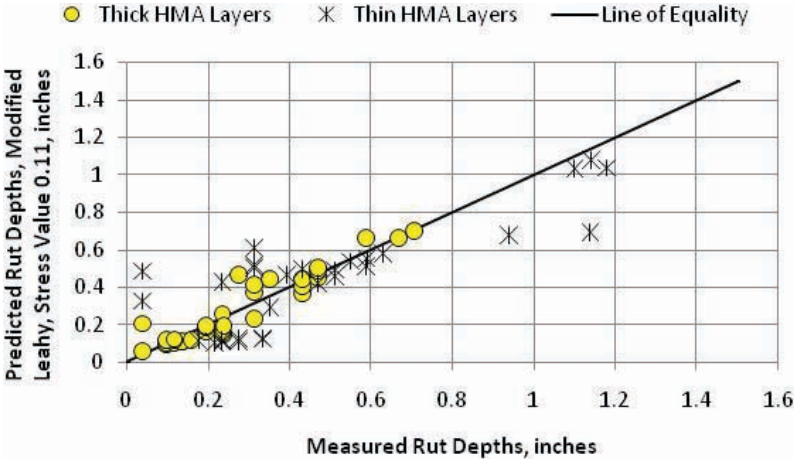

(a) Deviator stress parameter value of 0.11.

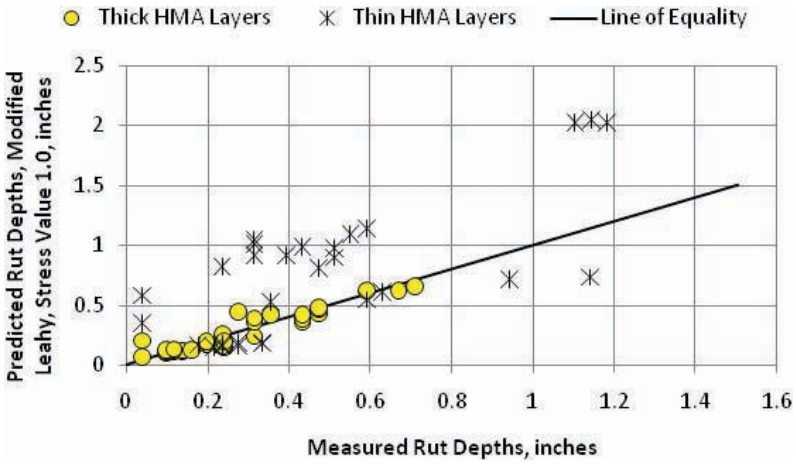

(b) Deviator stress parameter value of 1.0.

Figure 98. Effect of the deviator stress term in the modified Leahy function on reducing the difference between the predicted and measured rut depths.

volumetric properties to estimate the plastic strain parameters (similar to the NCHRP Project 1-40B procedure provided in Appendix C) is discussed in Section 3.3.

3.2.4 Adjustment of Laboratory-Derived Values

Figures 21 through 24 are examples comparing the predicted and measured rut depths for each transfer function for selected ALF, test track, and LTPP test sections—the same sections included in Figures 1 through 4 but using the global default values. As shown, all of the transfer functions can provide an accurate simulation of the measured rut depth evolution (ranging from very low to high rut depths) over a diverse range of mixtures, conditions, and pavement structures.

As stated in Chapter 2, the other important observation from these field-derived values is that the *N*-term exponent was found to be the same between all of the transfer functions. Using site- and mixture-specific plastic strain coefficients for each transfer function results in the same accuracy and precision of the time-series rut depth data—one transfer function is as accurate as the other transfer functions when using site-specific plastic deformation parameters. The question then becomes, does one transfer function result in a closer simulation of the time-series–measured rut depths using laboratory-derived plastic deformation coefficients that are adjusted to field-matched values?

All transfer functions embedded into the MEPDG Version 9-30A represent the steady-state or secondary region from repeated-load plastic deformation tests. The laboratory test results from the secondary region of the repeated-load confined, triaxial, and constant-height shear tests can be represented by Equation 25 and were determined in accordance with the procedure explained in Chapter 2. The plastic strain parameters for the WesTrack transfer function were estimated from repeated-load constant-height shear tests, while

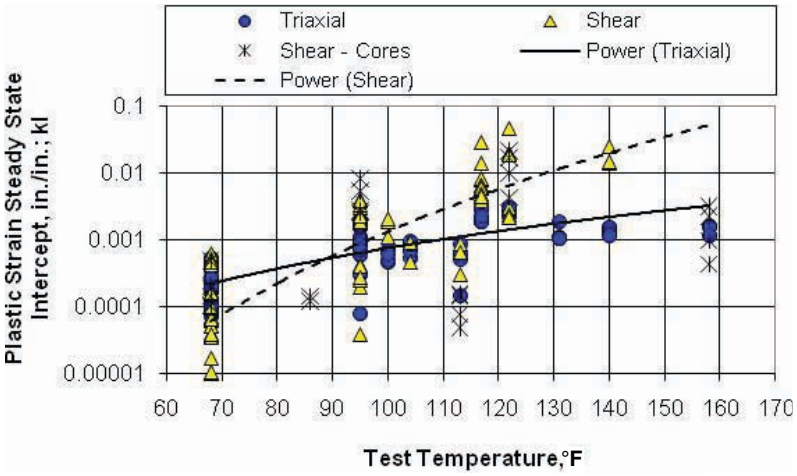

(a) Plastic strain intercept from secondary region.

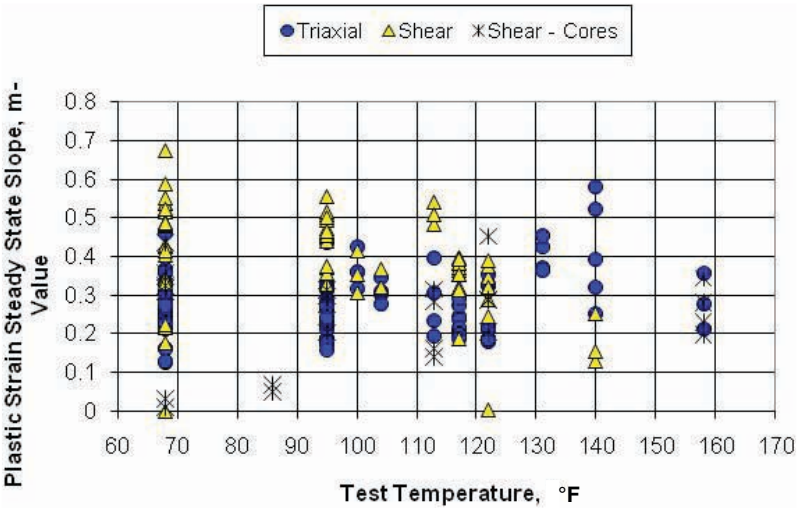

(b) Plastic strain slope or *m*-value from secondary region.

Figure 99. Correspondence between the* m*-value and intercept (from secondary region) and test temperature.

repeated-load triaxial tests were used to determine the plastic strain parameters for the other transfer functions.

Tables 24 and 25 summarize the results from the repeated-load plastic deformation tests for the triaxial and shear tests, respectively. The laboratory-derived values are not used directly as inputs to the MEPDG Version 9-30A, but need to be adjusted to field conditions for the different transfer functions. Adjustment of the laboratory-derived plastic deformation parameters is the calibration of the transfer functions, which is discussed in the next section of Chapter 3.

A comparison of the two plastic deformation parameter values was made in reviewing laboratory test results to identify any mixture anomalies that deviated from standard practice as well as to evaluate the accuracy of the NCHRP Project 1-40B mixture adjustment regression equation for k_{r3} (refer to Appendix C). Most of the mixtures included in the sampling template are considered traditional dense-graded mixtures. Although there is a trend between the two parameters, a universal relationship does not exist and is not present within the data, similar to the observation made from the laboratory-derived values (refer to Figure 101). Figure 102 was used to make some initial decisions about individual HMA mixtures in terms of their resistance to rutting. The following subsections provide a comparison between the laboratory- and field-derived plastic strain coefficient values for each transfer function.

3.2.4.1 *Field-Adjusted Secondary Region Slope or* m*-Value*

Figure 103 provides a comparison of the laboratory-derived and field-matched *m*-value or slope of the secondary

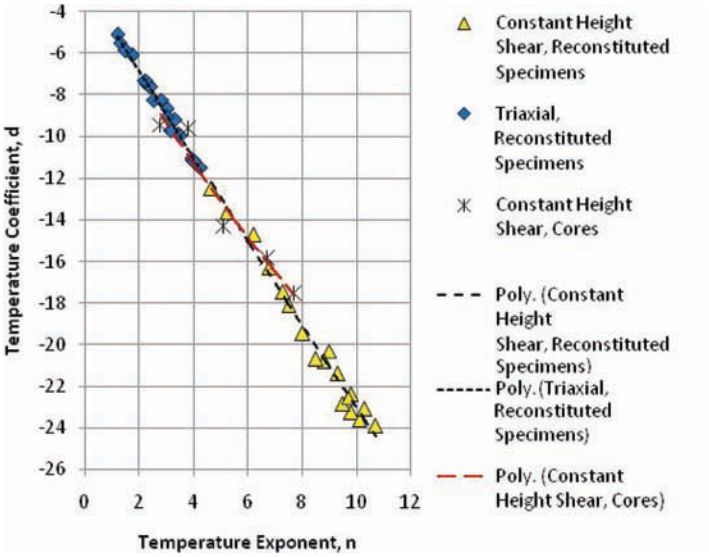

Figure 100. Relationship of temperature exponent (n-value) and coefficient (d-value) for both repeated load tests.

region of repeated-load shear and triaxial plastic deformation tests. Overall, there is reasonable correspondence between the laboratory-derived and field-matched *m*-values from both repeated load tests. There are anomalies or outliers, however, in the data set. Anomalies are defined as sections with material and/or construction defects (HMA stripping or moisture damage, checking during compaction, debonding, etc.) not simulated in the laboratory repeated-load tests or MEPDG computational methodology. An important observation of similarity between the transfer functions is that the *N*-term exponent or *m*-value is assumed to be independent of temperature, age, and dynamic modulus.

3.2.4.2 Field-Adjusted Secondary Region Intercept

Figures 104 and 105 provide a comparison of the laboratory-derived and field-matched intercepts for the repeated-load triaxial and shear tests, respectively. Sections with mixture anomalies (as defined in Section 3.2.4.1) were segregated between test sections and mixtures with and without anomalies. As shown, there is a lot of dispersion between the laboratory-derived and field-matched intercepts for both repeated load tests. Two reasons for the high variability are noted in the following.

1. Extensive variability exists in determining the laboratory-derived intercept from the repeated load tests. A slight change in the slope can result in a much greater change in the intercept from the secondary region (refer to Figures 46, 47, and 53).
2. The *m*-values between different test sections with the same mixture were assumed to be the same, so all of the error in the field-matched values is included in the intercept or coefficient of the transfer function.

The WesTrack shear stress- and strain-based transfer function was found to have reasonable correspondence between the laboratory-derived and field-matched secondary *m*-value and intercept. Thus, it was included in the recalibration.

The relationships between the laboratory-derived and field-matched intercepts for the Asphalt Institute and Verstraeten transfer functions have more variability, while the Kaloush and modified Leahy functions have a more defined relationship for the triaxial-based transfer functions. The temperature exponent is believed to be the reason for this scatter or dispersion in the data, so the Asphalt Institute transfer function was excluded from further consideration.

The Verstraeten transfer function also has extensive scatter between the field-matched and laboratory-derived intercepts. A reason for this increased dispersion is that only one pavement response value (deviator stress) is used to predict rutting so that transfer function was also excluded from further consideration. The Kaloush transfer function is also based on one response parameter (vertical elastic or resilient strain) but represents the baseline transfer function, so it was included in the recalibration.

An important observation from the analysis of residual errors and bias from the verification process (see Section 3.1.1) was the effect of HMA thickness and type of support layer. A consistent negative bias exists for thin HMA layers over crushed stone base layers and PCC pavements. Two approaches can be used to reduce the bias for the transfer function that include a stress term as a dependent variable (modified Leahy and WesTrack): (1) adjusting the value of the coefficient for the stress term and (2) including a thickness adjustment factor to the intercept. The approach taken was to determine a thickness adjustment factor to be consistent with the Kaloush transfer function that does not include stress as a dependent variable.

The reason for the thickness adjustment factor is that the depth functions do not adequately account for layer depth under all conditions. Various mechanistic analyses were conducted to explain and revise the depth function so that a thickness adjustment factor would not be required. The mechanistic analyses are explained in Appendix K and summarized in Section 3.6. In summary, a different mathematical relationship to account for thickness and depth of layer below the surface resulting in no bias was not identified. Thus, the depth function included in the MEPDG was left unchanged.

The thickness adjustment factors for the Kaloush, modified Leahy, and WesTrack transfer functions were determined

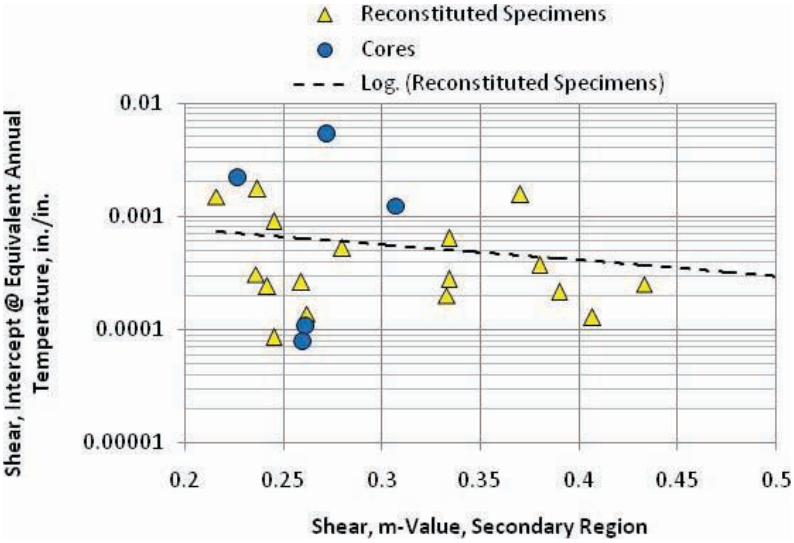

(a) Repeated-load constant-height shear tests.

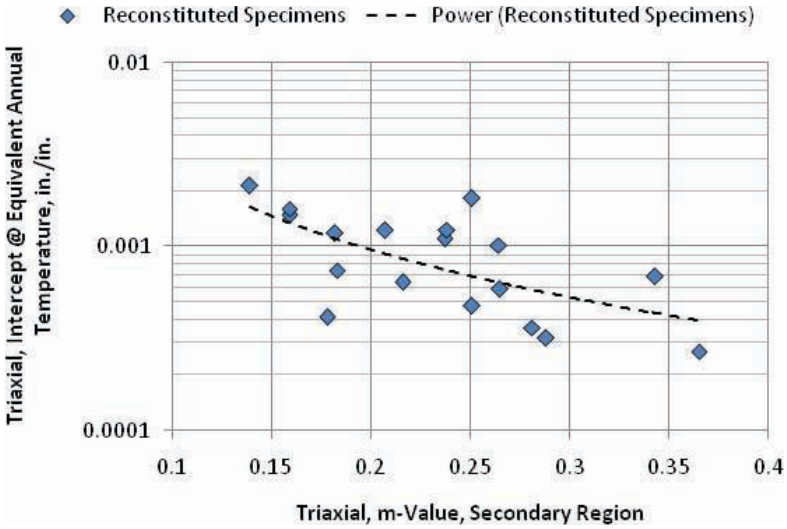

(b) Repeated-load triaxial tests.

Figure 101. Relationship of m-value and intercept (from secondary region) at equivalent annual temperature for the two repeated load tests.

by comparing the field-matched intercepts of each function between the thicker and thinner test sections of experiments with the same mixture—basically using the LTPP SPS-1, SPS-5, and SPS-6 projects in Tables 4 and 5. The thickness adjustment factors were then applied to all projects included in Tables 4 and 5.

Table 30 provides the thickness adjustment or shift factors for application to the intercept values of the transfer functions. Basically, the field-adjusted laboratory-derived intercept is multiplied by the thickness adjustment factor for the range of thickness and support layer listed in Table 30. That product is entered into the MEPDG Version 9-30A for the specific HMA layer.

3.2.5 Precision and Accuracy of Transfer Functions

This subsection summarizes the accuracy or bias and precision or standard error from the comparison of predicted and measured rut depths of each transfer function. The standard error is used in the MEPDG to evaluate and predict rut depths for different reliability levels. Table 31 summarizes the

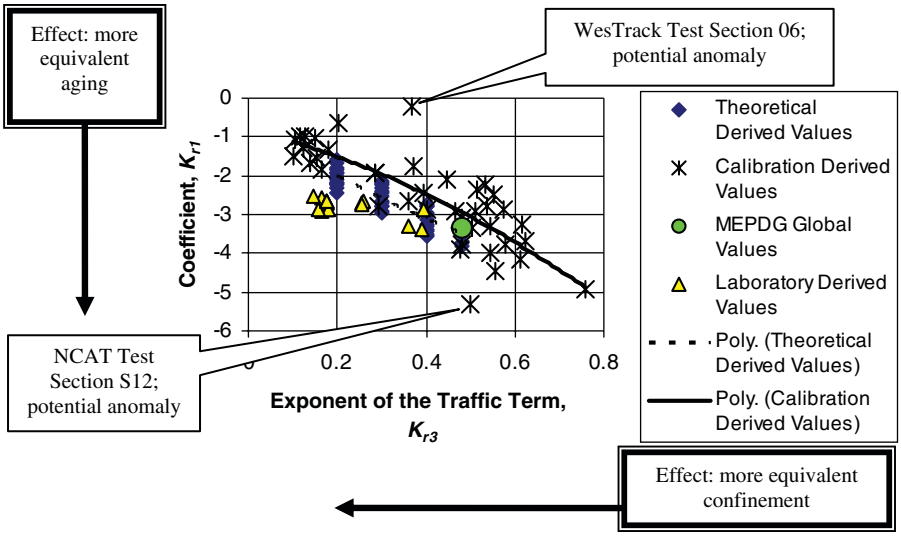

Figure 102. Relationship between the k_{r1} coefficient and k_{r3} N-exponent of the Kaloush rut-depth transfer function.

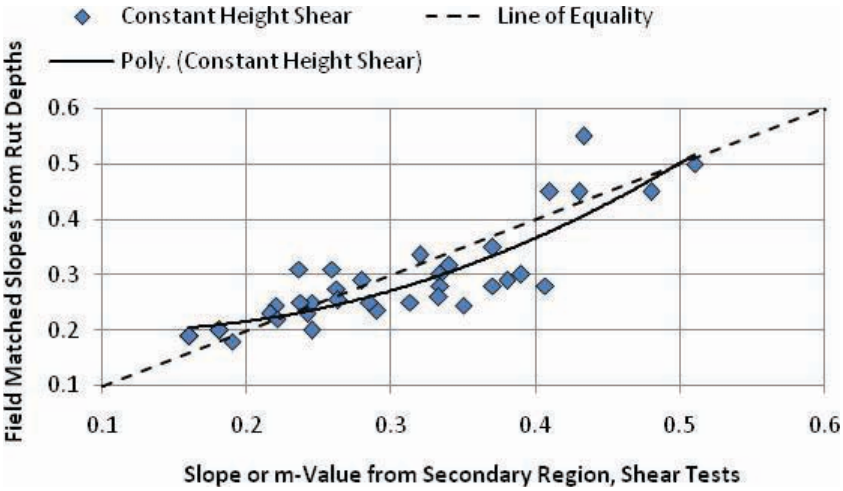

(a) Shear-based *m*-values or slopes from repeated load tests.

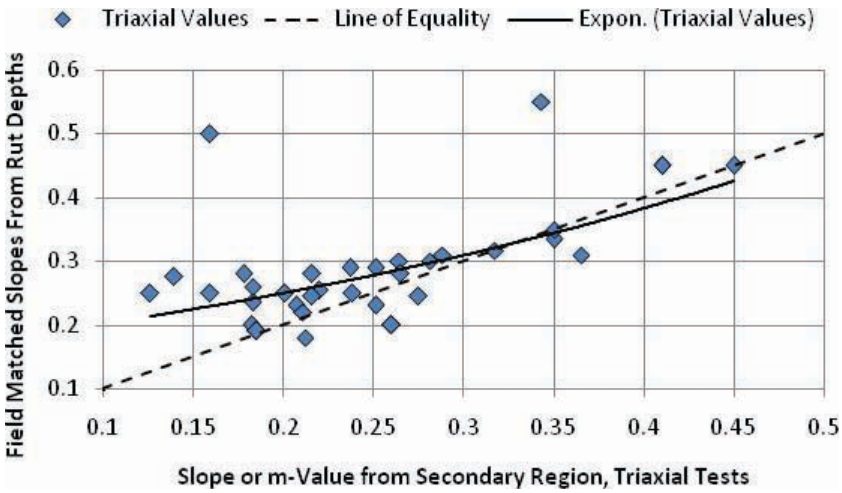

(b) Triaxial-based *m*-values or slopes from repeated load tests.

Figure 103. Relationship between field-matched and laboratory-measured slopes or m-values (N-term exponent).

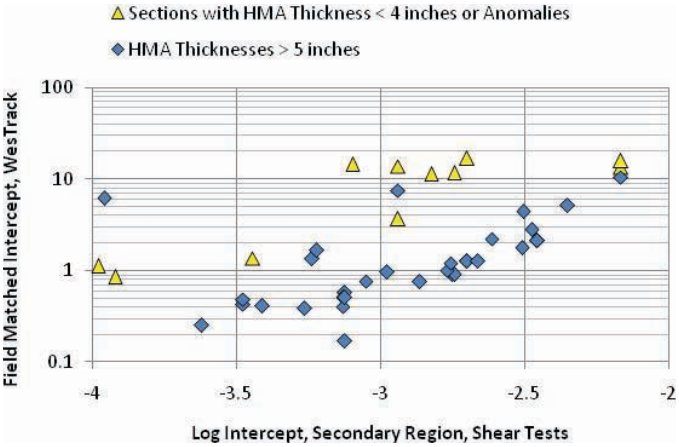

Figure 104. Comparison of field-matched intercept and laboratory-derived secondary region intercept from repeated-load shear-based tests.

other statistical parameters when using the redefined Input Level 1 to predict the rutting resistance of HMA mixtures. As shown, Input Level 1 using repeated-load plastic deformation tests has much lower standard errors in comparison to those provided in Table 27.

The standard errors reported in Table 31 exclude those test sections with anomalies as previously defined because moisture damage, stripping, checking, and debonding are not simulated in the laboratory test program or MEPDG, while those sections were included in the use of the global values for the plastic strain coefficients.

Figures 106 through 108 provide a comparison of the predicted and measured rut depths and residual errors. As shown, use of the field-adjusted laboratory-derived values for the plastic strain coefficients resulted in a significant improvement in the accuracy and precision of the three transfer functions. These results are considered acceptable, and more importantly, are considered indifferent.

A difference in the precision of the transfer functions was expected because the dispersion between the laboratory-derived

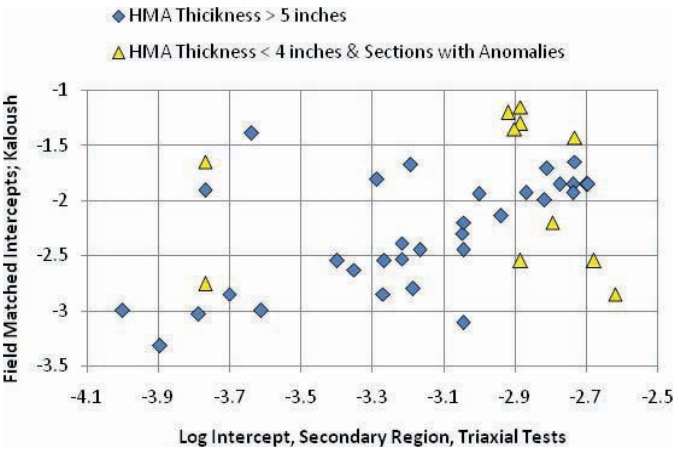

(a) Kaloush transfer function.

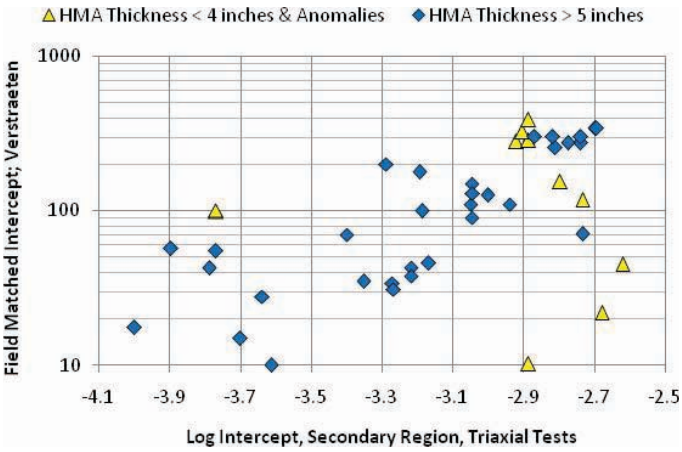

(b) Verstraeten transfer function

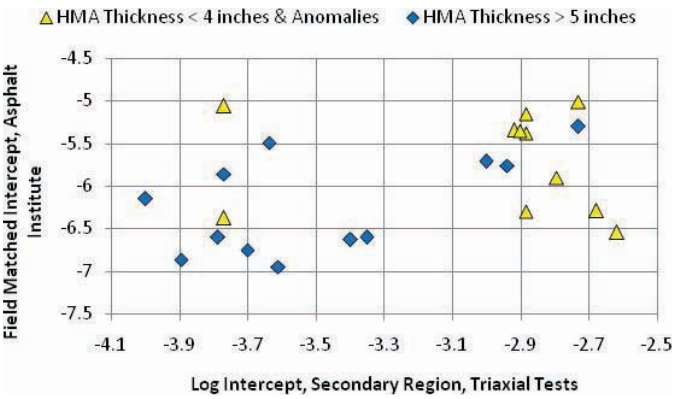

(c) Asphalt Institute transfer function.

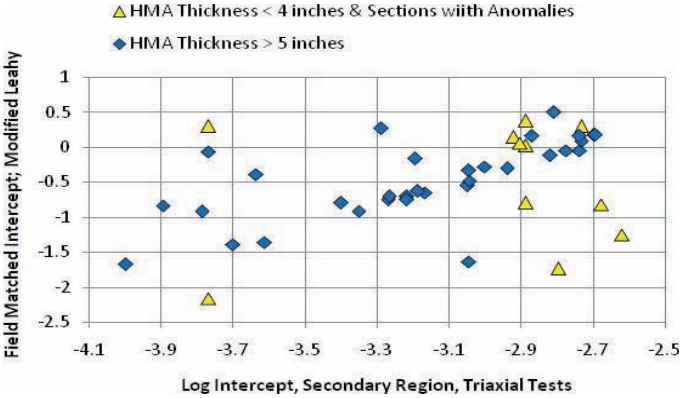

(d) Modified Leahy transfer function.

Figure 105. Comparison of field-matched intercept and laboratory-derived secondary region from repeated-load triaxial tests.

Table 30. Thickness adjustment or shift factors for determining the intercept value of the transfer functions.

HMA Mixture Application	HMA Layer Thickness, in.	Transfer Function		
		Kaloush	Modified Leahy	WesTrack
HMA overlays of PCC or semirigid pavements	<3.0	0.83	1.25	1.25
	3 to 4	0.90	1.10	1.0
	>4.0	1.0	1.0	1.0
HMA overlays of flexible pavements	<4.0	1.4	1.2	1.25
	4 to 6	1.2	1.2	1.1
	>6.0	1.0	1.0	1.0
New construction, unbound aggregate base or full depth	<4.0	1.05	1.2	1.2
	4.0 to 6.0	1.02	1.1	1.05
	6.0 to 8.0	1.0	1.0	1.0
	>8.0	1.0	1.0	1.0

Table 31. Statistical parameters of comparison between predicted and measured rut depths using repeated-load plastic deformation tests—Input Level 1.

Transfer Function	Statistical Parameters				
	Number of Data Points	Bias, in.	Standard Error, s_e	s_e/s_y	R^2
Calibration Data Set					
Kaloush (Equation 1)	296	-0.0072	0.1085	0.655	0.583
Modified Leahy (Equation 6)	296	0.0104	0.1045	0.611	0.699
WesTrack (Equation 8)	243	0.0095	0.091	0.585	0.712
Validation Data Set					
Kaloush (Equation 1)	60	-0.011	0.110	0.723	0.560
Modified Leahy (Equation 6)	60	0.0225	0.109	0.714	0.633
WesTrack (Equation 8)	60	0.0105	0.108	0.689	0.676

and field-matched intercepts of the three transfer functions was different [refer to Figures 104, 105(a), and 105(b)]. The indifference between the transfer functions in terms of precision is believed to be the result of:

- The measurement error (refer to Figure 91 and Section 3.2.1).
- The fact that some of the test sections with the higher measured rut depths occurred in the unbound layers, independent of the HMA transfer function used.
- Use of the lower value for the stress-term coefficient of the WesTrack transfer function.
- The fact that the intercept estimated from both repeated load tests has about the same error.

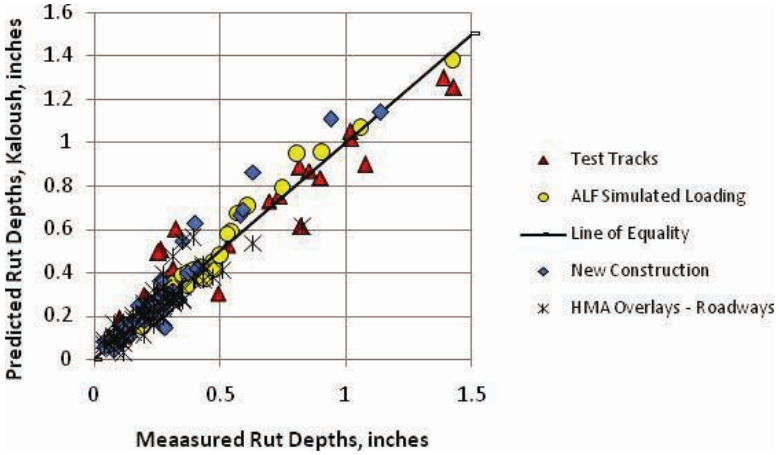

Comparison of measured and predicted rut depths for different pavement structures

Residual error as a function of total HMA thickness (new mixtures) for new construction and overlays

Residual error as a function of total HMA thickness (new construction) for neat and modified HMA mixtures

Figure 106. Comparison of predicted and measured rut depths for the Kaloush transfer function.

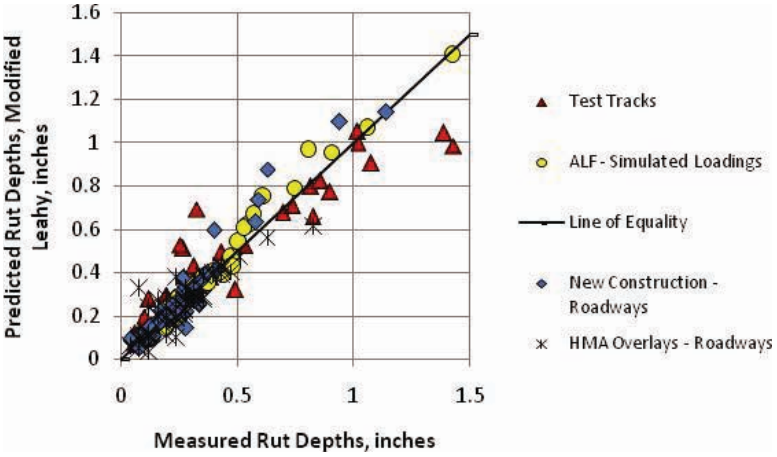

Figure 107. Comparison of predicted and measured rut depths for the modified Leahy transfer function.

- Use of the thickness adjustment factors for different structural conditions and HMA layer thickness (refer to Table 30).

It should also be noted that the standard errors reported in Table 31 exclude those test sections with anomalies as previously defined because moisture damage, stripping, checking, and debonding were not simulated in the laboratory test program or MEPDG.

3.2.6 Validation of Field-Adjusted Laboratory-Derived Plastic Strain Values

The AASHTO Local Calibration Guide for the MEPDG (2010) includes two approaches for validating the results from calibrating M-E–based transfer functions and their computational methodology: the traditional split-sample approach and jackknife testing. *Jackknifing* is a means of accomplishing reliable calibration and validation with limited sets of complete data from full-scale pavement sections. The specific application of jackknifing to the calibration of the MEPDG software is described in *NCHRP Research Results Digest 283: Jackknife Testing—An Experimental Approach to Refine Model Calibration and Validation* (Transportation Research Board, 2003a).

Split-sample validation differs from jackknifing in that the goodness-of-fit statistics for both calibration and prediction are based on $n/2$ values (for symmetric split sampling, the usual case) rather than n values. Traditional split-sample validation has the distinct disadvantage that, if n is small relative to the inference space being simulated, then $n/2$ is even smaller, which produces inaccurate calibrations, inaccurate coefficients, and less-reliable prediction accuracy. To overcome this deficiency, a method was proposed in the NCHRP Project 9-30 experimental plan that combines jackknifing and split-sample testing

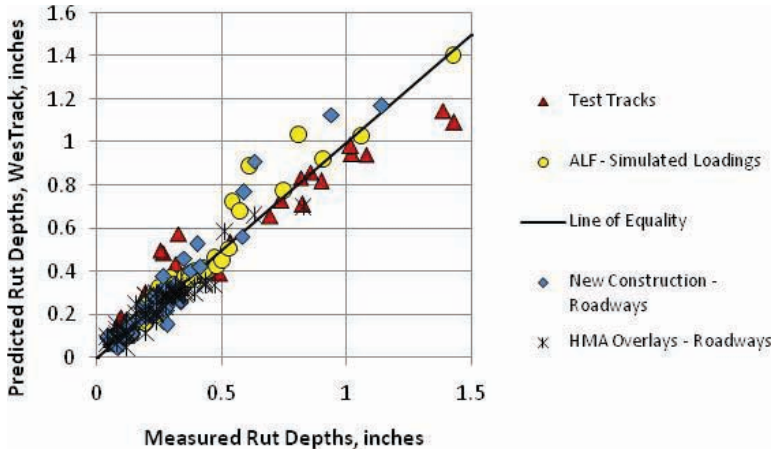

Figure 108. Comparison of predicted and measured rut depths for the WesTrack transfer function.

(Von Quintus, Andrei, and Schwartz, 2005). It is essentially an *n*/2 jackknifing scheme and has been termed split-sample jackknifing. Split-sample jackknifing can provide better measures of prediction accuracy than the traditional split-sample validation. The traditional split-sample approach, however, was used because it was believed that a sufficient number of sections were available.

Selected test sections were used to validate the results from the calibrated field-adjusted laboratory-derived values for the plastic strain coefficients for the Kaloush, modified Leahy, and WesTrack transfer functions. The test sections used for the validation process were selected from other test sections within the same experiment to develop the correspondence between the field-matched and laboratory-derived values.

Table 31 summarizes the statistical parameters for each transfer function. The statistical values derived from the calibration and validation data sets are similar. In addition, the slope of the correspondence between the predicted and measured values is similar to the line of equality, and it does go through the origin (refer to Figures 106 through 108).

3.3 Mixture Volumetric Adjustment Factors: Input Level 2

This section of Chapter 3 presents the relationship between the plastic strain coefficients and volumetric properties of each transfer function. This analysis was completed in estimating the laboratory-adjusted plastic strain coefficients from volumetric properties. The relationships reported under NCHRP Project 1-40B (refer to Appendix C) were initially used but were modified based on the results from the different transfer functions. The test sections used to develop the relationships to estimate the values for the plastic strain coefficients were designated in Tables 4 and 5 as those for Level 2 analysis. The other test sections designated in Tables 4 and 5 were used to compare the predicted and measured rut depths (discussed in Section 3.3.4).

Two factors found to be important from the analyses completed within this study that were excluded from the NCHRP Project 1-40B volumetric adjustment factors are (1) *m*-value as affected by modified mixtures and (2) HMA thickness. Thus, revisions were made to the initial relationships and are presented and discussed in the following sections.

3.3.1 Intercept of Transfer Functions

The field-adjusted, laboratory-derived intercept is required to estimate the transfer function intercept for each transfer function. A relationship was proposed for use from the NCHRP Project 1-40B procedure and is presented in Appendix C for the Kaloush transfer function, but that relationship was for the k_{r1} input variable to the MEPDG. The recommended relationships to estimate the intercept from the secondary region of triaxial and shear-based tests are provided as follows:

$$I_{Triaxial} = 10^{-3.6}\left(\frac{V_a}{V_{Design}}\right)^{0.52}\left(Log(VFA)\right)\left(F_{Index}\right)\left(C_{Index}\right) \quad (27)$$

$$I_{Shear} = 10^{-3.25}\left(\frac{V_a}{V_{Design}}\right)^{0.58}\left(Log(VFA)\right)\left(F_{Index}\right)\left(C_{Index}\right) \quad (28)$$

where

V_a = in-place air voids of the HMA layer, percent.
V_{Design} = design air void level for selecting the target asphalt content, percent.
VFA = voids filled with asphalt, percent.
F_{Index} = an index number related to the fine aggregate angularity (FAA) of the combined aggregate blend; refer to Table 32 for the recommended values.
C_{Index} = an index number related to the coarse aggregate angularity (CAA) of the combined aggregate blend; refer to Table 32 for the recommended values.

The values from Equation 27 were entered in Figure 105 to estimate the field-matched intercept for the Kaloush and

Table 32. Aggregate properties for determining the mixture volumetric adjustment factors for the intercept. (Values in table were taken directly from the NCHRP Project 1-40B procedure; refer to Appendix C.)

Fine Aggregate	Gradation	Fine Aggregate Angularity; AASHTO T 304				
		<45			>45	
FAA index value	External to restricted zone	1.0			0.9	
	Through restricted zone	1.05			1.0	
Coarse aggregate	**Gradation**	**Percentage Coarse Aggregate with Two Crushed Faces; AASHTO T 335**				
		0	**25**	**50**	**75**	**100**
CAA index value	Well graded	1.1	1.05	1.0	1.0	0.9
	Gap graded	1.2	1.1	1.05	1.0	0.9

modified Leahy transfer functions, while the value from Equation 28 was entered in Figure 104 to estimate the field-matched intercept for the WesTrack transfer function. The field-matched values were multiplied by the thickness adjustment factors provided in Table 30 for determining the inputs to the MEPDG Version 9-30A for the three transfer functions.

The NCHRP Project 1-40B procedure (provided in Appendix C) included a gradation factor that discriminated between fine- and coarse-graded mixtures. This same relationship was not exhibited as part of the laboratory and field-matched intercept values. It is expected that VFA and the fine and coarse aggregate angularity values adequately account for the effect of varying aggregate types and gradation.

3.3.2 Temperature Term Exponent of Kaloush Transfer Function

The Kaloush transfer function is the only one of the three recommended for use that includes temperature as a dependent variable in the transfer function. The NCHRP Project 1-40B procedure recommended the use of an adjustment that was based on air voids, effective asphalt content by volume, and gradation factors (see Appendix C). Results from this study that were reported and documented in Chapter 2 and the earlier parts of Chapter 3 suggest that this parameter be set and not changed. Thus, the temperature exponent was set to 1.5606, and all of the adjustment was to the intercept value to be consistent with the other two transfer functions, as discussed previously.

3.3.3 *m*-Value or *N*-Term Exponent of Transfer Functions

The adjustments recommended for use from the NCHRP 1-40B evaluation were based mostly on test sections that included neat HMA mixtures. The Asphalt Institute sponsored a study that determined the relative difference in performance between HMA neat and modified mixtures. That study reported a significant reduction in rut depths for HMA modified mixtures in comparison to HMA neat mixtures for dense-graded mixtures.

The Asphalt Institute recommended a correction or adjustment to the intercept value for the Kaloush transfer function to reduce the bias in predicting the rut depths of modified mixtures but not to the *m*-value or exponent to the *N*-term (refer to Figure 14). That decision was primarily made for simplicity, and few laboratory test results (repeated-load triaxial and shear tests) were available for predicting the rut depths of different HMA mixtures and pavement structures.

Results from this study, however, found a consistent difference in the *m*-value between HMA neat and modified mixtures for the same aggregate blend, as illustrated in Figure 109. As shown, the *m*-values of dense-graded HMA mixtures with modified asphalt are consistently lower than for neat asphalt for the same aggregate blend or job mix formula.

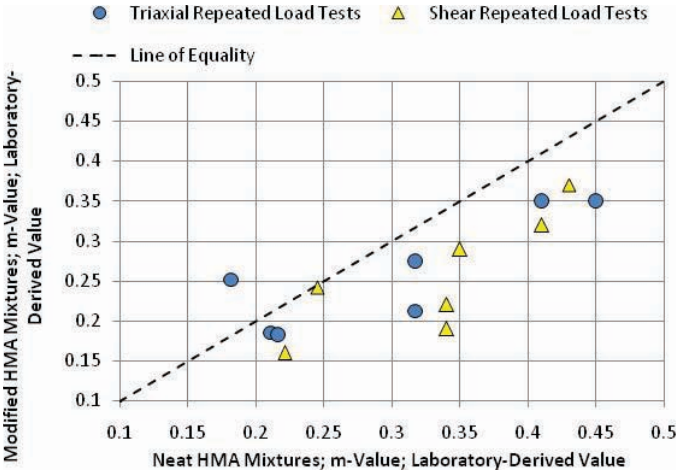

Figure 109. Laboratory-derived m-values for neat and modified HMA mixtures for the same gradation or aggregate blend.

Another important observation from Figure 109 is that the difference in *m*-values between the modified and neat mixtures appears to be the same for both the triaxial and shear tests. Thus, an adjustment is recommended for use in estimating the *m*-value when modified asphalt is substituted for neat asphalt, rather than making the adjustment to the intercept of the transfer function. The relationship for estimating the *m*-value for dense-graded mixtures is provided in Equation 29.

$$m - Value_{Neat} = 0.265\left(\frac{P_b}{P_{b(Opt)}}\right)^{0.75} \quad (29)$$

where

P_b = Asphalt content by weight at construction (the in-place value), percent.

$P_{b(Opt)}$ = Saturation or optimum asphalt content by weight, percent. This parameter defines the asphalt content at which the voids in mineral aggregate (VMA) start to increase or the density of the mixture starts to decrease.

For the use of modified asphalts, the *m*-value for neat asphalt mixtures is adjusted by Equation 30:

$$m - Value_{Modified} = m_b\left(m - Value_{Neat}\right) \quad (30)$$

where

m_b = an adjustment that accounts for the use of modified mixtures for the same aggregate blend of neat asphalt mixtures and is defined in the following:

For m-values less than or equal to 0.2: $m_b = 1.0$.

For m-values greater than 0.2:

$$m_b = 0.072 + (m - Value)0.64 \qquad (31)$$

3.3.4 Comparison of Predicted (Input Level 2) and Measured Rut Depths

The test sections included in Tables 4 and 5 and designed as calibration sections were used to predict the rut depths in comparison to the measured values. In other words, the test sections used to develop the relationships for the intercept and m-value were not used to determine the accuracy and precision arising from the use of those relationships. Figure 110 shows the comparison of the predicted and measured rut depths for the test sections designated as calibration sections in Tables 4 and 5.

Adjusting the plastic strain coefficients of the Kaloush transfer function to account for volumetric properties did result in an improvement (lower bias and standard error), but the statistical values are still considered poor. Figure 110 provides a comparison of the predicted and measured rut depths and summarizes the statistical values from Input Level 2. As shown, use of the volumetric properties and binder type to estimate values for the plastic strain coefficients improved the precision and accuracy of the three transfer functions in comparison to use of the one set of global values (Input Level 3; refer to Table 27), but they are still less than using Input Level 1 (refer to Table 31).

3.4 Assessment and Effectiveness of Rut-Depth Transfer Functions

The important criteria to be considered in the models' evaluation process are listed in the following in order of importance, as established from consensus of the participants.

- Model accuracy (consensus selection as the most important factor).
- Sensitivity to HMA mixture volumetric properties (binder type, aggregate blend, etc.).
- Sensitivity to temperature.
- Robustness.

As noted in Chapter 2, Section 2.1.1, it was the consensus of the participants that the rut depth predictions should be as accurate as possible, but the group did not reach consensus regarding any quantification of "acceptable" accuracy. It was also the consensus of the participants that the rut depth model should have the capability to predict rut depths over the entire range of values. In other words, the participants agreed that the rutting comparisons should not be limited to values below some maximum rut depth.

The approach for assessing the effectiveness of the different rut-depth prediction models took two forms: (1) an analysis and comparison of results related to the previously listed criteria and (2) an incremental benefit–cost (B-C) analysis.

3.4.1 Accuracy and Precision of Transfer Functions

The first approach simply compared the error terms and bias between the predicted and measured rut depths. The error term is important to the methodology used within the

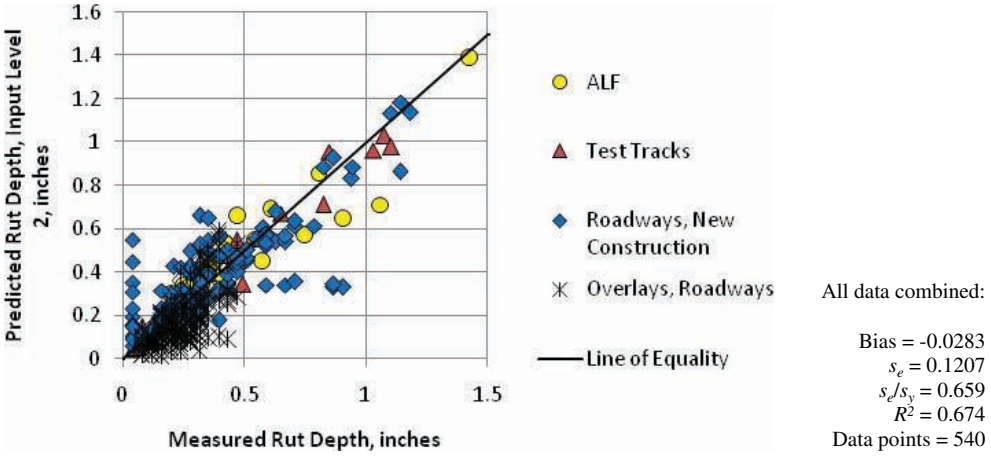

Figure 110. Comparison of predicted and measured rut depths for those test sections used for the Input Level 2 analysis.

MEPDG software for designing various pavement structures and mixtures at different reliability or confidence levels. The higher the error term, the greater the predicted rutting for the higher confidence or reliability level selected by the designer. The transfer function standard error terms for Input Level 1 are provided in Table 31.

The transfer function with the smaller error term defined the suggested improvements to the MEPDG and rut-depth prediction methodology currently embedded in the software. However, a significant difference between the error terms of alternate transfer functions and test methods in support of those transfer functions was not found. The modified Leahy transfer function has the lower standard error, but it is not substantially different from the standard errors of the other two transfer functions. In addition, the bias for the three transfer functions is less than the tolerable bias of 0.05 in., and the standard errors for the three transfer functions are within the rut-depth measurement error.

3.4.2 Benefit–Cost Analysis

The alternate transfer function with the lower standard error may have the higher materials characterization (testing) costs. Thus, a second approach was used for selecting the transfer function and supporting test methods for improving the MEPDG rut-depth prediction methodology included in the software.

The second method assesses the transfer functions using an incremental B-C ratio approach for determining which of the alternates considered has the greatest effectiveness. A similar process was used on an FHWA-sponsored project to determine the effectiveness of different testing programs and to optimize the number of tests based on performance criteria (Von Quintus, Andrei, and Schwartz, 1985). An explanation of the incremental B-C analysis and the assumptions used is provided in Appendix F.

The testing program needed for the HMA materials characterization and the total error term resulting from the MEPDG runs without any changes (using the global calibration values determined from NCHRP Project 1-37A) represent the baseline condition. The increased costs within the incremental benefit–cost ratio concept are the laboratory tests to establish the input values and/or calibration values. The benefit is a lower error term, defined as an increase in pavement life or reduced life-cycle costs considering the more accurate estimates of rutting using the same design life. Three alternates were considered:

1. Use of repeated load tests to estimate the values for the plastic strain coefficients; Input Level 1.
2. Use of volumetric properties from mixture design to estimate values for the plastic strain coefficients; Input Level 2.
3. Use of one set of global values for the plastic strain coefficients; Input Level 3.

The following summarizes the results from the incremental B-C analysis using results from laboratory tests and field performance.

3.4.2.1 Input Level 3 Versus Input Level 2

The standard error for Input Level 3 was set at 0.22 in. for all transfer functions, which represents the lower standard error of all transfer functions (Verstraeten) using the global plastic strain coefficients. The standard error for Input Level 2 was set at 0.121 in. (refer to Figure 110).

The difference in costs between these two alternates is negligible because the volumetric data is extracted from historical construction records or mixture designs. The only added cost is performing additional tests during mixture design to quantify the in-place properties. As such, the B-C ratio between these two alternates is large—significantly exceeding 1.0 for all conditions because the standard error was reduced by about 50% and the life related to rutting would be more than doubled. Input Level 3 is discarded and alternate 2 (Input Level 2) and 1 (Input Level 1) are compared.

3.4.2.2 Input Level 2 Versus Input Level 1

The costs assumed for the repeated-load triaxial and shear tests are summarized and discussed in Appendix F. The standard errors for Input Level 1 are provided in Table 31. The testing costs between the triaxial-based transfer functions (Kaloush and modified Leahy) were considered equal, and the standard errors were not substantially different, so these two became equal or were considered one option. The B-C ratios were only compared between the Kaloush and WesTrack (shear-based) transfer functions and associated testing costs and are provided in Appendix F. The incremental B-C ratios are also provided in Appendix F.

The standard error terms between these two options are also considered to be not substantially different. As such, no significant difference between the triaxial and shear-related transfer functions exists. The important or more significant finding from the incremental B-C analysis is that use of repeated load tests to estimate pavement life in terms of rutting resistance or failure is beneficial with ratios being greater than 1.0 for most conditions, as summarized in Tables 33 and 34. The difference between Tables 33 and 34 is the *m*-value used for the HMA layers, which represents the range of values determined from the calibration process.

As shown, the larger the paving project, the higher the reliability level selected and the higher the rut-depth trigger value, resulting in B-C ratios greater than 1.0. A value of 0.25 in. was

Table 33. Results from incremental benefit–cost analysis for comparing Input Levels 1 and 2 for lab-adjusted *m*-values of less than 0.35 (cells with B-C ratios greater than 1.0: use of repeated load testing is cost effective; benefit exceeds the cost).

Trigger Value, in.	Reliability Level, percent	HMA Overlay Project		
		Small Project, <$1M	Intermediate Project Size	Large Project, $5M
0.25	75	B-C > 1.0	B-C > 1.0	B-C > 1.0
	85			
	95			
0.50	75		B-C > 1.0	B-C > 1.0
	85	B-C > 1.0		
	95			
0.75	75			B-C > 1.0
	85		B-C > 1.0	
	95	B-C > 1.0		

The shaded cells have B-C ratios of less than one.

used for the lower trigger value or rut-depth design criteria, but that value would be considered impractical for most agencies. B-C ratios of less than 1.0 for the low failure criteria are related to the measurement error in comparison to the overall standard error of the transfer functions. In summary, for intermediate and higher volume roadways, repeated load testing is cost effective, while for lower volume roadways, Input Level 2 would be recommended.

3.4.3 Hypothesis Evaluation

The hypotheses used to develop the sampling template are listed in Section 2.4.2. This section discusses whether the specific hypotheses used to develop the sampling template were accepted or rejected. (Note: The hypotheses listed in Section 2.4.2 are reworded here.)

Hypothesis #1: The long-term aging model included in the MEPDG is assumed to be correct and will not result in a bias of the predicted rut depths between the transfer functions. The plastic strain parameters are assumed to be independent of time (i.e., dynamic modulus of the HMA is the only property that varies with time and depth). It was hypothesized that there would be no bias between roadway segments that include aging and the accelerated pavement tests and test tracks that exclude long-term aging. If a significant bias was found between the two conditions for all transfer functions, this would imply that the aging function needs to be revised or that aging should be applied to the plastic strain parameters of the transfer functions.

No significant difference was observed or found between the residual errors for test sections with no (or minor amounts of) long-term aging (ALF sections) and those with long-term aging (roadway sections). As such, increasing the dynamic modulus over time and closer to the surface is believed to be reasonable for distortion or rut depth analyses. Obviously,

Table 34. Results from incremental benefit–cost analysis for comparing Input Levels 1 and 2 for lab-adjusted *m*-values greater than 0.45 (cells with B-C ratios greater than 1.0: use of repeated load testing is cost effective; benefit exceeds the cost).

Trigger Value, in.	Reliability Level, percent	HMA Overlay Project		
		Small Project, <$1M	Intermediate Project Size	Large Project, $5M
0.25	75		B-C > 1.0	B-C > 1.0
	85	B-C > 1.0		
	95			
0.50	75			B-C > 1.0
	85		B-C > 1.0	
	95	B-C > 1.0		
0.75	75			B-C > 1.0
	85			
	95		B-C > 1.0	

The shaded cells have B-C ratios of less than one.

this statement might not be true for fracture or disintegration type distresses.

To directly evaluate the in-place plastic deformation properties over time requires a test method with the capability to test cores. Cores were taken along some of the test sections to confirm or reject this hypothesis. Repeated-load constant-height shear tests were performed on cores recovered from several test sections. The test results from the cores were presented and discussed in Chapter 2. Too few test sections were included in this analysis because some cores were damaged during the coring process and some of the mixtures exhibited moisture damage. From the few test results, it is believed that the assumption that the plastic strain coefficients are time independent is reasonable, but there is insufficient data to confirm or reject the hypothesis (refer to Figures 98 to 101).

Hypothesis #5: Dynamic modulus by itself will not eliminate the bias or explain the plastic deformation of HMA mixtures, and that bias is dependent on mixture characteristics but is independent of design features and strategies.

This hypothesis was accepted. A comparison of the bias and standard error using the Kaloush transfer function for selected sections found that both terms were unaffected by using calculated and measured dynamic modulus (refer to Figures 89 and 90). NCHRP Project 9-30(01) also reported that the residual errors of the MEPDG rut depth predictions were similar between different runs using dynamic modulus Input Levels 1 (measured dynamic modulus) and 3 (calculated dynamic modulus). In other words, the difference between the residual errors of runs made with Input Levels 1 and 3 was small; most of the error is from other sources (Von Quintus, Andrei, and Schwartz, 2005).

Hypothesis #6: The relative deviation or difference between measured and predicted rut depths for test sections in the same sampling cell is caused by material property differences, and that difference can be captured by repeated-load triaxial or constant-height shear tests. Similarly, laboratory HMA repeated-load triaxial or constant-height shear strain tests will discriminate between the rutting resistance of modified and neat HMA mixtures.

This hypothesis was accepted. Large standard errors were found between and across the cells of the sampling template. In addition, a different transfer function bias was observed between neat and modified HMA mixtures (refer to residual errors compared in Figures 84 through 88). Use of repeated-load triaxial and shear tests eliminated that difference in the bias and significantly reduced the standard error of the transfer functions.

Hypothesis #7: The depth correction or confinement functions included in the MEPDG Version 9-30A (refer to Equations 2 and 8) are a reasonable simulation of the effect of the upper HMA layers.

This hypothesis was accepted for the triaxial and shear-based transfer functions, even though a consistent difference in the transfer function intercept was identified for thin HMA layers (less than 5.0 in.) in comparison to thick HMA layers. The test sections where the greater difference was observed in the intercept values between thin and thick HMA layers were those exhibiting significant rutting in the unbound layers. In summary, it was unclear whether this consistent difference was a result of differences in the unbound layers or HMA. Thus, the hypothesis was not rejected. A thickness correction or adjustment factor was included for thin HMA layers for all transfer functions. The thickness adjustment factors are defined in Section 3.3.

Hypothesis #8: The rut-depth transfer function included in the MEPDG Version 1.1 (defined as the Kaloush function) provides an accurate simulation of the evolution of rut depths measured on HMA-surfaced pavements over the design life of the pavement.

This hypothesis was rejected using the *N*-term exponent or k_{r3} of 0.4756 (refer to Equation 1), which was based on repeated-load unconfined, uniaxial tests (refer to Figures 1 and 10). When using laboratory-derived values for the *m*-value or *N*-term exponent, the hypothesis was accepted for the three transfer functions (refer to Figures 7 to 10 and Figures 89 and 90). All transfer functions were found to provide an accurate simulation of the rut depth evolution and magnitude of rutting when using results from repeated load tests.

Hypothesis #9: Laboratory HMA repeated-load triaxial or constant-height shear strain tests provide a simulation of HMA rutting evolution.

Use of laboratory-derived values for the plastic strain coefficients (primarily the secondary region intercept values) resulted in a significant bias compared to the measured rut depths (refer to Figures 100 and 101). When the laboratory-derived values were adjusted to remove the bias, however, they provided an accurate simulation of the evolution of rutting (refer to Figures 4 to 8 and Figures 98 to 100). In other words, the adjustment factors for the laboratory-derived plastic strain coefficients are not equal to unity. Thus, this hypothesis was accepted after the field adjustment factors were applied to determine the layer-dependent Input Level 1 values for the plastic strain coefficients for the Kaloush, modified Leahy, and WesTrack transfer functions.

Hypothesis #10: After calibration, the MEPDG plastic-to-elastic axial strain ratio rut-depth transfer function will have the same accuracy and precision as the plastic shear strain and normal strain or deviator stress-based transfer functions.

This hypothesis was accepted after the effects of thin HMA layers were accounted for in estimating the Input Level 1 values for the plastic strain coefficients of the Kaloush, modified Leahy, and WesTrack transfer functions (refer to Table 31). It should be noted, however, that test sections with anomalous features were excluded from the comparison of measured and predicted rut depths.

3.4.4 Other Factors or Observations

This section identifies and discusses other observations from the data that are considered important to future use of the MEPDG.

3.4.4.1 Estimating the Intercept from Repeated Load Tests

As noted in Chapter 2, a major difference between the plastic axial and plastic shear strain accumulation is in the primary stage or region—the plastic shear strain accumulates at a much lower rate than the plastic axial strain (refer to Figures 68 and 70). Figure 111 shows the relationship between the intercepts for the primary and secondary regions from repeated-load triaxial and shear tests. As shown, there is more variation in the triaxial test data than for the shear test data. The important point of this observation is that the primary intercept (plastic strain at $N = 1$) can be much more easily defined and measured in comparison to the intercept defined from the secondary region (refer to Figures 68 and 70). Although the standard errors were found to be not substantially different between the transfer functions, the shear-defined intercept had less measurement error than the triaxial-defined intercept. It is believed that as additional data are collected with time, this observation will become more important.

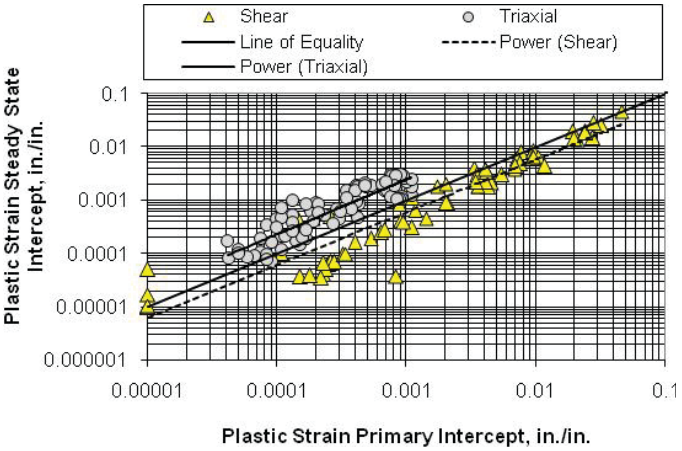

Figure 111. Correspondence between the primary and secondary intercept values from repeated load tests.

3.4.4.2 Nonlinearity Effects

As noted in Chapter 2, Figure 43 summarizes the influence of deviator stress on the slope of the plastic strain relationship—the average slope of the plastic strain relationship increases with increasing deviator stress. Inclusion of this effect into the MEPDG HMA rutting model was considered, but the standard errors were found to be more dependent on other factors. In summary, it is believed that nonlinearity has a minor effect on the plastic deformation coefficients of the different transfer functions.

3.4.4.3 Variability: Effect from Test Temperature

The plastic shear strains between the replicate test specimens have more dispersion in the data at the lower test temperatures (where the rut depth accumulation is less critical) and less dispersion between the replicates at higher test temperature (where the rut depth accumulation is critical). Conversely, the dispersion of the plastic vertical strains between the replicate test specimens is greater at the higher test temperature and lower for the lower test temperature—just the opposite for repeated shear tests. The lower variability between replicates at the higher test temperature where rutting occurs is considered a benefit from using repeated-load shear tests and will result in fewer replicates for the same level of confidence.

3.4.4.4 Laboratory Test Data Shape Characteristics Between Replicates

Another observation from the test data is that the same mixtures exhibited tertiary flow for the repeated-load triaxial-vertical strain tests on at least one of the replicates for the intermediate test temperature. None of the repeated-load constant-height shear specimens exhibited that characteristic for the lower and intermediate test temperatures. Figure 112 shows the rut depths measured with time for two LTPP SPS projects. (Figure 91 shows the variability in rut depth measurements as well as the relative change over time for four additional LTPP projects.) As shown, the rut depths increase at a uniform rate or at a decreasing rate—similar to the rate of increasing shear strains from the repeated-load constant-height shear test. None of the test sections included in the calibration–validation process exhibited tertiary flow characteristics such as accelerated rutting past some level of traffic.

3.4.4.5 Laboratory Test Data Variability and Equivalent Temperature Concept

An important observation from the laboratory test results from the repeated-load triaxial and shear tests is the variability

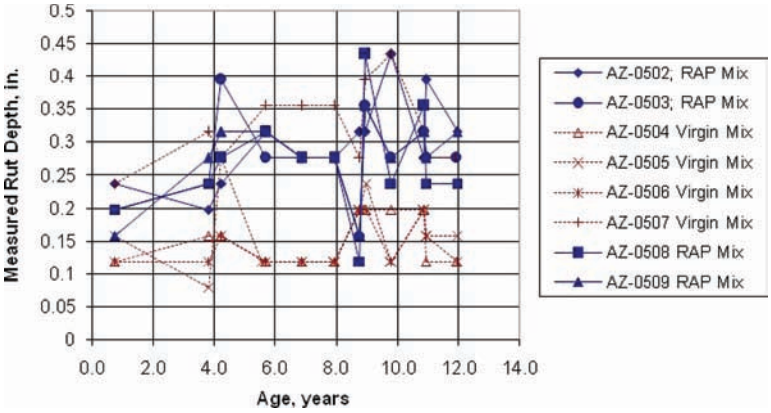

(a) Rut depths measured on the Arizona SPS-5 test sections.

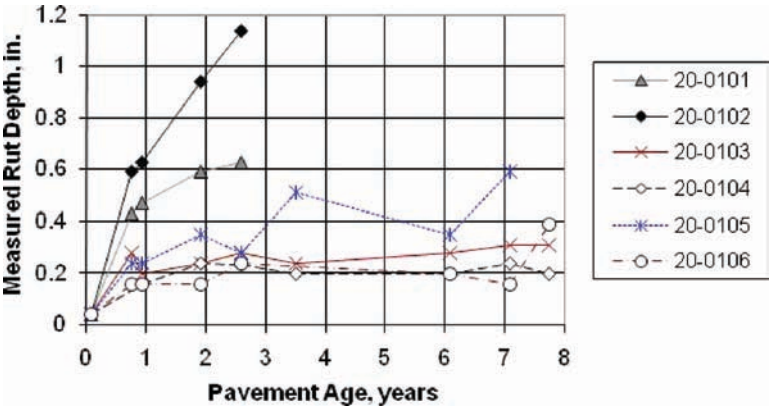

(b) Rut depths measured on the Kansas SPS-1 test sections.

Figure 112. Rut depths measured over time for two LTPP SPS projects.

between replicate test specimens and test temperatures. Figure 113 shows an example from the repeated-load triaxial and shear tests for the Arizona SPS-5 binder mixture. As shown, the variability in the results for plastic strain accumulation in the triaxial-based test for the lower test temperature is consistent, or the variability between replicates is smaller at the lower test temperature. Conversely, the variability between replicates is smaller at the higher test temperature for the shear-based test. The results provided in Figure 113 are typical of other mixtures included in the production and exploratory test program, discussed in Chapter 2 and presented in Appendix E.

Rutting occurs at the higher test temperature, so the test with the lower amount of variability at the higher test temperature should require fewer tests for the same level of confidence. This observation suggests that the transfer function based on triaxial test results should have the higher standard error because of the greater dispersion in the test data for the same number of tests. However, the equivalent annual pavement temperature was used to determine values for the plastic strain coefficients. The equivalent annual pavement temperature used to determine the plastic strain coefficients is near the midrange test temperature used in the laboratory. For the midrange test temperature, the variability is still higher for the repeated-load triaxial tests in comparison to the shear tests, but it is much less. This is believed to be a reason why the predicted versus measured rut depths for the three transfer functions (Kaloush, modified Leahy, and WesTrack) were found to be not substantially different.

Another important observation from the laboratory tests is that many of the repeated-load triaxial tests exhibited tertiary flow and accelerated plastic strain at the midrange and high test temperature, while almost none of the repeated-load shear tests exhibited these characteristics (refer to Figure 113). Tests exhibiting tertiary flow increase the error in estimating the slope and intercept from the secondary region because it is more difficult to determine for some test specimens or mixtures.

3.5 Application: Mixture Design and Acceptance

The Kaloush, modified Leahy, and WesTrack transfer functions were used to prepare a brief analysis of the test results that can be used to judge the rutting resistance of HMA mixtures

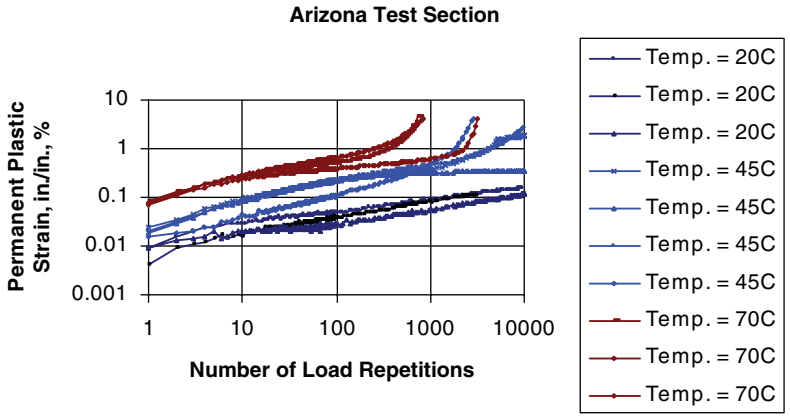

(a) Repeated-load triaxial test results for the Arizona SPS-5 binder mixture.

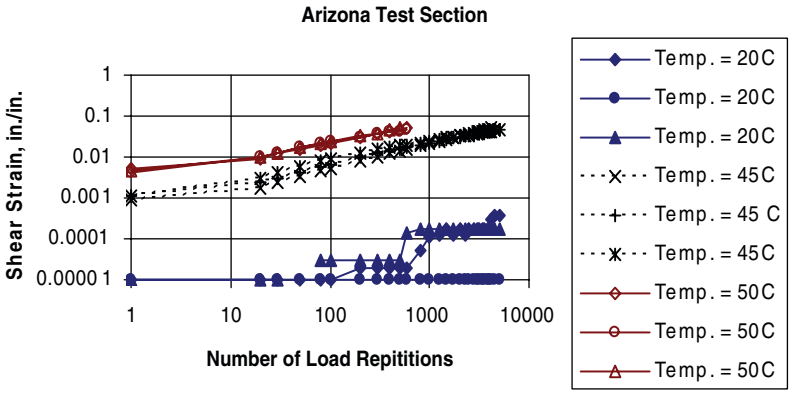

(b) Repeated-load shear test results for the Arizona SPS-5 binder mixture.

Figure 113. Results from repeated-load triaxial and shear tests for different temperatures for one mixture in the LTPP program.

without running or executing the MEPDG Version 9-30A software for all projects. Figure 114 shows a graphical analysis of the rutting resistance of dense-graded HMA mixtures. The intercept or coefficient and *m*-value or slope for each transfer function represents the field-matched values.

The two lines or boundaries represent 0.25 in. and 0.75 in. of rutting of the HMA mixtures. In other words, all combinations of *m*-values and the intercept or coefficient of the transfer function that fall along the good resistance to rutting line will exhibit 0.25 in. of rutting, while any combination of *m*-values and the intercept falling along the poor resistance to rutting will exhibit 0.75 in. of rutting. These boundary conditions were developed for a conventional HMA structure in a mild climate on a high-volume roadway. Similar graphs can be prepared for other structures, traffic volumes, and climates.

Laboratory repeated-load tests are performed in the laboratory, and the laboratory-derived intercept and *m*-value are determined in accordance with the procedure documented in Chapter 2. The field-adjusted laboratory-derived values are then determined in accordance with the appropriate Figures 103 to 105. The field-adjusted values for both plastic strain coefficients are plotted on the appropriate graph in Figure 114. If the points plot below the good resistance to rutting line, the mixture is considered resistant to rutting. Conversely, if the points plot above the poor resistance to rutting line, the mixture is susceptible to distortion.

3.6 Advanced Mixture Characterization and Rut-Depth Simulation Models

Most practical applications for evaluating stress and strain responses in pavement structures, including the MEPDG, use linear elasticity theory to model the mechanical behavior of materials. This simplified modeling technique conveniently reduces computational time, but it is incapable of taking into consideration more complex behavior of materials, such as inelastic deformations observed in HMA at certain loading and environmental conditions. To overcome such limitations, empirical expressions are used to correlate elastic to plastic deformations to predict rutting of flexible pavement structures.

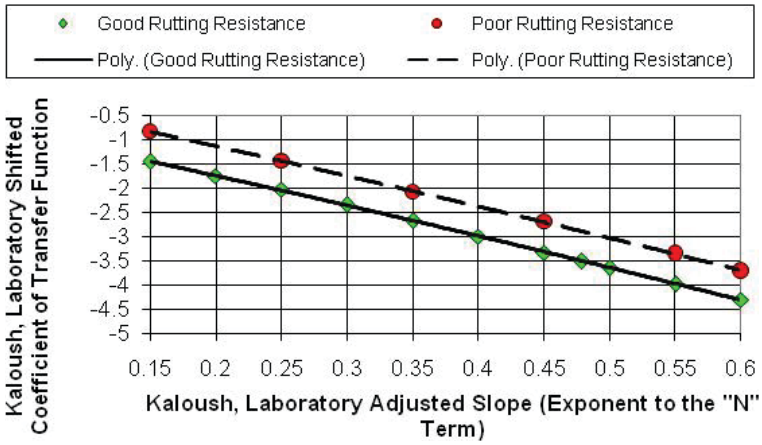

(a) Kaloush transfer function.

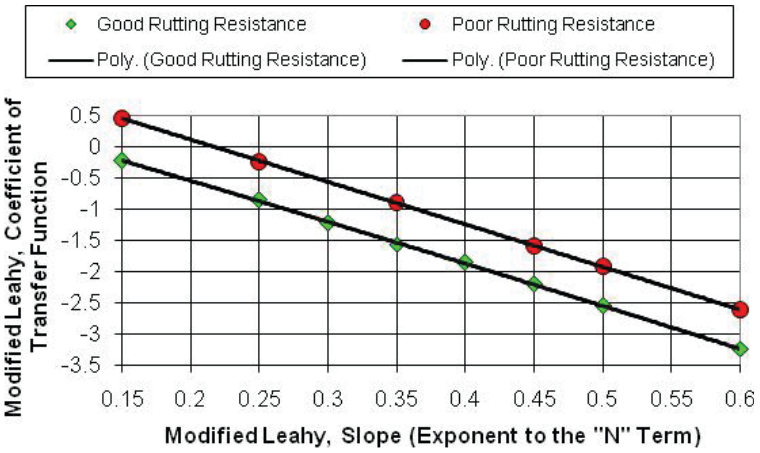

(b) Modified Leahy transfer function.

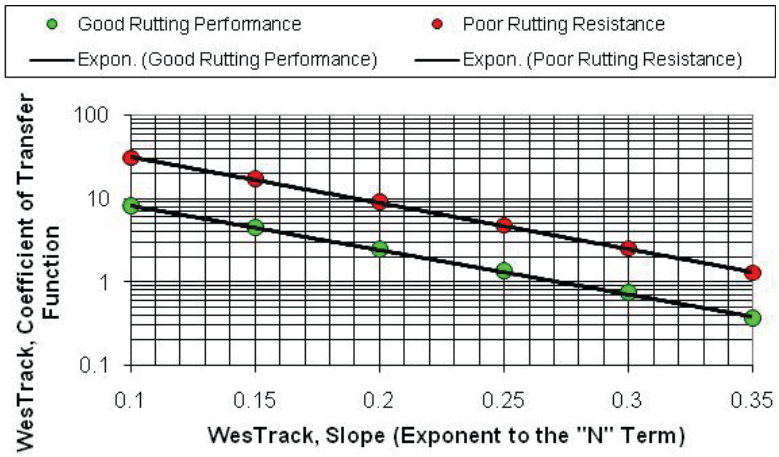

(c) WesTrack transfer function.

Figure 114. Comparison of predicted and measured rut depths for those test sections used for the validation process.

Advanced mixture characterization tools, however, provide qualitative information about the mechanics of deformation at various critical locations within the pavement structure. The focus of the advanced mixture characterization effort in this project was to use a more fully mechanistic tool to explain rutting formulations in flexible pavement structures and confirm or make proposals for revising some of the empirical formulations included in the MEPDG. These could include, for example, the depth functions embedded in the MEPDG and the test conditions for the triaxial and shear repeated-load tests. Another focus of this effort was to create a material property database that could be used for verifying more fully mechanistic models for evaluating the distortion of HMA mixtures.

This part of Chapter 3 includes a summary of the advanced mixture characterization studies conducted to help explain and propose changes to the MEPDG rut-depth prediction computational methodology. Appendix K provides more detailed discussion on the results from the advanced mixture characterization and modeling tools.

3.6.1 Advanced Mixture Characterization Tests

The advanced materials characterization testing was completed by subcontractors: the University of Maryland and North Carolina State University. The advanced materials characterization testing was to provide data used to verify and confirm the more mechanistic-based rut-depth prediction model. Data collected from these tests can also be used as a future resource to advance the state of the art of fully mechanistic modeling. The specific material properties and tests for the advanced mixture characterization included:

- Linear viscoelastic relaxation modulus and creep compliance: determined from axial dynamic modulus testing.
- Continuum damage properties in tension and compression: determined from constant-strain-rate tests to failure at low temperatures, which include minimal viscoplasticity effects on the measured responses. Additional constant-strain-rate tests to failure at higher temperatures can be used for model validation.
- Viscoplasticity properties in tension and compression: determined from creep and recovery tests at elevated temperatures.
- Additional calibration–validation tests: indirect tension; repeated-load permanent deformation at various stress states/temperatures.

The objective was to take projects constructed under controlled conditions for which traffic, climate, and other input parameters were well defined. Materials from these projects were characterized using the full suite of material characterization tests that can be used to validate or verify advanced constitutive models. HMA mixtures from the FHWA ALF were used for this effort. Results from these tests were documented and included in the project database for future use.

3.6.2 Model Formulation

ABAQUS was selected as the vehicle for the modeling effort because it is a robust commercial finite-element package with good support resources and a wide base of users in many engineering fields. ABAQUS has powerful preprocessing and post-processing capabilities to simplify modeling and analysis of results. It also includes several features useful for more advanced analysis (e.g., dynamic analysis, advanced nonlinear models for unbound materials, tire–pavement interactions). Most importantly, ABAQUS permits the development and inclusion of user-defined material (UMAT) subroutines.

Two user-defined model components or materials subroutines were included in ABAQUS: a viscoelastic continuum damage (VECD) model and a viscoplastic (VP) model. The combined VEPCD model is a viscoelastic continuum damage formulation with extension to viscoplasticity. Total strains are decomposed into three parts: viscoelastic, damage, and viscoplastic. Microstructural damage is incorporated in the viscoelastic component via the elastic–viscoelastic correspondence principle and is defined as a function of internal-state variables. The viscoplastic strain is computed separately and integrated to the viscoelastic/damage strain through the use of the total strain decomposition.

The viscoelastic with damage component is based upon work by Ha and Schapery (Ha and Schapery, 1998; Schapery, 1999). The viscoplastic component is formulated using Perzyna's viscoplastic theory with HiSS flow surface (Desai and Zhang, 1987). Details of the implementation, calibration, and validation of this model in the context of HMA were documented by Gibson (2006). The constitutive model developed by Gibson (2006) at the University of Maryland was implemented into the ABAQUS commercial finite-element program.

The VEPCD model was relatively simple to calibrate using three sets of tests performed over an appropriate range of temperatures and loading rates. The calibration tests included, as noted previously: (a) a conventional dynamic modulus test to determine the undamaged viscoelastic properties, (b) unconfined and confined constant-strain-rate tests to failure at low temperatures to determine the damage functions,

and (c) unconfined and confined cyclic creep and recovery tests to failure at high temperatures to determine the viscoplastic properties.

The HMA layer was also modeled in two ways: as a linear elastic material and as a nonlinear material using the Drucker–Prager frictional plasticity model in ABAQUS assuming a linear yield surface and a piecewise linear hardening law. The unbound pavement layers were modeled as linear elastic materials in both cases. The Drucker–Prager plasticity model for HMA was calibrated using unconfined and confined axial strength test data for a typical dense-graded HMA mixture. Although not a perfect match to the measured data, the predictions based on finite element analyses are qualitatively acceptable for providing insights for the improvement of mechanistic–empirical procedures.

The plasticity model in predicting the rutting with the number of axle load simulations in some of the FHWA ALF test pads did result in a consistent bias, but an evolution of rutting was predicted that closely matched the values measured over time. Results from the studies to confirm the applicability of the depth function, evolution of rutting using actual wheel load simulations from the ALF, and results for determining the test conditions used in the laboratory repeated-load tests are documented in Appendix K.

CHAPTER 4

Conclusions and Proposals for Implementation and Future Research

4.1 Conclusions

The objective of this research effort was to propose revisions to the HMA rut-depth transfer function in the MEPDG software developed under NCHRP Project 1-37A for consideration by NCHRP and the AASHTO Joint Task Force on Pavements. The following are key conclusions and findings from this study relative to improving the MEPDG for use in evaluating an HMA mixture's resistance to rutting or distortion.

1. The most important conclusion from this project, in the authors' opinion, is that repeated-load plastic deformation tests (shear and triaxial) are cost effective. The benefit–cost ratio was above 1.0 for most conditions analyzed for the threshold rut depths that are typically used by agencies in defining when to rehabilitate HMA pavements and overlays (refer to Tables 32 and 33). In other words, use of values derived for Input Level 1 will be beneficial to agencies in managing and designing HMA mixtures and pavements to ensure long life and minimal maintenance costs.

   The standard error based on the use of repeated load testing (Input Level 1) was found to be lower than the standard error based on the use of volumetric properties (Input Level 2) to estimate the values for the plastic strain coefficients of each transfer function. The use of Input Level 3 or the use of one set of global values for the plastic strain coefficients is not recommended.
2. Another important conclusion is that the Kaloush, modified Leahy, and WesTrack transfer functions provide similar accuracy and precision for predicting rut depths after calibration using repeated-load plastic deformation tests. In other words, the standard error and bias were found to be not substantially different between the three transfer functions after calibration in using repeated-load plastic deformation tests (refer to Table 31). All three transfer functions were found to provide a reasonable simulation or prediction of the rut depth evolution in significantly different climates, levels of truck traffic, and pavement structures, and are proposed for future use (refer to Figures 21 through 24).
3. With regard to the use of repeated-load plastic deformation tests (triaxial or shear), results from the repeated-load plastic deformation tests can be used, with an adjustment to field-matched values (laboratory-derived, field-adjusted plastic strain values) to predict the rut depth of HMA mixtures over time. In previous versions of the MEPDG and the current version of DARWin-ME, no guidance is provided for taking the results from repeated-load plastic deformation tests and entering mixture-specific values in the software. Results from this study provide adjustment factors or relationships that can be applied to the laboratory-derived slope or *m*-value and intercept from the secondary region of the repeated load tests and used directly as inputs to the software (refer to Figures 103 to 105).
4. Although all three transfer functions are proposed for future use in evaluating the rutting resistance of HMA mixtures, it is proposed that the WesTrack transfer function be included in the future versions of DARWin-ME. This proposal arises from the ability to test field cores using the repeated-load constant-height shear test. The ability to test field cores with the in-place properties over time is especially important to carry out forensic investigations, settle disputes between owner and contractor on warranty projects, and establish the change in mixture properties over time that is especially important for warm-mix asphalt, polymer-modified, and high-RAP mixtures. Additional reasons for including the WesTrack transfer function and using the repeated-load constant-height shear test in future versions of DARWin-ME are:
   a. The intercept from the secondary or steady-state region can be more easily or more accurately estimated from the primary intercept that is easily measured from the

laboratory tests (refer to Figure 111). Less variability was observed between the primary and secondary intercepts for the shear-based tests, which suggests that fewer test specimens are needed at the same level of confidence.

b. The variability between sample replicates for the higher test temperatures, where rutting occurs, is lower for the repeated-load constant-height shear tests in comparison to the triaxial tests. The triaxial test was observed to have the higher variability between replicates for the higher test temperature. Again, less variability at the critical temperature suggests that fewer test specimens are needed at the same level of confidence.

c. Few of the test specimens tested in the constant-height shear test exhibited tertiary flow characteristics in comparison to the number of test specimens exhibiting tertiary flow from the triaxial test. None of the test sections included in the study (ALF test pads, test tracks, and roadway sections) exhibited actual tertiary flow under real traffic conditions.

d. The disadvantage in using the repeated-load shear-based tests is the compaction mold. Little effort has been directed toward compacting samples for shear testing using a form of rolling wheel compaction—no commercial equipment is currently available that would be comparable to the Superpave gyratory compactor for compacting samples for triaxial testing.

5. The use of layer- or mixture-dependent values for the plastic strain coefficients is proposed in designing mixtures for a specific location or depth within the pavement structure. The use of one set of values for the plastic strain coefficients of the transfer functions will result in less precise estimates of pavement life relative to distortion for all three transfer functions. In addition, dynamic modulus by itself did not explain the difference in rutting between different mixtures and other conditions. For example, differences in dynamic modulus are not sufficient to explain the difference in *m*-values and rutting between modified and neat HMA mixtures (refer to Figure 109).
6. The transfer functions that include a stress term as an independent variable correctly accounted for the thickness effect on rut depth for some structures, but not all (refer to Figures 97 and 98). In other words, the value for the coefficient of the stress term (deviator stress or shear stress) was defined to minimize the thickness adjustment factors for some of the pavement structures.
7. Without question, the global *m*-value or *N*-term exponent for the Kaloush transfer function (0.4791) is too large. Laboratory-derived and field-matched values were found to be significantly less than that value of the global exponent [refer to Figure 103(b)]. In addition, repeated-load confined, triaxial tests are proposed for use with the Kaloush and modified Leahy transfer functions. Unconfined tests will result in higher *m*-values that do not represent the rut depth evolution from multiple test sections (as an example, refer to Figures 89 and 90).
8. The depth functions included in the MEPDG and DARWin-ME were found to be reasonable in estimating the rut depths for varying HMA thicknesses. Although thickness adjustment factors were recommended (refer to Table 30), the overall effect of thickness is believed to be reasonable. No other revision or correction is proposed other than the thickness correction or adjustment factors.
9. The aging model included in the MEPDG was found to provide reasonable results, and no bias was found between the ALF, test tracks, and roadway segments once the laboratory-derived values were used in predicting the rut depths for sections with different levels of aging.

4.2 Proposals for Implementation and Future Research

It is proposed that the three transfer functions identified from this research project (Kaloush, modified Leahy, and WesTrack) be implemented in the MEPDG and future versions of DARWin-ME. Any one of the transfer functions can provide an acceptable simulation in terms of accuracy and precision of the measured rut depths over a diverse range of dense-graded mixtures and pavement structures. More importantly, repeated-load plastic deformation tests in support of the transfer functions to determine the values for the plastic strain coefficients were found to be cost effective. At a minimum, it is proposed that the WesTrack and repeated-load constant-height shear tests be included in the program, along with the Kaloush transfer function, for the reasons noted in Section 4.1.

Potential topics for problem statements that are identified for future research projects are listed and briefly explained in the following.

- The repeated-load constant-height shear tests can be used to evaluate the effects of long-term aging on the performance of HMA wearing surfaces and base mixtures because of their applicability or ability to test thin layers. This item is considered a significant benefit over current triaxial tests in terms of measuring the in-place properties from cores for warm-mix asphalt, high RAP content, and modified HMA mixtures. However, AASHTO provisional standard practice PP 3 for preparing reconstituted shear-based test specimens from bulk HMA mixtures or individual material components by means of the rolling wheel compactor has expired. Additional work is proposed in the future to improve on the compaction molds and procedures for preparing shear test specimens and to identify critical features of rolling wheel compaction to reduce the

amount of variability between replicate test specimens. This proposal assumes that the WesTrack transfer function and use of repeated-load constant-height shear tests will be included in a future version of the DARWin-ME software.

- The current methodology included in the MEPDG and DARWin-ME uses monthly average temperature values on a quartile basis, and those values are used to predict pavement distress. The MEPDG and DARWin-ME do not tie temperature to a time or to a traffic level. It is assumed that truck traffic is equally distributed during the day. A proposed improvement to the MEPDG and DARWin-ME is to tie temperature to traffic, similar to the methodology used for PCC pavements. Use of the MEPDG or DARWin-ME would then provide more accurate and precise estimates of rutting for which truck traffic occurs within a specific segment of the daytime or nighttime hours.
- It is proposed that support be continued for the Materials Reference Library for storing materials and mixtures for future use in calibrating and validating distress transfer functions and future fully mechanistic models (advanced mixture characterization methods in support of fully mechanistic models) for both fracture and distortion type of distresses.

APPENDIX A

Proposed Addendum to AASHTO Publication MEPDG-1: *Mechanistic–Empirical Pavement Design Guide, Interim Edition: A Manual of Practice*

The intent of Appendix A is to provide a summary of the procedure to determine the HMA plastic deformation parameter inputs to the MEPDG Version 9-30A to predict rutting so that it can be used as a reference to the MEPDG *Manual of Practice* that was published in 2008. This assumes that the AASHTO DARWin committee will recommend that one or multiple rut-depth transfer functions be included in the official MEPDG software released or updated with time for the AASHTO members. The procedural manual was prepared as a standalone document so that it can be easily converted to an AASHTO Recommended Practice, if proposed for publication and use by NCHRP.

A.1 Introduction

This manual presents the procedures and guidelines for determining values for the plastic deformation constants of hot-mix asphalt (HMA) mixtures for selected rut-depth transfer functions that are included in the *Mechanistic–Empirical Pavement Design Guide* (MEPDG) software referred to as Version 9-30A. The rut-depth transfer functions included in the MEPDG Version 9-30A software are referred to as the Kaloush, WesTrack, modified Leahy, Verstraeten, and Asphalt Institute transfer functions. All of these transfer functions are discussed in detail in the research report, but the Kaloush, modified Leahy, and WesTrack functions are proposed for use in mixture and structural design.

The guidelines are based on the calibration of the Kaloush, modified Leahy, and WesTrack rut-depth transfer functions using repeated-load plastic deformation tests, measured material properties, and rut-depth time-series data from field and other full-scale pavement sections. Based on the results from the NCHRP Project 9-30A study (comparison of measured and predicted rut depths), these three transfer functions can be used with similar accuracy and precision.

A.2 Scope of Manual

The manual provides guidelines for using repeated-load triaxial and constant-height shear tests with different rut-depth transfer functions for evaluating the rutting susceptibility of dense-graded HMA mixtures in accordance with the MEPDG rut-depth computational methodology. This includes analyses of repeated-load plastic deformation tests to determine mixture- and layer-specific inputs to the MEPDG for different transfer functions.

The transfer functions proposed for use and included in the MEPDG Version 9-30A software are listed in the following and are defined in greater detail in Section A.6 of this manual.

1. Kaloush vertical strain transfer function; the transfer function included in the original MEPDG software developed in NCHRP Project 1-37A (Kaloush and Witczak, 2000).
2. WesTrack shear strain and shear stress transfer function (Epps et al., 2000).
3. Modified Leahy vertical strain and deviator stress transfer function—a modified form of the original Leahy or Asphalt Institute transfer function. The modified Leahy transfer function excludes the temperature and asphalt property factors included in the original Leahy (Asphalt Institute) transfer function because dynamic modulus of the mixture is used to compute the HMA mixture response for predicting rut depths.

The original Leahy or Asphalt Institute and Verstraeten transfer functions were included in the NCHRP Project 9-30A study but excluded from the procedural manual. The reasons for excluding both transfer functions are provided in Chapter 3, Data Interpretation and Application, of *NCHRP Report 719.*

As part of the repeated-load triaxial and shear tests and corresponding transfer functions, the NCHRP Project 1-40B HMA mixture adjustment factors are included as Level 2 inputs in accordance with the MEPDG input hierarchical definition; regression equations or relationships are used to estimate the values of the plastic strain coefficients from HMA volumetric properties.

A.3 Significance and Use

The procedures included in the manual are intended to be used for the design and evaluation of individual dense-graded HMA mixtures and/or layers using laboratory repeated-load plastic deformation tests instead of default values that were determined from the global calibration effort for each transfer function.

The MEPDG software developed in NCHRP Project 1-37A uses the same set of default values for the plastic deformation coefficients for all layers and assumes that dynamic modulus tests will account for any difference in rutting between the different layers. Use of only dynamic modulus tests, however, did not improve on the accuracy and precision of the transfer functions. The MEPDG Version 1.0 software was modified so that HMA layer-specific coefficients could be entered into the software. This modified software package is referred to as MEPDG Version 9-30A.

Use of repeated-load tests and measured HMA plastic deformation constants for each layer improved the goodness-of-fit and overall accuracy of the rut-depth transfer functions and prediction methodology included in the MEPDG Version 9-30A software. Repeated load testing is recommended for use in calculating the level of rutting of HMA mixtures for rehabilitation and new pavement construction during design and/or to create a materials library on a mixture-specific basis.

The following paragraphs summarize the conditions most appropriate for using the specific test procedure and transfer functions listed in Section A.2: Scope of Manual. A more detailed discussion on the use of each test procedure and transfer function (in comparing the predicted rut depth and standard error terms) is included in Chapter 3 of *NCHRP Report 719.*

- Repeated-load triaxial tests and corresponding rut-depth transfer functions (Kaloush and modified Leahy) can be used during the mixture design stage and mixture production when the component materials or bulk mixture can be sampled for preparing test specimens in accordance with AASHTO TP 79. The height-to-diameter requirement required for the test specimens eliminates the use of cores for HMA lifts of less than 4 in. in thickness. The test procedure can be used for lift thicknesses that are greater than 6 in. For lift thicknesses of 4 in. to 6 in., test specimens can be cored laterally along a larger sample extracted from the HMA mat with the assumption that aggregate alignment has little to no impact on the plastic deformation parameters. That assumption or hypothesis is believed to be false (Von Quintus et al., 1991). In addition, coring the test specimens laterally from a larger sample is not included within this procedural manual. This height-to-diameter requirement also restricts the use of this procedure to determine the MEPDG inputs for forensic investigations or follow-up studies when there are disputes between the owner and contractor over any warranty work and actual materials are unavailable to reconstitute the HMA mixture, since most HMA lifts or layers are less than 4 in. in thickness.
- Repeated-load constant-height shear tests and the WesTrack rut-depth transfer function can be used during the mixture design stage, mixture verification, and forensic investigations when cores are the only samples available for testing. The restriction on the use of this test method is that laboratory rolling-wheel compaction molds for preparing the test specimens are unavailable on a production basis. Gyratory-compacted specimens have been used with success but require the use of oversize gyratory samples (larger diameter samples) so that the test specimen can be cored from the gyratory-compacted sample (Witczak, 2007; Witczak et al., 2002). The use of the gyratory compactor is known to result in variable air voids across the radial axis as well as along the vertical axis of the compacted specimen. AASHTO TP 79 requires that the gyratory-compacted specimens be cored to test the center portion of the specimen. Coring the center portion of the gyratory specimen reduces the air void gradients within the test specimen and is a preferred surface for mounting the LVDTs on the test specimen.

A.4 Summary of Analysis Procedure

The MEPDG does not directly include flow number as a mixture input parameter. Repeated-load plastic deformation tests are used to determine values for the coefficients to the rut-depth transfer functions included in the MEPDG Version 9-30A software. The laboratory-derived coefficients are adjusted or shifted to represent field conditions. The shift factors were developed using multiple test sections included in the FHWA-LTPP program, full-scale test track test sections, and roadway segments.

A.4.1 Hierarchical Input Level and Plastic Strain Constants

The procedures used to determine the plastic deformation constants are based on the input hierarchical structure included in the MEPDG.

1. Input Level 1 represents the use of repeated load tests: (1) repeated-load triaxial (confined) tests or (2) repeated-load constant-height shear tests. The plastic vertical strain

or plastic shear strain measured over a defined number of load cycles is used to determine the coefficient and slope (exponent for the loading cycles term) of different rut-depth transfer functions. These laboratory-derived plastic deformation constants are determined over multiple test temperatures or at the equivalent test temperature and shifted or adjusted to represent field conditions. The adjusted values are entered into the MEPDG Version 9-30A software for each HMA layer.

2. Input Level 2 represents the use of HMA material component and mixture volumetric properties to estimate the plastic deformation properties for each layer.
3. Input Level 3 simply uses the default values for the plastic deformation coefficients that are determined either globally or locally.

Input Level 1 is recommended for use for all design–build and warranty type projects and for HMA mixture and structural design verification by the agency when the contractor is responsible for mixture design (refer to Section A.6.2). Input Level 2 is recommended for use during pavement structural designs when access to the HMA materials is unavailable to the owner or pavement designer (refer to Section A.6.3). In this case, the plastic deformation parameters for the specific rut-depth transfer function should be determined using historical construction data stored within the agency's or contractor's construction-materials database. Input Level 3 is not recommended for use other than for paper studies. It is included in the previous list to be inclusive of all hierarchical input levels allowed within the MEPDG.

A.4.2 Shift Factors: Field-Matched Values for the Plastic Strain Coefficients

Results from the repeated-load plastic deformation triaxial and constant-height shear tests were used to directly predict rut depths of numerous LTPP and full-scale test track test sections using the rut-depth transfer functions. The laboratory-derived parameters resulted in a large positive bias and high standard error of the estimate for each transfer function. Thus, measured rut depths were used to determine the parameters for each project that reduced the bias and standard error. Figure A.1 shows an example of the comparison of measured and predicted rut depths for two projects through matching the transfer function parameters to the measured rut depths.

The laboratory-adjusted values were combined for all projects to define the common shift factors or laboratory-adjusted parameters of each transfer function to minimize the bias and standard error. The shift factors apply to both the multiple temperature and equivalent temperature options (discussed in Section A.6).

A.4.3 Test Temperature Option and Number of Test Specimens

Two test temperature options are available for use that are applicable to all rut-depth transfer functions: (A) the multiple test temperature option and the (B) equivalent test temperature option. The number of test specimens is dependent on whether the multiple temperature or equivalent temperature option is selected.

A.4.3.1 Option A: Multiple Test Temperatures

The multiple temperature option uses three test temperatures that are defined as (1) 50% reliability PG high temperature minus 5°C, (2) 20°C, and (3) the middle temperature between the first two. For the multiple test temperature option, two test specimens at each temperature are required for a total of six test specimens. The multiple test temperature option should be used for pavement structural designs, during the final mixture design stage, and for detailed forensic investigations.

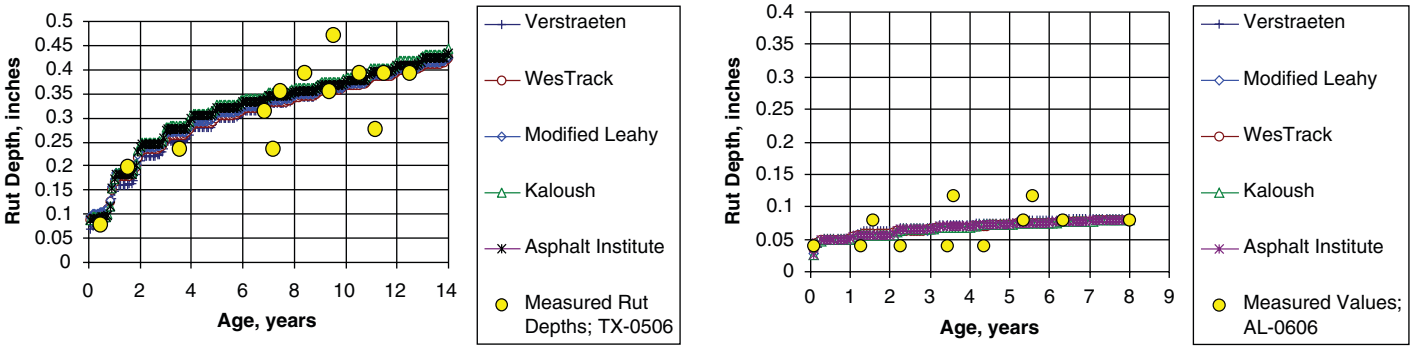

Figure A.1. Measured and predicted rut depths, using different transfer functions, after the plastic deformation coefficients were matched to field conditions.

A.4.3.2 Option B: Equivalent Test Temperatures

The equivalent temperature option uses one test temperature that is defined as the equivalent temperature that will result in the same level of rutting at the end of the design period with the rutting predicted using temperatures defined for that climate and structure. For the equivalent test temperature option, three total test specimens are required. The equivalent test temperature option should be used for mixture design verification and acceptance of HMA mixtures during construction.

A.5 Repeated-Load Plastic Deformation Testing

This section of the procedural manual provides guidance on preparing and testing the test specimens for measuring values for the plastic deformation coefficients relative to a specific rut-depth transfer function.

A.5.1 Target Air Void Level

The target air void level for all test specimens should be the average air void level expected after rolling (the expected mean air void level from the construction specifications). When cores are recovered for testing using the repeated-load constant-height shear test with the multiple temperature option, the cores should be grouped in accordance with Section A.5.3 of this manual.

A.5.2 Short-Term Aging the HMA Mixtures

The test specimen preparation process for reconstituting the materials during the mixture design stage includes the short-term aging procedure to simulate HMA production. Mixtures for all specimens should be short-term oven-aged for 4 hours at 135°C in accordance with AASHTO R 30, Mixture Conditioning of Hot Mix Asphalt (HMA), prior to compaction. (The short-term aging procedure recommended for use in AASHTO TP 79 or an equivalent procedure should be used.)

The short-term aging procedure should not be used on test specimens prepared from bulk mixtures sampled during construction or on cores since they already include short-term aging.

A.5.3 Repeated Load Testing for MEPDG Input Level 1

This section of the procedure manual is divided into two parts that relate to the repeated-load test procedure selected. Two test options can be used to determine the inputs to the MEPDG Version 9-30A software: (I) repeated-load triaxial (confined) tests and (II) repeated-load constant-height shear tests.

A.5.3.1 Option I: Repeated-Load Triaxial (Confined) Tests

The required number of test specimens should be prepared depending on whether the multiple test temperature or equivalent test temperature option is being used (refer to Section A.4.3 of this manual). All test specimens should be prepared from reconstituted samples of the aggregate and asphalt that are blended and compacted to the volumetric conditions after construction or bulk mixture sampled during production.

A.5.3.1.1 Test Specimen Preparation. Specimens for triaxial testing are fabricated in accordance with AASHTO PP 60, Preparation of Cylindrical Performance Test Specimens Using the Superpave Gyratory Compactor. This is the specimen fabrication standard developed for making specimens for the Asphalt Mixture Performance Tester in NCHRP Project 9-29.

All triaxial test specimens should be prepared in accordance with AASHTO TP 79, Compaction of Triaxial Test Specimens for Dynamic Modulus and Repeated Load Permanent Deformation Tests. The specimen size used in all repeated-load triaxial tests was 100 mm by 150 mm. This test procedure has a stringent height-to-diameter requirement, so testing cores under Option I is not covered within this procedure manual. As noted previously, materials should be sampled and reconstituted during the mixture design stage or bulk HMA sampled during production.

A.5.3.1.2 Grouping of Test Specimens. The air void tolerance for all test specimens should be in accordance with AASHTO TP 79. When the multiple test temperature option is selected, sort the test specimens into three subsets of two specimens each (or the number of test specimens selected for each test temperature) so that the average air voids of the different subsets are approximately equal. Grouping of the test specimens is not required when the equivalent temperature option is selected because all test specimens are tested at the same test temperature.

A.5.3.1.3 Testing Conditions. The repeated axial load and confining pressure recommended for use in measuring the repeated-load plastic deformation parameters using confined triaxial tests of each test specimen are:

- Repeated axial load applied to the test specimen is 70 psi.
- Confining pressure is 10 psi.

A.5.3.1.4 Testing Procedure. The dynamic modulus and repeated-load plastic deformation tests should be measured in accordance with AASHTO TP 79, Determining the Dynamic

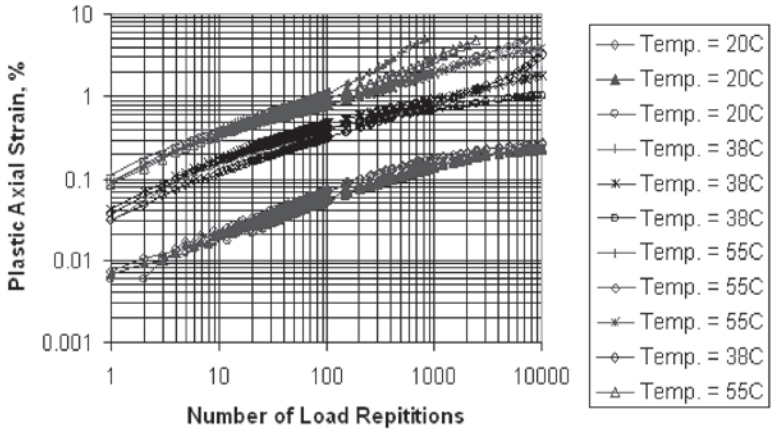

Figure A.2. Test results from a repeated-load triaxial (confined) plastic deformation test.

Modulus and Flow Number for HMA Using the AMPT. The plastic and total strains should be measured and stored in the data acquisition system in accordance with AASHTO TP 79. Figure A.2 shows a graphical example of the test results.

A.5.3.2 Option II: Repeated-Load Constant-Height Shear Tests

The required number of test specimens should be prepared depending on whether the multiple test temperature or equivalent test temperature option is being used (refer to Section A.4.3 of this manual). The laboratory test specimens for this test procedure can consist of laboratory specimens reconstituted during the mixture design stage, bulk HMA mixtures sampled during production, or cores recovered from the pavement.

A.5.3.2.1 HMA Mixture Preparation: Reconstituting HMA Component Materials. All repeated-load constant-height shear test specimens that are reconstituted in the laboratory should be prepared in accordance with AASHTO PP 60 regarding the reconstituting, mixing, and short-term aging of the mixture, if applicable. The same short-term aging of the HMA mixture is used for these test specimens as for the triaxial test specimens.

A.5.3.2.2 Test Specimen Preparation. The test specimens require a minimum diameter of 6 in. and minimum height of 2 in. This subsection is divided into two parts: one addresses the compaction of reconstituted mixtures in the laboratory and bulk mixtures sampled during procedure, and the other addresses the use of cores.

Compaction of Test Specimens: Reconstituted Samples and Bulk Mixtures Sampled During Construction. Most gyratory compactors compact 6-in. diameter specimens, which means that the compacted specimen cannot be cored to remove the higher air void level near the outside edges of the specimen. Based on results from projects sponsored by SHRP, FHWA, and NCHRP, the radial air void gradient will affect the shear properties of the mix. As a result, it is recommended that the test specimens be compacted using a rolling wheel compactor.

Fabrication of specimens for simple shear testing using rolling wheel compaction should follow AASHTO PP 3, Preparing Hot Mix Asphalt (HMA) Specimens by Means for the Rolling Wheel Compactor. This standard was developed during SHRP but was deleted from the AASHTO Provisional Standards in 2003. Chapter 2 of *NCHRP Report 719* provides details on the rolling wheel mold and procedure that was used to compact all test specimens for repeated-load shear tests.

A test pad can be constructed in the laboratory using the procedure and equipment documented in Chapter 2 of the report or in the field using full-scale equipment (placement and compaction equipment) through the use of a control strip in terms of mixture design confirmation prior to construction. Laboratory rolling-wheel compaction molds can be easily constructed. The setup and mold size, however, should be adjustable to allow preparation of a variable-length slab that is 30-in. wide and 4-in. thick. The variable length is needed because the amount of materials can vary for compacting the full-size, 30-in. by 30-in. slab specified in AASHTO PP 3. The test pad can be rolled using a small self-propelled roller with a static drum weight of 3,000 lbs.

The required number of 6-in.-diameter test specimens should be cored from the test pad. The thickness of the pad should be 4 in. to allow the extracted core to be sawed on the bottom and top to ensure parallel surfaces. The cutting or sawing process should be done in accordance with AASHTO PP 60.

Cores Recovered from the In-Place HMA Mat. The location for coring the HMA mixture is not covered in this procedure manual. The location and number of cores should

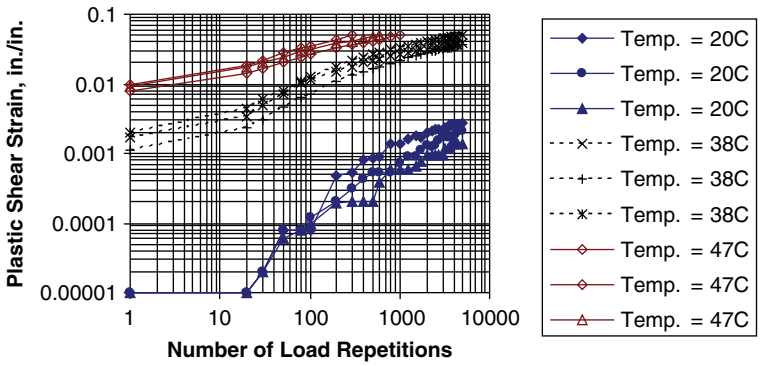

Figure A.3. Test results from a repeated-load constant-height shear test.

be determined at random points that are typically used in quality assurance programs. The number of cores should be estimated to ensure statistical accuracy using typical quality assurance methods and depends on the variability of the air voids along the project.

The top and bottom of each core should be sawed in accordance with PP 60 to ensure that the surfaces of the core are parallel.

After sawing, measure the bulk specific gravity in accordance with AASHTO T 166 or T 275, whichever applies, and calculate the air voids for each test specimen in accordance with AASHTO T 269.

A.5.3.2.3 Grouping of Test Specimens. The air void tolerance for all test specimens should be in accordance with AASHTO TP 79. When the multiple test temperature option is selected, sort the test specimens into three subsets of two specimens each (or the number of test specimens selected for each test temperature) so that the average air voids of the different subsets are approximately equal. Grouping of the test specimens is not required when the equivalent temperature option is selected because all test specimens are tested at the same test temperature.

A.5.3.2.4 Testing Procedure. The repeated shear testing should be conducted in accordance with AASHTO T 320, Determining the Permanent Shear Strain and Stiffness of Asphalt Mixtures Using the Superpave Shear Tester. In this test, a repeated shear stress of 10 psi is applied to the specimen while applying sufficient axial stress to keep the height of the specimen constant. The test specimen has LVDTs to monitor the shear deformation and the axial deformation. The shear pulse is 0.1 s with a 0.6 s rest period. The test should be continued to 5,000 cycles or to a plastic shear strain of 5%.

The plastic shear and total shear stains should be measured and stored in the data acquisition system in accordance with AASHTO TP 79. Figure A.3 shows a graphical example of the test results.

A.6 Analysis of Repeated-Load Test to Determine Plastic Deformation Coefficients

This part of the procedure manual overviews the different rut-depth transfer functions included in the MEPDG Version 9-30A and determination of values for the plastic deformation coefficients of those transfer functions using laboratory repeated-load test results.

A.6.1 Rut-Depth Transfer Functions

A.6.1.1 Transfer Functions Based on Repeated-Load Triaxial (Confined) Test Results

HMA plastic deformation properties recommended for use in the MEPDG Version 1.0 were determined from repeated-load unconfined tests in a low stress range. This is adequate if only relative comparisons of different HMA mixtures are made. For mixture evaluation and predicting rut depths, however, relative comparisons can be inadequate. Stress state depends on tire pressure, tire type, axle load, temperature, layer thicknesses, pavement type, and so on.

To estimate the roadway conditions to be simulated in the laboratory and to be consistent with the structural evaluation procedures used, elastic layer theory or other response models can be used to calculate the stresses and strains in an HMA layer under different loading, environmental, and structural conditions. Of course, all assumptions used with elastic layer theory apply to these recommendations, and the normal and principal stresses calculated on an element in an HMA layer will not necessarily be the same as those in a triaxial test specimen. Thus, the octahedral shear stress theory (distortion energy theory) was used to calculate the confining stress

and vertical stress in the laboratory test specimen to result in an equivalent maximum octahedral shear stress calculated in the HMA layer itself. The octahedral shear stress is given by:

$$\tau_{OCT} = \frac{1}{3}\left[(\sigma_1 - \sigma_2)^2 + (\sigma_2 - \sigma_3)^2 + (\sigma_3 - \sigma_1)^2\right]^{0.5} \quad \text{(A.1)}$$

The octahedral shear stress at failure represents the critical shearing stress at yielding. For an analysis of stress, elastic layer theory was used to calculate the normal and principal stresses that exist in an element within the HMA layer for determining the appropriate laboratory loading conditions. This allows factors such as contact pressures, tire types, and total loads to be considered in the laboratory during mixture design and analysis to ensure that the HMA mixture can sustain the imposed stresses. The stress predicted using the octahedral shear stress theory was used in triaxial compression tests.

The maximum octahedral shear stress generally occurs under the wheel load at a depth of 2 in. to 4 in. below the surface, while the maximum shear stress occurs near the outside edge of the tire nearer the surface to values within the inside edge of the tire at depths of 2 in. to 4 in. below the surface. As reported by many others, the lateral and vertical stresses computed with elastic layer theory vary with structure, depth, and radius from the center of the wheel loads.

An exploratory test program was implemented to determine the range of confining pressures and vertical stresses that should be used in the laboratory test program for mixture characterization based on compression type tests. The test conditions, in terms of repeated axial stress (or deviator stress), and confining pressure recommended for use in most pavement analysis for HMA mixtures were determined from this exploratory program and are listed and included in Section A.5.3.1.3 of this manual.

A.6.1.1.1 Kaloush-Witczak Vertical Resilient Strain Transfer Function (Original Transfer Function Included in the MEPDG Developed in NCHRP Project 1-37A). The following equation is the plastic strain relationship included in the MEPDG to predict rut depth in the HMA layer increments.

$$\varepsilon_p = \varepsilon_r K_Z \beta_{r1} 10^{kr1} (T)^{kr2\beta r2} (N)^{kr3\beta r3} \quad \text{(A.2)}$$

where

ε_p = incremental plastic strain at the mid-depth of a thickness increment.
ε_r = resilient strain calculated at the mid-depth of a thickness increment.
T = temperature at the mid-depth of a thickness increment.
N = number of axle load applications of a specific axle type and load interval within a specific time interval.
β_{r1}, β_{r2}, β_{r3}, = local calibration coefficients, all equal to 1.0 for the global calibration effort and within NCHRP Project 9-30A.
k_{r1} = plastic deformation factor or coefficient (for the global calibration effort in NCHRP Project 1-40D, the coefficient equals –3.35412).
k_{r2} = plastic deformation factor related to the effect of temperature (for the global calibration effort in NCHRP Project 1-40D, the temperature exponent equals 1.5606).
k_{r3} = plastic deformation factor related to the effect of wheel load (for the global calibration effort in NCHRP Project 1-40D, the loading cycle's exponent equals 0.4791).
K_Z = depth function and equal to:

$$K_Z = (C_1 + C_2 D)(0.328196)^D \quad \text{(A.3)}$$

$$C_1 = -0.1039 H_{HMA}^2 + 2.4868 H_{HMA} - 17.342 \quad \text{(A.4)}$$

$$C_2 = 0.0172 H_{HMA}^2 - 1.7331 H_{HMA} + 27.428 \quad \text{(A.5)}$$

where

D = depth to the mid-depth of the thickness increment, in.
H_{HMA} = total thickness of the HMA layer.

The plastic deformation factors (k_{r1}, k_{r2}, and k_{r3}) are determined from repeated-load plastic deformation tests conducted in the laboratory and adjusted to field conditions. The k_{r3} factor is the slope within the steady-state or secondary range, k_{r1} is the intercept of the log–log relationship between the number of load applications and cumulative plastic strain, and the k_{r2} factor is the effect of temperature on the intercept.

A.6.1.1.2 Modified Leahy Vertical Strain and Deviator Stress Transfer Function (Based on Original Leahy or Asphalt Institute Transfer Function). Leahy performed uniaxial (unconfined) repeated-load plastic deformation tests on HMA test specimens spanning three asphalt content levels, two binder types, two aggregate types, three stress levels, and three temperatures. The final model recommended by Leahy (referred to as the Asphalt Institute transfer function) was based on multiple terms that were included in the transfer function. That transfer function is included in the MEPDG Version 9-30A, but was found to exhibit a higher standard error and larger shift factor. As a result the original equation was modified to exclude some of the terms that can be accounted for through the dynamic modulus of the HMA. The modified equation is provided in the following equation.

$$Log\left(\frac{\varepsilon_p}{\varepsilon_r}\right) = -0.50 + 0.25LogN + 0.110Log\sigma_d + 0.930LogV_{beff} + 0.5011LogV_a \quad \text{(A.6)}$$

where

ε_p = accumulated plastic strain at N repetitions of load.
ε_r = resilient strain of the HMA material as a function of temperature and time rate of loading.
N = number of load repetitions.
σ_d = deviator stress, psi.
V_{beff} = effective asphalt content, percent by volume.
V_a = air void content or voids total mix, percent.

A.6.1.2 Transfer Functions Based on Repeated-Load Constant-Height Shear Test Results

A.6.1.2.1 WesTrack Shear Strain and Shear Stress Transfer Function. The WesTrack model was recently developed to determine the importance of different mixture properties and their variance as related to rutting in establishing performance-related specifications. Two models were developed from the study:

- The Level I analysis is an empirical model relating mix properties to rut depth, while Level II is based on M-E principles. For Level I, rut depth is a function of ESAL's, air voids, asphalt content (percent by weight), and the percent of aggregate finer than the number 200 sieve.
- The Level II analysis consists of calculating the permanent shear strain (γ) at 50 mm below the surface, shear stress (τ), and compressive strain (εv) on top of the subgrade. Total rut depth measured at the surface is expressed as a function of the number of load repetitions by combining the rut depth predicted in the HMA layer and unbound layers.

The Level II analysis was included in the MEPDG Version 9-30A software. In simple loading, plastic shear strain in the HMA was assumed to accumulate according to the following equation.

$$\gamma_p = ae^{(b\tau)}\gamma_e N^c \quad \text{(A.7)}$$

where

γ_p = plastic or inelastic shear strain at a depth of 2 in. (50 mm) below the surface or below the top of the additional layers included in the structure.
γ_e = elastic shear strain at the same depth noted previously.
N = number of axle load applications.
a,b,c = regression constants.

Table A.1. Suggested values of *K* as a function of HMA layer thickness.

HMA Thickness, in.	*K*-Value
5 to 7	5.5
7 to 9	7.0
9 to 12	8.5
>12	10.0

The rutting that is estimated in the HMA layer due to shear deformation is determined from the following equation.

$$RD_{HMA} = K\gamma_{p,t} \quad \text{(A.8)}$$

where

K = a coefficient related to the thickness of the HMA layer (Table A.1).

A.6.2 HMA Mixture Evaluation Procedure: MEPDG Level 1 Input Determination

The following lists the steps used for determining/evaluating the rutting susceptibility of HMA mixtures using repeated-load plastic deformation tests—referred to in other documents as the flow number test. Two options are available, both of which are discussed.

A.6.2.1 Option A: Multiple Temperature Option

The multiple temperature option uses three test temperatures, which are defined as: (1) 50% reliability PG high temperature minus 5°C, (2) 20°C, and (3) middle-range temperature between the first two.

1. Determine the laboratory-derived slope or *m*-value of the steady-state or secondary region for each test specimen.

   The steady-state region is the area where the slope becomes constant between the number of loading cycles and accumulated plastic strain (refer to Figures A.2 and A.3). NCHRP Project 9-30A found that the average slopes between all test temperatures were approximately equal. Test specimens with significantly different slopes should be investigated to determine the reason for the different slopes. An additional test specimen can be prepared and tested when the variability is high and there is no obvious reason for the difference in the steady-state slopes.

   The average steady-state slope for both laboratory repeated-load tests should be determined based on a moving decade of loading cycles. (For example: 1 to 10, 2 to 20, 3 to 30, . . . ; 10 to 100, 20 to 200, 30 to 300, . . . ; 100 to 1000, 200 to 2000, 300 to 3000, . . . ; etc.) Once the slope becomes relatively constant (defined as the steady-state

region of the laboratory test), that value should be used as the exponent for the load cycle term (N) of the rut-depth transfer functions or m-value.

Two other opposite possibilities exist over the entire number of loading cycles for the laboratory repeated-load tests: (1) the slope continues to decrease over the entire number of loading cycles, and (2) the slope starts to increase at an increasing rate (refer to Figure A.2, which shows examples for each of these conditions for individual test specimens). Determining the slope for these conditions is discussed in the following.

a. When a test specimen starts to exhibit continual decrease in plastic strains with continued loading cycles, the average slope should be determined for the region prior to that decrease—when the slope is relatively constant.
b. When a test specimen exhibits accelerated plastic deformation (slope continually increases, typically referred to as tertiary flow and characteristic of repeated-load confined, triaxial tests), that part of the test should be excluded from determining the slope in the steady-state region of the test.

Systematic differences exist between the repeated-load confined, triaxial test and repeated-load constant-height shear test. At the beginning of the repeated-load triaxial test, the accumulated plastic axial strain increases but at a decreasing rate until the rate of change becomes relatively constant, as shown in Figure A.2. Conversely, at the beginning of the repeated-load shear test, the rate of the accumulated plastic shear strain is small and then the rate of change becomes relatively constant, as shown in Figure A.3. The initial areas for both of these tests should be excluded from determining the slope of the steady-state region. *NCHRP Report 719* discusses this difference in greater detail and provides examples for determining the slope in the steady-state regions from both tests for the different conditions noted here.

2. Determine the laboratory-derived representative slope from all test specimens.

The methodology included in the MEPDG assumes that the steady-state slope is independent of test temperature for all of the rut-depth transfer functions. Any change in temperature is accounted for in the temperature exponent of the Kaloush transfer function and/or through the effects of temperature on dynamic modulus for the other transfer functions that exclude temperature as an independent variable.

a. If the slope does not consistently change with test temperature, average all slopes.
b. If the slope consistently changes with test temperature (increasing or decreasing with test temperature), determine the representative slope at the equivalent temperature. Equivalent temperature is defined under Option B.

3. Determine the laboratory-derived intercept or coefficient of the transfer functions for each test specimen. The laboratory-derived intercept will be test-temperature–dependent.
   a. For the Kaloush transfer function that includes temperature as a parameter, determine the temperature dependency of the intercept through the exponent of the temperature term; the exponent to the temperature term should be determined from the laboratory test results.
   b. For the modified Leahy and WesTrack transfer functions, which exclude the temperature term, the representative slope should be determined at the equivalent temperature.
4. Using only the test specimens that were used to determine the representative laboratory slope, determine the laboratory intercept at the equivalent temperature. The equivalent temperature is defined and discussed in Section A.6.2.2 of this manual.
5. The field-matched parameters are determined for the HMA mixture and structure using the relationships noted in the following.
   a. Figures A.4 and A.5 are used to adjust the laboratory-derived representative slope value to the field-matched slope value for the two different repeated load tests. Figure A.4 is for adjusting the m-value or slope from repeated-load triaxial tests, while Figure A.5 is for adjusting the m-value from repeated-load shear tests.
   b. Figure A.6 through A.8 are used to adjust the laboratory-derived intercept to the field-matched intercept value, which are all transfer-function–dependent.
   c. The temperature exponent for the Kaloush transfer functions is not adjusted from the laboratory-measured values.
6. The field-matched intercepts for each transfer function from Figures A.6 to A.8 are multiplied by the thickness adjustment factors provided in Table A.2. The thickness adjustment factors for the Kaloush, modified Leahy, and WesTrack transfer functions were determined by comparing the field-matched intercepts of each function between the thicker and thinner test sections of experiments with the same mixture—basically using the LTPP SPS-1, SPS-5, and SPS-6 projects.
7. The field-matched parameters for each transfer function are then entered into the MEPDG software for predicting the rut depth for that mixture and pavement structure.

   If the total predicted rut depth is less than the threshold value for rutting, the mixture is considered adequate. If the predicted rutting is greater than the threshold value, however, a revised mixture design maybe needed.

   Note: It is assumed that the HMA mixture is not susceptible to moisture damage, adequate bond exists between the individual lifts, and compaction of the HMA

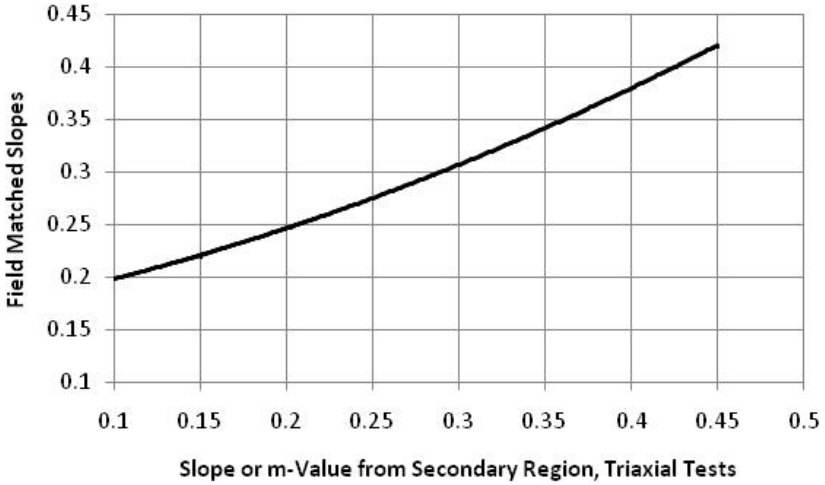

Figure A.4. Determining the field-matched slopes from laboratory-derived values from repeated-load triaxial tests, Kaloush and modified Leahy transfer functions. (Refer to Figure 103(b) in Chapter 3 regarding the dispersion in the data.)

mixtures excludes the occurrence of checking and other construction defects.

A.6.2.2 Option B: Equivalent Temperature Option

The equivalent temperature option uses one test temperature, which is defined as the equivalent temperature and will result in the same level of rutting at the end of the design period with the rutting predicted using temperatures defined for that climate and structure. The following lists the steps and determination of the values for the plastic strain coefficients based on the equivalent temperature concept.

1. Determine the equivalent or representative temperature for the climate and structure of the project.

   Two methods can be used to determine the equivalent or representative temperature for a specific climate and area:

   a. Use the midrange temperature of the multiple temperature option discussed previously as the equivalent temperature. The equivalent temperatures for the sites included in the NCHRP Project 9-30A study were found to be close to this temperature. This temperature, however, is less precise and accurate and should be used where local calibration has yet to be performed.

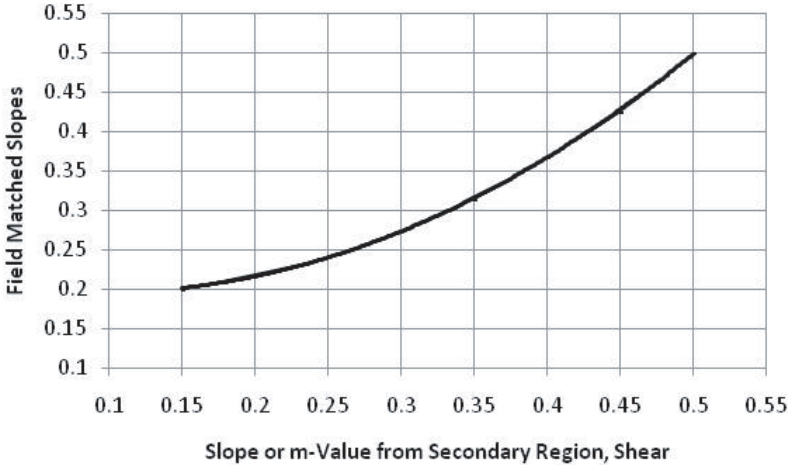

Figure A.5. Determining field-matched slopes from laboratory-derived values from repeated-load constant-height shear tests, WesTrack transfer function. (Note: Refer to Figure 103(a) in Chapter 3 regarding the dispersion in the data.)

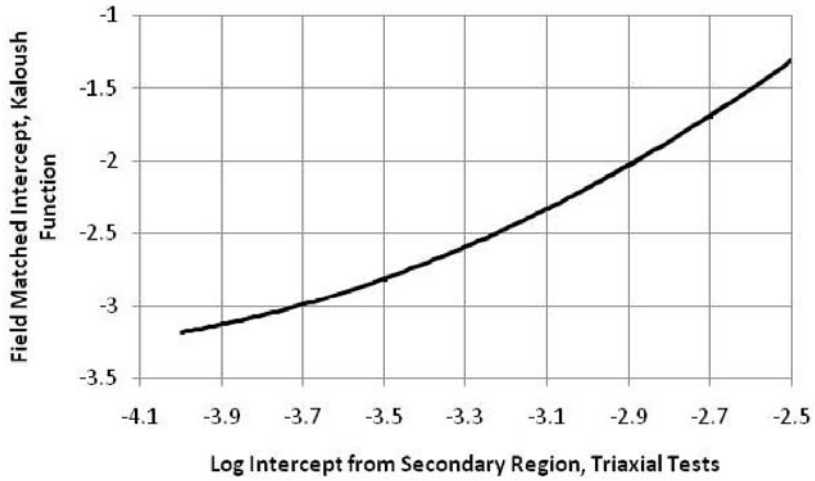

Figure A.6. Determining the field-matched intercept or coefficient of the Kaloush transfer function from repeated-load triaxial tests. (Note: Refer to Figure 105(a) in Chapter 3 regarding the dispersion in the data.)

b. Use the MEPDG to estimate the equivalent temperature that will result in the same level of rutting for multiple roadway segments using the actual climate data within a specific site or region. This method is considered the more accurate one because it uses the MEPDG rut-depth computational methodology directly in determining that temperature and can be completed during the local calibration process.

The following paragraphs briefly discuss using the MEPDG Version 9-30A to estimate the equivalent temperature.

a. Determine an initial estimate for the laboratory-adjusted transfer function parameters. The initial values can be extracted from historical data, if available, or the Input Level 2 values determined for the mixture(s) in question or proposed for use. In other words, values for the plastic strain coefficients can be estimated using the relationships for Input Level 2 estimates that are provided in Section A.6.3, which are similar to the NCHRP Project 1-40B volumetric adjustment factors (Von Quintus, 2006).
b. Execute the MEPDG to predict the rut depth using a range of constant temperatures for the trial pavement structure and design truck traffic. Constant temperatures of 10°C, 20°C, 40°C, and 50°C will normally be

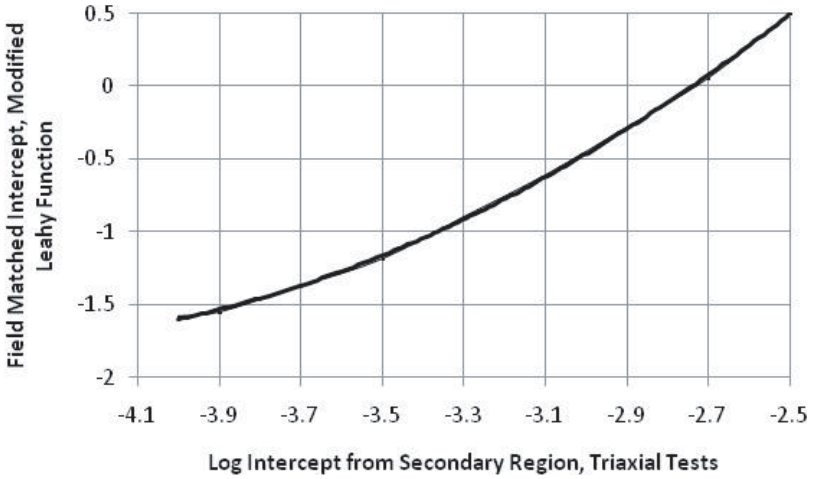

Figure A.7. Determining the field-matched intercept or coefficient of the modified Leahy transfer function from repeated-load triaxial tests. (Note: Refer to Figure 105(d) in Chapter 3 regarding the dispersion in the data.)

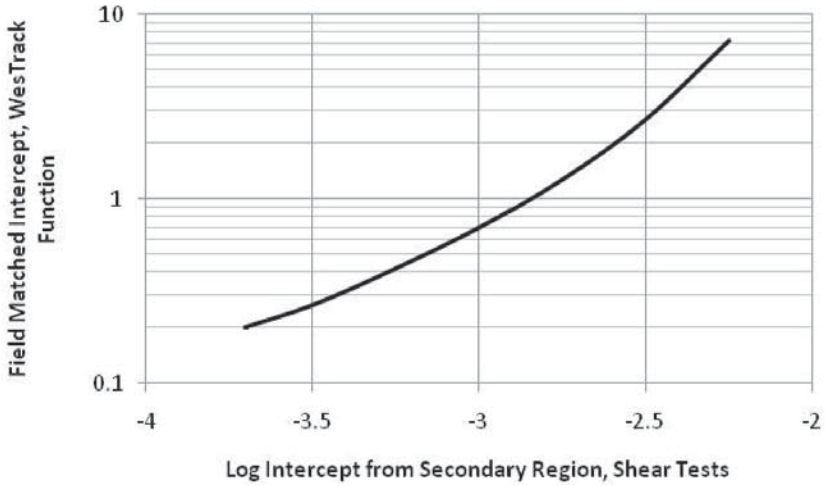

Figure A.8. Determining the field-matched intercept or coefficient of the WesTrack transfer function from repeated-load constant-height shear tests. (Note: Refer to Figure 104 in Chapter 3 regarding the dispersion in the data.)

sufficient. These constant temperature files are available within the MEPDG Version 9-30A software. Plot maximum predicted rut depth at the end of the design period as a function of temperature. Figure A.9 is an example.

c. Execute the MEPDG to predict the rut depth using the actual climatic files and the same default values, trial structure, and design truck traffic used in the previous step.
d. Use the maximum rut depth predicted over the design period to determine the equivalent temperature that results in that same value. In other words, the maximum calculated rut depth using the actual climate data from step c is entered in Figure A.9 to find the single temperature value that results in that same rut depth. This temperature is defined as the equivalent or representative temperature for the specific structure, climate, and truck traffic.
2. Three test specimens are prepared and tested at the defined equivalent temperature. The test specimens are compacted at the average in-place air voids determined by the specifications. This value can be determined from recent historical construction records.
3. Determine the laboratory-derived slope or *m*-value within the steady-state or secondary region for each test specimen (the exponent for the *N*-term for the transfer functions).
4. Determine the laboratory-derived intercept from the steady-state or secondary region for each test specimen (the coefficient for the transfer functions).
5. The field-matched parameters are determined for the HMA mixture and structure using the relationships noted as follows.
   a. Figures A.4 are A.5 are used to adjust the laboratory-derived representative slope or *m*-value to the field-matched slope or *m*-value for the two repeated load test procedures.

Table A.2. Thickness adjustment or shift factors for determining the intercept value of the transfer functions.

HMA Mixture Application	HMA Layer Thickness, in.	Transfer Function		
		Kaloush	Modified Leahy	WesTrack
HMA overlays of PCC or semirigid pavements	<3.0	0.83	1.25	1.25
	3 to 4	0.90	1.10	1.0
	>4.0	1.0	1.0	1.0
HMA overlays of flexible pavements	<4.0	1.4	1.2	1.25
	4 to 6	1.2	1.2	1.1
	>6.0	1.0	1.0	1.0
New construction, unbound aggregate base or full depth	<4.0	1.05	1.2	1.2
	4.0 to 6.0	1.02	1.1	1.05
	6.0 to 8.0	1.0	1.0	1.0
	>8.0	1.0	1.0	1.0

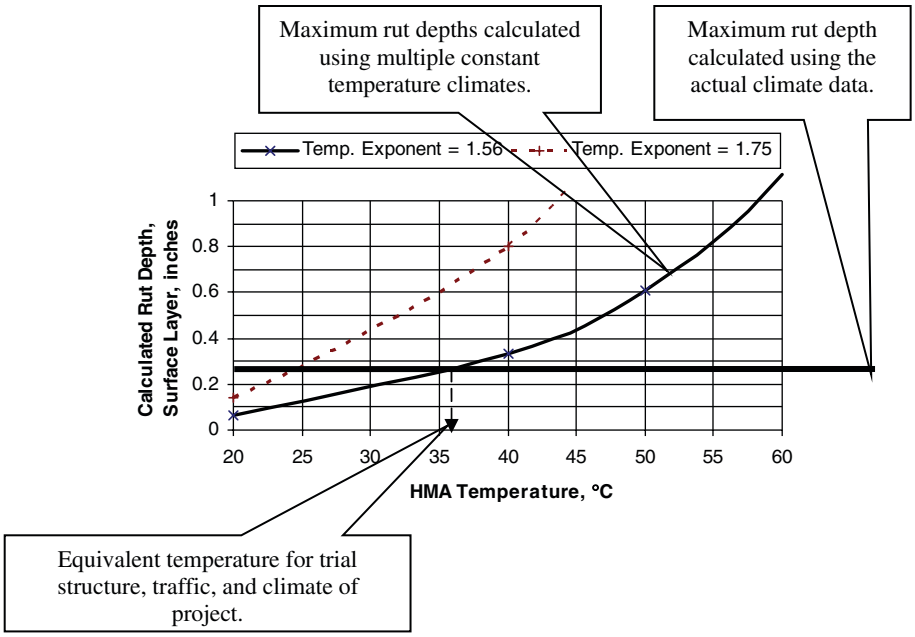

Figure A.9. Example of rut depths predicted with MEPDG (Kaloush transfer function) using a constant temperature environment to estimate the equivalent annual pavement temperature.

b. Figures A.6 through A.9 are used to adjust the laboratory-derived intercept to the field-matched intercept.
c. The temperature exponent for the Kaloush transfer function is not adjusted from the laboratory-measured values.

6. The field-matched parameters for the intercept are multiplied by the appropriate thickness adjustment factor provided in Table A.2.
7. The field-matched parameters for the slope and intercept are then entered into the MEPDG software for the appropriate transfer function for predicting the rut depth for that mixture.

   If the total predicted rut depth is less than the threshold value for rutting, the mixture is considered adequate. If the predicted rutting is greater than the threshold value, however, a revised mixture design maybe needed.

A.6.3 HMA Mixture Evaluation Procedure: MEPDG Level 2 Input Determination

This section of the procedure manual estimates values for the plastic deformation parameters from the HMA material and volumetric properties for predicting rutting in HMA mixtures. Section A.6.3.4 defines those properties that are used to estimate the laboratory-derived intercept and *m*-value from repeated-load plastic deformation tests.

A.6.3.1 Intercept of Transfer Functions

The field-adjusted, laboratory-derived intercept is required to estimate the transfer function intercept for each transfer function. The recommended relationships to estimate the laboratory-derived intercept from the secondary region of triaxial and shear-based tests are provided in the following equations.

$$I_{Triaxial} = 10^{-3.6}\left(\frac{V_a}{V_{Design}}\right)^{0.52}\left(Log(VFA)\right)\left(F_{Index}\right)\left(C_{Index}\right) \quad \text{(A.9)}$$

$$I_{Shear} = 10^{-3.25}\left(\frac{V_a}{V_{Design}}\right)^{0.58}\left(Log(VFA)\right)\left(F_{Index}\right)\left(C_{Index}\right) \quad \text{(A.10)}$$

where

V_a = in-place air voids of the HMA layer, percent.
V_{Design} = design air void level for selecting the target asphalt content, percent.
VFA = voids filled with asphalt, percent.
F_{Index} = an index number related to the fine aggregate angularity (FAA) of the combined aggregate blend; refer to Table A.3 for the recommended values.
C_{Index} = an index number related to the coarse aggregate angularity (CAA) of the combined aggregate blend; refer to Table A.3 for the recommended values.

The values from Equation A.9 are applied to Figures A.6 and A.7 to estimate the field-matched intercept for the Kaloush and modified Leahy transfer functions, respectively, while the value from Equation A.10 is applied to Figure A.8 to estimate the field-matched intercept for the WesTrack transfer func-

Table A.3. Aggregate properties for determining the mixture adjustment factors

Fine Aggregate	Gradation	Fine Aggregate Angularity; AASHTO T 304				
		<45		>45		
FAA index value	External to restricted zone	1.0		0.9		
	Through restricted zone	1.05		1.0		
Coarse Aggregate	**Gradation**	**Percentage Coarse Aggregate with Two Crushed Faces; AASHTO TP 61**				
		0	**25**	**50**	**75**	**100**
CAA index value	Well graded	1.1	1.05	1.0	1.0	0.9
	Gap graded	1.2	1.1	1.05	1.0	0.9

tion. The field-matched values are multiplied by the thickness adjustment factors provided in Table A.2 for determining the inputs to the MEPDG Version 9-30A for the three transfer functions.

A.6.3.2 Temperature Term Exponent of Kaloush Transfer Function

The Kaloush transfer function is the only one of the three recommended for use that includes temperature as a dependent variable. The temperature exponent should be set to 1.5606.

A.6.3.3 m-*Value or* N-*Term Exponent of Transfer Functions*

The relationship for estimating the *m*-value for dense-graded designed aggregate blends is provided in Equation A.11.

$$m-Value_{Neat} = 0.265\left(\frac{P_b}{P_{b(Opt)}}\right)^{0.75} \quad \text{(A.11)}$$

where

P_b = Asphalt content by weight at construction (the in-place value), percent.

$P_{b(Opt)}$ = Saturation or optimum asphalt content by weight, percent. This parameter defines the asphalt content at which the VMA starts to increase or the density of the mixture starts to decrease. An example and demonstration in determining this variable are provided in Section A.6.3.4 of this manual.

For the use of modified asphalts, the *m*-value for neat asphalt mixtures is adjusted by Equation A.12:

$$m-Value_{Modified} = m_b\left(m-Value_{Neat}\right) \quad \text{(A.12)}$$

where

m_b = an adjustment that accounts for the use of modified mixtures for the same aggregate blend of neat asphalt mixtures and defined below.

For *m*-values less than or equal to 0.2 : $m_b = 1.0$

For *m*-values greater than 0.2 :

$$m_b = 0.072 + \left(m-Value\right)0.64 \quad \text{(A.13)}$$

A.6.3.4 HMA Properties Used in Determining Level 2 Inputs

A.6.3.4.1 Design Air Void Content to Select Target Asphalt Content. ***Design Air Void Content to Select Target Asphalt Content,*** $\mathbf{V_{a(design)}}$: This parameter is determined from mixture design charts (air voids as a function of asphalt content) and is the air void content at the target asphalt content (or the value expected during production of the mixture). Figure A.10 shows an example in determining this value or parameter for a specific mixture. The reality of this parameter is dependent on how close the laboratory compactive effort simulates the field compaction that occurs under the rollers and truck traffic.

In most cases, the HMA mixture design will be unavailable when the structural design is completed. In this cases, it is recommended that the agency's policy on design air void content be used. This will be 4% in most cases; however, some agencies now use 3% and 5% for some of their mixtures to select the asphalt content for production.

A.6.3.4.2 Saturation Asphalt Content by Weight. ***Saturation asphalt content by weight,*** $\mathbf{P_{b(Sat)}}$: This parameter is determined from the mixture design charts (mixture density as a function of asphalt content) and is the asphalt content where the density begins to significantly decrease or where the VMA begins to significantly increase. This value is determined in the laboratory and is not a well-defined parameter. Figure A.11(a) shows an example of a sensitive HMA mixture in determining this value, while Figure A.11(b) shows an example for a nonsensitive mixture.

In most cases, the saturation asphalt content will be unknown when the structural design is completed. In this case, it is recommended that previous mixture design records be reviewed to select a reasonable ratio between the target asphalt content

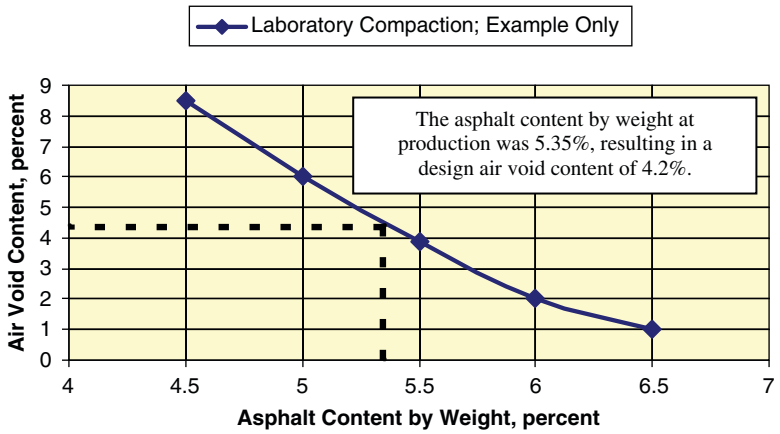

Figure A.10. Graphical example determining the design air void content from the laboratory mixture design chart.

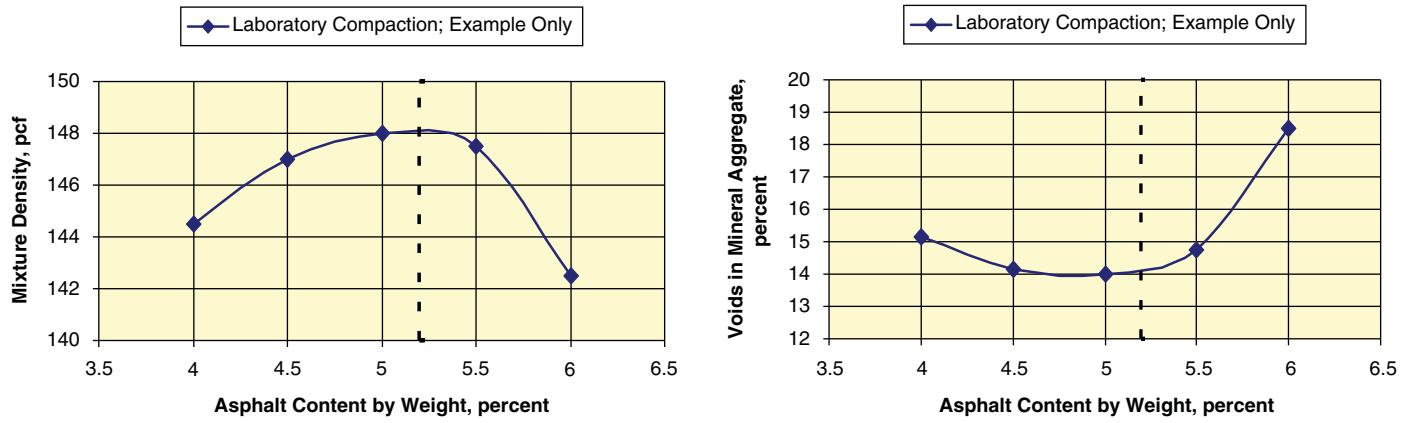

(a) Example for a sensitive mixture.

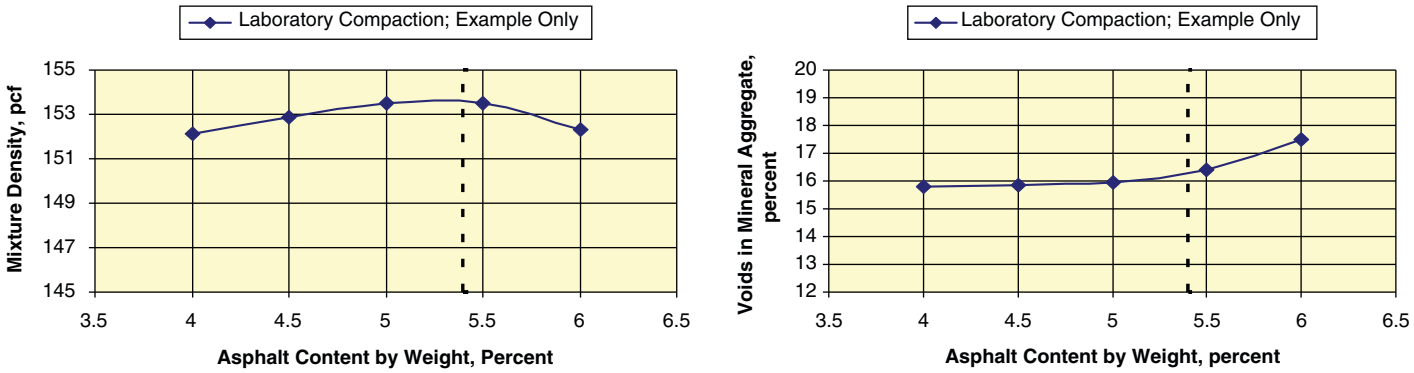

(b) Example for a nonsensitive mixture.

Figure A.11. Graphical example determining the saturation asphalt content from the laboratory mixture design chart.

and saturation asphalt content by weight. This value generally varies from 0.90 to 1.0 for HMA mixtures that are resistant to rutting. The asphalt content where the density begins to significantly decrease and VMA begins to significantly increase should never be selected for mixtures to be placed on higher volume roadways.

This parameter is dependent on the laboratory compaction device and compaction effort used in the laboratory. The assumption is that the laboratory compaction device and effort accurately simulate the compaction from the rollers and truck traffic over time.

A.6.3.4.3 Fine Aggregate Angularity Index. ***Fine aggregate angularity index, F_{Index}***: An index number or value related to the fine aggregate angularity of the combined fine aggregate of a mixture (refer to Table A.3). The FAA index is entered into the MEPDG software. Most agencies measure the FAA value during mixture design and for aggregate source approval (AASHTO T 304).

A.6.3.4.4 Coarse Aggregate Angularity Index. ***Coarse aggregate angularity index, C_{Index}***: An index number or value related to the coarse aggregate angularity of the combined coarse aggregate of a mixture. Few agencies measure the CAA value in the laboratory (AASHTO T 326), but most do have required limits for the minimum amount of coarse aggregate with two crushed faces for varying truck volumes (AASHTO TP 61). For high-volume roadways, most agencies require 100% crushed coarse aggregate. The C_{Index} value, as used in the MEPDG, is related to the amount of crushed coarse aggregate (refer to Table A.3). The CAA index is entered into the MEPDG software.

A.6.3.5 Estimation of Repeated-Load Plastic Deformation Parameters: Input Level 2

The following provides a few notes that should be remembered regarding use of the mixture adjustment factors in predicting rutting of HMA mixtures.

1. These mixture adjustment factors were not optimized in terms of minimizing the residual errors of the predicted rut depths.
2. The ratio of the actual asphalt content to saturation asphalt content by weight should be less than 1.1 and greater than 0.90. It is possible that this ratio can be greater than 1.1 and less than 0.90 for some mixture designs because of the differences in compaction devices and compaction effort used in the laboratory. It is recommended that the range of this value be limited to the values listed because too little data outside that range was included in the initial development of this factor.
3. The design air void content based on the actual asphalt content should be within a range of less than or equal to 5.0% and greater than or equal to 3.0%.
4. The C_{Index} values for 0% coarse aggregate with two crushed faces was estimated because all mixtures included in the original evaluation to estimate the C_{Index} value were greater than 50%.

Cited AASHTO Standard and Provisional Practices and Methods of Test

R 30, Mixture Conditioning of Hot Mix Asphalt (HMA)
T 304, Uncompacted Void Content of Fine Aggregate
T 320, Determining the Permanent Shear Strain and Stiffness of Asphalt Mixtures Using the Superpave Shear Tester (SST)
T 326, Uncompacted Void Content of Coarse Aggregate (As Influenced by Particle Shape, Surface Texture, and Grading)
T 335, Determining the Percentage of Fracture in Coarse Aggregate
PP 3, Preparing Hot-Mix Asphalt (HMA) by Means of the Rolling Wheel Compactor
PP 60, Preparation of Cylindrical Performance Test Specimens Using the Superpave Gyratory Compactor (SGC)
TP 79, Determining the Dynamic Modulus and Flow Number for Hot Mix Asphalt (HMA) Using the Asphalt Mixture Performance Tester (AMPT)

References for Procedural Manual

Kaloush, K. E. and M. W. Witczak. Development of a Permanent to Elastic Strain Ratio Model for Asphalt Mixtures. Inter-Team Technical Report for NCHRP Project 1-37A, "Development of the 2002 Guide for the Design of New and Rehabilitated Pavement Structures." ERES Consultants, Inc., 2000.

Von Quintus, H. L., J. A. Scherocman, C. S. Hughes, and T. W. Kennedy. *NCHRP Report 338: Asphalt-Aggregate Mixture Analysis System: AAMAS.* TRB, National Research Council, Washington, D.C., 1991.

Von Quintus, H. L. History and Hypothesis Behind the HMA Mixture Adjustment Factors for Rutting and Area Fatigue Cracking Predictions. White Paper prepared for NCHRP Project 1-40B, "User Manual and Local Calibration Guide for the Mechanistic–Empirical Pavement Design Guide and Software." Applied Research Associates, Inc., 2006.

Epps, J. A., A. Hand, S. Seeds, T. Scholz, S. Alavi, C. Ashmore, C. L. Monismith, J. A. Deacon, J. T. Harvey, and R. Leahy. *NCHRP Report 455: Recommended Performance-Related Specification For Hot-Mix Asphalt Construction.* Part II: Performance-Related Specification. TRB, National Research Council, Washington, D.C., 2000.

Witczak, M. W. *NCHRP Report 580: Simple Performance Tests for Permanent Deformation of Hot Mix Asphalt, Volume II: Flow Number and Flow Time.* Transportation Research Board of the National Academies, Washington, D.C., 2007.

Witczak, M. W., K. Kaloush, T. Pellinen, M. El-Basyouny, and H. L. Von Quintus. *NCHRP Report 465: Simple Performance Test for Superpave Mix Design.* TRB, National Research Council, Washington, D.C., 2002.

APPENDIX B

Software Modifications or Alterations to the MEPDG for Predicting Rut Depths

Appendix B identifies and discusses the enhancements and modifications that were made to the MEPDG Version 1.0 software under NCHRP Project 9-30A to facilitate use of other rut-depth transfer functions. This modified version of the software is referred to as MEPDG Version 9-30A.

B.1 Incorporate Other Rut-Depth Transfer Functions

Three rut-depth transfer functions were included in the software. These functions were (1) the WesTrack shear strain and shear stress transfer function, (2) the Verstraeten deviator stress transfer function, and (3) the Asphalt Institute vertical elastic strain and deviator stress transfer function. Screen shots for each of the transfer functions are included within this part of Appendix B to explain the entry of each permanent deformation parameter for the specific transfer functions recommended for use from the facilitated workshop.

This is the screen for using the Kaloush transfer function that is included in the original version of the MEPDG (refer to Equation 1).

This screen is also used to enter the permanent deformation parameters derived from the NCHRP Project 1-40B procedure. This procedure adjusts the permanent deformation parameters based on the volumetric properties of the in-place HMA mixture during construction and is included as Appendix C. Those values are then entered into the appropriate window for each parameter.

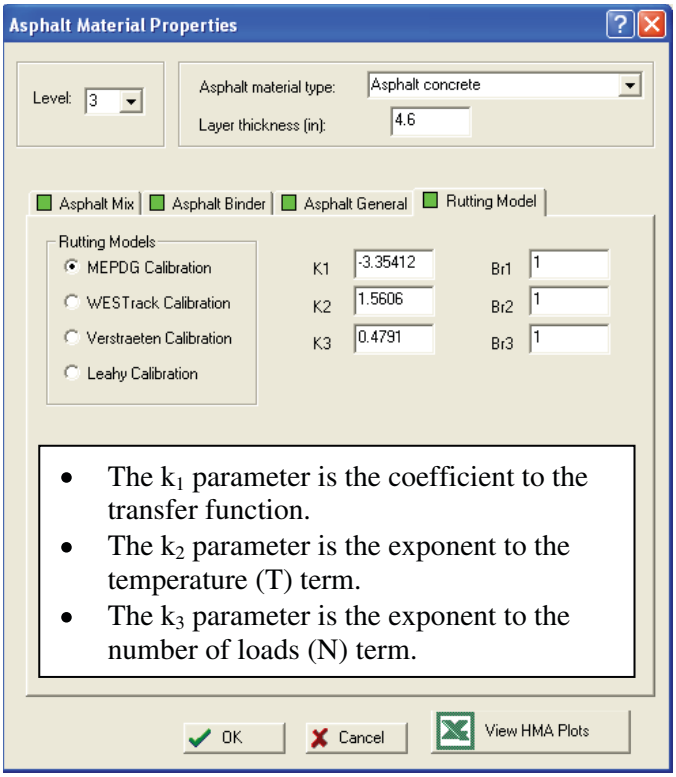

For the Kaloush and all other transfer functions, *N* is the number of axles (single, tandem, or tridem) within a specific axle load interval for a specific truck class within a specified period of time.

This is the screen for using the WesTrack transfer function (refer to Equation 8). The default values are shown in the input fields for the permanent deformation parameters. The field-adjusted or calibrated values are entered into each appropriate field or window.

The local calibration factors (B_a, B_b, and B_c terms) must be set to unity or the values determined from calibration prior to making any runs with the software.

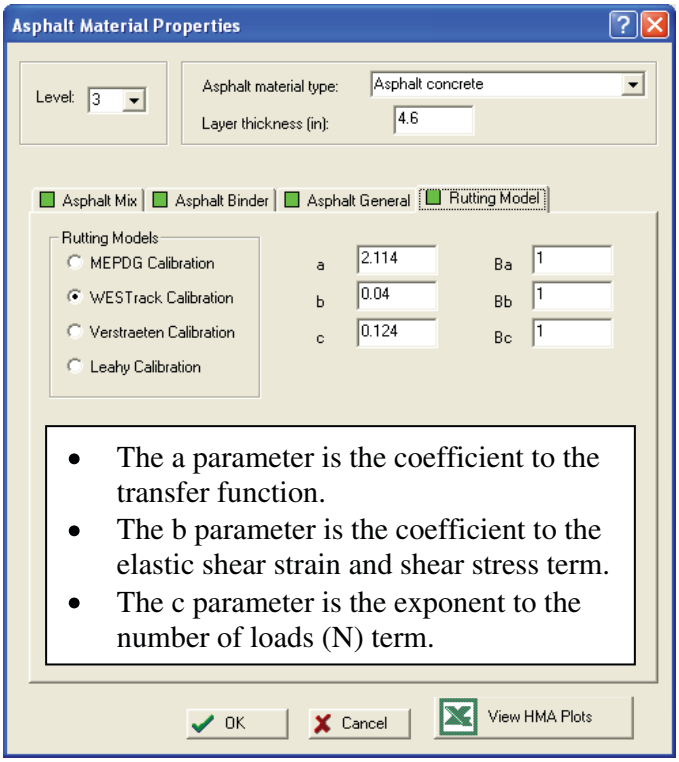

This is the screen for using the Verstraeten transfer function (refer to Equation 7). The default values are shown in the input fields for the permanent deformation parameters. The field-adjusted or calibrated values are entered into each appropriate field or window.

The local calibration factors (B_A and B_b terms) must be set to unity or the values determined from calibration prior to making any runs with the software.

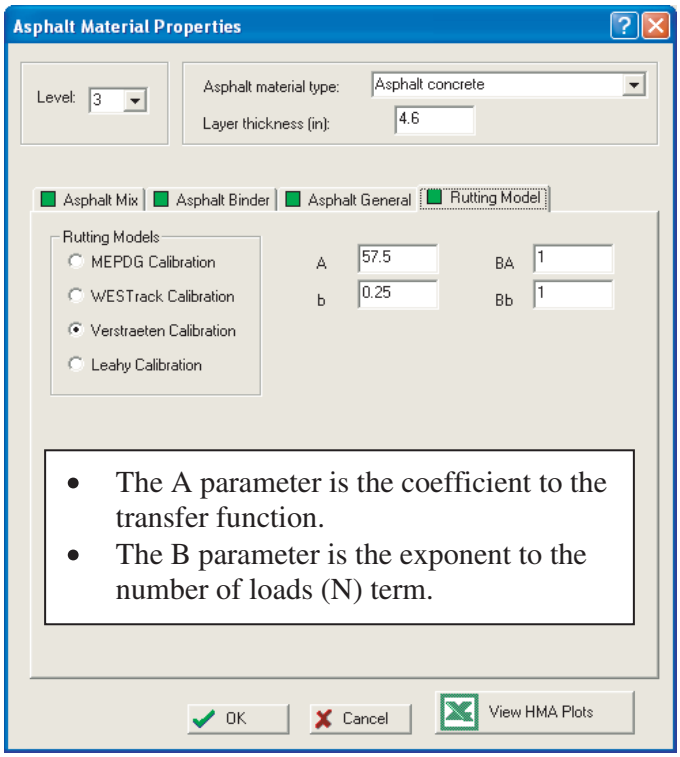

This is the screen for using the Asphalt Institute or *original* Leahy transfer function (refer to Equation 5). The default permanent deformation values are shown in the input fields. The field-adjusted or calibrated values are entered into each appropriate field or window. The following defines the parameters not listed on the screen shot.

- The C3 parameter is the exponent to the temperature (T) term.
- The C4 parameter is the exponent to the deviator stress (σ_d) term.
- The C5 parameter is the exponent to the asphalt viscosity (η) term.
- The C6 parameter is the exponent to the effective asphalt content by volume (V_{beff}) term.
- The C7 parameter is the exponent to the HMA air void (V_a) term.

The local calibration factors (*B1* through *B7* terms) must be set to unity or the values determined from calibration prior to making any runs with the software.

This screen is also used to enter the permanent deformation parameters for the *modified* Leahy transfer function. A value of zero is entered for those terms not included in the modified Leahy transfer function and the global intercept value is changed. In summary, zero is entered for C3 and C5, and a value of –0.505 is entered for C1 (refer to Equation 6). The values for the other coefficients are assumed to be the same as for the *original* Asphalt Institute or Leahy regression equation.

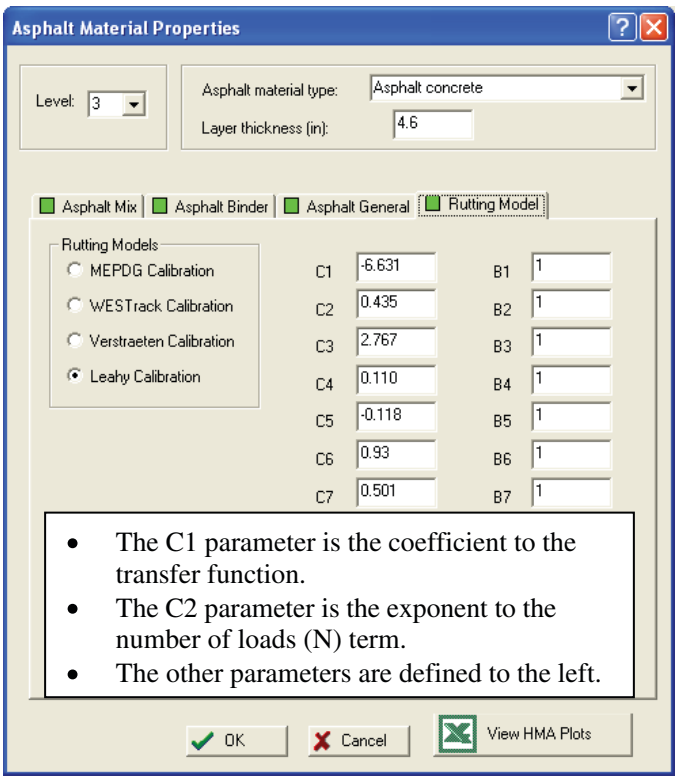

B.2 HMA Layer-Specific Plastic Deformation Coefficients

Based on local calibration studies completed for Wisconsin, Ohio, Montana, and Missouri, a significant bias was found between the measured and predicted rut depths. This bias was initially eliminated through the use of thickness correction factors for some of these projects. The bias, however, can be eliminated by using different permanent deformation parameters for each HMA structural layer. Specifically, the rut depths measured along the Wisconsin SPS-1 and SPS-9 test sections were evaluated and compared, and it was found that the rut depths with time can be stratified into two groups: those Wisconsin test sections with ATB layers and those without ATB layers. The initial analysis attributed this difference to thickness differences between the test sections, but it could also be attributed to the ATB layer. Trenches were used to confirm that most of the rutting was initiated in the ATB layer. It was impossible to determine the cause for the bias except through destructive sampling.

All versions of the MEPDG software released to date use one set of permanent deformation parameters for the Kaloush rut-depth transfer function that are used for all HMA layers. The MEPDG computational methodology assumes that the differences in HMA dynamic modulus will correctly account for differences in rutting susceptibility of different layers. The MEPDG software was revised to permit the user to enter layer-specific permanent deformation parameters that are determined from laboratory repeated-load tests. As noted in Chapter 2, this revision can significantly alter the local calibration factors determined from individual projects and/or HMA mixtures.

B.3 Plastic Deformation Coefficients for Unbound Layers

The local calibration factor for the unbound aggregate granular base and subbase layers could not be entered for a specific cross section, while local calibration factors could be entered for fine- and coarse-grained subgrade soils. The MEPDG was revised so that the local calibration parameter can be entered for the coarse-grained granular base and subbase layers. This revision did not result in significant changes to the predicted total amount of rutting.

B.4 Lateral Wander Effects

Lateral wander of traffic influences the number of axle load applications over a point for predicting distress. An increase in wander will result in less permanent deformation within a pavement system.

The standard deviation is used to define the practical limits of the width of the lateral distribution of wheel loads. The MEPDG software assumes a uniform distribution of wheel or axle loads between the limits defined by the standard deviation of wheel loads. A normal distribution is believed to provide a more realistic distribution of wheel loads for computing total rutting across all lane widths. The MEPDG was revised to include a normal distribution in the lateral location of the wheel loads for calculating the pavement responses in computing total rut depth.

This revision had a minimal effect on the calibration and computed rut depths because the same default values have been used for all roadway sections. Minor differences, however, were observed where the wander was varied within the loading cycle of the WesTrack experiment. The remainder of this section explains the computational methodology that was used in computing rut depths for different lane widths and lateral wander.

The MEPDG approach assumes that the wander is normally distributed and that the standard deviation for the normal distribution plot σ_d represents the wander in inches. The MEPDG approach is graphically shown and explained in Figure B.1.

The load positions used for rutting-related response calculation are shown in Figure B.1. The area under the normal distribution curve is divided into 21 parts, each representing 1/21 of the total distribution. For each of these areas, a representative coordinate (distance between rutting path and center point of considering dual wheel load) in the wander direction is found by multiplying the standard normal deviate by the wander standard deviation, mathematically defined as:

$$x = ZR[i] * \sigma_d$$

where

$i = 0, 1, 2, \ldots, 20.$
Z = depth below the surface.
R = radial distance from center of wheel path.

The pavement response must be evaluated at the critical wheel positions in the traffic direction in addition to the wander direction. For a single wheel loading, the representative location in the traffic direction is chosen as the midpoint between the dual wheels. For tandem and tridem axles, MEPDG selects the maximum vertical strain after evaluating two load positions.

In the case of tandem axles (refer to Figure B.2), the first set of responses is determined as a combination of responses resulting from loading cases 2 and 4, and the second set of responses is determined from a combination of responses resulting from loading cases 1, 3, and 5.

In the case of tridem axles [refer to Figures B.3(a) and B.3(b)], the first set of responses is determined as a combination of responses resulting from loading cases 1, 3, 5, 7, and 9, and the second set of responses is determined as a combination of responses resulting from loading cases 2, 4, 6, and 8. For permanent deformation calculations, the MEPDG Version 9-30A software chooses the maximum of two responses.

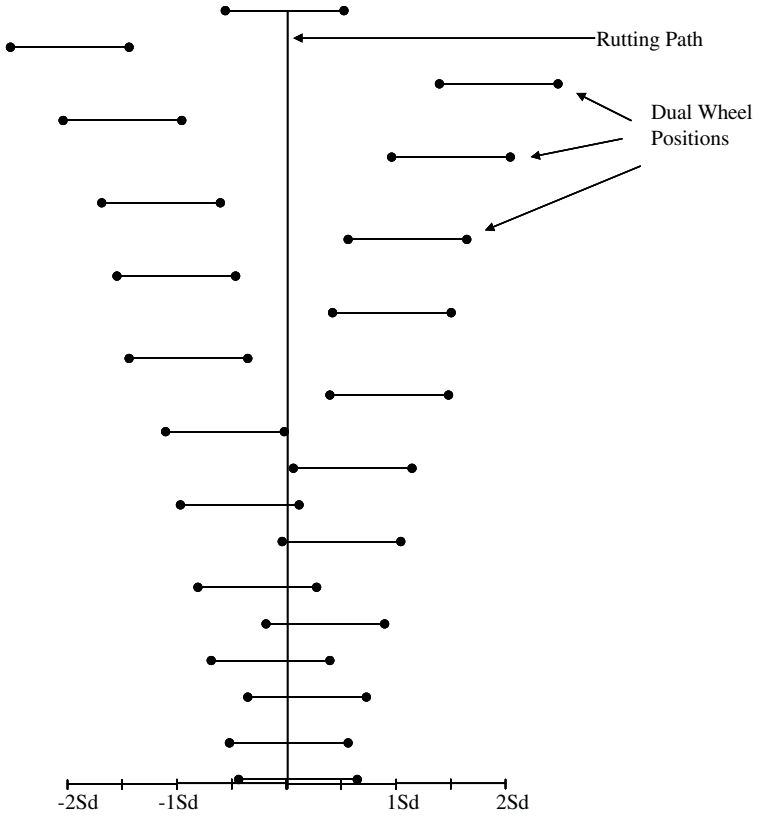

Figure B.1. Rutting analysis wander approach.

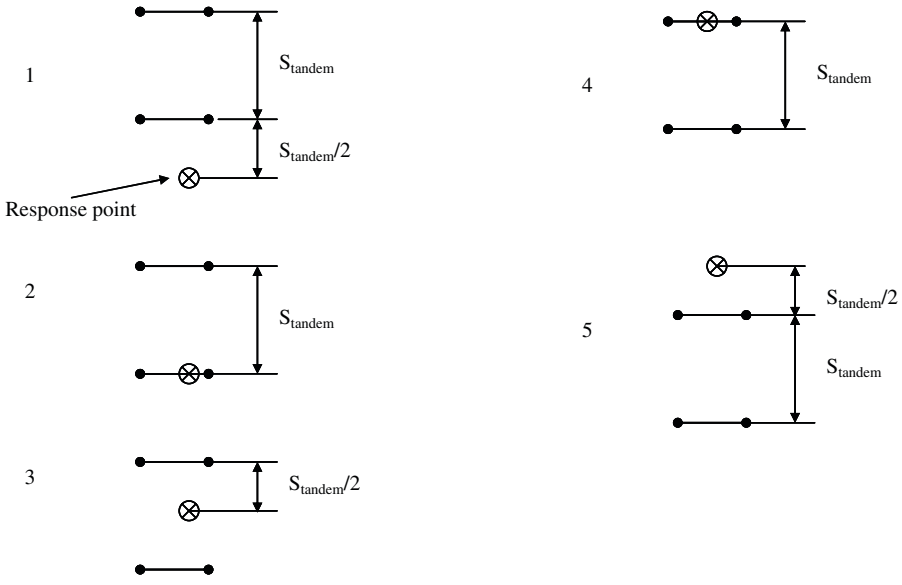

Figure B.2. Tandem load locations in the traffic directions.

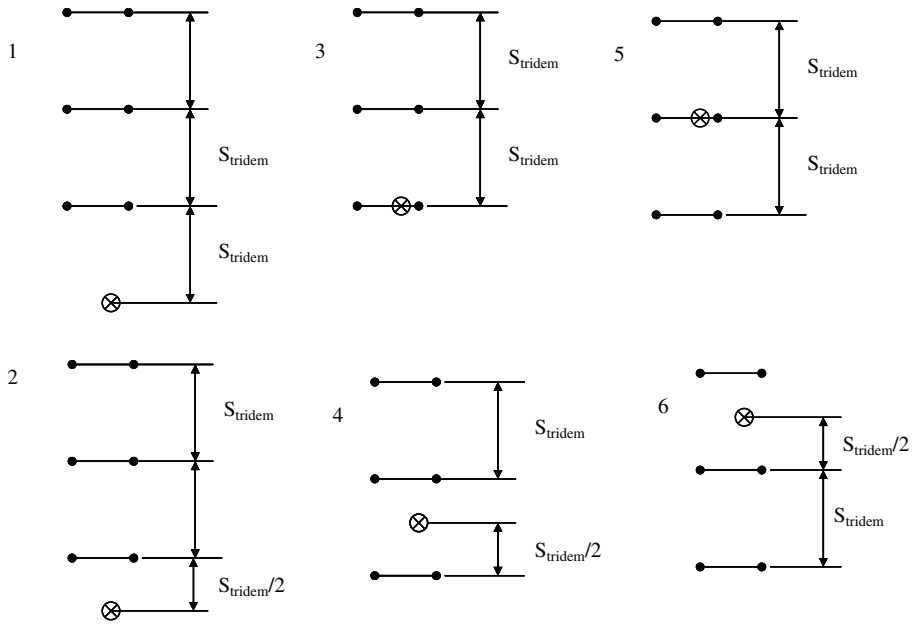

Figure B.3(a). Tridem load locations in the traffic direction.

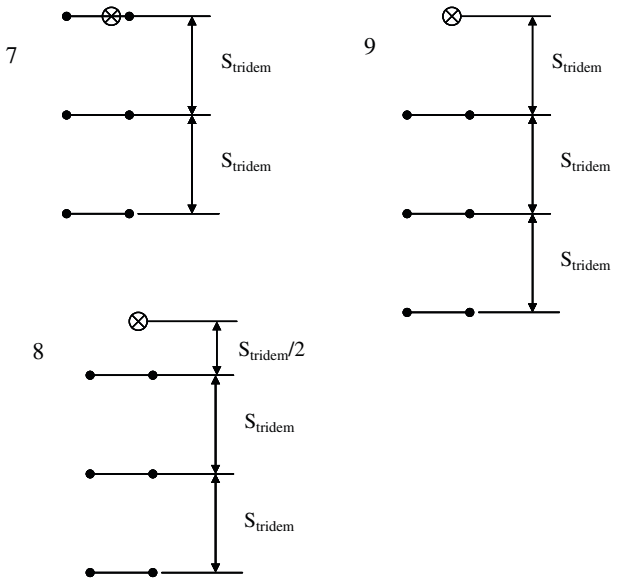

Figure B.3(b). Tridem load locations in the traffic direction.

B.5 Revisions to Computational Methodology

The rut-depth transfer functions based on vertical or compressive (MEPDG, Verstraeten, Asphalt Institute) and shear (WesTrack) strains require different responses computed at different locations within APADS. (APADS is the software package or routine to compute pavement responses in the MEPDG for calculating rut depths and other distresses.) The difficult part of adding transfer functions to the program that use different responses was identifying the correct fields that include the responses needed for calculating the rut depths for each transfer function. NCHRP Project 1-37A personnel directly involved in developing APADS assisted in identifying the correct fields to be extracted from APADS because the documentation and comments included in the source code are minimal, making it difficult to ensure that the correct parameter is being called from a specific part of the program.

The approach used in the MEPDG for permanent deformation prediction is based on incremental permanent strain accumulation calculated as a function of resilient strain, applied traffic, and temperature distribution within a given

sub-season. A sub-season is defined as a period corresponding to one-fifth of a design increment over which a constant temperature is assumed for stiffness calculations. Permanent deformation is estimated for each sub-season at the mid-depth of each sub-layer within the pavement system.

To estimate the permanent deformation of each individual sub-layer, the system verifies the type of layer, applies the model corresponding to the material type of the sub-layer, and computes the plastic strain accumulated at the end of each sub-season. The overall permanent deformation for a given sub-season is the sum of permanent deformation for each individual layer, including the unbound layers and subgrade. The following sections of Appendix B summarize the revisions made to the original program to facilitate use of the additional transfer functions and the response computed in support of those transfer functions.

B.5.1 Processing Temperature Profile Data for Other Rut-Depth Transfer Functions

A base unit of one month is typically used for rutting computations. In situations where the pavement is exposed to freezing and thawing cycles, the base unit of 1 month is changed to 15 days' (half a month) duration to account for rapid changes in the pavement material properties during freezing and thawing. While rutting computations are based on a 2-week or monthly average temperature, the influence of extreme temperatures, above and below the average, are directly accounted for in the design analysis. In order to include the extreme temperatures during a given month (or during 15 days for a freeze/thaw period), the following approach was used in the analysis scheme.

The solution sequence from the Integrated Climatic Model (ICM) provides temperature data at intervals of 0.1 hours (6 min) over the analysis period. This temperature distribution for a given month (or 15 days) is represented by a normal distribution with a certain mean value (μ) and standard deviation (σ), $N(\mu,\sigma)$, as shown in Figure B.4.

The frequency distribution of temperature data obtained using the ICM is assumed to be normally distributed, as shown in Figure B.4. The frequency diagram obtained from the ICM represents the distribution at a specific depth and time. A given month (or bimonthly for freeze/thaw) may have extreme temperatures (even at a low frequency of occurrence) that could be significant for rutting.

Using the average temperature value may not capture the damage caused by extreme temperatures. In order to account for the extreme temperature, the temperatures over a given interval are divided into five different sub-seasons. For each sub-season the sub-layer temperature is defined by a temperature that represents 20% of the frequency distribution of the pavement temperature. This sub-season also represents the conditions with 20% of the monthly traffic. This is accomplished by computing pavement temperatures corresponding to standard normal deviates of −1.2816, −0.5244, 0, 0.5244, and 1.2816. These values correspond to accumulated frequencies of 10%, 30%, 50%, 70%, and 90% within a given month.

B.5.2 Calculate Stresses and Strains for Other Rut-Depth Transfer Functions

It is necessary to use the pavement response model for the layered pavement structure to calculate vertical compressive stresses (strains) for all cases to be analyzed. The number of cases depends on the damage increment. The following increments are used in the software:

- Pavement age: by year.
- Season: by month or half a month.
- Load configuration: axle type.
- Load level: discrete load levels in 1,000-lb to 3,000-lb increments, depending on axle type.
- Temperature: pavement temperature quintile for the HMA dynamic modulus.

For rutting, the MEPDG software modifies the actual pavement response for the effects of wander and uses this modified response for the calculation of the incremental permanent deformations within each sub-layer. A good approximation is to assume that the wander is normally distributed. The standard

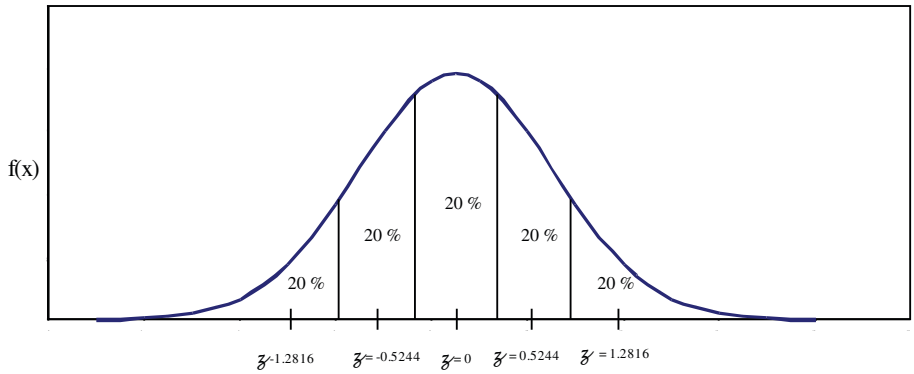

Figure B.4. Temperature distribution for a given analysis period.

deviation for the normal distribution plots represents the wander in inches. The area under the normal distribution curve can be divided into 20 quintiles; each represents 5% of the total traffic distributions. In the traffic direction, the MEPDG software defines for each axle type (single, tandem, tridem) the analysis locations where the maximum response is most likely to occur.

Given a particular layered pavement cross section, the vertical resilient strain at any given depth (along a vertical axis, defined in the *x, y* plane) is defined by knowledge of the three-dimensional stress state and the elastic properties (modulus and Poisson's ratio) of the HMA layer in question from:

$$\varepsilon_{rz} = \frac{1}{E^*}\left(\sigma_z - \mu\sigma_x - \mu\sigma_y\right) \tag{B.1}$$

The complex modulus of HMA mixtures is employed in the MEPDG through a master curve. Thus, dynamic modulus (E^*) is expressed as a function of the mix properties, temperature, and time of the load pulse. Knowledge of the predicted vertical resilient strain at any point, along with the plastic strain relationship, allows the direct calculation of the plastic strain, ε_p, at any given point within the HMA layer, after N repetitions of load, to be computed. The incremental rut depth for each sub-layer in the HMA layer can be determined from:

$$\Delta R_{d_i} = \varepsilon_{p_i}\left(\Delta h_i\right) \tag{B.2}$$

Finally, by simply summing all incremental ΔR_d through the entire layer, the software obtains the total layer rut depth from:

$$R_d = \sum_{i=1}^{n} \Delta R_{d_i} \tag{B.3}$$

B.5.3 Calculate Plastic Deformation Using Other Rut-Depth Transfer Functions

Transfer functions for plastic deformation (rutting) in the MEPDG software provide the plastic strain under specific pavement conditions for a total number of load repetitions. A special strain hardening approach is used to incorporate seasonal differences in a cumulative deformation subsystem because conditions vary from one season to another (e.g., temperature, resilient strain, moisture content, resilient modulus of the supporting layers).

For the general solution, plastic deformation is estimated for each layer at each computational location using pavement responses calculated at the mid-depth of each sub-layer. Computations of plastic deformations are done at locations defined by the analysis module for regular traffic. In the following model description, the equivalent number of load cycles for each sub-season is found by solving the plastic deformation model for N with the deformation accumulated up to the current sub-season and the material properties and load conditions prevailing in the current sub-season. The software implementation of the Witczak–Kaloush transfer function consists of two steps.

1. In the first step, the additional number of load applications, designated as N_{virt}, just prior to the sub-season under analysis is estimated from Equation B.4:

$$\ln\left(N_{virt}\right) = \left(\ln\left(\varepsilon_p/\varepsilon_r\right) - \ln\left(k_1\right) + 3.35412\ln(10) - 1.5606\ln(T)\right)/0.4791 \tag{B.4}$$

   The initial coefficients used in estimating N_{virt} were uncalibrated values proposed by Witczak and Kaloush based on laboratory testing.
2. In the second step, the software uses the MEPDG rut-depth transfer function based on vertical plastic strain to calculate the sub-season plastic deformation corresponding to current resilient deformation ε_r, sub-season temperature, and total increment of axle applications defined as:

$$N_{Tot} = N_{Traf} + N_{Virt} \tag{B.5}$$

B.5.4 Verstraeten Plastic Deformation or Rut-Depth Transfer Function

The Verstraeten deviator stress transfer function predicts plastic deformation as a function of material properties, stress level, and number of load applications, as shown in Equation B.6. This is the same as Equation 7 in Chapter 2; it is repeated here for ready reference purposes.

$$\varepsilon_p = A\frac{\sigma_1 - \sigma_3}{E^*}\left(\frac{N}{1000f}\right)^{b_{AC}} \tag{B.6}$$

where

ε_p = permanent or plastic shear strain, in./in.
σ_1 and σ_3 = vertical and radial stresses, psi.
E^* = dynamic modulus of HMA mixture
N = number of load cycles at stress level.
f = frequency of load, Hz.
A and b_{AC} = regression coefficients.

The deviator stress ($\sigma_1 - \sigma_3$) divided by dynamic modulus (E^*) is a measure of the resilient strain in this transfer function. As summarized in Chapter 2, the recommended values for the regression coefficients of conventional HMA mixtures are A = 57.5 and b_{AC} = 0.25. These are considered the global default values for this transfer function, but they represent laboratory test conditions.

The Verstraeten model was not developed for incremental rut-depth accumulation purposes, similar to the Witczak–Kaloush transfer function prior to calibrating the MEPDG. To correctly implement this within the MEPDG computational framework, some assumptions were made

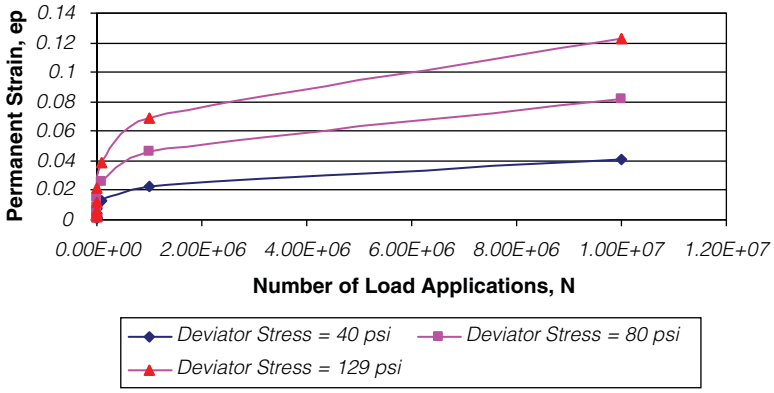

Figure B.5. Plastic deformation accumulation as a function of N and σ_d—Verstraeten transfer function.

regarding strain hardening that takes place as the load cycles are applied to the pavement. Figure B.5 presents the model's behavior as a function of N and σ_d.

The time-hardening principle embedded in the MEPDG software to estimate the accumulation of plastic strains in the HMA layers under different site conditions is also applied to the Verstraeten transfer function. To implement this model within the MEPDG framework, the N_{virt} expression in the software (Equation B.4) was changed as follows:

$$\ln(N_{virt}) = 4\left[\ln\left(\frac{E^*\varepsilon_p}{\sigma_1-\sigma_3}\right)-\ln(57.5)\right]+\ln(1000f) \qquad \text{(B.7)}$$

The increment of plastic deformation is computed for a given stress state, load frequency, modulus, and N computed in accordance with Equation B.6. The depth function is used to calculate the incremental plastic strains and rut depths for each sub-layer in accordance with the MEPDG computational methodology. As part of the facilitated workshop, the applicability of the depth correction function for the deviator-stress–based transfer function was questioned. It was the opinion of some participants that the depth correction function may need to be revised. Calibration work completed within this project concluded that the depth correction function was applicable to the deviator-stress–based transfer function (refer to Chapter 3).

B.5.5 WesTrack Plastic Deformation or Rut-Depth Transfer Function

The WesTrack plastic shear strain transfer function was developed using data from the SHRP research studies and WesTrack field experiment. The M-E–based formulation for predicting HMA rut depths using plastic shear strain and shear stress is shown in Equation B.8. This is the same as Equation 8 in Chapter 2; it is repeated here for ready reference purposes.

$$\gamma_p = ae^{b\tau}\gamma_e N^c \qquad \text{(B.8)}$$

where

γ_p = plastic shear strain at a depth of 2 in. beneath the tire edge.
τ = corresponding elastic shear stress.
γ_e = corresponding resilient shear strain.
a, b, c = regression coefficients.

The time-hardening principle included in the MEPDG is also used to estimate the accumulation of plastic strains in the HMA under varying site conditions. To implement this transfer function within the MEPDG framework, the N_{virt} expression in the software (Equation B.4) was changed as follows:

$$\ln(N_{virt}) = \left(\ln(\gamma_p/\gamma_r)-\ln(a)-b\tau\right)/c \qquad \text{(B.9)}$$

Next, the increment of the plastic shear strain is computed for a given stress state, load frequency, modulus, and N computed in accordance with Equation B.8. The rutting that is estimated in the HMA layer due to the plastic deformation is determined from the following equation, where K is a coefficient related to the thickness of the HMA layer. The K-values were included in Table 2 in Chapter 2. The depth function included in the MEPDG is turned off when using the WesTrack transfer function.

$$PD = K\gamma_p \qquad \text{(B.10)}$$

APPENDIX C

Step-By-Step Procedure for Adjusting the Global Calibration Parameters of the MEPDG (Kaloush) Rut-Depth Transfer Function

Extracted from "Local Calibration Adjustments for the HMA Distress Prediction Models," Von Quintus (2005), Preliminary Draft Final Report for NCHRP Project 1-40B. The hypotheses and assumptions for these adjustments are included in an interim report, "History and Hypothesis Behind the HMA Mixture Adjustment Factors for Rutting and Area Fatigue Cracking Predictions" (Von Quintus, 2006), also prepared under NCHRP Project 1-40B.

This appendix lists the steps used in the recalibration process of the MEPDG software rut-depth and fatigue cracking prediction models, adjusting the global calibration coefficients determined from the NCHRP Project 1-37A calibration procedure.

The plastic deformation prediction equation embedded in the MEPDG software to predict rutting over time is given in Equation C.1.

$$\frac{\varepsilon_p}{\varepsilon_r} = \beta_{r1}(10)^{k_{r1}}(T)^{\beta_{r2}(k_{r2})}(N)^{\beta_{r3}(k_{r3})} \quad \text{(C.1)}$$

where

T = temperature, °F.
N = number of load applications for a specific temperature range or season.
k_{r1} = global calibration coefficient = −3.4488, for all HMA mixes.
k_{r2} = global calibration coefficient = 1.5606, for all HMA mixes.
k_{r3} = global calibration coefficient = 0.4791, for all HMA mixes.
$\beta_{r1,r2,r3}$ = local calibration coefficients for rutting (for Option A, all = 1.0).

Differences in volumetric properties are taken into account through changes in the dynamic modulus. It has been found, however, that HMA mixtures with similar dynamic modulus values can have significantly different plastic deformation constants and resulting rut depths. The following lists the steps used to revise the previous plastic deformation equation to account for volumetric differences known to have a significant effect on the plastic deformation constants. It should be noted that this procedure does not take into account any differences in performance between neat and polymer-modified mixtures. The local calibration factors in Equation C.1 will need to take these types of differences into account.

1. Extract or collect the volumetric properties for each HMA layer that were measured at the time of construction. These properties include the air voids, effective asphalt content by volume, and gradation, all of which can usually be obtained from construction and mix design records. In addition, these volumetric properties are required inputs for the MEPDG, so no additional data or information is needed for the recalibration process.
2. Determine the gradation index, *GI,* for each HMA mixture. The gradation index is defined as the absolute difference between the actual gradation and the maximum density line (FHWA 0.45 power gradation chart) using sieve sizes 3/8, #4, #8, #16, #30, and #50. Table C.1 lists the percent passing for these sieve sizes that follow the maximum density line as defined by the FHWA 0.45 power gradation curves for different size mixtures. The gradation index is used to refine the adjustment factors for rutting predictions.

$$GI = \sum_{i=3/8}^{\#50} \left| P_i - P_{i(0.45)} \right| \quad \text{(C.2)}$$

where

GI = gradation index.
P_i = percent passing sieve i.
$P_{i(0.45)}$ = percent passing sieve i for the FHWA 0.45 maximum density line (refer to Table C.1).

Table C.1. Maximum density line gradations using the FHWA 0.45 power gradation analysis.

Sieve Size, in.	Percent Passing for Mixtures with Different Top Sieve Size					
	3/8	½	¾	1	1½	1¾
1¾	—	—	—	—	—	100
1½	—	—	—	—	100	93
1	—	—	—	100	83	78
¾	—	—	100	88	73	68.5
½	—	100	83.5	73.5	61	57
3/8	100	88	73.5	64.5	53.5	50
No. 4	74	64.5	54	47	39	36.3
No. 8	54.5	47	39	34	28.5	26.5
No. 16	39.5	34	28.5	25.5	20.5	18.5
No. 30	29	25.5	21	18	15.5	14
No. 50	20.5	18	15	13.5	11	10

3. Determine the design air voids for each HMA mixture. The design air void level used within an agency is a policy decision that does not vary by mixture type. The design air void level is usually 4% for most dense-graded HMA mixtures and is obtained from the mix design method. Some agencies vary this value for surface and base mixtures.
4. Determine the optimum effective asphalt content by volume for each HMA mixture. The optimum effective asphalt content is dependent on the surface area and other surface characteristics of the aggregate. Surface area and texture are difficult to define, so a specific compaction effort has been used in previous work.

   Regarding the Marshall mixture design method, the optimum asphalt content was defined as 75 blows per face for all dense-graded mixtures, which is used for most high-volume roadways. For the Superpave mix design method, there is insufficient data to determine this value and only one compaction effort is generally available for a specific mixture. For simplicity and ease of use, this value is defined at *N*-design. Results from the recalibration effort will need to be evaluated to determine if the rut-depth residual error is *N*-design or truck volume category dependent.
5. Make an adjustment to the k_{r1} parameter (intercept coefficient) based on volumetric properties and gradation for each HMA layer by using Equation C.3. This value (k_{r1}) replaces the global calibration factor included in the MEPDG software.

$$k_{r1} = Log\left[1.5093x10^{-3}\left(K_{r1}\right)\left(V_a\right)^{0.5213}\left(V_{be}\right)^{1.0057}\right] - 3.4488 \quad \text{(C.3)}$$

where

V_a = in-place air voids after compaction, percent.
V_{be} = effective asphalt content by volume, percent.
K_{r1} = intercept coefficient, refer to Figure C.1.

It is expected that some additional adjustments to Figure C.1 may be made as more sections are added to the database for determining the effect of the aggregate gradation and other volumetric mixture properties on the permanent deformation properties of the mixture.

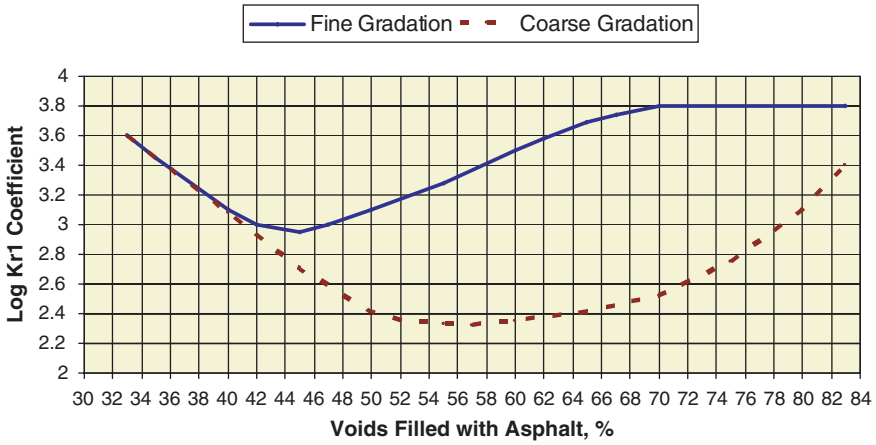

Figure C.1. Estimate of the K_{r1} intercept parameter from VFA and gradation.

Table C.2. Fine aggregate angularity index used to adjust plastic deformation parameters, F_{Index}.

Gradation—External to Restricted Zone	Fine Aggregate Angularity	
	<45	> 5
Dense grading—external to restricted zone	1.00	0.90
Dense grading—through restricted zone	1.05	1.0

Table C.3. Coarse aggregate angularity index used to adjust plastic deformation parameters, C_{Index}.

Type of Gradation	Percent Crushed Material with Two Faces				
	0	25	50	75	100
Well graded	1.1	1.05	1.0	1.0	0.9
Gap graded	1.2	1.1	1.05	1.0	0.9

6. Make an adjustment to the k_{r2} parameter (the temperature sensitivity exponent) based on volumetric properties and gradation for each HMA layer by using the following equation. This value (k_{r2}) replaces the global calibration factor included in the MEPDG software.

$$k_{r2} = 1.5606\left(\frac{V_a}{V_{a(design)}}\right)^{0.25}\left(\frac{P_b}{P_{b(opt)}}\right)^{1.25}\left(F_{Index}\right)\left(C_{Index}\right) \quad \text{(C.4)}$$

where

$V_{a(design)}$ = design air voids used to select the optimum asphalt content, percent.
P_b = asphalt content by weight, percent.
$P_{b(opt)}$ = optimum asphalt content by weight, percent.
F_{Index} = fine aggregate angularity index, refer to Table C.2.
C_{Index} = coarse aggregate angularity index, refer to Table C.3.

7. Make an adjustment to the k_{r3} parameter (sensitivity to load coefficient) based on volumetric properties and gradation for each HMA layer by using the following equation. This value (k_{r3}) replaces the global calibration factor included in the MEPDG software.

$$k_{r3} = 0.4791\left(K_{r3}\right)\left(\frac{P_b}{P_{b(opt)}}\right) \quad \text{(C.5)}$$

where

k_{r3} = slope coefficient; for fine-graded mixtures $k_{r3} = 0.40$, and for coarse-graded mixtures $k_{r3} = 0.70$.

8. Most flexible pavements and HMA overlays will consist of multiple HMA layers, each with different volumetric properties. The *k* coefficients are determined for each HMA layer. However, only one set of plastic deformation constants or coefficients can be used as local calibration factors to the MEPDG software for all HMA mixtures in the pavement structure. Determination of the adjustment coefficients should be based on the HMA mixtures that make up the upper 8 in. by calculating a weighted adjustment based on layer thickness. The following guidelines are provided to determine the rutting *kr* coefficients for a specific run or problem.
   a. Calculate the *k* coefficients for each HMA layer and use a weighted value based on thickness for the HMA mixtures that compose the top 8 in. It should be noted that a depth of 8 in. is based on previous experience and engineering judgment. This thickness guideline needs to be verified and confirmed in future studies. The LTPP SPS-1 and SPS-5 projects should provide the data needed to confirm this guideline.
   b. HMA surface layers that are less than 1 in. in thickness and underlain by at least 3 in. of dense-graded HMA mixtures can be ignored in calculating the *k*-values.
   c. Asphalt-treated open-graded drainage layers:
      i. Asphalt-treated open-graded drainage layers that are 8 in. or more below dense-graded HMA mixtures should be ignored in making these calculations.
      ii. Asphalt-treated open-graded drainage layers that are within 8 in. of the surface should be included in calculating the *k*-values. It should be noted that a thickness of 8 in. of dense-graded mixtures above any drainage layer is based on previous experience and engineering judgment. This guideline needs to be verified and confirmed in future studies. The LTPP SPS-1 projects can provide the data to support or reject this guideline.

APPENDIX D

Dynamic Modulus Test Results

Appendix D provides a summary of the dynamic modulus tests conducted in accordance with AASHTO TP 79 and the resulting master curves for the primary HMA mixtures included in the production test program. The results from dynamic modulus tests completed under other studies are not included in this appendix.

Mix ID	ARIZONA VIRGIN	
DATE	5/25/2007	
TECHNICIAN	Bennett	
VMA	14.1	Volume, %
VFA	67	Volume, %
Reference Temp	20	C

			1		2	3	
Temperature C	Frequency Hz	Modulus Ksi	Phase Angle Degree	Modulus Ksi	Phase Angle Degree	Modulus Ksi	Phase Angle Degree
4	10	3323.01	4.22	3065.3	4.4		
4	1	2920.38	6.66	2705.7	6.6		
4	0.1	2443.2	9.32	2306.6	9.1		
4	0.01	1894.08	11.27	1814.6	11.0		
20	10	2151.61	11.2	2028.6	11.0		
20	1	1558.74	16.7	1494.3	16.4		
20	0.1	972.004	23.8	944.5	23.1		
20	0.01	513.496	31.2	487.7	29.8		
40	10	674.099	30.7	600.2	30.9		
40	1	291.329	37.5	270.0	36.1		
40	0.1	108.811	36.5	103.0	34.7		
40	0.01	38.0716	26.9	39.9	25.6		

Project:	ARIZONA VIRGIN
Date:	05/25/07
Technician:	Bennett
Sample Description:	AZV-1 and AZV-2
Notes:	N/A
Shift Factors:	Arrhenius log10 (a(T)) = EA/19.147143*(1/T - 1/Tr)
Master Curve Model:	log10 (E*) = Delta + (Max - Delta) / (1+EXP (Beta + Gamma* log10 (tr)))
Reference Temperature:	20 C

Data:

VMA:	14.1	%
VFA:	67	%

		1		2		3	
Temp	Frequency	Modulus	Phase	Modulus	Phase	Modulus	Phase
C	Hz	Ksi	Degree	Ksi	Degree	Ksi	Degree
4	10	3323.0	4.2	3065.3	4.4		
4	1	2920.4	6.7	2705.7	6.6		
4	0.1	2443.2	9.3	2306.6	9.1		
4	0.01	1894.1	11.3	1814.6	11.0		
20	10	2151.6	11.2	2028.6	11.0		
20	1	1558.7	16.7	1494.3	16.4		
20	0.1	972.0	23.8	944.5	23.1		
20	0.01	513.5	31.2	487.7	29.8		
40	10	674.1	30.7	600.2	30.9		
40	1	291.3	37.5	270.0	36.1		
40	0.1	108.8	36.5	103.0	34.7		
40	0.01	38.1	26.9	39.9	25.6		

Final Parameters:

	Max	3442.7 ksi
	Delta	2.0
	Beta	-2.1381
	Gamma	0.5417
	EA	236476

Goodness of Fit:

R2	0.9994
Se/Sy	0.02

Project:	ARIZONA VIRGIN
Date:	05/25/07
Sample Description:	AZV-1 and AZV-2
Notes:	N/A
Shift Factors:	Arrhenius log10 (a(T)) = EA/19.147143*(1/T - 1/Tr)
Master Curve Model:	log10 (E*) = Delta + (Max - Delta) / (1+EXP (Beta + Gamma* log10 (tr)))
Reference Temperature:	20 C

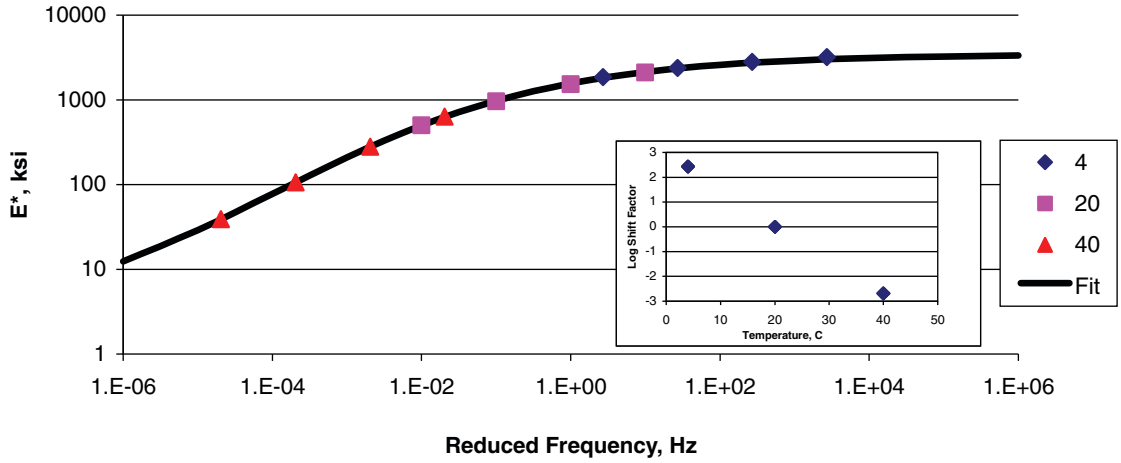

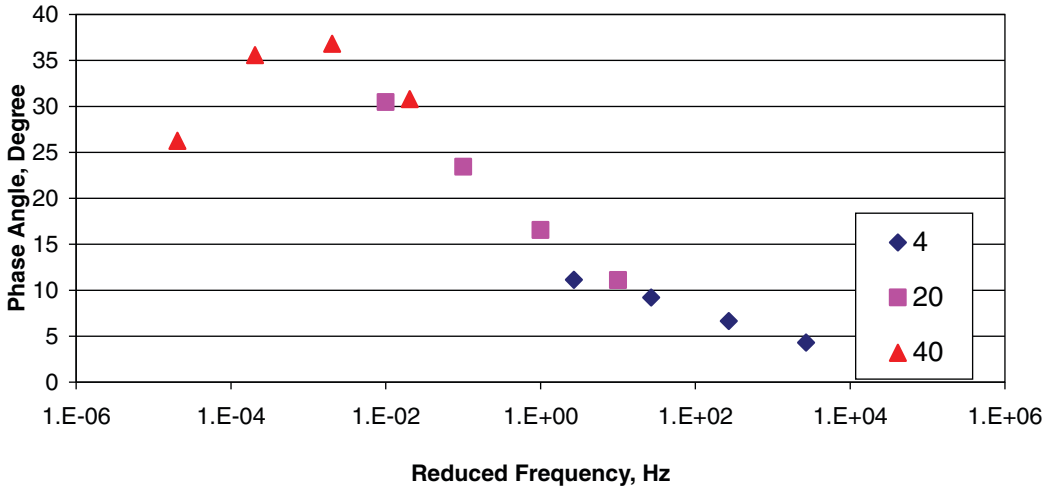

Mix ID	MISSISSIPPI VIRGIN	
DATE	06/15/07	
TECHNICIAN	Bennett	
VMA	15	Volume, %
VFA	75	Volume, %
Reference Temp	20	C

			1		2		3
Temperature C	Frequency Hz	Modulus Ksi	Phase Angle Degree	Modulus Ksi	Phase Angle Degree	Modulus Ksi	Phase Angle Degree
4	10	1975.8	10.1	2260.6	11.0		
4	1	1521.8	14.9	1656.8	15.5		
4	0.1	1023.7	20.5	1091.1	21.6		
4	0.01	594.7	23.9	655.4	25.8		
20	10	829.3	23.4	989.7	23.8		
20	1	463.4	29.6	547.3	30.4		
20	0.1	231.7	34.2	259.7	33.6		
20	0.01	109.4	30.8	109.6	31.5		
40	10	190.8	34.8	210.3	35.5		
40	1	84.2	30.5	87.0	31.2		
40	0.1	47.7	24.5	49.8	22.4		
40	0.01	31.5	15.2	29.7	14.6		

Project:	MISSISSIPPI VIRGIN
Date:	06/15/07
Technician:	Bennett
Sample Description:	MTV-1 and MTV-2
Notes:	N/A
Shift Factors:	Arrhenius log10 (a(T)) = EA/19.147143*(1/T - 1/Tr)
Master Curve Model:	log10 (E*) = Delta + (Max - Delta) / (1+EXP (Beta + Gamma* log10 (tr)))
Reference Temperature:	20 C

Data:

VMA:	15	%	
VFA:	75	%	

		1		2		3	
Temp	Frequency	Modulus	Phase	Modulus	Phase	Modulus	Phase
C	Hz	Ksi	Degree	Ksi	Degree	Ksi	Degree
4	10	1975.8	10.1	2260.6	11.0		
4	1	1521.8	14.9	1656.8	15.5		
4	0.1	1023.7	20.5	1091.1	21.6		
4	0.01	594.7	23.9	655.4	25.8		
20	10	829.3	23.4	989.7	23.8		
20	1	463.4	29.6	547.3	30.4		
20	0.1	231.7	34.2	259.7	33.6		
20	0.01	109.4	30.8	109.6	31.5		
40	10	190.8	34.8	210.3	35.5		
40	1	84.2	30.5	87.0	31.2		
40	0.1	47.7	24.5	49.8	22.4		
40	0.01	31.5	15.2	29.7	14.6		

Final Parameters:

Max	3433.7	ksi
Delta	13.6	
Beta	-0.6551	
Gamma	0.5540	
EA	209666	

Goodness of Fit:

R2	0.9977
Se/Sy	0.04

Project:	MISSISSIPPI VIRGIN
Date:	06/15/07
Sample Description:	MTV-1 and MTV-2
Notes:	N/A
Shift Factors:	Arrhenius log10 (a(T)) = EA/19.147143*(1/T - 1/Tr)
Master Curve Model:	log10 (E*) = Delta + (Max - Delta) / (1+EXP (Beta + Gamma* log10 (tr)))
Reference Temperature:	20 C

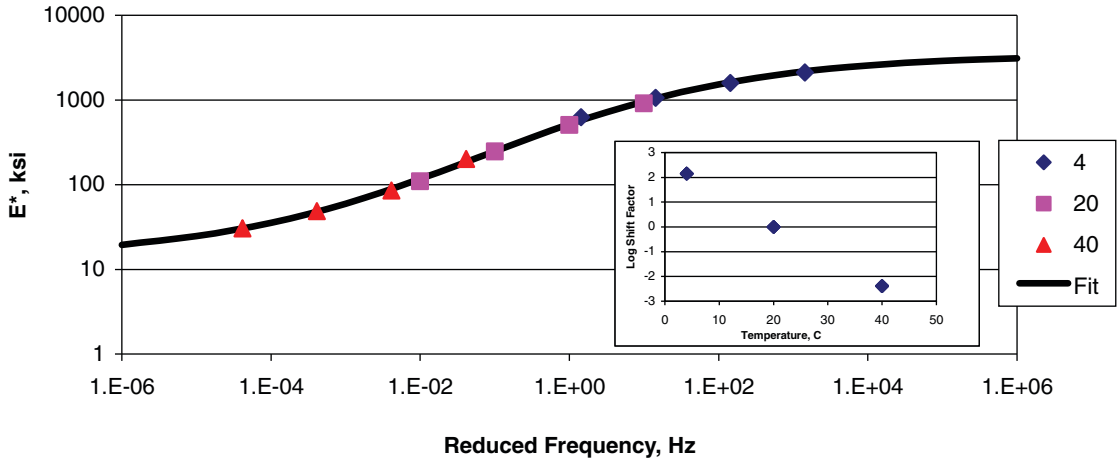

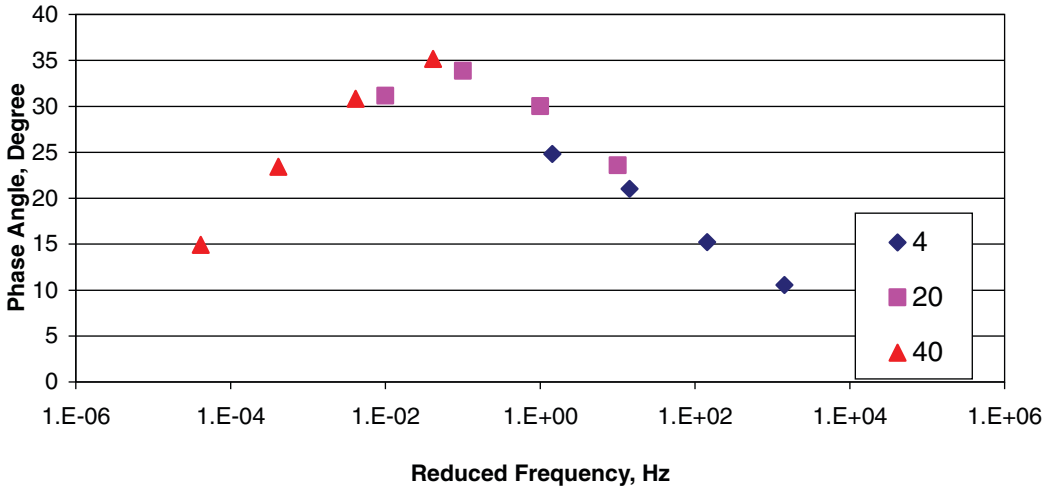

Mix ID	MONTANA	VIRGIN
DATE	06/05/07	
TECHNICIAN	Bennett	
VMA	14.9	Volume, %
VFA	76	Volume, %
Reference Temp	20	C

			1		2		3
Temperature C	Frequency Hz	Modulus Ksi	Phase Angle Degree	Modulus Ksi	Phase Angle Degree	Modulus Ksi	Phase Angle Degree
4	10	2229.3	10.8	2260.6	11.0		
4	1	1652.5	15.5	1656.8	15.5		
4	0.1	1095.0	21.0	1091.1	21.6		
4	0.01	623.4	26.2	655.4	25.8		
20	10	924.9	24.5	989.7	23.8		
20	1	517.4	31.8	547.3	30.4		
20	0.1	245.3	34.6	259.7	33.6		
20	0.01	105.5	30.6	109.6	31.5		
35	10	307.2	36.0	311.8	35.5		
35	1	137.2	34.8	137.1	34.1		
35	0.1	62.0	28.7	60.4	27.5		
35	0.01	33.3	19.3	32.9	18.6		

Project:	MONTANA VIRGIN
Date:	06/05/07
Technician:	Bennett
Sample Description:	MTV-1 and MTV-2
Notes:	N/A
Shift Factors:	Arrhenius log10 (a(T)) = EA/19.147143*(1/T - 1/Tr)
Master Curve Model:	log10 (E*) = Delta + (Max - Delta) / (1+EXP (Beta + Gamma* log10 (tr)))
Reference Temperature:	20 C

Data:

VMA:	14.9	%					
VFA:	76	%					
		1		2		3	
Temp	Frequency	Modulus	Phase	Modulus	Phase	Modulus	Phase
C	Hz	Ksi	Degree	Ksi	Degree	Ksi	Degree
4	10	2229.3	10.8	2260.6	11.0		
4	1	1652.5	15.5	1656.8	15.5		
4	0.1	1095.0	21.0	1091.1	21.6		
4	0.01	623.4	26.2	655.4	25.8		
20	10	924.9	24.5	989.7	23.8		
20	1	517.4	31.8	547.3	30.4		
20	0.1	245.3	34.6	259.7	33.6		
20	0.01	105.5	30.6	109.6	31.5		
35	10	307.2	36.0	311.8	35.5		
35	1	137.2	34.8	137.1	34.1		
35	0.1	62.0	28.7	60.4	27.5		
35	0.01	33.3	19.3	32.9	18.6		

Final Parameters:

Max	3444.4	ksi
Delta	8.9	
Beta	-0.8019	
Gamma	0.5468	
EA	208131	

Goodness of Fit:

R2	0.9986
Se/Sy	0.03

Project:	MONTANA VIRGIN
Date:	06/05/07
Sample Description:	MTV-1 and MTV-2
Notes:	N/A
Shift Factors:	Arrhenius log10 (a(T)) = EA/19.147143*(1/T - 1/Tr)
Master Curve Model:	log10 (E*) = Delta + (Max - Delta) / (1+EXP (Beta + Gamma* log10 (tr)))
Reference Temperature:	20 C

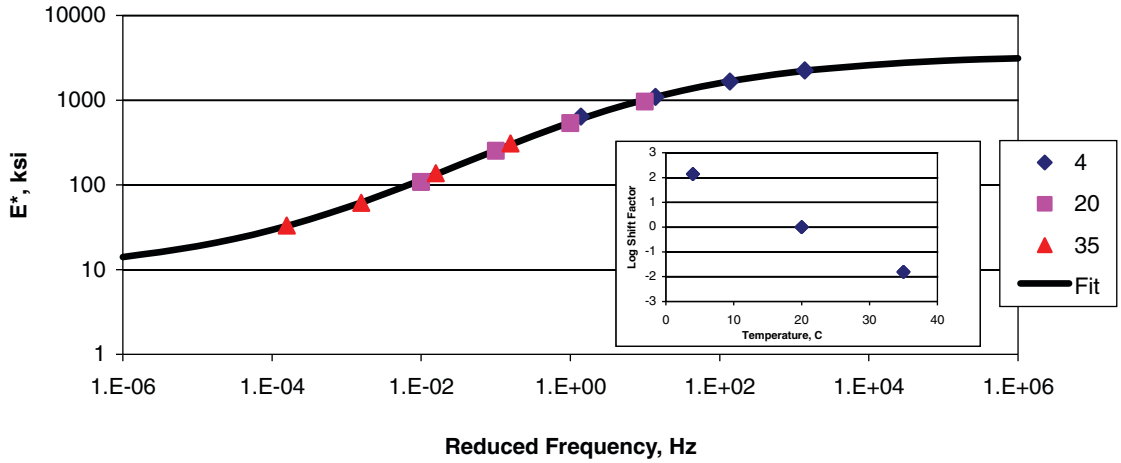

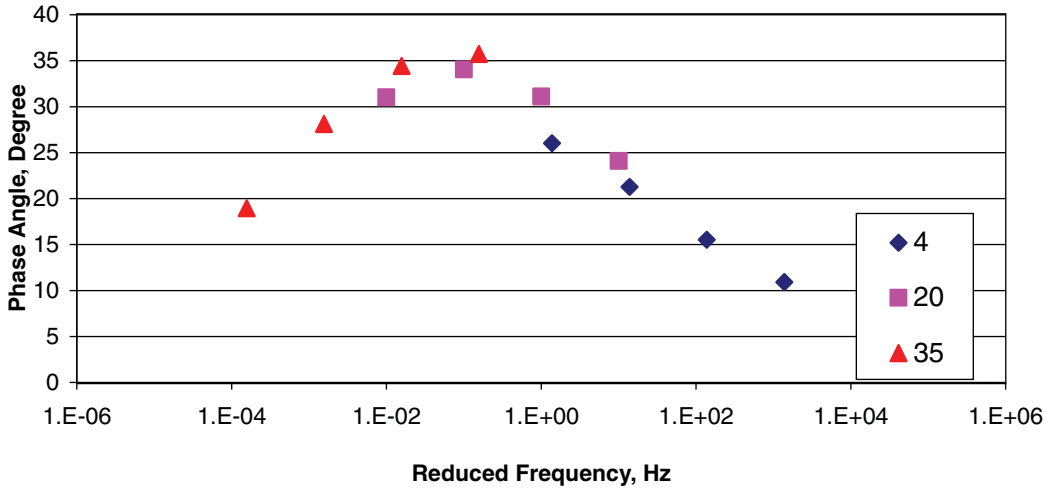

APPENDIX E

Repeated-Load Test Results

Appendix E provides a summary of the repeated-load plastic deformation tests conducted in accordance with AASHTO TP 79 and TP 320 for the core mixtures included in the production test program. The results from repeated-load plastic deformation tests completed under other studies are not included in this appendix.

E.1 Repeated-Load Triaxial Tests

Alabama; HMA Overlay

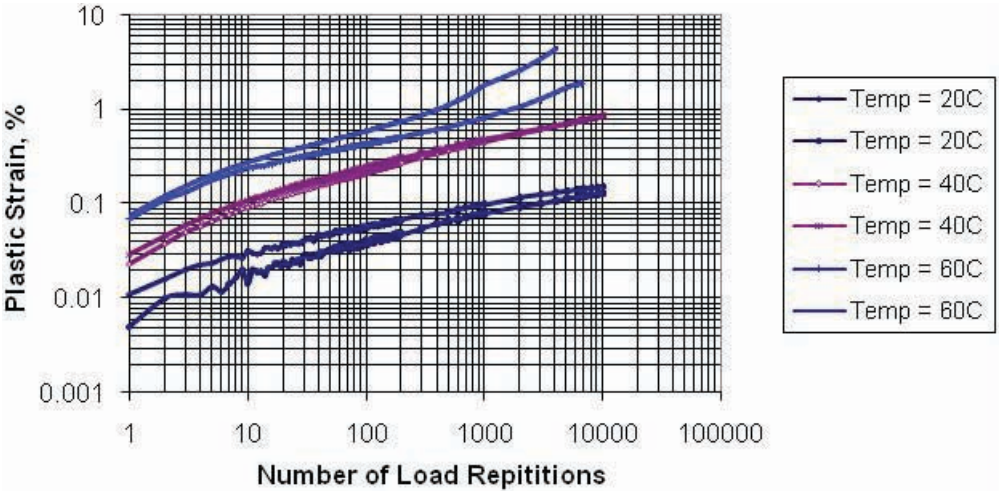

Arizona; HMA Overlay Without RAP

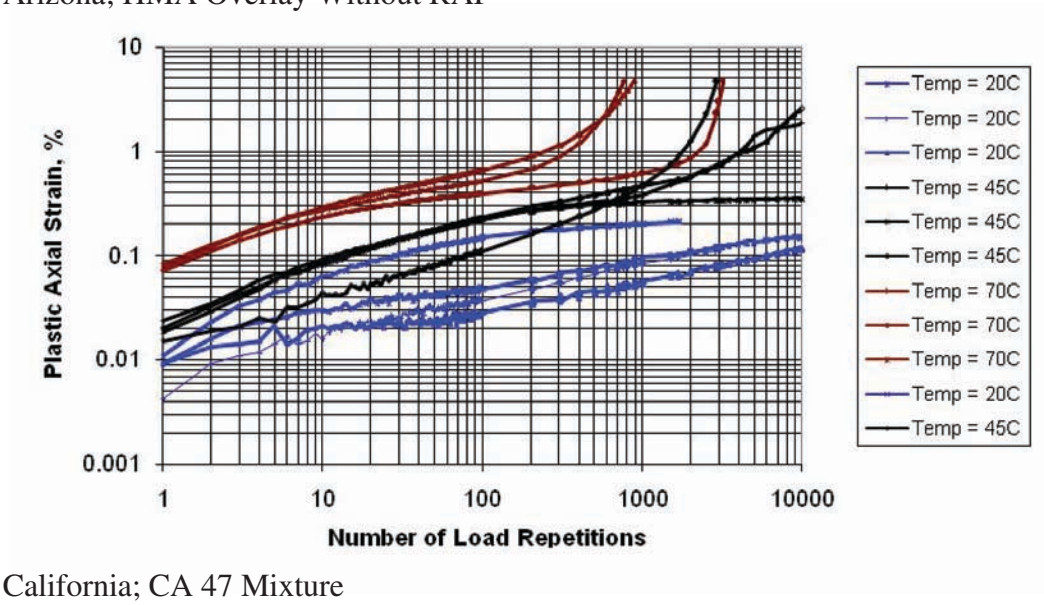

California; CA 47 Mixture

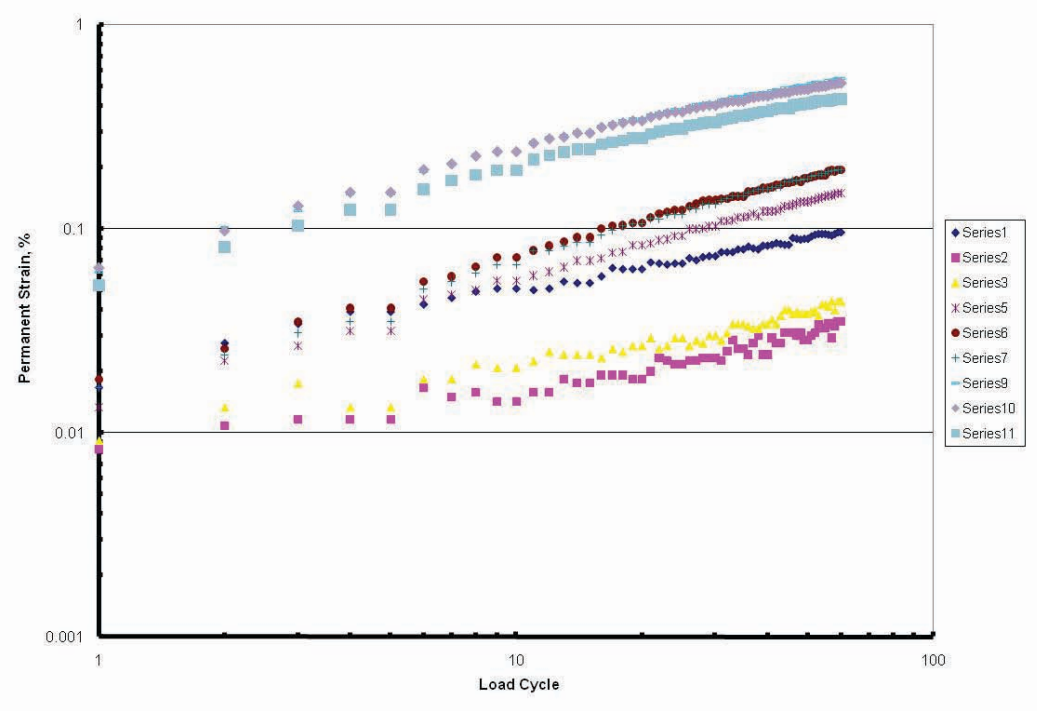

California; CA 47M Mixture

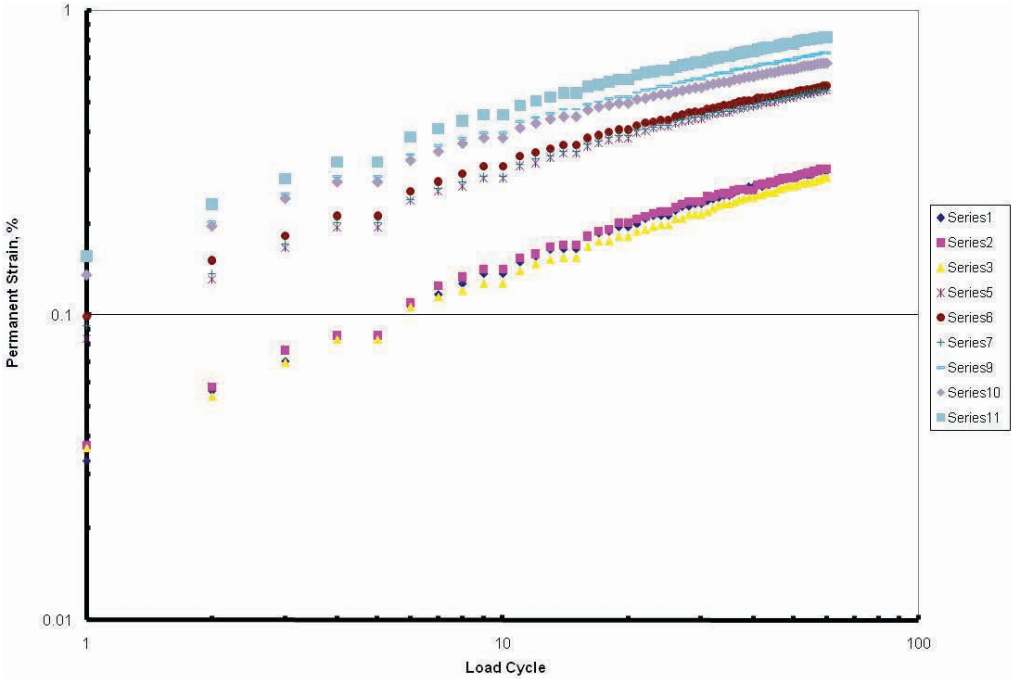

California; CA 52 Mixture

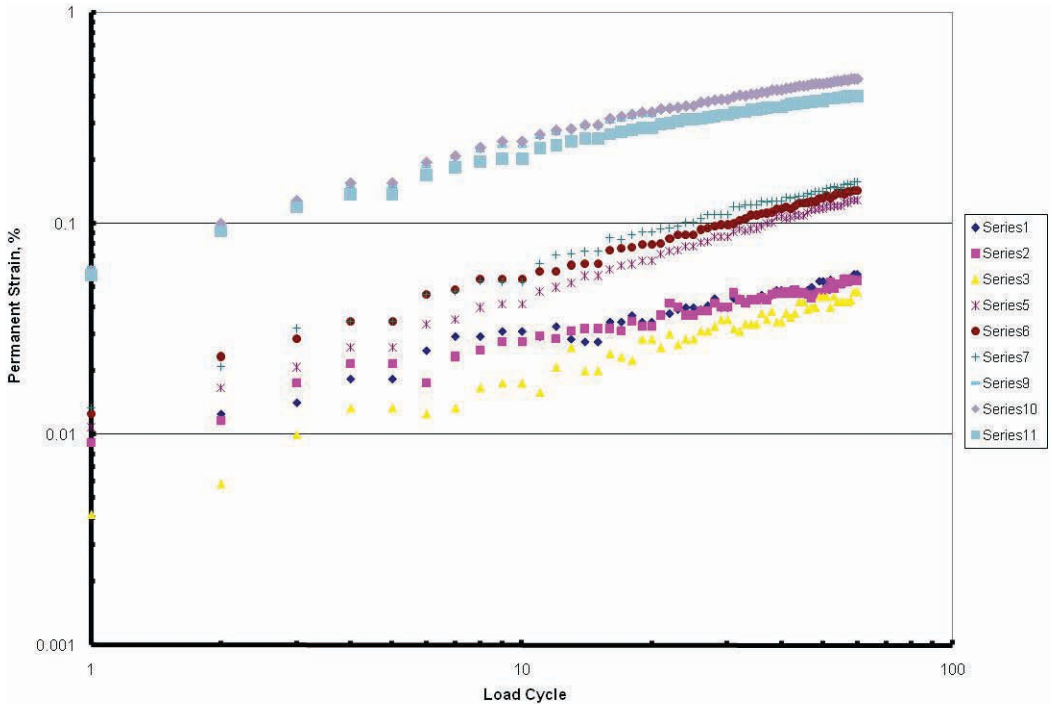

Colorado; HMA Mixture Without RAP

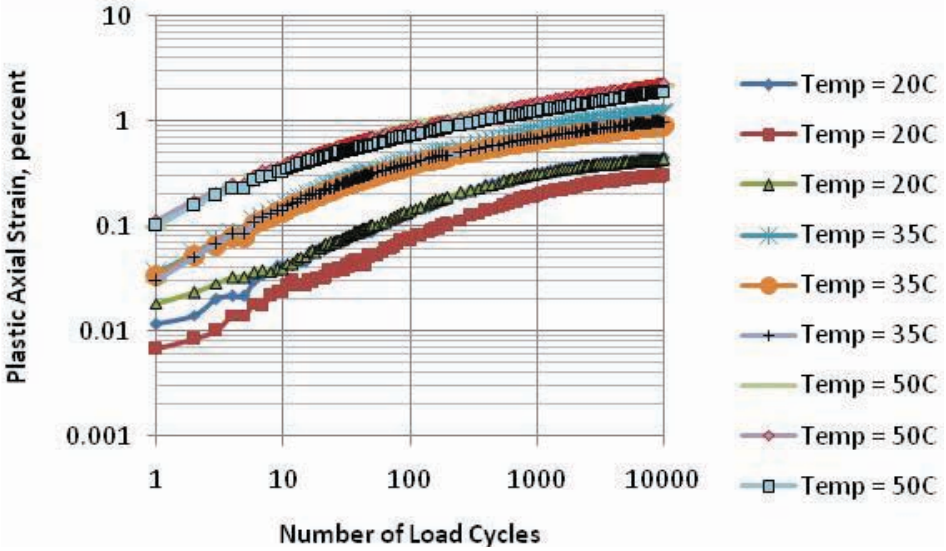

Colorado; HMA Mixture with RAP

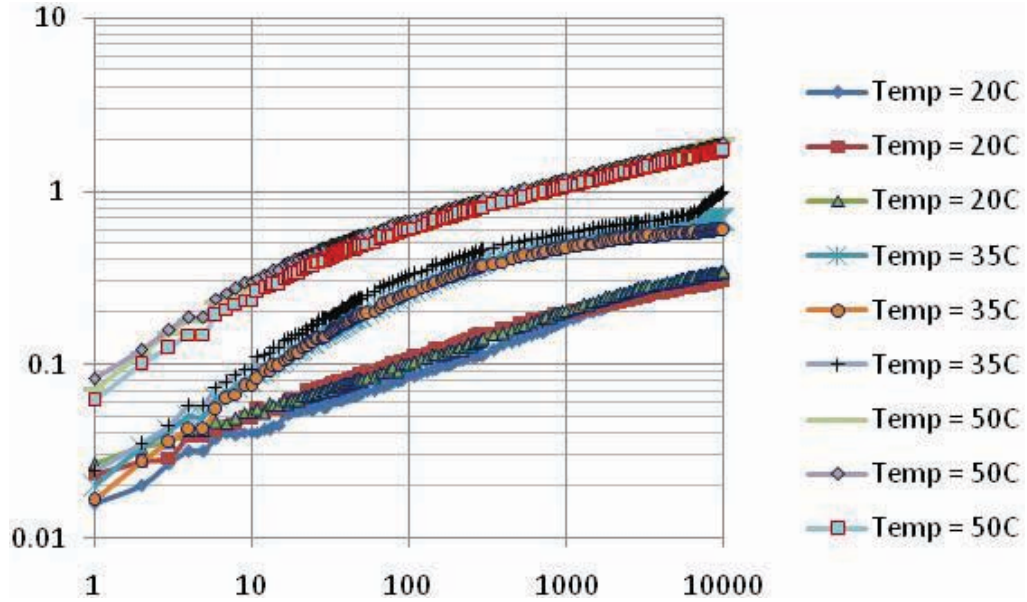

Mississippi; HMA Overlay Without RAP

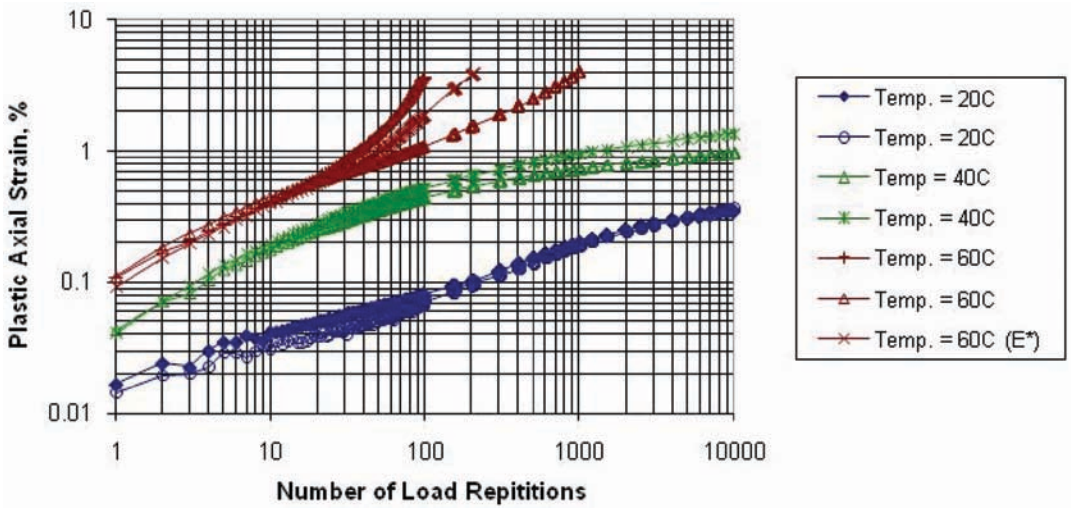

Missouri; HMA Overlay; Binder Mixture with RAP

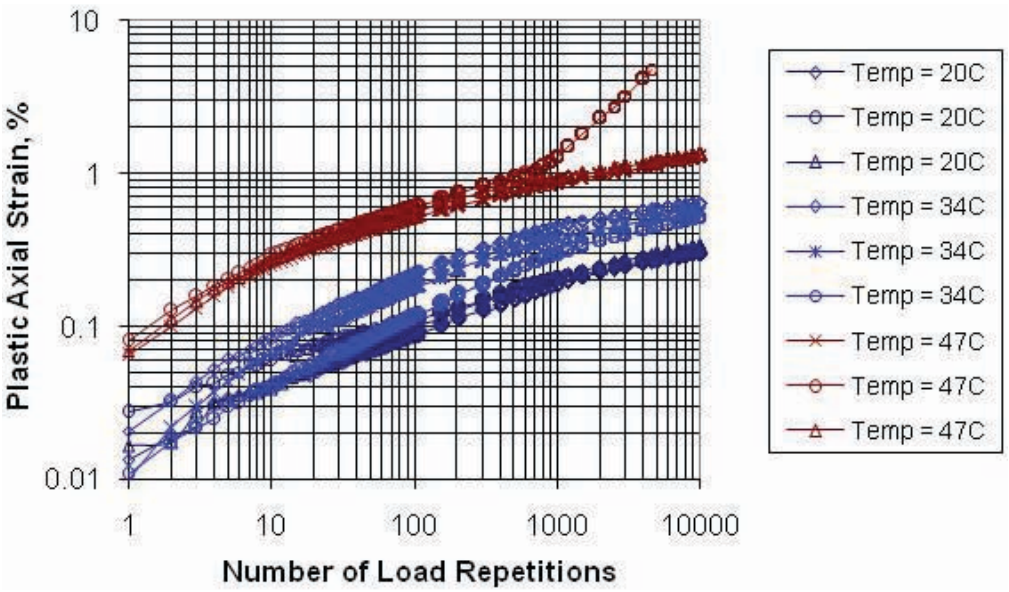

Missouri; HMA Overlay; Binder Mixture Without RAP

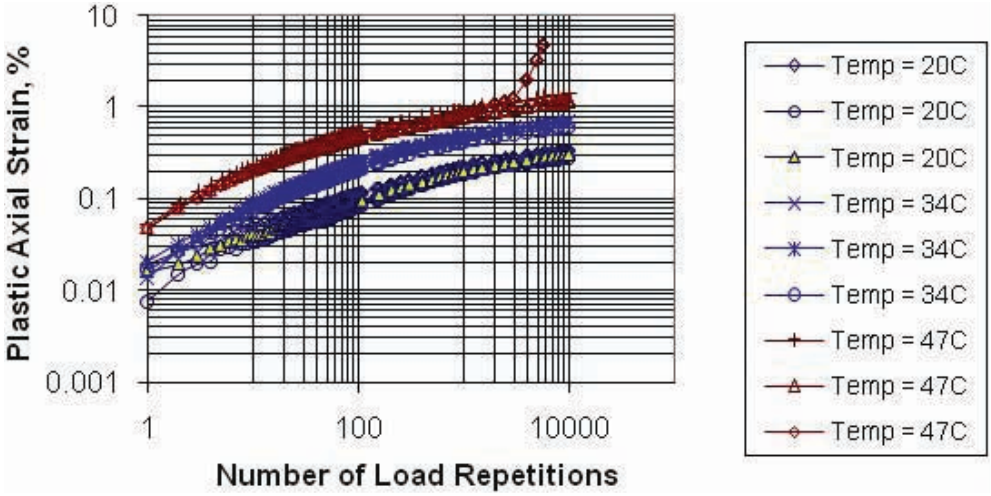

Missouri; HMA Overlay; Surface Mixture Without RAP

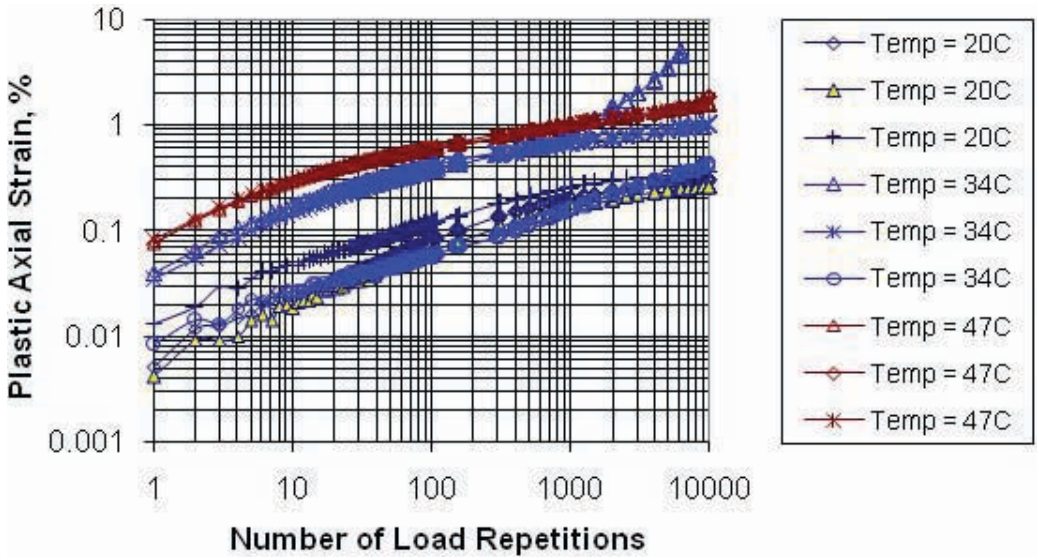

Montana; HMA Overlay; Binder Mixture Without RAP

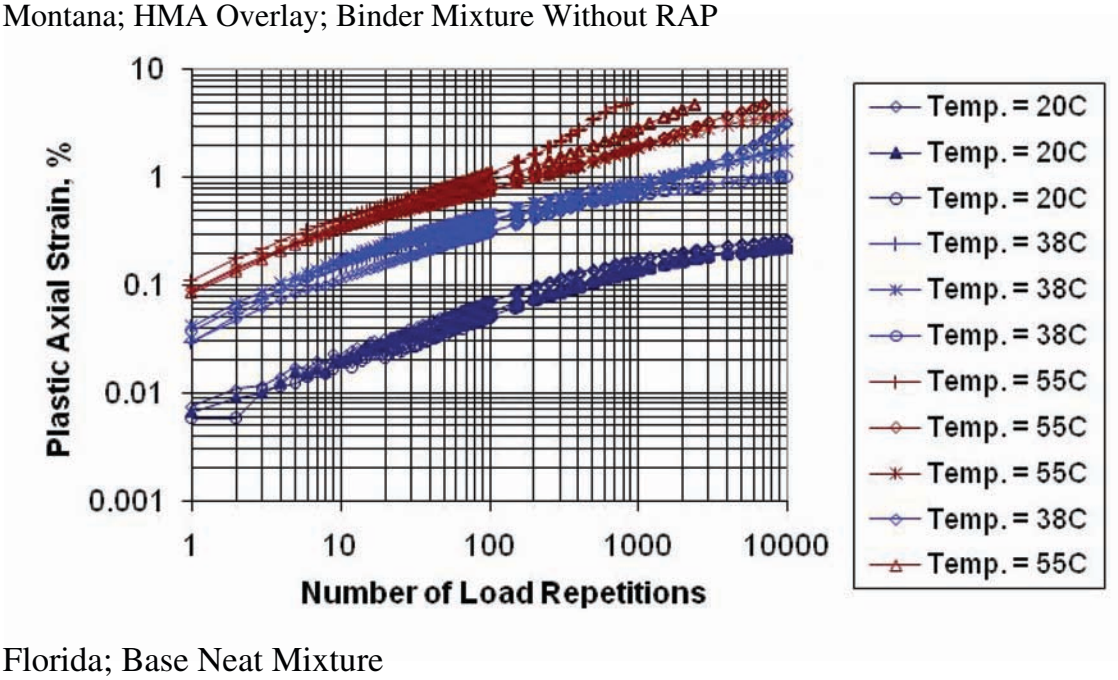

Florida; Base Neat Mixture

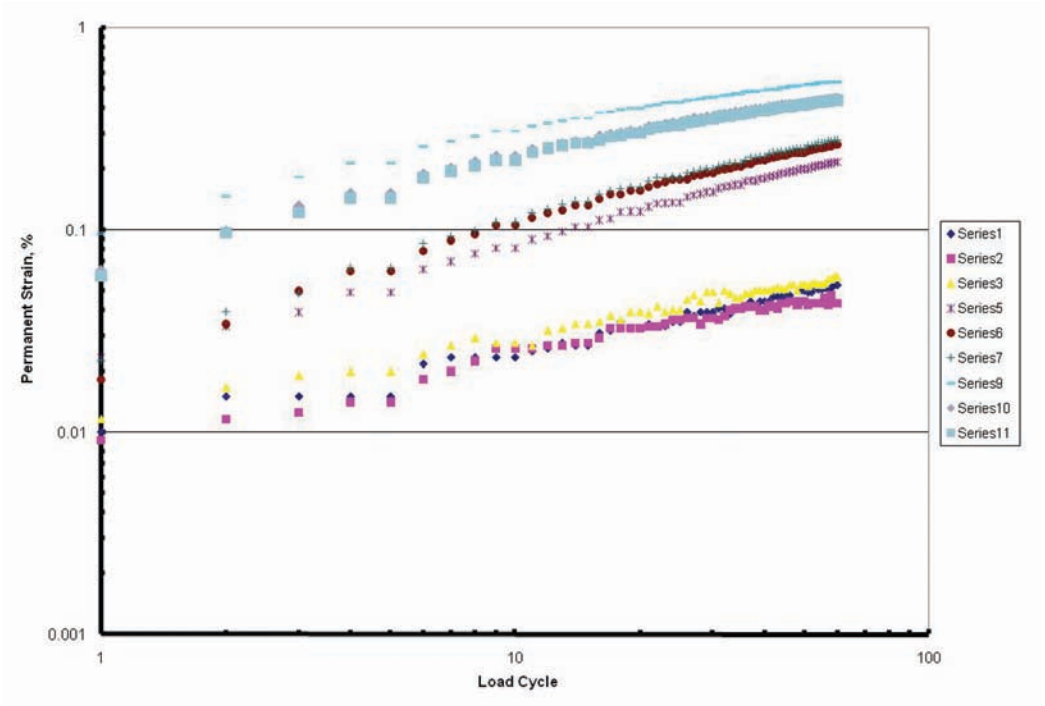

Florida; Binder Modified Mixture

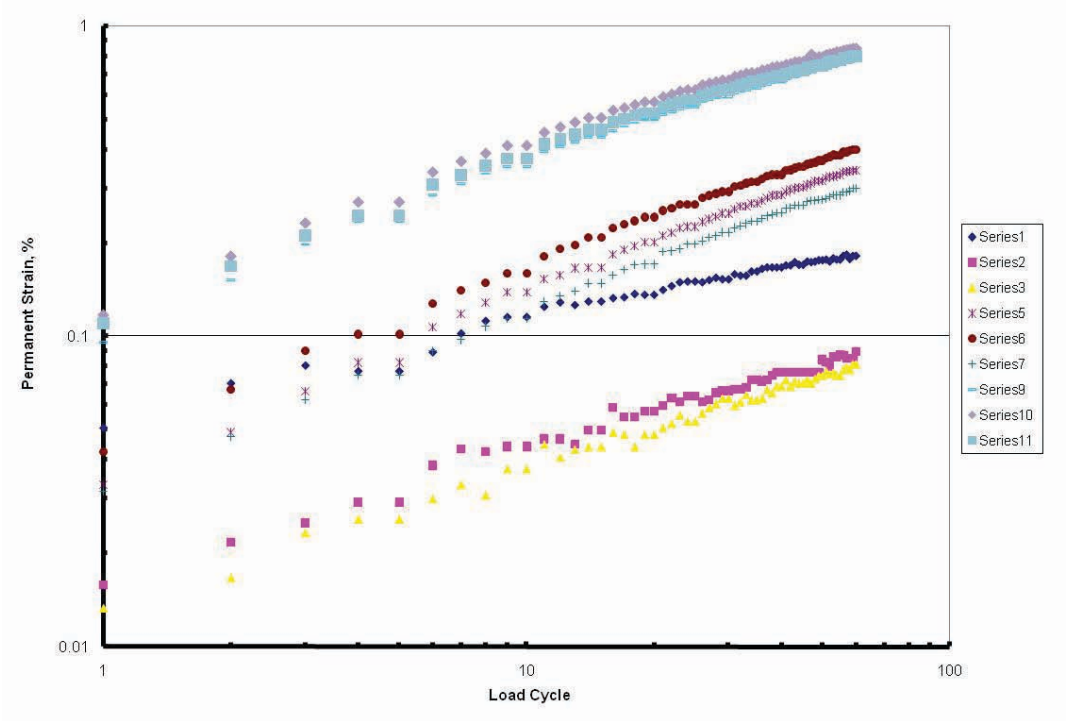

Florida; Binder Neat HMA Mixture

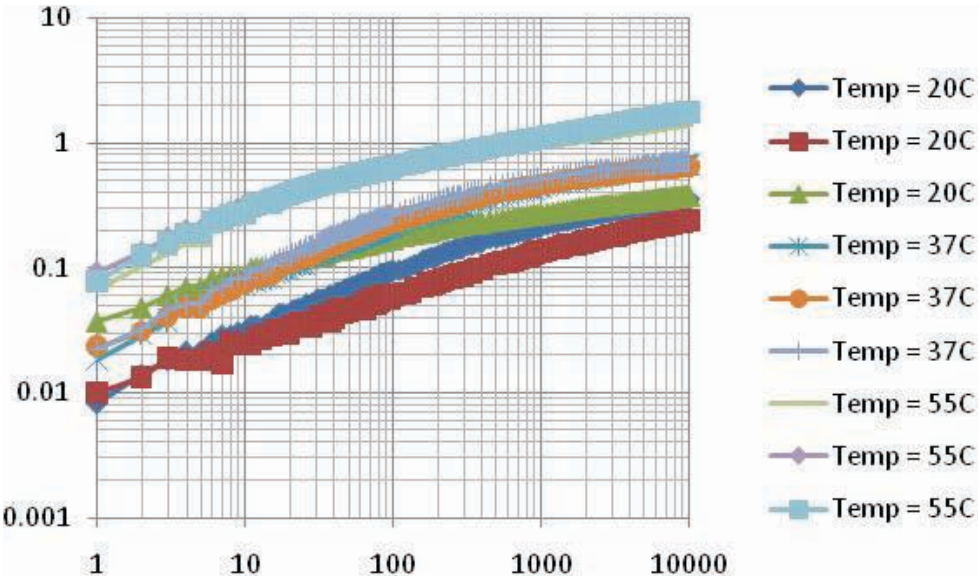

Indiana; HMA Mixture 7A

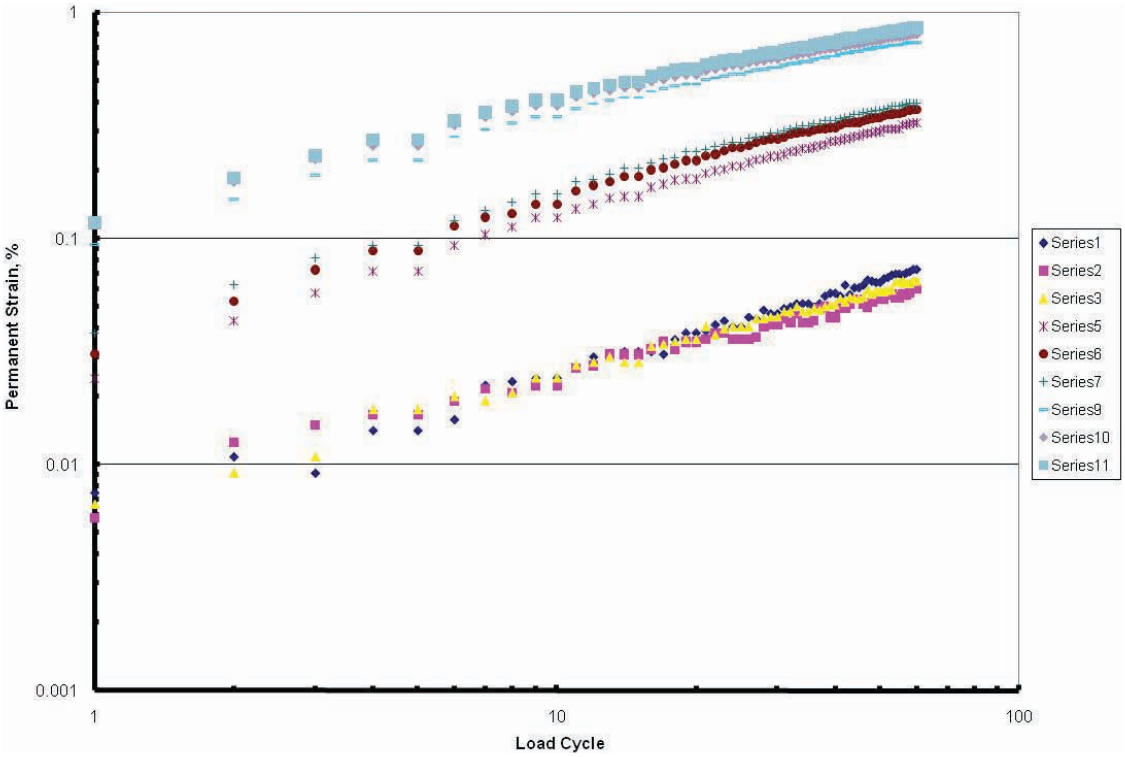

Indiana; HMA Mixture 7B

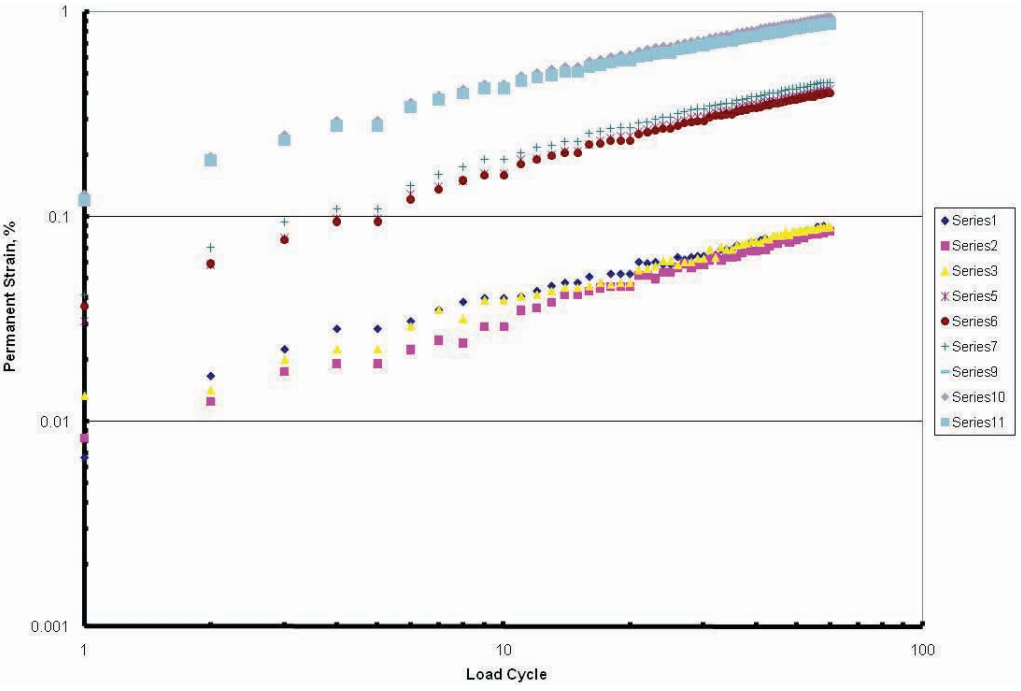

Indiana; HMA Mixture 8B

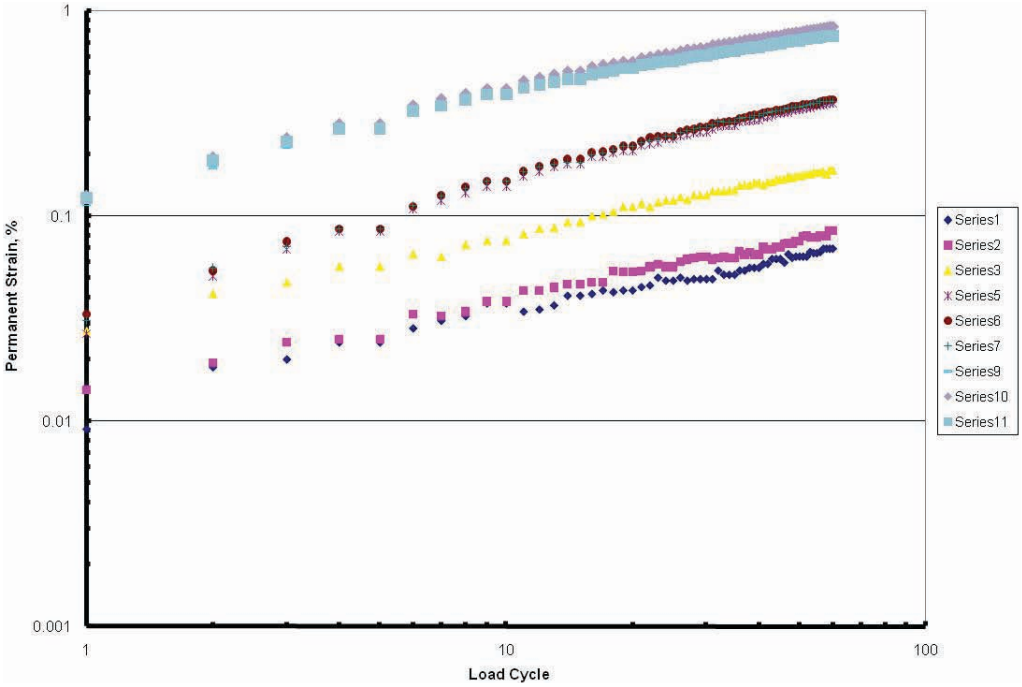

Wisconsin; ATB Mixture

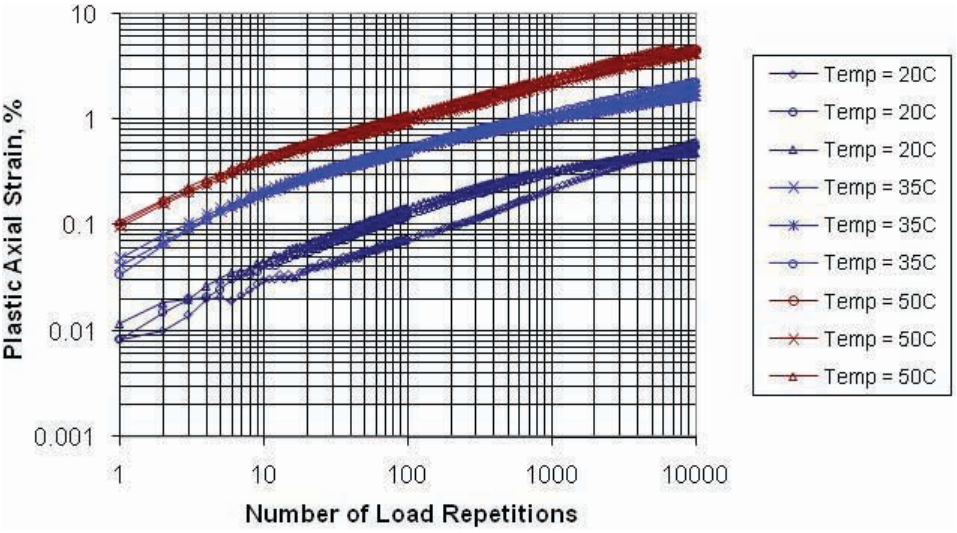

Wisconsin; HMA Binder Mixture

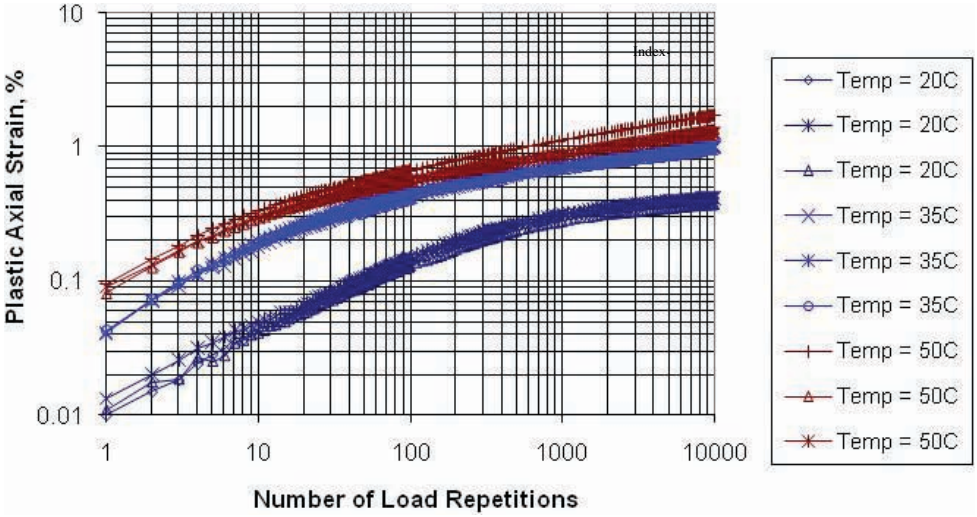

Wisconsin; HMA Surface Mixture

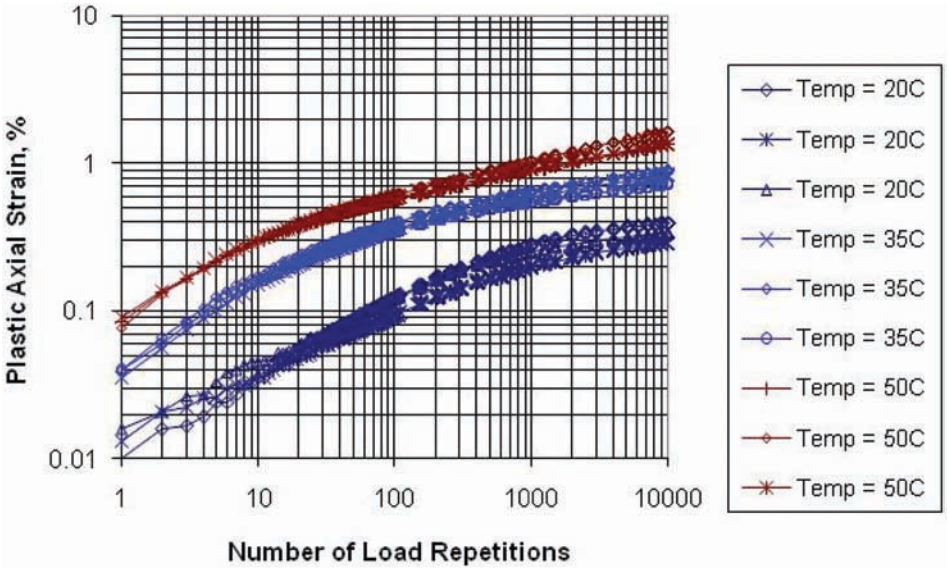

E.2 Repeated-Load Constant-Height Shear Tests

Alabama; HMA Overlay

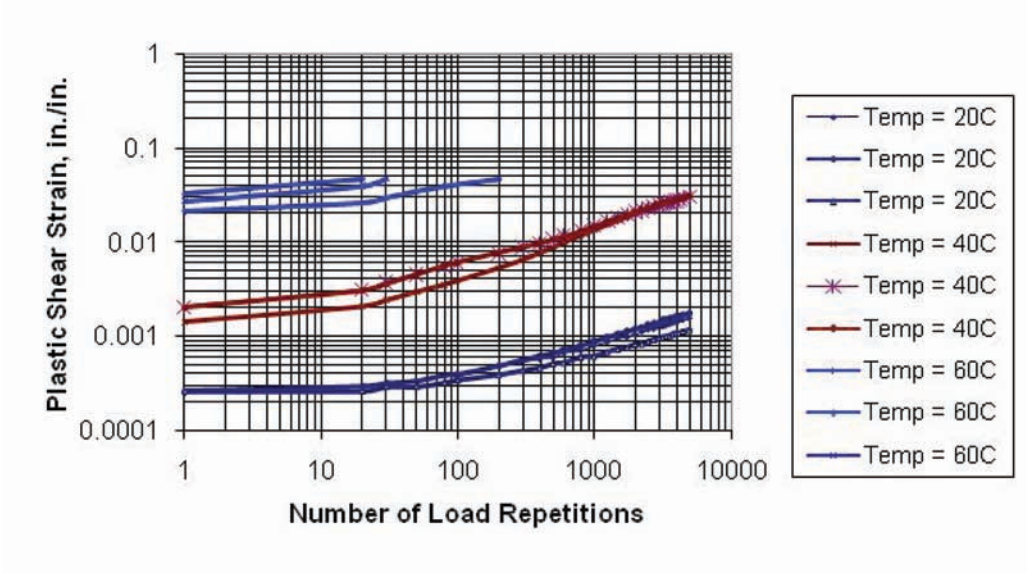

Arizona; HMA Overlay Without RAP

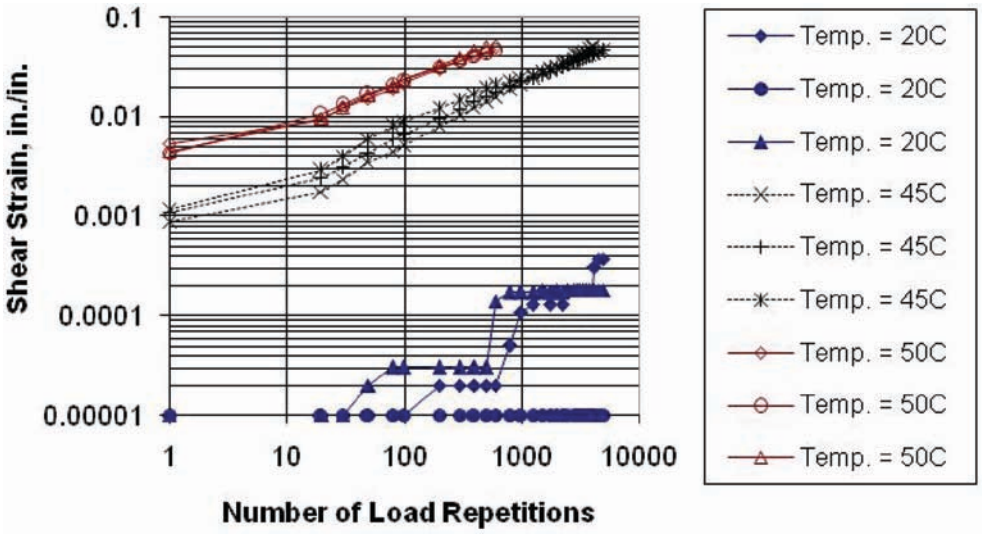

Arizona; HMA Overlay with RAP – Cores

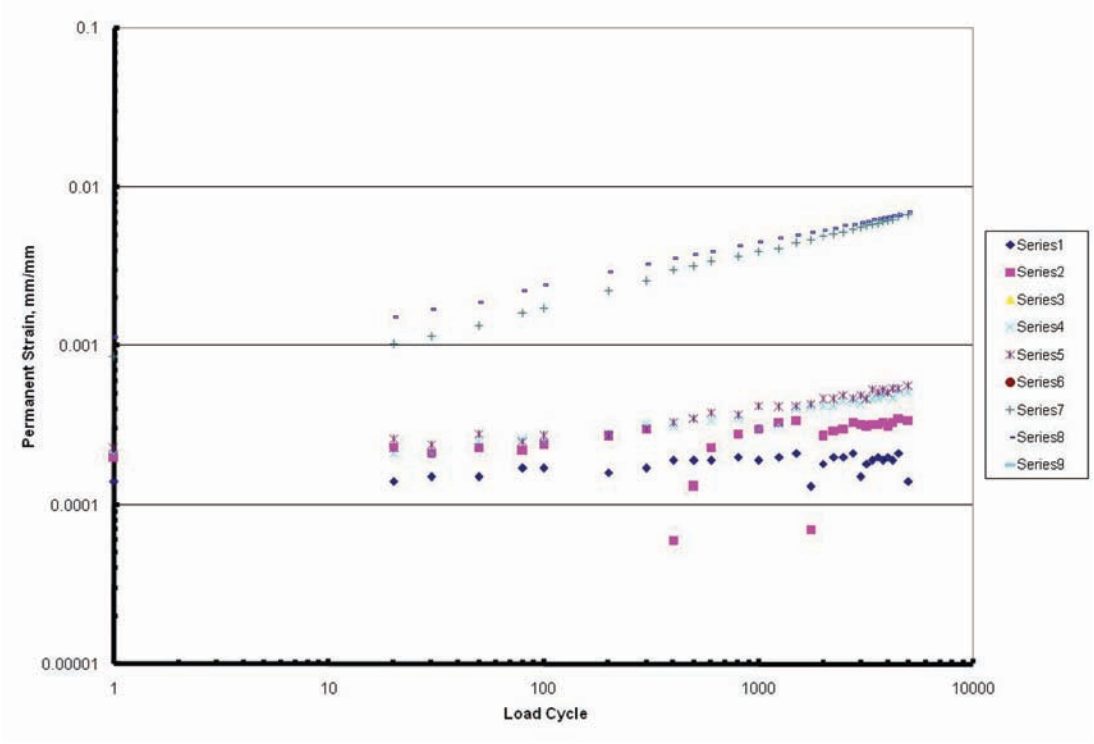

Arizona; HMA Overlay Without RAP – Cores

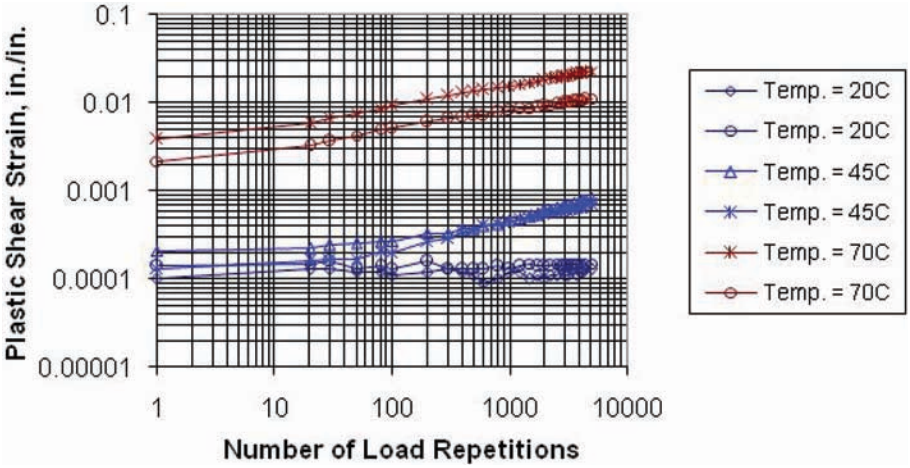

California; CA 47 Mixture

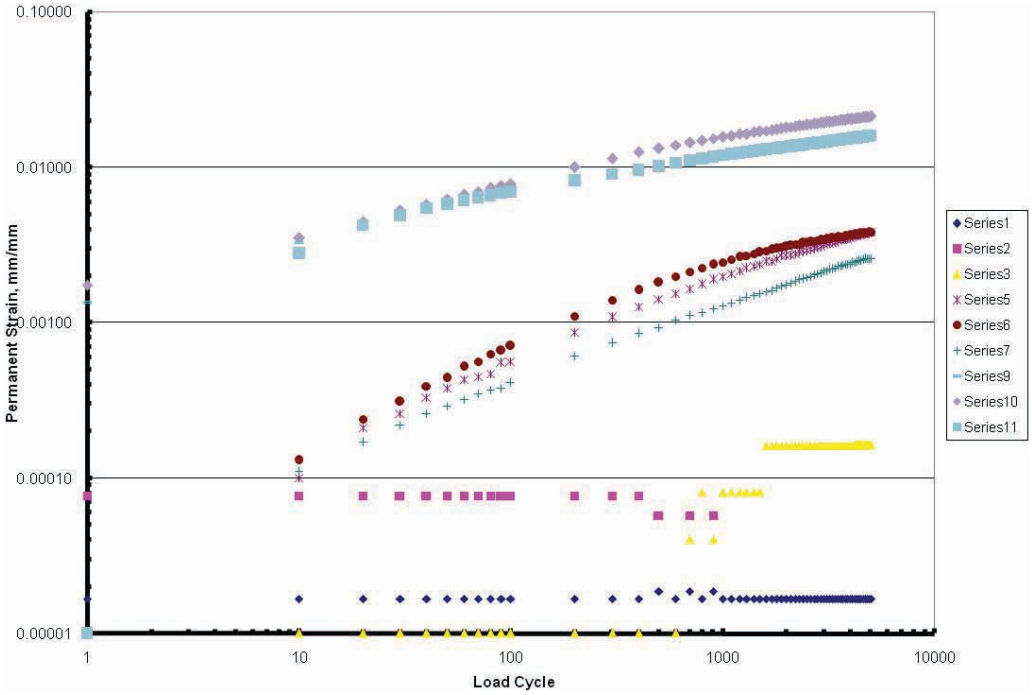

California; CA 47M Mixture

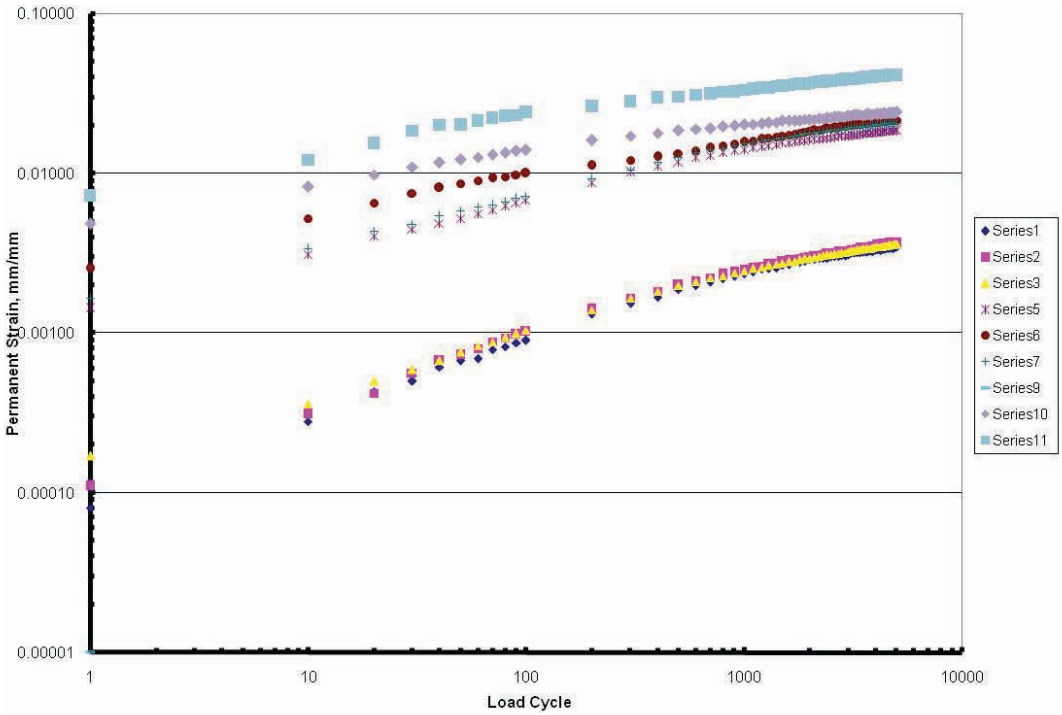

California; CA 57 Mixture

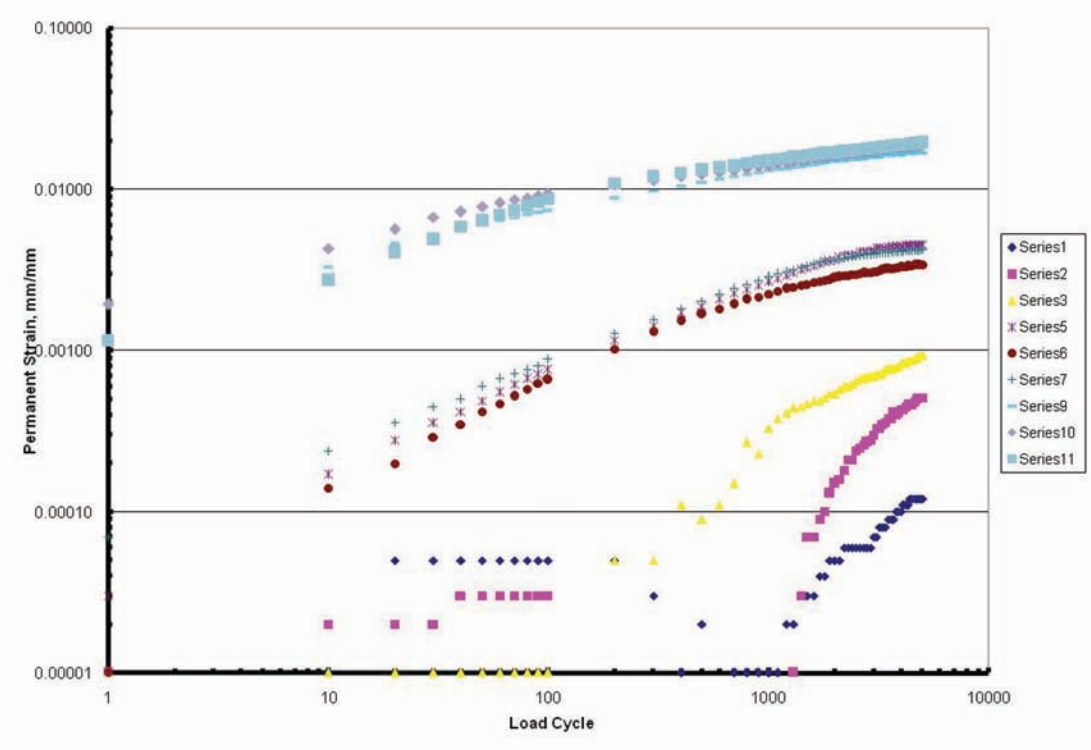

Missouri; HMA Overlay; Binder Mixture with RAP

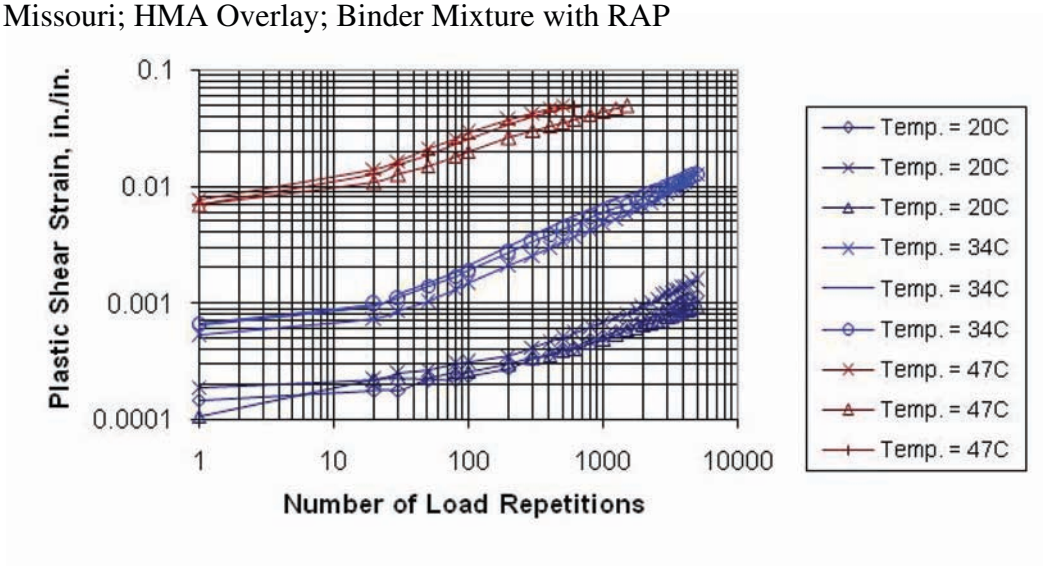

Missouri; HMA Overlay; Binder Mixture Without RAP

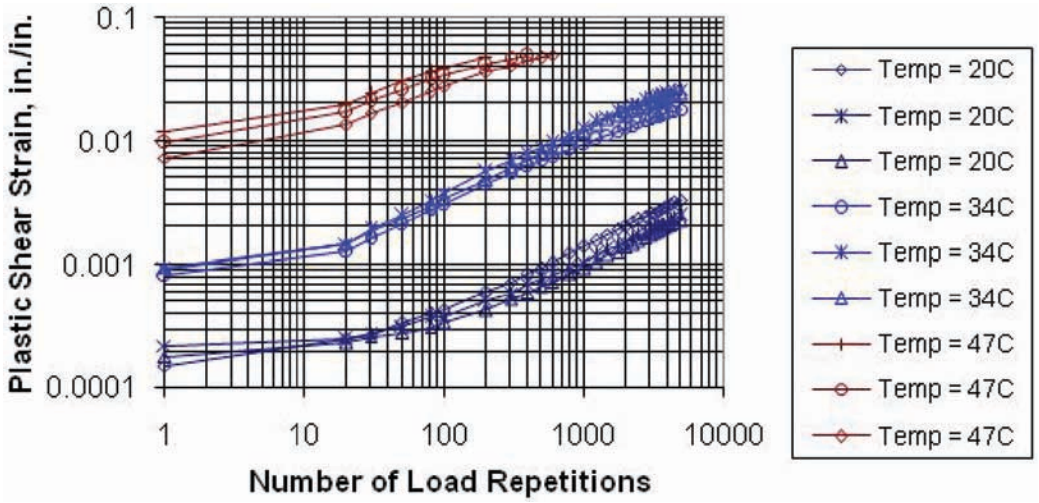

Missouri; HMA Overlay; Surface Mixture Without RAP

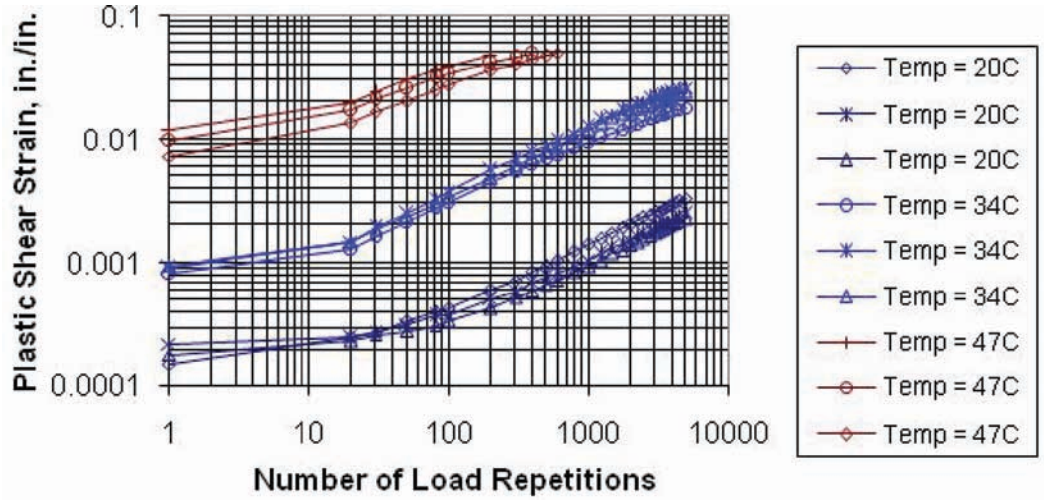

Montana; HMA Overlay; Binder Mixture Without RAP

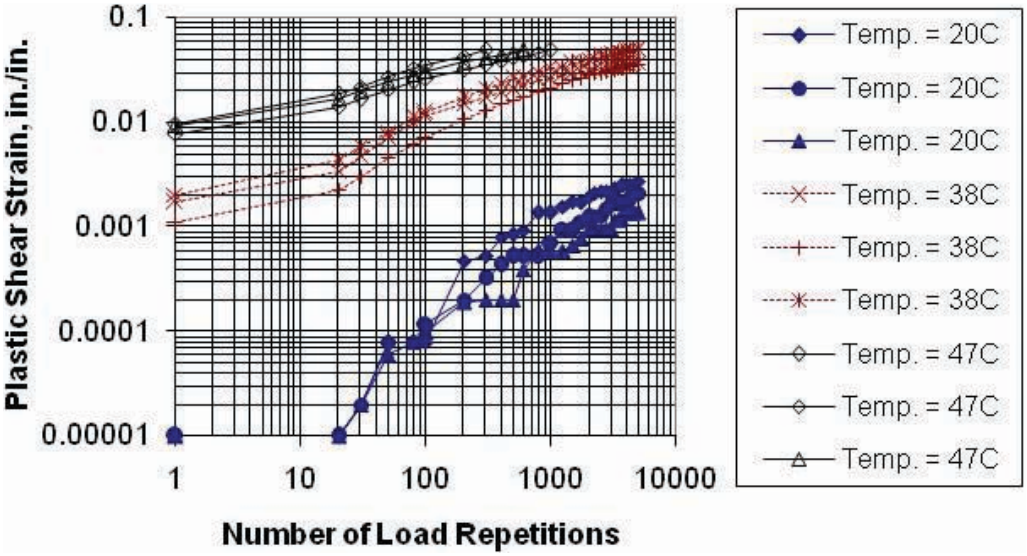

Florida; HMA Neat Base Mixture

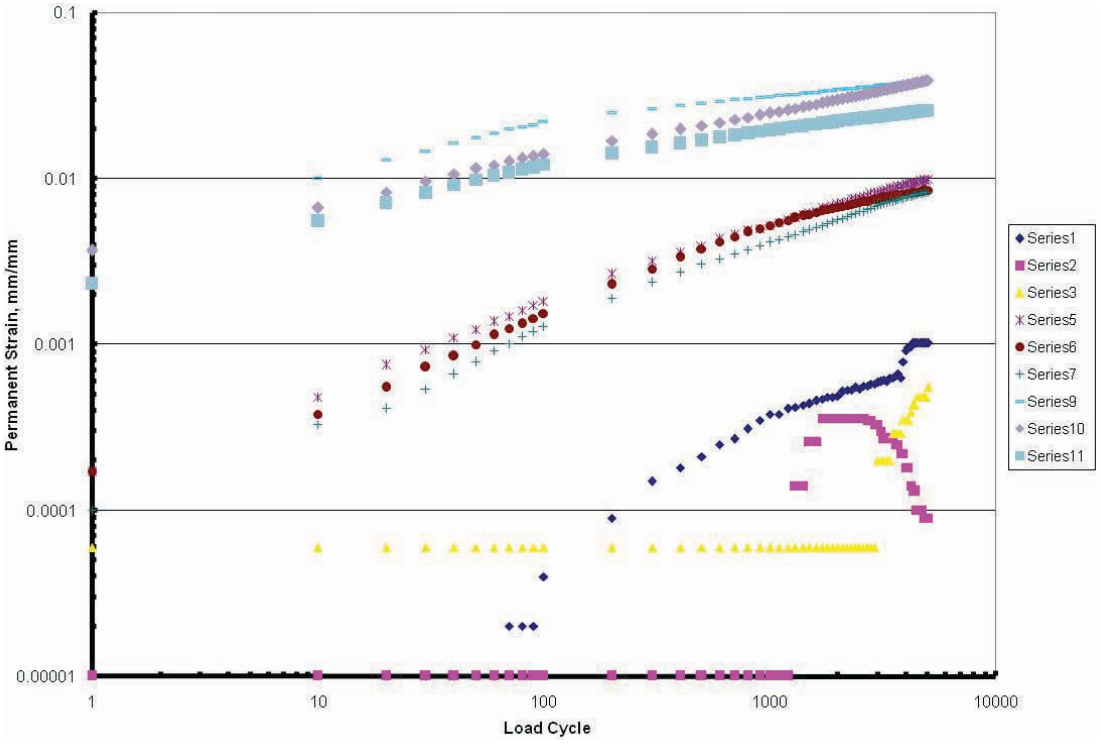

Florida; HMA Modified Binder Mixture

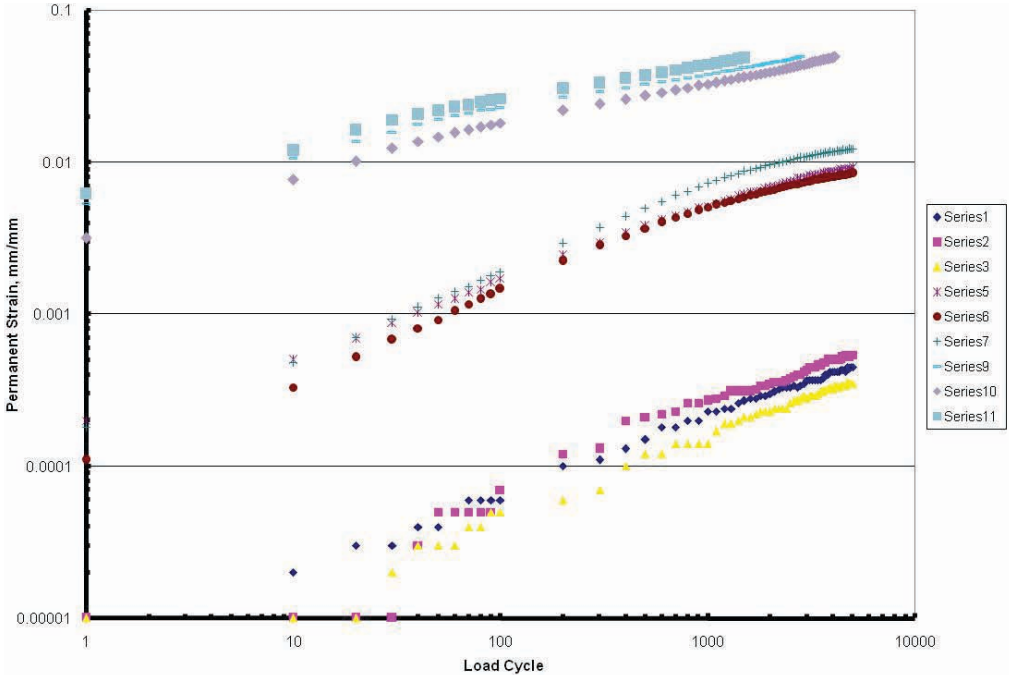

Florida; HMA Neat Binder Mixture

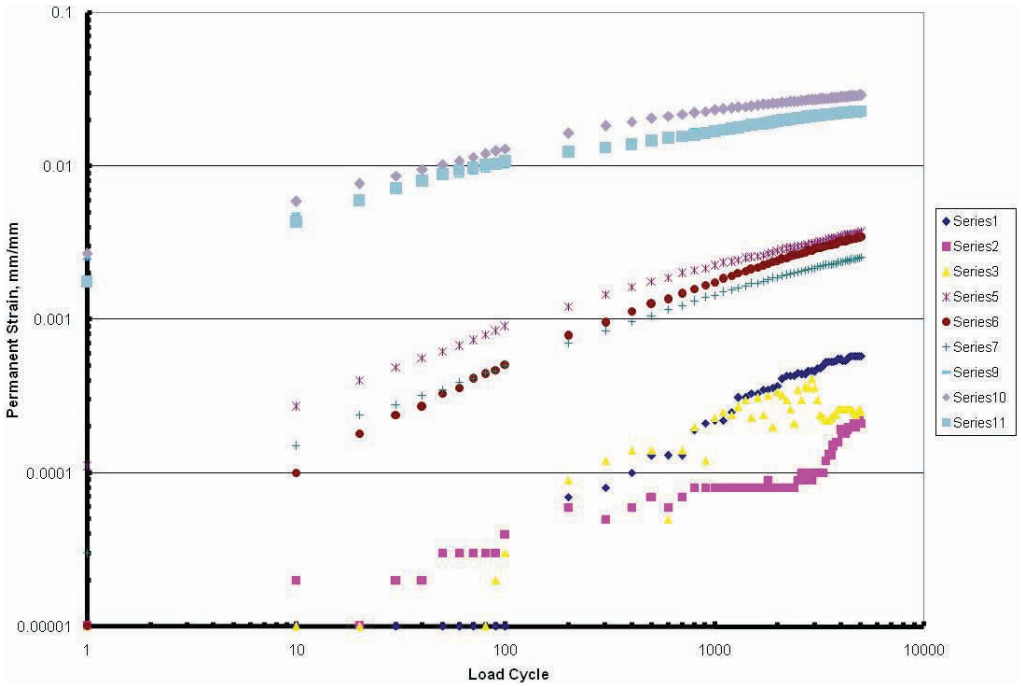

Indiana; HMA Mixture 7A

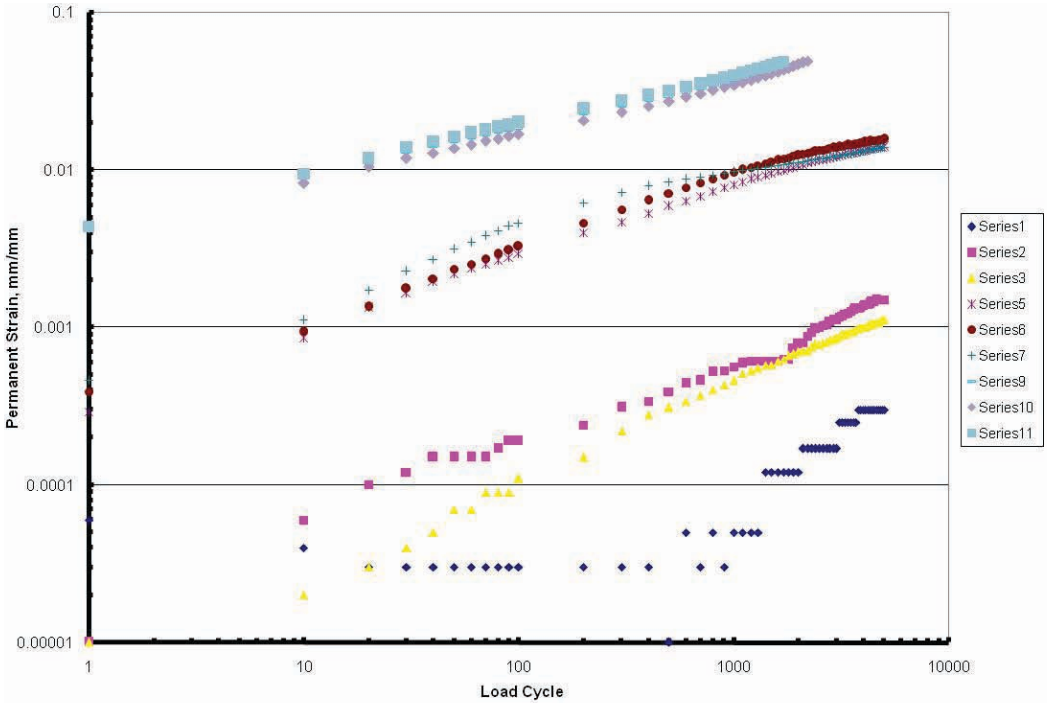

Indiana; HMA Mixture 7B

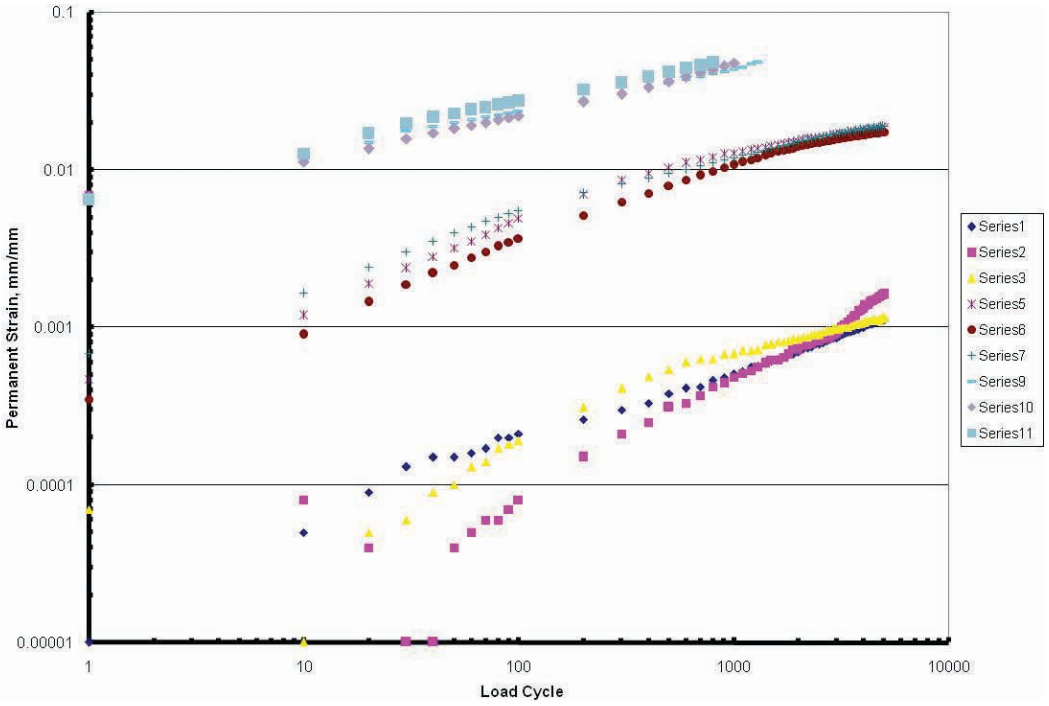

Indiana; HMA Mixture 8B

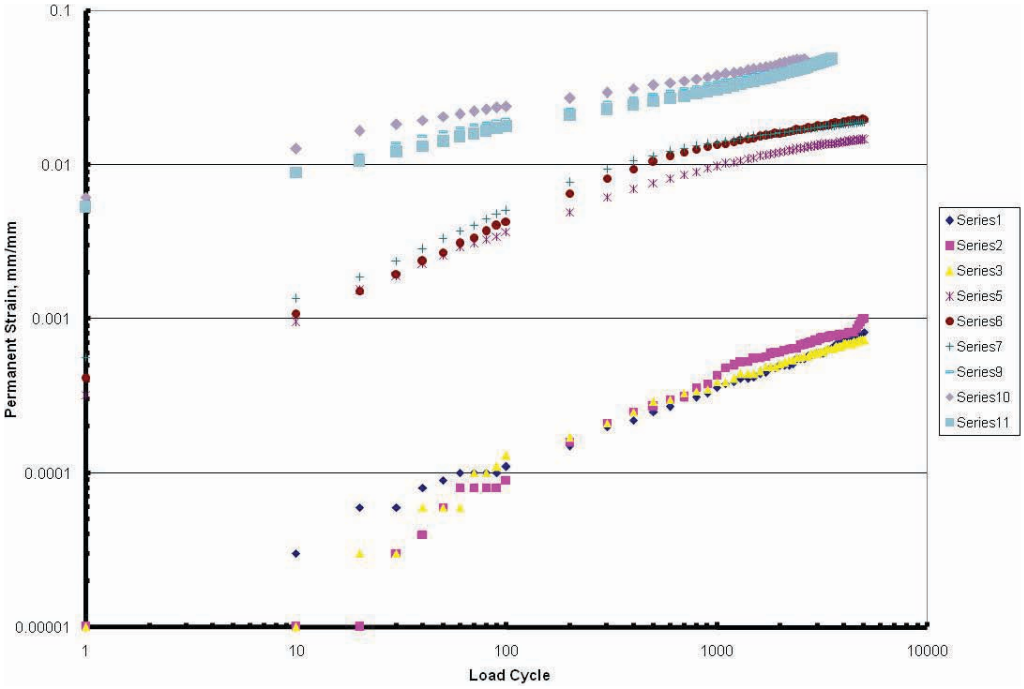

Wisconsin; HMA ATB Mixture

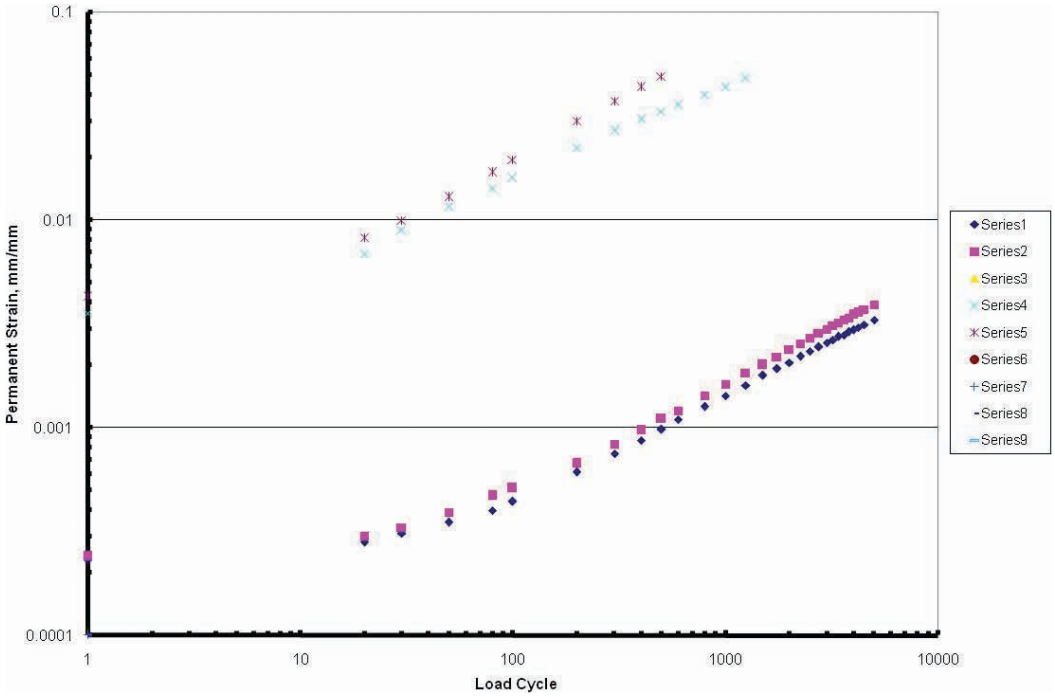

Wisconsin; HMA Binder Mixture

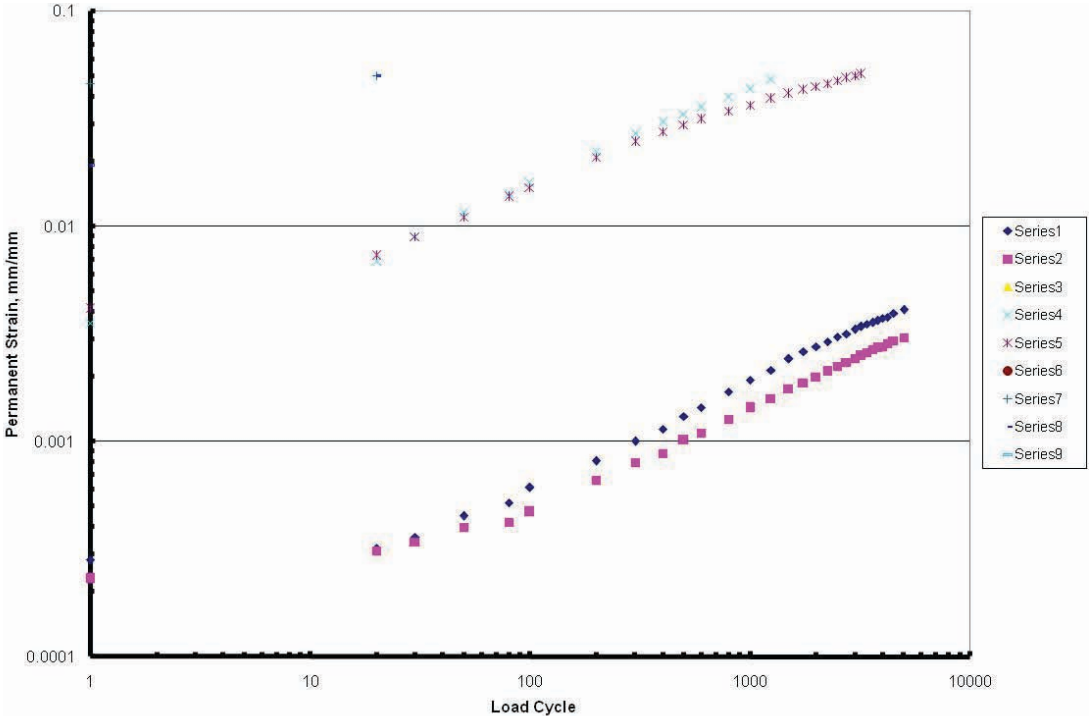

Wisconsin; HMA Surface Mixture

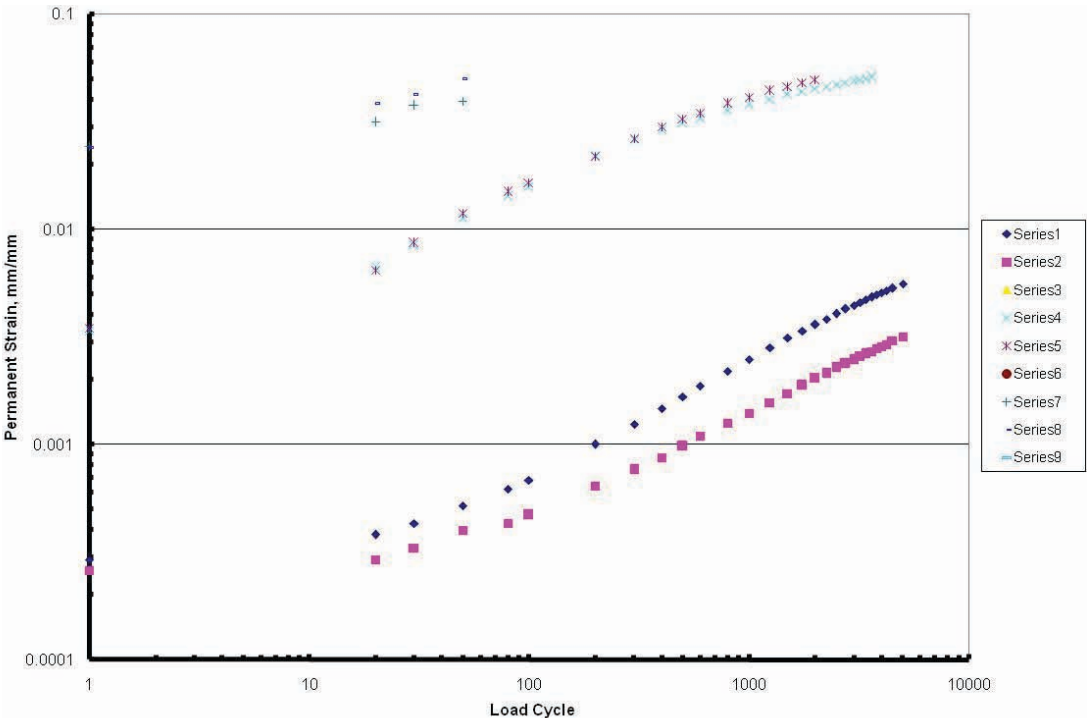

Wisconsin; ATB Mixture – Cores

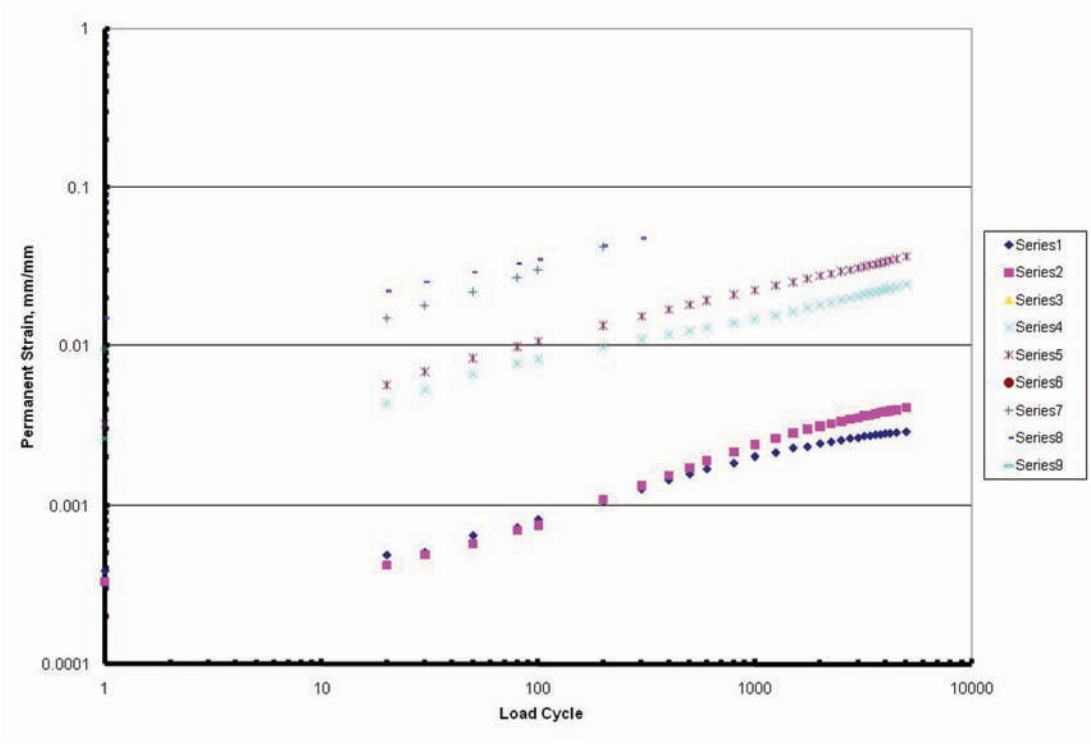

Wisconsin; HMA Binder Mixture – Cores

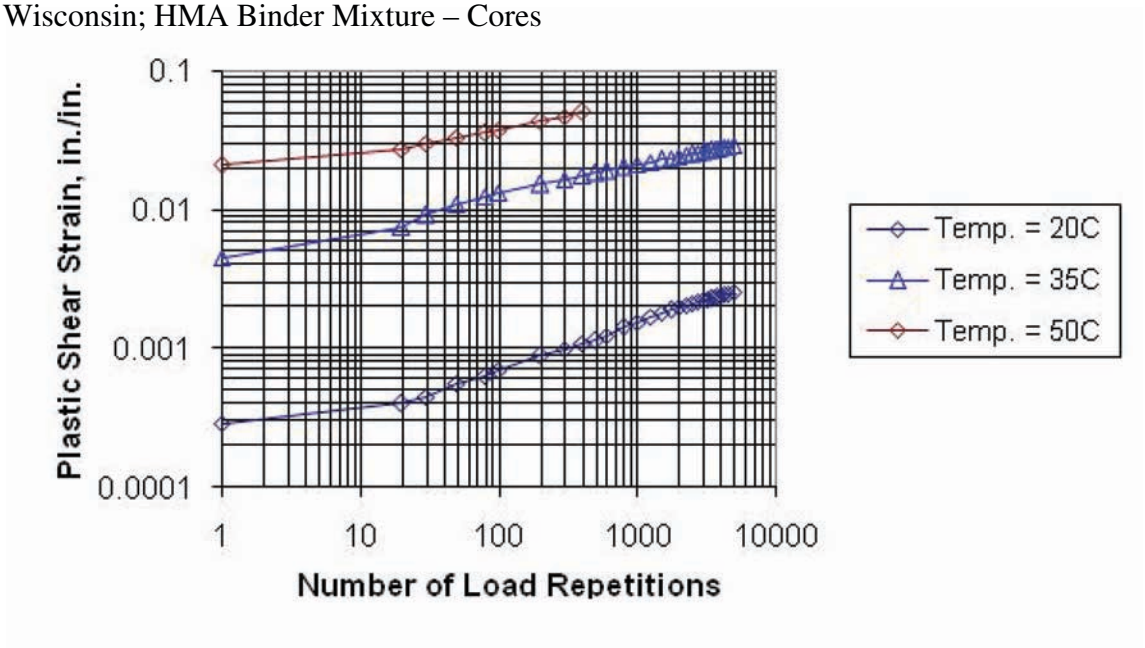

Wisconsin; HMA Surface Mixture – Cores

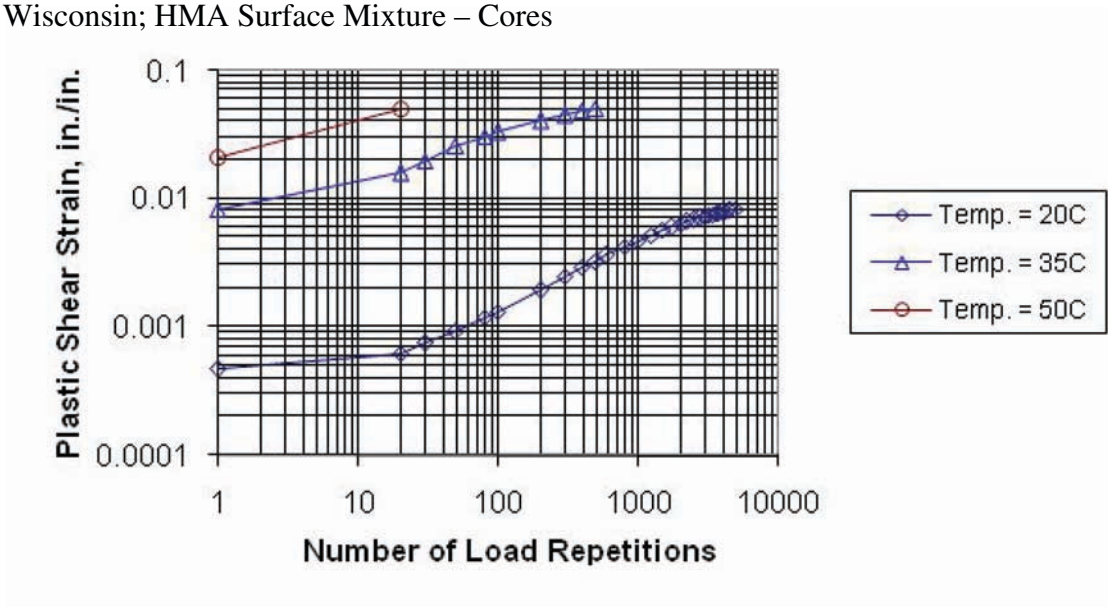

APPENDIX F

Incremental Benefit–Cost Analysis: Comparison of Alternate Transfer Functions and Test Methods

F.1 Introduction

This appendix discusses the approach used to assess the accuracy and material testing requirements for the different transfer functions. The approach for assessing the effectiveness of the different rut-depth prediction models took two forms.

1. The first was to compare the error terms and bias between the predicted and measured rut depths. The error term is important to the methodology used within the MEPDG software for designing various pavement structures and mixtures at different reliability or confidence levels. The higher the error term, the greater the predicted rutting for the higher confidence or reliability level selected by the designer.

   The transfer function with the smaller error term will define the suggested improvements to the MEPDG and rut-depth prediction methodology currently embedded in the software. It is expected, however, that there may not be a statistical or significant difference between the error terms of alternate transfer functions and test methods in support of those transfer functions. In addition, the alternate transfer function with the lower standard error may have the higher materials characterization (testing) costs. Thus, a second approach will be used for selecting the transfer function and supporting test methods for improving the MEPDG rut-depth prediction methodology included in the software.
2. The second method uses an incremental benefit–cost ratio approach for determining which of the alternate transfer functions will have the greatest effectiveness. The testing program needed for the HMA materials characterization and the total error term resulting from the MEPDG runs without any changes (using the global calibration values determined from NCHRP Project 1-37A) represent the baseline condition. The increased costs within the benefit–cost ratio concept will be the increased costs from the testing program to establish the input values and/or calibration values. The benefit will be a reduction in error term, defined as an increase in pavement life or reduced life-cycle costs considering the more accurate estimates of rutting using the same design life. A similar process was used on an FHWA-sponsored project to determine the effectiveness of different testing programs and to optimize the number of tests based on performance criteria (Von Quintus et al., 1985).

   The alternative with the greatest benefit–cost ratio would be the one recommended as an improvement to the MEPDG rut-depth prediction model. The incremental benefit–cost ratio may be dependent on the failure condition or the maximum permissible rut depth within the HMA layers. Thus, three levels of rutting criteria will be used within the HMA layers (0.25 in., 0.50 in., and 0.75 in.) to determine whether the benefit–cost ratios are failure-level–dependent.

This appendix documents the incremental benefit–cost analysis method and steps used in comparing the different transfer functions and test methods. It also provides the background, reasoning, and assumptions used for the incremental benefit–cost analysis. The examples included use material properties and predicted rut depths from the different transfer functions and testing methods.

F.2 Benefit–Cost Analysis: Procedure for Determining Cost Effectiveness

The basis for determining cost effectiveness of different rut-depth transfer functions and material testing methods is an incremental benefit–cost analysis. This is a widely accepted method of comparing multiple alternatives while ensuring that a change from the existing (i.e., do nothing) situation is warranted. The do-nothing alternate represents the baseline condition or use of MEPDG Level 3 inputs for

predicting rut depths. Each alternative, including the baseline or do-nothing condition, has certain costs with which it is associated; the following are some of the more common ones that have been used:

- Design and testing,
- Construction,
- Maintenance,
- User, and
- Rehabilitation.

For each alternative, construction, maintenance, user, and rehabilitation costs are combined into an equivalent uniform annual cost or present worth cost over the life of the pavement. Similarly, design and testing costs are converted to equivalent uniform annual or present worth costs. Alternatives are then arranged in order of increasing testing costs from the baseline condition. A challenger/defender approach is used to directly compare alternatives in terms of benefit–cost ratios. If the B-C ratio is greater than 1, the challenger becomes the defender to the next challenging alternative. Conversely, if its B-C ratio is less than 1, the defender remains a defender to the next challenger. This procedure continues until all alternatives have been examined, as shown in Figure F.1.

The components required for this approach include (1) the initial cost of construction, (2) cost for various materials test programs, (3) the accuracy of the distress prediction transfer function and model, (4) the sensitivity of distress (rut depth for this example) to the material properties derived from the test program, (5) the rehabilitation or maintenance strategies that may result from various distress levels, and (6) the costs for rehabilitation or maintenance strategies once the design criteria are exceeded.

User costs should also be considered because under certain circumstances these costs tend to dominate the analysis. These user costs fall into two categories. First are the user costs associated with major rehabilitation activities. These costs include the extra time expended by the traveling public while traversing an area of pavement undergoing major rehabilitation. Second are the user costs (time, gas, oil, tires, etc.) associated with minor rehabilitation activities as well as simply traversing rough roads. These costs occur on a day-to-day basis.

Incremental cost is the added cost or cost difference between the different testing programs between defender and challenger in support of the rut-depth transfer function, while incremental benefit is the reduction between defender and challenger in uniform annual costs to build, maintain, and rehabilitate the road. A cash flow diagram for two different

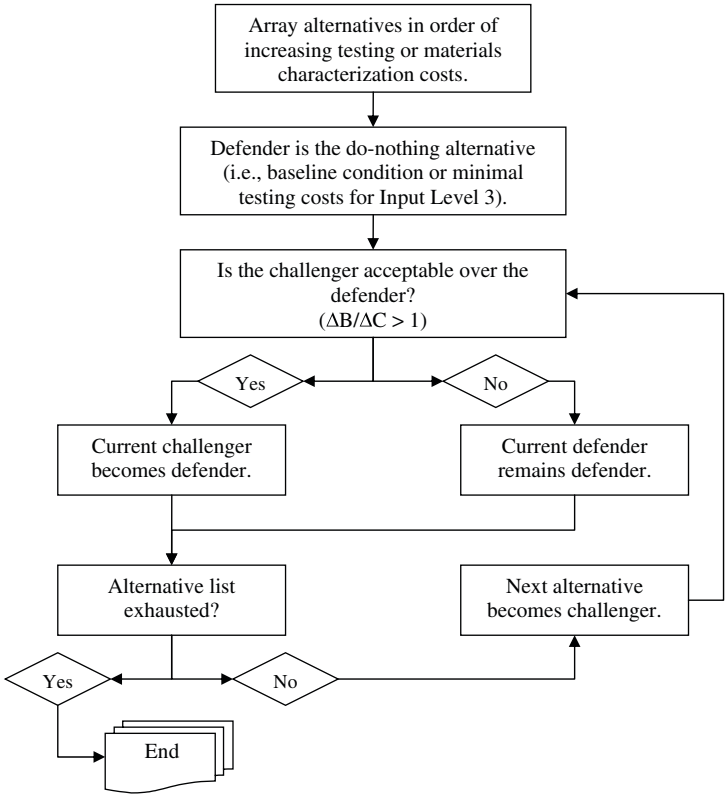

Figure F.1. Flow diagram of the challenger/defender procedure for analysis of multiple alternatives.

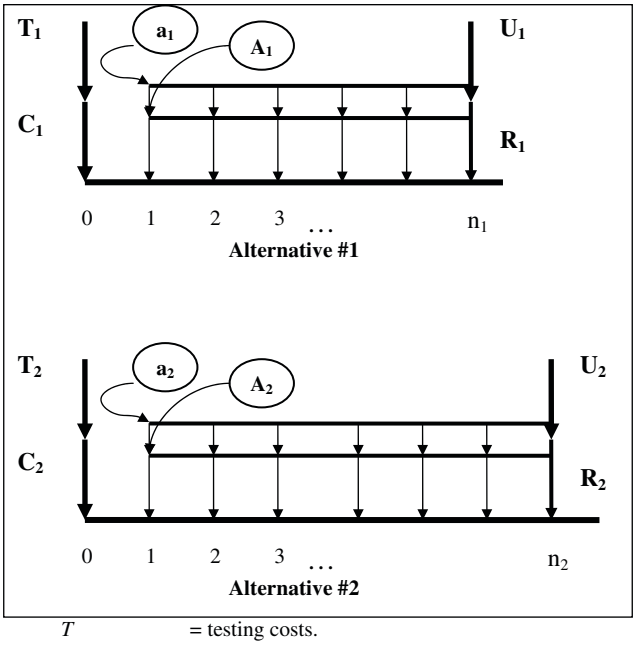

T	= testing costs.
C	= construction costs.
U	= user costs associated with rehabilitation.
R	= rehabilitation costs.
A	= annual user costs.
a	= annual maintenance costs.

Figure F.2. Benefit–cost analysis for two alternatives resulting from different test methods or material properties in support of different transfer functions.

alternatives is illustrated in Figure F.2. The incremental benefit–cost ratio between these two strategies is simply defined by Equation F.1.

$$\Delta B/\Delta C = \frac{A_{s1} - A_{s2}}{A_{t2} - A_{t2}} \tag{F.1}$$

where

$A_{s1,s2}$ = total annual costs of alternatives 1 and 2 (excluding the testing costs).

$A_{t1,t2}$ = annual cost of testing for alternatives 1 and 2.

$$A_{s1} = C_1\left(\frac{A}{P}, i, n_1\right) + a_1 + A_1 + (U_1 + R_1)\left(\frac{A}{F}, i, n_1\right) \tag{F.2}$$

$$A_{t1} = T_1\left(\frac{A}{P}, i, n_1\right) \tag{F.3}$$

A = equivalent uniform cost.
P = actual present worth cost.
i = interest rate.
n = number of compounding periods.

As noted previously, an incremental benefit–cost ratio greater than 1 means that more benefit is received from the increased cost. If this is the case, the challenger becomes the defender to the next alternative. Otherwise, the original defender remains the defender to the next challenger (refer to Figure F.1).

F.3 Cost Evaluation

In judging the attractiveness of alternative testing programs and transfer functions, it is necessary to recognize the time value of money. Because capital may be loaned at interest, the value of money is greater at present than the same unit at a later date. Two methods are considered for evaluating, on an economic basis, multiple alternatives: present worth and equivalent uniform annual costs.

Using the concept of equivalence and by taking into account the interest rate and number of compounding periods, it can be stated that any future payment or series of payments can be represented by a single, equivalent present worth. Conversely, an actual present worth or a future payment can be represented by an equivalent uniform annual cost. Figures F.3 and F.4 illustrate the concepts of present worth and equivalent uniform annual cost using standard cash flow diagrams, respectively. The factors in parenthesis (e.g., P/A, i, n) are compound interest factors that are tabulated in most engineering economy textbooks.

F.3.1 Present Worth Analysis

Present worth analysis is a widely accepted method because future expenditures or receipts are transformed into present equivalent dollars. In comparing two or more alternatives, future payments or series of payments for each case are converted to present values. The alternative that has the lowest present value is considered (at least from an economic standpoint) the most attractive.

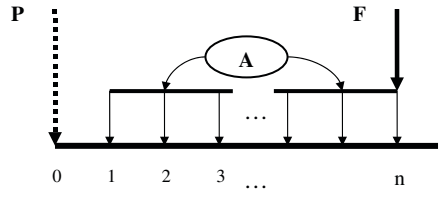

$$P = A\left(\frac{P}{A}, i, n\right) + F\left(\frac{P}{F}, i, n\right) \tag{F.4}$$

where

P	= equivalent present worth.
A	= actual series of payments.
F	= actual future payment.
n	= number of compounding periods.
i	= interest rate per period.
$\left(\frac{P}{A}, i, n\right)$	= uniform series, present worth factor.
$\left(\frac{P}{F}, i, n\right)$	= single payment, present worth factor.

Figure F.3. Equivalent present worth of actual future series of payments.

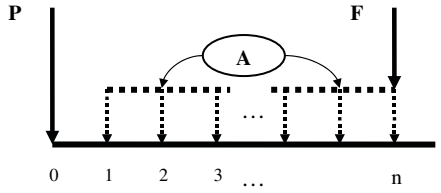

$$A = P\left(\frac{A}{P},i,n\right) + F\left(\frac{A}{F},i,n\right) \quad \text{(F.5)}$$

where

A	= equivalent uniform cost.
P	= actual present worth.
F	= actual future payment.
n	= number of compounding periods.
i	= interest rate.
$\left(\frac{A}{P},i,n\right)$	= uniform series capital recovery factor.
$\left(\frac{A}{F},i,n\right)$	= uniform series sinking fund factor.

Figure F.4. Actual present worth represented by equivalent uniform annual cost.

In this approach the most important assumption is that the alternatives are equal in all respects except costs. In most cases, however, alternatives under consideration have different potential service lives. Techniques have been devised to overcome this difficulty. The most common method is to assume that an alternative can be considered a sequence of identical alternatives. In other words, each alternative will be replaced with an identical successor at the end of its service life, and this process will continue until all alternatives reach the end of their service lives at the same time.

F.3.2 Equivalent Annual Cost Analysis

In this method of comparing multiple alternatives, all present and future values are converted to equivalent uniform annual costs (simply termed *annual cost*). In comparing multiple alternatives, that which has the lowest annual cost is the most attractive. For this method for the annual cost comparison, no assumption is made concerning equal service lives. That is, alternatives may be directly compared with no sequential repetition of alternatives.

F.3.3 Differences Between Methods

The obvious difference between the two methods is that the present worth analysis requires equal service lives of alternatives for direct comparison, with unequal service lives requiring special treatment. The special treatment requires sequential repetition of alternatives until all alternatives reach the end of their service life at the same time. It should be noted that from a mathematical standpoint, both methods are exact and always predict the same alternative as most attractive. In fact, if the sequential alternative repetition technique is used, the computed present values can be converted into annual costs that are numerically equal to those obtained from a conventional annual cost comparison.

In general, the present worth of an alternative that requires an investment *I,* service life *n,* and interest rate *i,* with *k* equal to the number of sequences, can be expressed in terms of the single payment present worth factor.

$$\text{Present worth} = I\left[1 + \frac{1}{(1+i)^n} + \frac{1}{(1+i)^{2n}} + \cdots + \frac{1}{(1+i)^{(k-1)n}}\right]$$

$$= I\frac{\left(1-(1+i)^{kn}\right)(1+i)^n}{\left(1-(1+i)^n\right)(1+i)^{kn}} \quad \text{(F.6)}$$

This expression is the sum of *k* terms in a geometric series. To convert this present worth to an equivalent annual cost, multiply by the uniform series capital recovery factor expressed in terms of *k.*

$$\text{Annual cost} = I\frac{i(1+i)^n}{(1+i)^n - 1} \quad \text{(F.7)}$$

This expression is simply the equivalent annual cost of the alternative, which could have been computed directly by using an annual cost analysis. Thus, the equivalent annual cost will be used as a basis for computing benefits and costs. This circumvents the difficulties encountered when using a present value analysis to compare alternatives with different lives.

In summary, all costs and benefits are converted to equivalent uniform annual costs. For multiple (i.e., three or more) alternatives, the incremental benefit–cost analysis should be performed using a challenger/defender approach (refer to Figure F.1).

F.4 Assumptions

The following lists the assumptions that were used in the incremental benefit–cost analysis of the different alternatives considering different transfer functions and test methods in support of those transfer functions.

- Calibration of the rut-depth transfer functions eliminates all model bias. Thus, at a 50% reliability level the rut depth predictions are the same between all of the transfer functions or test methods for the same set of calibration data. This condition assumes that the different transfer functions used the same set of data so that the overall standard error was determined for the same critical rut depth between all transfer functions and test methods. The median rut depth used in the global calibration from NCHRP Project 1-40D was approximately 0.35 in., and few rut depths exceeded 0.50 in.

Table F.1

Critical Rut Depth, in.	Median Age, years	
	New Construction	HMA Overlays
0.25	16	12
0.50	22	21
0.75	27	>30

- Most new and rehabilitation pavement designs are based on a 20-year design period. Survivability analyses have been completed over the years to estimate the expected service life prior to exceeding a critical distress value for life-cycle cost analyses. A couple of these studies were completed using LTPP data, and many of these test sections were included in the global calibration process of the MEPDG. As such, these survivability analyses were used to estimate the median age at which the critical rut depth was exceeded. These ages are listed in Table F.1.

  For simplicity, the median ages exceeding the critical rut depths for new construction were used in the example. It may be more appropriate to keep the median age constant at the point at which the critical rut depth would be exceeded at a 50% reliability level and then determine the time or age at which the critical rut depth is exceeded for the different reliability levels.
- One type of HMA mixture is used for each example. Open-graded and other specialty mixtures were excluded from the examples.
- All laboratories have basic equipment needed to prepare HMA mixture designs using volumetric principles. Overall laboratory overhead costs are the same between the different strategies and are assumed to be $100,000 per year. The cost to complete a standard HMA mixture design based on volumetric principles is assumed to be $25,000 per mixture and includes all of the ancillary activities (transportation and shipping, material sampling, mixing, compaction, testing, etc.).
- The initial costs of the specific laboratory test equipment to measure the permanent deformation properties of the HMA are different but are depreciated over the same time period. The initial cost for the test equipment needed in support of the transfer function is provided in Table F.2. These costs have also been reported or estimated for testing individual specimens and are also included in Table F.2. It was assumed that at least one specialized laboratory technician would be required to operate the more sophisticated test equipment. An additional laboratory supervisor would not be needed, but some of that person's time would be needed in terms of overhead costs. The following lists and defines the costs that should be included in the cost estimates for testing.
  - **Direct labor costs:** Technicians' and supervisors' salaries. As noted, one additional laboratory technician was assumed to operate the more sophisticated equipment.
  - **Testing equipment costs:** Nonexpendable equipment depreciation. Annual depreciation cost of testing equipment is a measure of the annual consumption of value throughout the equipment's useful life. Expendable supplies were included within the annual maintenance category of the equipment.
  - **Travel costs and vehicle costs:** Vehicle and equipment rental, subsistence, mileage, and maintenance costs. Transportation costs are generally considered minimal and omitted from cost computations. Shipment of materials would also be included in this category, which was combined with the annual maintenance costs of the equipment.
  - **Administrative overhead and engineering costs:** These are indirect labor costs and include holidays, vacation, sick leave, and other benefits.

Table F.2. Summary of test equipment costs included in the incremental benefit–cost analysis.

Test Method	Initial Test Equipment Costs	Additional Costs for Sample Preparation	Maintenance Cost of Equipment	Additional Overhead Costs in Support of Test Equipment	Cost for Sample Prep and Testing; One Set of Specimens
Baseline condition; Level 3 inputs	0	0	0	0	0
Loaded wheel tester	50,000	7,500	7,000	10,000	2,500
Simple performance test for dynamic modulus	40,000	3,000	7,000	10,000	2,000
Repeated-load permanent deformation, confined	40,000	6,000	7,000	10,000	3,000
Repeated shear, constant height	65,000	3,000	7,000	10,000	2,500

Note: All costs in dollars.

Table F.3. Number of test specimens needed to support the transfer function.

Test Method	Number of Test Specimens	Number of Compacted Samples
Baseline condition	0	0
Loaded wheel tester	3	3
Simple performance tester for dynamic modulus	2 cored from gyratory-compacted samples	2 gyratory samples
Repeated-load permanent deformation tests, confined	6 cored from gyratory-compacted samples	6 gyratory samples
Repeated shear, constant height tests	6 cored from rolling wheel compacted sample	1 rolling wheel compacted sample

Note: All test methods include HMA mixture design equipment based on volumetric principles.

- Table F.3 lists the number of test specimens and samples that were used in estimating the laboratory testing costs and sample preparation costs for one set of test specimens summarized in Table F.2.
- All costs are computed on the basis of a project being one lane and a mile in length.
- The initial construction costs between the different alternatives is the same because the same set of calibration data is used between all transfer functions and test methods in support of those transfer functions; assumed to be \$250,000 per lane mile ($C_1 = C_2$; refer to Figure F.2).
- It is assumed that the pavement has been designed such that the failure condition is rutting rather than any other distress for all conditions. The rehabilitation strategy is to remove and replace the HMA wearing surface because of rutting. Thus, the rehabilitation cost is the same between the different strategies but occur at different times; assumed to be \$75,000 per lane mile ($R_1 = R_2$; refer to Figure F.2).
- The annual user and maintenance costs are assumed to be the same for all alternatives because the failure mode is assumed to be the same. In addition, the user delay cost associated with the pavement rehabilitation strategy is assumed to be the same because the rehabilitation strategy is the same. The only difference is the time of the rehabilitation. The annual user and maintenance costs and user delay costs are assumed to be \$100,000 per lane mile ($A_1 = A_2$, $a_1 = a_2$, and $U_1 = U_2$; refer to Figure F.2).
- The standard error between the prediction models is different. The specific values used in the examples are provided in the next section.

F.5 Standard Error: Test Method and Transfer Function Dependent

Table F.4 lists the standard errors that were derived from limited testing for selected projects to demonstrate the incremental benefit–cost analysis procedure. The standard deviation of the residual error for the rut depth predictions was determined from the calibration process completed in NCHRP Projects 1-37A and 1-40D using mostly LTPP test sections. Equation F.8 is the relationship included in the MEPDG software for the rut-depth transfer function.

$$s_e = 0.24\left(RD^{0.8026} + 0.001\right) \quad \text{(F.8)}$$

where

RD = predicted average rut depth, in.

This same type of relationship was also used for the other transfer functions, as summarized in Table F.4. The prediction model error is often termed the *standard error estimate* (s_e) and can be used to establish confidence intervals for the prediction model. This error explains the scatter of the data about the 1:1 line between the predicted and observed distress quantities and is composed of four components. The components of error associated with *se* are listed in Table F.5 and can be mathematically expressed as follows, assuming that no correlation exists between the contributing errors to the overall error.

$$s_e^2 = e_m^2 + e_i^2 + e_l^2 + e_r^2 \quad \text{(F.9)}$$

where

s_e = total error of prediction (the standard error estimate associated with the actual versus predicted performance quantity, sometimes referred to as the calibration error).

e_i = error caused by using laboratory or field measurements to estimate the model inputs needed to compute the performance indicator using some functional form and material properties.

e_m = error caused by inaccuracies in measuring the distress along the test section used in the calibration process.

Table F.4. Standard error relationships from limited testing and projects.

Transfer Function	Test Method[1]	Standard Error Relationship	Standard Error at Critical Rut Depth, in.		
			0.25	0.50	0.75
MEPDG	Input Level 3[2]	$0.24\left(RD^{0.8026}+0.001\right)$	0.079	0.138	0.191
MEPDG	Input Level 1[3]	$0.24\left(RD^{0.8026}+0.001\right)$	0.079	0.138	0.191
MEPDG	Mix adjust.[4]	$0.20\left(RD^{0.75}+0.001\right)$	0.071	0.119	0.161
MEPDG	Loaded wheel[5]	$0.16\left(RD^{0.50}+0.001\right)$	0.080	0.113	0.138
Kaloush, strain	RLPD, plastic strain	$0.17\left(RD^{0.65}+0.001\right)$	0.069	0.109	0.141
Leahy, stress	RLPD, plastic strain	$0.17\left(RD^{0.70}+0.0001\right)$	0.065	0.105	0.139
WesTrack, shear	RSCH, plastic strain	$0.12\left(RD^{0.40}+0.001\right)$	0.069	0.091	0.107

RLPD = Repeated-load plastic deformation tests.
RSCH = Repeated shear constant height tests.

1. All of the different conditions considered within these examples assume that only one set of permanent deformation constants is used for all mixtures within a flexible pavement or HMA overlay (i.e., layer independent, as currently assumed in Version 1.0 of the MEPDG).
2. This condition represents the baseline condition where only Level 3 inputs are used, similar to the global calibration process.
3. This condition represents the baseline condition, with the exception that the simple performance test is used to measure the dynamic modulus of the HMA mixtures.
4. This condition represents the baseline condition, with the exception that the NCHRP Project 1-40B mixture adjustment factors are used to determine the coefficients and exponents of the MEPDG rut-depth transfer function. Layer-dependent coefficients and exponents were used.
5. This condition represents the use of a loaded wheel tester or torture test to estimate the coefficients and exponents of the MEPDG rut-depth transfer function.

e_r = error due to replication, referred to as pure error.
e_l = error caused by inappropriate assumptions or an incorrect model form, referred to as lack-of-fit or model error.

The quantification of the sources of variability is important when refining the calibration–validation process to reduce the overall error. As an example, decreasing the input error of pavement material properties will have little effect on reducing the total error or uncertainty of the predictions for the condition if the majority of the total error is caused by measurement error of the distress observations. It has been reported that the majority of the standard error is measurement error, which could explain the smaller difference in the standard error than expected between the different transfer functions.

F.6 Comparison of Alternates

The incremental benefit–cost analysis used in the example follows the process summarized in Figure F.1. The benefit is defined as the reduction in pavement costs over the service life of the pavement, while the cost is defined as the increase in testing costs over the service life of the pavement. The detailed data and information used in the incremental benefit–cost analysis is summarized in the exhibits included at the end of this appendix. Exhibit F.1 provides a summary of the benefit/cost (B/C) ratios for different rut depth threshold

Table F.5. Summary of calibration error dependency (Von Quintus et al., 2004).

Components of Calibration Error	Error Is:		
	Distress Dependent	Input Level Dependent	Prediction Equation Dependent
Measurement error	Yes	No	No
Input error	No	Yes	Yes (see note)
Model error	No	No	Yes
Pure error	Yes	Yes	Yes

Note: The prediction equation was listed as being independent of input error in the body of the report because the assumption was that the prediction methodology would not be changed (i.e., one set of permanent deformation constants was applicable to all HMA mixtures). If different inputs are used for each HMA layer, then the calibration error of the prediction equation becomes dependent on the input error.

Shaded cells show where the components of the calibration factor were independent of the error parameter.

values and reliability levels. The following summarizes the results from these comparisons.

1. Use of the mixture adjustment factors from NCHRP Project 1-40B (regression equations used to estimate the plastic deformation constants for the MEPDG rut-depth transfer function) was found to have a benefit–cost ratio significantly greater than 1.0 in comparison to the do-nothing alternate or baseline condition (MEPDG Input Level 3 in Table F.4).
2. All of the laboratory test methods were found to have a benefit–cost ratio greater than 1.0, in comparison to use of the mixture adjustment factors, for the lower rut-depth trigger value and higher reliability level. One reason for this finding is the measurement error. As reported in NCHRP Project 9-30, the measurement error will be a significant factor in determining the cost effectiveness of the different test methods in support of the alternate transfer functions.
3. The median service life used in the example was dependent on the critical rut depths and determined from the survivability analyses completed in other projects using the LTPP database (refer to Section F.4). An additional incremental benefit–cost ratio evaluation was completed using the overall median service life for HMA overlays. Using a constant median service life (based on a 50% reliability level) will increase the benefit (reduced equivalent annual cost from the longer service lives), while little effect will be incurred on the incremental testing cost.

F.7 Detailed Data and Information Summary for Alternate Comparisons

This part of Appendix F includes the detailed data and information used in the preliminary incremental benefit–cost analysis for comparing the different alternates. Figure F.5 illustrates the typical rut depth versus age relationship that was used to estimate the number of compound periods or age at which the critical rut depth will be exceeded. A relationship similar to Figure F.5 was prepared for each alternate.

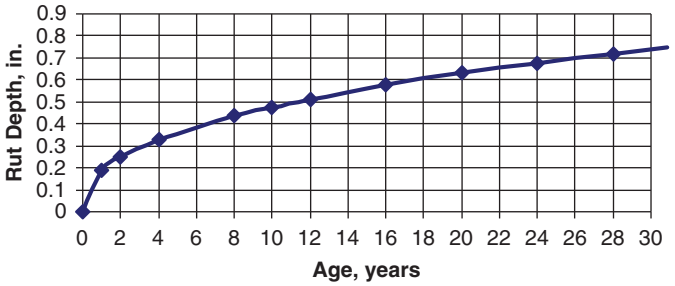

Figure F.5. Typical increase in rut depth with age to estimate the effect of larger standard errors on reduced service life for rutting.

- Exhibit F.1: A summary of the benefit–cost ratios for different threshold values and reliability levels.
- Exhibit F.2: A summary of the cost analysis spreadsheet for the pavement and testing costs for a threshold rut depth of 0.25 in. and different reliability levels (75%, 85%, and 95%).
- Exhibit F.3: A summary of the cost analysis spreadsheet for the pavement and testing costs for a threshold rut depth of 0.50 in. and different reliability levels (75%, 85%, and 95%).
- Exhibit F.4: A summary of the cost analysis spreadsheet for the pavement and testing costs for a threshold rut depth of 0.75 in. and different reliability levels (75%, 85%, and 95%).

Exhibit F.1.

Cost Element	Test Method in Support of the Transfer Function					
	Baseline	Mix Adjust.	Loaded Wheel	SPT	RLPD	RSCH
Critical Rut Depth=0.25 and Reliability=75 percent						
Total Equivalent Annual Pavement Costs	180589	131281	129249	115678	109895	92694
Total Equivalent Annual Testing Costs	39937	38865	57606	54223	54824	55468
Benefit		49308	2032	15603	21386	38587
Costs		1072	18741	15358	15959	16603
B/C Ratio		46.0	0.1	1.0	1.3	2.3
Critical Rut Depth=0.25 and Reliability=85 percent						
Total Equivalent Annual Pavement Costs	515806	311842	291194	243810	211077	148430
Total Equivalent Annual Testing Costs	47224	42790	70843	62190	61994	60533
Benefit		203964	20648	68032	100765	163412
Costs		4434	28053	19400	19204	17743
B/C Ratio		46.0	0.7	3.5	5.2	9.2
Critical Rut Depth=0.25 and Reliability=95 percent						
Total Equivalent Annual Pavement Costs	2060310	1207000	1010627	870375	774516	421790
Total Equivalent Annual Testing Costs	80800	62250	129649	101146	101925	85373
Benefit		853310.0	196373.0	336625.0	432484.0	785210.0
Cost		18550.0	67399.0	38896.0	39675.0	23123.0
B/C Ratio		46.0	2.9	8.7	10.9	34.0
Critical Rut Depth=0.50 and Reliability=75 percent						
Total Equivalent Annual Pavement Costs	177430	115678	112889	110294	107501	94901
Total Equivalent Annual Testing Costs	39868	38526	56268	53888	54654	55669
Benefit		61752.0	2789.0	5384.0	8177.0	20777.0
Cost		1342.0	17742.0	15362.0	16128.0	17143.0
B/C Ratio		46.0	0.2	0.4	0.5	1.2
Critical Rut Depth=0.50 and Reliability=85 percent						
Total Equivalent Annual Pavement Costs	432534	200171	191394	181161	173024	134104
Total Equivalent Annual Testing Costs	45414	40362	62685	58295	59298	59231
Benefit		232363.0	8777.0	19010.0	27147.0	66067.0
Cost		5052.0	22323.0	17933.0	18936.0	18869.0
B/C Ratio		46.0	0.4	1.5	1.4	3.5
Critical Rut Depth=0.50 and Reliability=95 percent						
Total Equivalent Annual Pavement Costs	1448343	571852	564453	541186	485642	295915
Total Equivalent Annual Testing Costs	67497	48442	93179	80679	81453	73935
Benefit		876491	7399	30666	86210	275937
Cost		19055	44737	32237	33011	25493
B/C Ratio		46.0	0.2	1.0	2.6	10.8
Critical Rut Depth=0.75 and Reliability=75 percent						
Total Equivalent Annual Pavement Costs	111156	84757	83777	81949	80152	75358
Total Equivalent Annual Testing Costs	38427	37853	53889	52126	52716	53893
Benefit		26399	980	2808	4605	9399
Cost		574	16036	14273	14863	16040
B/C Ratio		46.0	0.1	0.3	0.3	0.6
Critical Rut Depth=0.75 and Reliability=85 percent						
Total Equivalent Annual Pavement Costs	220698	117151	112889	107873	102492	89816
Total Equivalent Annual Testing Costs	40809	38558	56268	53738	54370	55207
Benefit		103547	4262	9278	14659	27335
Cost		2251	17710	15180	15812	16649
B/C Ratio		46.0	0.2	0.6	0.9	1.6
Critical Rut Depth=0.75 and Reliability=95 percent						
Total Equivalent Annual Pavement Costs	774516	265121	243810	226070	204420	142103
Total Equivalent Annual Testing Costs	52848	41774	66970	61087	61523	59958
Benefit		509395	21311	39051	60701	123018
Cost		11074	25196	19313	19749	18184
B/C Ratio		46.0	0.8	2.0	3.1	6.8

Exhibit F.2.

Summary of Pavement Costs

Critical Rut Depth	0.25	Median Pavement Service Life	16
Reliability Level	75		

Cost Element	Test Method in Support of the Transfer Function					
	Baseline	Mix Adjust.	Loaded Wheel	SPT	RLPD	RSCH
Interest Rate	0.05	0.05	0.05	0.05	0.05	0.05
Number of Compound Periods	7.83	11.75	12	14	15.08	19.67
Capitol Recovery Factors	0.0733	0.0887	0.0898	0.0990	0.1044	0.1305
	0.4653	0.7741	0.7959	0.9799	1.0871	1.6109
Compound Interest Factors; Capital Recovery	0.1575	0.1146	0.1128	0.1010	0.0960	0.0810
Sinking Fund Compound Interest Factors	0.1075	0.0646	0.0628	0.0510	0.0460	0.0310
Construction Costs	1,000,000	1,000,000	1,000,000	1,000,000	1,000,000	1,000,000
Equivalent Annual Constr. Costs; Capital Recovery	157469	114592	112825	101024	95996	81038
Annual Maintenance Costs	2000	2000	2000	2000	2000	2000
Annual User Costs	5000	5000	5000	5000	5000	5000
Total Annual Costs	7000	7000	7000	7000	7000	7000
Rehabilitation Costs	125,000	125,000	125,000	125,000	125,000	125,000
User Delay Costs	25000	25000	25000	25000	25000	25000
Total Rehabilitation Costs	150000	150000	150000	150000	150000	150000
Equivalent Annual Rehab Costs; Sinking Fund	16120	9689	9424	7654	6899	4656
Total Equivalent Annual Pavement Costs	180589	131281	129249	115678	109895	92694

Summary of Testing Costs

Critical Rut Depth, in.	0.25	Median Pavement Service Life	10
Reliability Level, %	75		

Cost Element	Test Method in Support of the Transfer Function					
	Baseline	Mix Adjust.	Loaded Wheel	SPT	RLPD	RSCH
Interest Rate	0.05	0.05	0.05	0.05	0.05	0.05
Number of Compound Periods	7.83	11.75	12	14	15.08	19.67
Capital Recovery Factors	0.0733	0.0887	0.0898	0.0990	0.1044	0.1305
	0.4653	0.7741	0.7959	0.9799	1.0871	1.6109
Compound Interest Factors; Capital Recovery	0.1575	0.1146	0.1128	0.1010	0.0960	0.0810
Mixture Design Costs	25000	25000	25000	25000	25000	25000
Initial Test Equipment Costs	0	0	50000	40000	40000	65000
Initial Compaction Equipment Costs	0	0	2500	0	0	2500
Initial Specimen Equipment Prep Costs	0	0	3000	1500	1500	3000
Total Initial Equipment & Mix Design Costs	25000	25000	80500	66500	66500	95500
Annual Initial Equipment & Mix Design Costs	3937	2865	9082	6718	6384	7739
Unit Sample Prep Costs	0	0	2500	1500	1500	3000
Number of Compacted Samples	0	0	3	2	6	1
Total Sample Prep Costs	0	0	7500	3000	9000	3000
Unit Specimen Test Costs	0	0	2000	1000	1000	1000
Number of Test Specimens	0	0	3	2	6	6
Total Specimen Testing Costs	0	0	6000	2000	6000	6000
Total Specimen Prep & Testing Costs	0	0	13500	5000	15000	9000
Annual Specimen Prep & Testing Costs	0	0	1523	505	1440	729
Annual Equipment Maintenance Costs	6000	6000	7000	7000	7000	7000
Annual Equipment Overhead Costs	30000	30000	40000	40000	40000	40000
Total Equivalent Annual Testing Costs	39937	38865	57606	54223	54824	55468

(continued on next page)

Exhibit F.2. (Continued).

Summary of Pavement Costs

Critical Rut Depth: 0.25
Reliability Level: 85
Median Pavement Service Life: 16

Cost Element	Test Method in Support of the Transfer Function					
	Baseline	Mix Adjust.	Loaded Wheel	SPT	RLPD	RSCH
Interest Rate	0.05	0.05	0.05	0.05	0.05	0.05
Number of Compound Periods	2.42	4.17	4.5	5.5	6.5	10
Capitol Recovery Factors	0.0563	0.0613	0.0623	0.0654	0.0687	0.0814
	0.1253	0.2256	0.2455	0.3078	0.3732	0.6289
Compound Interest Factors; Capital Recovery	0.4490	0.2716	0.2536	0.2124	0.1840	0.1295
Sinking Fund Compound Interest Factors	0.3990	0.2216	0.2036	0.1624	0.1340	0.0795
Construction Costs	1,000,000	1,000,000	1,000,000	1,000,000	1,000,000	1,000,000
Equivalent Annual Constr. Costs; Capital Recovery	448962	271602	253647	212443	183980	129505
Annual Maintenance Costs	2000	2000	2000	2000	2000	2000
Annual User Costs	5000	5000	5000	5000	5000	5000
Total Annual Costs	7000	7000	7000	7000	7000	7000
Rehabilitation Costs	125,000	125,000	125,000	125,000	125,000	125,000
User Delay Costs	25000	25000	25000	25000	25000	25000
Total Rehabilitation Costs	150000	150000	150000	150000	150000	150000
Equivalent Annual Rehab Costs; Sinking Fund	59844	33240	30547	24367	20097	11926
Total Equivalent Annual Pavement Costs	515806	311842	291194	243810	211077	148430

Summary of Testing Costs

Critical Rut Depth, in.: 0.25
Reliability Level, %: 85
Median Pavement Service Life: 16

Cost Element	Test Method in Support of the Transfer Function					
	Baseline	Mix Adjust.	Loaded Wheel	SPT	RLPD	RSCH
Interest Rate	0.05	0.05	0.05	0.05	0.05	0.05
Number of Compound Periods	2.42	4.17	4.5	5.5	6.5	10
Capital Recovery Factors	0.0563	0.0613	0.0623	0.0654	0.0687	0.0814
	0.1253	0.2256	0.2455	0.3078	0.3732	0.6289
Compound Interest Factors; Capital Recovery	0.4490	0.2716	0.2536	0.2124	0.1840	0.1295
Mixture Design Costs	25000	25000	25000	25000	25000	25000
Initial Test Equipment Costs	0	0	50000	40000	40000	65000
Initial Compaction Equipment Costs	0	0	2500	0	0	2500
Initial Specimen Equipment Prep Costs	0	0	3000	1500	1500	3000
Total Initial Equipment & Mix Design Costs	25000	25000	80500	66500	66500	95500
Annual Initial Equipment & Mix Design Costs	11224	6790	20419	14127	12235	12368
Unit Sample Prep Costs	0	0	2500	1500	1500	3000
Number of Compacted Samples	0	0	3	2	6	1
Total Sample Prep Costs	0	0	7500	3000	9000	3000
Unit Specimen Test Costs	0	0	2000	1000	1000	1000
Number of Test Specimens	0	0	3	2	6	6
Total Specimen Testing Costs	0	0	6000	2000	6000	6000
Total Specimen Prep & Testing Costs	0	0	13500	5000	15000	9000
Annual Specimen Prep & Testing Costs	0	0	3424	1062	2760	1166
Annual Equipment Maintenance Costs	6000	6000	7000	7000	7000	7000
Annual Equipment Overhead Costs	30000	30000	40000	40000	40000	40000
Total Equivalent Annual Testing Costs	47224	42790	70843	62190	61994	60533

Exhibit F.2. (Continued).

Summary of Pavement Costs

Critical Rut Depth	0.25
Reliability Level	95
Median Pavement Service Life	16

Cost Element	Test Method in Support of the Transfer Function					
	Baseline	Mix Adjust.	Loaded Wheel	SPT	RLPD	RSCH
Interest Rate	0.05	0.05	0.05	0.05	0.05	0.05
Number of Compound Periods	0.58	1	1.2	1.4	1.58	3
Capitol Recovery Factors	0.0514	0.0525	0.0530	0.0535	0.0540	0.0579
	0.0287	0.0500	0.0603	0.0707	0.0801	0.1576
Compound Interest Factors; Capital Recovery	1.7920	1.0500	0.8792	0.7573	0.6739	0.3672
Sinking Fund Compound Interest Factors	1.7420	1.0000	0.8292	0.7073	0.6239	0.3172
Construction Costs	1,000,000	1,000,000	1,000,000	1,000,000	1,000,000	1,000,000
Equivalent Annual Constr. Costs; Capital Recovery	1792009	1050000	879241	757282	673927	367209
Annual Maintenance Costs	2000	2000	2000	2000	2000	2000
Annual User Costs	5000	5000	5000	5000	5000	5000
Total Annual Costs	7000	7000	7000	7000	7000	7000
Rehabilitation Costs	125,000	125,000	125,000	125,000	125,000	125,000
User Delay Costs	25000	25000	25000	25000	25000	25000
Total Rehabilitation Costs	150000	150000	150000	150000	150000	150000
Equivalent Annual Rehab Costs; Sinking Fund	261301	150000	124386	106092	93589	47581
Total Equivalent Annual Pavement Costs	2060310	1207000	1010627	870375	774516	421790

Summary of Testing Costs

Critical Rut Depth, in.	0.25
Reliability Level, %	95
Median Pavement Service Life	16

Cost Element	Test Method in Support of the Transfer Function					
	Baseline	Mix Adjust.	Loaded Wheel	SPT	RLPD	RSCH
Interest Rate	0.05	0.05	0.05	0.05	0.05	0.05
Number of Compound Periods	0.58	1	1.2	1.4	1.58	3
Capital Recovery Factors	0.0514	0.0525	0.0530	0.0535	0.0540	0.0579
	0.0287	0.0500	0.0603	0.0707	0.0801	0.1576
Compound Interest Factors; Capital Recovery	1.7920	1.0500	0.8792	0.7573	0.6739	0.3672
Mixture Design Costs	25000	25000	25000	25000	25000	25000
Initial Test Equipment Costs	0	0	50000	40000	40000	65000
Initial Compaction Equipment Costs	0	0	2500	0	0	2500
Initial Specimen Equipment Prep Costs	0	0	3000	1500	1500	3000
Total Initial Equipment & Mix Design Costs	25000	25000	80500	66500	66500	95500
Annual Initial Equipment & Mix Design Costs	44800	26250	70779	50359	44816	35068
Unit Sample Prep Costs	0	0	2500	1500	1500	3000
Number of Compacted Samples	0	0	3	2	6	1
Total Sample Prep Costs	0	0	7500	3000	9000	3000
Unit Specimen Test Costs	0	0	2000	1000	1000	1000
Number of Test Specimens	0	0	3	2	6	6
Total Specimen Testing Costs	0	0	6000	2000	6000	6000
Total Specimen Prep & Testing Costs	0	0	13500	5000	15000	9000
Annual Specimen Prep & Testing Costs	0	0	11870	3786	10109	3305
Annual Equipment Maintenance Costs	6000	6000	7000	7000	7000	7000
Annual Equipment Overhead Costs	30000	30000	40000	40000	40000	40000
Total Equivalent Annual Testing Costs	80800	62250	129649	101146	101925	85373

Exhibit F.3.

Summary of Pavement Costs

Critical Rut Depth	0.5
Reliability Level	75
Median Pavement Service Life	22

Cost Element	Test Method in Support of the Transfer Function					
	Baseline	Mix Adjust.	Loaded Wheel	SPT	RLPD	RSCH
Interest Rate	0.05	0.05	0.05	0.05	0.05	0.05
Number of Compound Periods	8	14	14.5	15	15.58	18.92
Capitol Recovery Factors	0.0739	0.0990	0.1014	0.1039	0.1069	0.1259
	0.4775	0.9799	1.0288	1.0789	1.1386	1.5171
Compound Interest Factors; Capital Recovery	0.1547	0.1010	0.0986	0.0963	0.0939	0.0830
Sinking Fund Compound Interest Factors	0.1047	0.0510	0.0486	0.0463	0.0439	0.0330
Construction Costs	1,000,000	1,000,000	1,000,000	1,000,000	1,000,000	1,000,000
Equivalent Annual Constr. Costs; Capital Recovery	154722	101024	98599	96342	93914	82957
Annual Maintenance Costs	2000	2000	2000	2000	2000	2000
Annual User Costs	5000	5000	5000	5000	5000	5000
Total Annual Costs	7000	7000	7000	7000	7000	7000
Rehabilitation Costs	125,000	125,000	125,000	125,000	125,000	125,000
User Delay Costs	25000	25000	25000	25000	25000	25000
Total Rehabilitation Costs	150000	150000	150000	150000	150000	150000
Equivalent Annual Rehab Costs; Sinking Fund	15708	7654	7290	6951	6587	4944
Total Equivalent Annual Pavement Costs	177430	115678	112889	110294	107501	94901

Summary of Testing Costs

Critical Rut Depth, in.	0.5
Reliability Level, %	75
Median Pavement Service Life	22

Cost Element	Test Method in Support of the Transfer Function					
	Baseline	Mix Adjust.	Loaded Wheel	SPT	RLPD	RSCH
Interest Rate	0.05	0.05	0.05	0.05	0.05	0.05
Number of Compound Periods	8	14	14.5	15	15.58	18.92
Capital Recovery Factors	0.0739	0.0990	0.1014	0.1039	0.1069	0.1259
	0.4775	0.9799	1.0288	1.0789	1.1386	1.5171
Compound Interest Factors; Capital Recovery	0.1547	0.1010	0.0986	0.0963	0.0939	0.0830
Mixture Design Costs	25000	25000	25000	25000	25000	25000
Initial Test Equipment Costs	0	0	50000	40000	40000	65000
Initial Compaction Equipment Costs	0	0	2500	0	0	2500
Initial Specimen Equipment Prep Costs	0	0	3000	1500	1500	3000
Total Initial Equipment & Mix Design Costs	25000	25000	80500	66500	66500	95500
Annual Initial Equipment & Mix Design Costs	3868	2526	7937	6407	6245	7922
Unit Sample Prep Costs	0	0	2500	1500	1500	3000
Number of Compacted Samples	0	0	3	2	6	1
Total Sample Prep Costs	0	0	7500	3000	9000	3000
Unit Specimen Test Costs	0	0	2000	1000	1000	1000
Number of Test Specimens	0	0	3	2	6	6
Total Specimen Testing Costs	0	0	6000	2000	6000	6000
Total Specimen Prep & Testing Costs	0	0	13500	5000	15000	9000
Annual Specimen Prep & Testing Costs	0	0	1331	482	1409	747
Annual Equipment Maintenance Costs	6000	6000	7000	7000	7000	7000
Annual Equipment Overhead Costs	30000	30000	40000	40000	40000	40000
Total Equivalent Annual Testing Costs	39868	38526	56268	53888	54654	55669

Exhibit F.3. (Continued).

Summary of Pavement Costs

Critical Rut Depth: 0.5
Reliability Level: 85
Median Pavement Service Life: 22

Cost Element	Test Method in Support of the Transfer Function					
	Baseline	Mix Adjust.	Loaded Wheel	SPT	RLPD	RSCH
Interest Rate	0.05	0.05	0.05	0.05	0.05	0.05
Number of Compound Periods	2.92	6.92	7.3	7.8	8.25	11.42
Capitol Recovery Factors	0.0577	0.0701	0.0714	0.0732	0.0748	0.0873
	0.1531	0.4016	0.4278	0.4631	0.4956	0.7457
Compound Interest Factors; Capital Recovery	0.3766	0.1745	0.1669	0.1580	0.1509	0.1170
Sinking Fund Compound Interest Factors	0.3266	0.1245	0.1169	0.1080	0.1009	0.0670
Construction Costs	1,000,000	1,000,000	1,000,000	1,000,000	1,000,000	1,000,000
Equivalent Annual Constr. Costs; Capital Recovery	376551	174496	166864	157966	150890	117047
Annual Maintenance Costs	2000	2000	2000	2000	2000	2000
Annual User Costs	5000	5000	5000	5000	5000	5000
Total Annual Costs	7000	7000	7000	7000	7000	7000
Rehabilitation Costs	125,000	125,000	125,000	125,000	125,000	125,000
User Delay Costs	25000	25000	25000	25000	25000	25000
Total Rehabilitation Costs	150000	150000	150000	150000	150000	150000
Equivalent Annual Rehab Costs; Sinking Fund	48983	18674	17530	16195	15134	10057
Total Equivalent Annual Pavement Costs	432534	200171	191394	181161	173024	134104

Summary of Testing Costs

Critical Rut Depth, in.: 0.5
Reliability Level, %: 85
Median Pavement Service Life: 22

Cost Element	Test Method in Support of the Transfer Function					
	Baseline	Mix Adjust.	Loaded Wheel	SPT	RLPD	RSCH
Interest Rate	0.05	0.05	0.05	0.05	0.05	0.05
Number of Compound Periods	2.92	6.92	7.3	7.8	8.25	11.42
Capital Recovery Factors	0.0577	0.0701	0.0714	0.0732	0.0748	0.0873
	0.1531	0.4016	0.4278	0.4631	0.4956	0.7457
Compound Interest Factors; Capital Recovery	0.3766	0.1745	0.1669	0.1580	0.1509	0.1170
Mixture Design Costs	25000	25000	25000	25000	25000	25000
Initial Test Equipment Costs	0	0	50000	40000	40000	65000
Initial Compaction Equipment Costs	0	0	2500	0	0	2500
Initial Specimen Equipment Prep Costs	0	0	3000	1500	1500	3000
Total Initial Equipment & Mix Design Costs	25000	25000	80500	66500	66500	95500
Annual Initial Equipment & Mix Design Costs	9414	4362	13433	10505	10034	11178
Unit Sample Prep Costs	0	0	2500	1500	1500	3000
Number of Compacted Samples	0	0	3	2	6	1
Total Sample Prep Costs	0	0	7500	3000	9000	3000
Unit Specimen Test Costs	0	0	2000	1000	1000	1000
Number of Test Specimens	0	0	3	2	6	6
Total Specimen Testing Costs	0	0	6000	2000	6000	6000
Total Specimen Prep & Testing Costs	0	0	13500	5000	15000	9000
Annual Specimen Prep & Testing Costs	0	0	2253	790	2263	1053
Annual Equipment Maintenance Costs	6000	6000	7000	7000	7000	7000
Annual Equipment Overhead Costs	30000	30000	40000	40000	40000	40000
Total Equivalent Annual Testing Costs	45414	40362	62685	58295	59298	59231

(continued on next page)

Exhibit F.3. (Continued).

Summary of Pavement Costs

Critical Rut Depth	0.5
Reliability Level	95
Median Pavement Service Life	22

Cost Element	Test Method in Support of the Transfer Function					
	Baseline	Mix Adjust.	Loaded Wheel	SPT	RLPD	RSCH
Interest Rate	0.05	0.05	0.05	0.05	0.05	0.05
Number of Compound Periods	0.83	2.17	2.2	2.3	2.58	4.42
Capitol Recovery Factors	0.0521	0.0556	0.0557	0.0559	0.0567	0.0620
	0.0413	0.1117	0.1133	0.1188	0.1341	0.2407
Compound Interest Factors; Capital Recovery	1.2599	0.4977	0.4913	0.4710	0.4227	0.2578
Sinking Fund Compound Interest Factors	1.2099	0.4477	0.4413	0.4210	0.3727	0.2078
Construction Costs	1,000,000	1,000,000	1,000,000	1,000,000	1,000,000	1,000,000
Equivalent Annual Constr. Costs; Capital Recovery	1259864	497698	491264	471031	422732	257752
Annual Maintenance Costs	2000	2000	2000	2000	2000	2000
Annual User Costs	5000	5000	5000	5000	5000	5000
Total Annual Costs	7000	7000	7000	7000	7000	7000
Rehabilitation Costs	125,000	125,000	125,000	125,000	125,000	125,000
User Delay Costs	25000	25000	25000	25000	25000	25000
Total Rehabilitation Costs	150000	150000	150000	150000	150000	150000
Equivalent Annual Rehab Costs; Sinking Fund	181480	67155	66190	63155	55910	31163
Total Equivalent Annual Pavement Costs	1448343	571852	564453	541186	485642	295915

Summary of Testing Costs

Critical Rut Depth, in.	0.5
Reliability Level, %	95
Median Pavement Service Life	22

Cost Element	Test Method in Support of the Transfer Function					
	Baseline	Mix Adjust.	Loaded Wheel	SPT	RLPD	RSCH
Interest Rate	0.05	0.05	0.05	0.05	0.05	0.05
Number of Compound Periods	0.83	2.17	2.2	2.3	2.58	4.42
Capital Recovery Factors	0.0521	0.0556	0.0557	0.0559	0.0567	0.0620
	0.0413	0.1117	0.1133	0.1188	0.1341	0.2407
Compound Interest Factors; Capital Recovery	1.2599	0.4977	0.4913	0.4710	0.4227	0.2578
Mixture Design Costs	25000	25000	25000	25000	25000	25000
Initial Test Equipment Costs	0	0	50000	40000	40000	65000
Initial Compaction Equipment Costs	0	0	2500	0	0	2500
Initial Specimen Equipment Prep Costs	0	0	3000	1500	1500	3000
Total Initial Equipment & Mix Design Costs	25000	25000	80500	66500	66500	95500
Annual Initial Equipment & Mix Design Costs	31497	12442	39547	31324	28112	24615
Unit Sample Prep Costs	0	0	2500	1500	1500	3000
Number of Compacted Samples	0	0	3	2	6	1
Total Sample Prep Costs	0	0	7500	3000	9000	3000
Unit Specimen Test Costs	0	0	2000	1000	1000	1000
Number of Test Specimens	0	0	3	2	6	6
Total Specimen Testing Costs	0	0	6000	2000	6000	6000
Total Specimen Prep & Testing Costs	0	0	13500	5000	15000	9000
Annual Specimen Prep & Testing Costs	0	0	6632	2355	6341	2320
Annual Equipment Maintenance Costs	6000	6000	7000	7000	7000	7000
Annual Equipment Overhead Costs	30000	30000	40000	40000	40000	40000
Total Equivalent Annual Testing Costs	67497	48442	93179	80679	81453	73935

Exhibit F.4.

Summary of Pavement Costs

Critical Rut Depth	0.75
Reliability Level	75
Median Pavement Service Life	27

Cost Element	Test Method in Support of the Transfer Function					
	Baseline	Mix Adjust.	Loaded Wheel	SPT	RLPD	RSCH
Interest Rate	0.05	0.05	0.05	0.05	0.05	0.05
Number of Compound Periods	14.83	23	23.5	24.5	25.58	29.08
Capitol Recovery Factors	0.1031	0.1536	0.1574	0.1652	0.1742	0.2066
	1.0618	2.0715	2.1474	2.3047	2.4836	3.1322
Compound Interest Factors; Capital Recovery	0.0971	0.0741	0.0733	0.0717	0.0701	0.0660
Sinking Fund Compound Interest Factors	0.0471	0.0241	0.0233	0.0217	0.0201	0.0160
Construction Costs	1,000,000	1,000,000	1,000,000	1,000,000	1,000,000	1,000,000
Equivalent Annual Constr. Costs; Capital Recovery	97092	74137	73284	71694	70132	65963
Annual Maintenance Costs	2000	2000	2000	2000	2000	2000
Annual User Costs	5000	5000	5000	5000	5000	5000
Total Annual Costs	7000	7000	7000	7000	7000	7000
Rehabilitation Costs	125,000	125,000	125,000	125,000	125,000	125,000
User Delay Costs	25000	25000	25000	25000	25000	25000
Total Rehabilitation Costs	150000	150000	150000	150000	150000	150000
Equivalent Annual Rehab Costs; Sinking Fund	7064	3621	3493	3254	3020	2394
Total Equivalent Annual Pavement Costs	111156	84757	83777	81949	80152	75358

Summary of Testing Costs

Critical Rut Depth, in.	0.75
Reliability Level, %	75
Median Pavement Service Life	27

Cost Element	Test Method in Support of the Transfer Function					
	Baseline	Mix Adjust.	Loaded Wheel	SPT	RLPD	RSCH
Interest Rate	0.05	0.05	0.05	0.05	0.05	0.05
Number of Compound Periods	14.83	23	23.5	24.5	25.58	29.08
Capital Recovery Factors	0.1031	0.1536	0.1574	0.1652	0.1742	0.2066
	1.0618	2.0715	2.1474	2.3047	2.4836	3.1322
Compound Interest Factors; Capital Recovery	0.0971	0.0741	0.0733	0.0717	0.0701	0.0660
Mixture Design Costs	25000	25000	25000	25000	25000	25000
Initial Test Equipment Costs	0	0	50000	40000	40000	65000
Initial Compaction Equipment Costs	0	0	2500	0	0	2500
Initial Specimen Equipment Prep Costs	0	0	3000	1500	1500	3000
Total Initial Equipment & Mix Design Costs	25000	25000	80500	66500	66500	95500
Annual Initial Equipment & Mix Design Costs	2427	1853	5899	4768	4664	6299
Unit Sample Prep Costs	0	0	2500	1500	1500	3000
Number of Compacted Samples	0	0	3	2	6	1
Total Sample Prep Costs	0	0	7500	3000	9000	3000
Unit Specimen Test Costs	0	0	2000	1000	1000	1000
Number of Test Specimens	0	0	3	2	6	6
Total Specimen Testing Costs	0	0	6000	2000	6000	6000
Total Specimen Prep & Testing Costs	0	0	13500	5000	15000	9000
Annual Specimen Prep & Testing Costs	0	0	989	358	1052	594
Annual Equipment Maintenance Costs	6000	6000	7000	7000	7000	7000
Annual Equipment Overhead Costs	30000	30000	40000	40000	40000	40000
Total Equivalent Annual Testing Costs	38427	37853	53889	52126	52716	53893

(continued on next page)

Exhibit F.4. (Continued).

Summary of Pavement Costs

Critical Rut Depth	0.75
Reliability Level	85
Median Pavement Service Life	27

Cost Element	Test Method in Support of the Transfer Function					
	Baseline	Mix Adjust.	Loaded Wheel	SPT	RLPD	RSCH
Interest Rate	0.05	0.05	0.05	0.05	0.05	0.05
Number of Compound Periods	6.17	13.75	14.5	15.5	16.5	20.75
Capitol Recovery Factors	0.0676	0.0978	0.1014	0.1065	0.1118	0.1376
	0.3513	0.9559	1.0288	1.1303	1.2368	1.7522
Compound Interest Factors; Capital Recovery	0.1923	0.1023	0.0986	0.0942	0.0904	0.0785
Sinking Fund Compound Interest Factors	0.1423	0.0523	0.0486	0.0442	0.0404	0.0285
Construction Costs	1,000,000	1,000,000	1,000,000	1,000,000	1,000,000	1,000,000
Equivalent Annual Constr. Costs; Capital Recovery	192346	102305	98599	94237	90428	78536
Annual Maintenance Costs	2000	2000	2000	2000	2000	2000
Annual User Costs	5000	5000	5000	5000	5000	5000
Total Annual Costs	7000	7000	7000	7000	7000	7000
Rehabilitation Costs	125,000	125,000	125,000	125,000	125,000	125,000
User Delay Costs	25000	25000	25000	25000	25000	25000
Total Rehabilitation Costs	150000	150000	150000	150000	150000	150000
Equivalent Annual Rehab Costs; Sinking Fund	21352	7846	7290	6636	6064	4280
Total Equivalent Annual Pavement Costs	220698	117151	112889	107873	103492	89816

Summary of Testing Costs

Critical Rut Depth, in.	0.75
Reliability Level, %	85
Median Pavement Service Life	27

Cost Element	Test Method in Support of the Transfer Function					
	Baseline	Mix Adjust.	Loaded Wheel	SPT	RLPD	RSCH
Interest Rate	0.05	0.05	0.05	0.05	0.05	0.05
Number of Compound Periods	6.17	13.75	14.5	15.5	16.5	20.75
Capital Recovery Factors	0.0676	0.0978	0.1014	0.1065	0.1118	0.1376
	0.3513	0.9559	1.0288	1.1303	1.2368	1.7522
Compound Interest Factors; Capital Recovery	0.1923	0.1023	0.0986	0.0942	0.0904	0.0785
Mixture Design Costs	25000	25000	25000	25000	25000	25000
Initial Test Equipment Costs	0	0	50000	40000	40000	65000
Initial Compaction Equipment Costs	0	0	2500	0	0	2500
Initial Specimen Equipment Prep Costs	0	0	3000	1500	1500	3000
Total Initial Equipment & Mix Design Costs	25000	25000	80500	66500	66500	95500
Annual Initial Equipment & Mix Design Costs	4809	2558	7937	6267	6013	7500
Unit Sample Prep Costs	0	0	2500	1500	1500	3000
Number of Compacted Samples	0	0	3	2	6	1
Total Sample Prep Costs	0	0	7500	3000	9000	3000
Unit Specimen Test Costs	0	0	2000	1000	1000	1000
Number of Test Specimens	0	0	3	2	6	6
Total Specimen Testing Costs	0	0	6000	2000	6000	6000
Total Specimen Prep & Testing Costs	0	0	13500	5000	15000	9000
Annual Specimen Prep & Testing Costs	0	0	1331	471	1356	707
Annual Equipment Maintenance Cost	6000	6000	7000	7000	7000	7000
Annual Equipment Overhead Costs	30000	30000	40000	40000	40000	40000
Total Equivalent Annual Testing Costs	40809	38558	56268	53738	54370	55207

Exhibit F.4. (Continued).

Summary of Pavement Costs

Critical Rut Depth: 0.75
Reliability Level: 95
Median Pavement Service Life: 27

Cost Element	Test Method in Support of the Transfer Function					
	Baseline	Mix Adjust.	Loaded Wheel	SPT	RLPD	RSCH
Interest Rate	0.05	0.05	0.05	0.05	0.05	0.05
Number of Compound Periods	1.58	5	5.5	6	6.75	10.58
Capitol Recovery Factors	0.0540	0.0638	0.0654	0.0670	0.0695	0.0838
	0.0801	0.2763	0.3078	0.3401	0.3900	0.6756
Compound Interest Factors; Capital Recovery	0.6739	0.2310	0.2124	0.1970	0.1782	0.1240
Sinking Fund Compound Interest Factors	0.6239	0.1810	0.1624	0.1470	0.1282	0.0740
Construction Costs	1,000,000	1,000,000	1,000,000	1,000,000	1,000,000	1,000,000
Equivalent Annual Constr. Costs; Capital Recovery	673927	230975	212443	197017	178191	124003
Annual Maintenance Costs	2000	2000	2000	2000	2000	2000
Annual User Costs	5000	5000	5000	5000	5000	5000
Total Annual Costs	7000	7000	7000	7000	7000	7000
Rehabilitation Costs	125,000	125,000	125,000	125,000	125,000	125,000
User Delay Costs	25000	25000	25000	25000	25000	25000
Total Rehabilitation Costs	150000	150000	150000	150000	150000	150000
Equivalent Annual Rehab Costs; Sinking Fund	93589	27146	24367	22053	19229	11100
Total Equivalent Annual Pavement Costs	774516	265121	243810	226070	204420	142103

Summary of Testing Costs

Critical Rut Depth, in.: 0.75
Reliability Level, %: 95
Median Pavement Service Life: 27

Cost Element	Test Method in Support of the Transfer Function					
	Baseline	Mix Adjust.	Loaded Wheel	SPT	RLPD	RSCH
Interest Rate	0.05	0.05	0.05	0.05	0.05	0.05
Number of Compound Periods	1.58	5	5.5	6	6.75	10.58
Capital Recovery Factors	0.0540	0.0638	0.0654	0.0670	0.0695	0.0838
	0.0801	0.2763	0.3078	0.3401	0.3900	0.6756
Compound Interest Factors; Capital Recovery	0.6739	0.2310	0.2124	0.1970	0.1782	0.1240
Mixture Design Costs	25000	25000	25000	25000	25000	25000
Initial Test Equipment Costs	0	0	50000	40000	40000	65000
Initial Compaction Equipment Costs	0	0	2500	0	0	2500
Initial Specimen Equipment Prep Costs	0	0	3000	1500	1500	3000
Total Initial Equipment & Mix Design Costs	25000	25000	80500	66500	66500	95500
Annual Initial Equipment & Mix Design Costs	16848	5774	17102	13102	11850	11842
Unit Sample Prep Costs	0	0	2500	1500	1500	3000
Number of Compacted Samples	0	0	3	2	6	1
Total Sample Prep Costs	0	0	7500	3000	9000	3000
Unit Specimen Test Costs	0	0	2000	1000	1000	1000
Number of Test Specimens	0	0	3	2	6	6
Total Specimen Testing Costs	0	0	6000	2000	6000	6000
Total Specimen Prep & Testing Costs	0	0	13500	5000	15000	9000
Annual Specimen Prep & Testing Costs	0	0	2868	985	2673	1116
Annual Equipment Maintenance Costs	6000	6000	7000	7000	7000	7000
Annual Equipment Overhead Costs	30000	30000	40000	40000	40000	40000
Total Equivalent Annual Testing Costs	52848	41774	66970	61087	61523	59958

Cited AASHTO Standard and Provisional Practices and Methods of Test

R 30, Mixture Conditioning of Hot Mix Asphalt (HMA)

T 166, Bulk Specific Gravity of Compacted Hot Mix Asphalt (HMA) Using Saturated Surface-Dry Specimens

T 269, Percent Air Voids in Compacted Dense and Open Asphalt Mixtures

T 275, Bulk Specific Gravity of Compacted Hot Mix Asphalt (HMA) Using Paraffin-Coated Specimens

T 304, Uncompacted Void Content of Fine Aggregate

T 320, Determining the Permanent Shear Strain and Stiffness of Asphalt Mixtures Using the Superpave Shear Tester (SST)

T 326, Uncompacted Void Content of Coarse Aggregate (As Influenced by Particle Shape, Surface Texture, and Grading)

T 335, Determining the Percentage of Fracture in Coarse Aggregate

PP 3, Preparing Hot-Mix Asphalt (HMA) by Means of the Rolling Wheel Compactor

PP 60, Preparation of Cylindrical Performance Test Specimens Using the Superpave Gyratory Compactor (SGC)

PP 61, Developing Dynamic Modulus Master Curves for Hot Mix Asphalt (HMA) Using the Asphalt Mixture Performance Tester (AMPT)

TP 79, Determining the Dynamic Modulus and Flow Number for Hot Mix Asphalt (HMA) Using the Asphalt Mixture Performance Tester (AMPT)

References

AASHTO. *AASHTO Guide for Design of Pavement Structures.* American Association of State Highway and Transportation Officials, Washington, D.C., 1993.

AASHTO. *Manual of Practice for the Mechanistic–Empirical Pavement Design Guide.* American Association of State Highway and Transportation Officials, Washington, D.C., 2008.

AASHTO. *Manual of Practice for Local Calibration of the Mechanistic–Empirical Pavement Design Guide.* American Association of State Highway and Transportation Officials, Washington, D.C., 2010.

Archilla, A. R., L.-L. Kobayashi, and L. G. Diaz. Using Permanent Deformation Tests and the MEPDG to Quantify Permanent Deformation Improvements from Modified Binders. *Journal of the Association of Asphalt Paving Technologists,* Volume 77, 2008, pp. 1005–1033.

ARA. *Guidelines for Implementing NCHRP 1-37A M-E Design Procedures in Ohio: Volume 4—MEPDG Models Validation and Recalibration.* Final Report for Job Number 134300, Ohio Department of Transportation, Office of Research and Development, Columbus, Ohio, 2008.

ARA. *Implementing the AASHTO Mechanistic–Empirical Pavement Design Guide in Missouri, Volume II: MEPDG Model Validation and Calibration.* Final Report CM08.01, MODOT Study R104-002, Missouri Department of Transportation, Construction and Materials Division, Jefferson City, Missouri, 2009.

ARA, Inc., ERES Consultants Division. *Guide for Mechanistic–Empirical Design of New and Rehabilitated Pavement Structures.* Final Report, NCHRP Project 1-37A. Transportation Research Board of the National Academies, Washington, D.C., 2004.

Asphalt Institute. *Quantifying the Effects of PMA for Reducing Pavement Distress.* Informational Series #215, First Edition, Asphalt Institute, Lexington, Kentucky, 2005.

Biligiri, K. P. Rational Modeling of Tertiary Flow for Asphalt Mixtures. *Transportation Research Record: Journal of the Transportation Research Board, No. 2001.* Transportation Research Board of the National Academies, Washington, D.C., 2007, pp. 63–72.

Daleiden, J. F., J. B. Rauhut, B. Killingsworth, E. O. Antwi, and M. I. Darter. *SHRP Report SHRP-P-394: Evaluation of the AASHTO Design Equations and Recommended Improvements.* TRB, National Research Council, Washington, D.C., 1994.

Desai, C. S. and D. Zhang. Viscoplastic Model for Geologic Materials with Generalized Flow Rule. *International Journal for Numerical and Analytical Methods in Geomechanics,* Vol. 11, 1987, pp. 603–662.

Epps, J. A., A. Hand, S. Seeds, T. Scholz, S. Alavi, C. Ashmore, C. L. Monismith, J. A. Deacon, J. T. Harvey, and R. Leahy. *NCHRP Report 455: Recommended Performance-Related Specification For Hot-Mix Asphalt Construction.* Part II: Performance-Related Specification. TRB, National Research Council, Washington, D.C., 2000.

FHWA. *Determining Modified Asphalt Binder Properties for the Superpave Specification: Report on the Construction of Pavements with Modified Asphalt Binders.* Pooled Fund Study TPF-5(019), Federal Highway Administration, Turner-Fairbank Highway Research Center, McLean, Virginia, 2004.

Gibson, N. H. *A Viscoelastoplastic Continuum Damage Model for the Compressive Behavior of Asphalt Concrete.* PhD. Dissertation. University of Maryland, College Park, MD, 2006.

Ha, K. and R. A. Schapery. A Three-Dimensional Viscoelastic Constitutive Model for Particulate Composites with Growing Damage and Its Experimental Verification. *International Journal of Solids and Structures,* Vol. 35, No. 26–27, 1998, pp. 3497–3517.

Kaloush, K. E. and M. W. Witczak. Development of a Permanent to Elastic Strain Ratio Model for Asphalt Mixtures. Inter-Team Technical Report for NCHRP Project 1-37A, "Development of the 2002 Guide for the Design of New and Rehabilitated Pavement Structures." ERES Consultants, Inc., September 2000.

Kenis, W. J. Predictive Design Procedures: A Design Method for Flexible Pavements Using the VESYS Structural Subsystem. *Proceedings—Volume 1,* 4th International Conference on the Structural Design of Asphalt Pavements, Ann Arbor, MI, 1977.

Kenis, W. J., J. A. Sherwood, and T. F. McMahon. Verification and Application of the VESYS Structural Subsystem. *Proceedings—Volume 1,* 5th International Conference on the Structural Design of Asphalt Pavements, Delft, The Netherlands, 1982, pp. 333–334.

Leahy, R. B. *Permanent Deformation Characteristics of Asphalt Concrete.* Ph.D. Dissertation. University of Maryland, College Park, MD, 1989.

Monismith, C. L. and K. Wallace. Pavement Design Considerations for Two-Layer Pavements Containing Open-Graded Asphalt Mixtures. *Journal of Association of Asphalt Paving Technologists,* Vol. 51, 1982, pp. 1–34.

Monismith, C. L., R. G. Hicks, F. N. Finn, J. Sousa, J. Harvey, S. Weissman, J. Deacon, J. Coplantz, and G. Paulsen. *SHRP Report SHRP-A-415: Permanent Deformation Response of Asphalt Aggregate Mixes.* TRB, National Research Council, Washington, D.C., 1994.

Monismith, C. L., J. A. Deacon, and J. T. Harvey. *WesTrack: Performance Models for Permanent Deformation and Fatigue.* Pavement Research Center, Institute of Transportation Studies, University of California, Berkeley, 2000.

Monismith, C. L., L. Popescu, and J. T. Harvey. Rut Depth Estimation for Mechanistic–Empirical Pavement Design Using Simple Shear

Test Results. *AAPT Volume* #75, Association of Asphalt Paving Technologists, 2006.

Rauhut, J. B., J. C. O'Quinn, and W. R. Hudson. *Sensitivity Analysis of FHWA Structural Model VESYS II.* Report Number FHWA-RD-76-23, Federal Highway Administration, Office of Research and Development, Washington, D.C., 1976.

Rauhut, J. B. Permanent Deformation Characterization of Bituminous Mixtures for Pavement Rutting Predictions. *Transportation Research Record 777*. TRB, National Research Council, Washington, D.C., 1980.

Rauhut, J. B., R. L. Lytton, and D. I. Darter. *Pavement Damage Functions for Cost Allocation: Volume 2—Descriptions of Detailed Studies.* Report Number FHWA/RD-84/-19, Federal Highway Administration, Office of Engineering and Highway Operations, McLean, Virginia, 1984.

Rauhut, J. B., A. A. Eltahan, and A. L. Simpson. *Common Characteristics of Good And Poorly Performing AC Pavements.* Report Number FHWA-RD-99-193, Federal Highway Administration, Office of Engineering and Highway Operations—Research and Development, McLean, Virginia, 1999.

Rauhut, J. B., H. L. Von Quintus, and A. Eltahan. *Performance of Rehabilitated Asphalt Concrete Pavements in the LTPP Experiments—Data Collected Through February 1997.* Report No. FHWA-RD-00-029, Federal Highway Administration, Office of Infrastructure Research and Development, Washington, D.C., 2000.

Schapery, R. A. Nonlinear Viscoelastic and Viscoplastic Constitutive Equations with Growing Damage. *International Journal of Fracture,* Vol. 97, 1999, pp. 33–66.

SHRP. *SHRP Report SHRP-P-338: Distress Identification Manual for the Long-Term Pavement Performance Project.* TRB, National Research Council, Washington, D.C., 1993.

SHRP, Monismith, C. L., R. G. Hicks, F. N. Finn, J. Sousa, J. Harvey, S. Weissman, J. Deacon, J. Coplantz, and G. Paulsen. *SHRP Report SHRP-A-415: Permanent Deformation Response of Asphalt Aggregate Mixes,* Strategic Highway Research Program, TRB, National Research Council, Washington, D.C., 1994.

SHRP and D. R. Jones, IV. *SHRP Materials Reference Library: Asphalt Cements: A Concise Data Compilation.* TRB, National Research Council, Washington, D.C., 1993–1995. http://onlinepubs.trb.org/onlinepubs/shrp/SHRP-A-645.pdf.

Sousa, J. B., J. A. Deacon, S. Weissman, J. T. Harvey, C. L. Monismith, R. B. Leahy, G. Paulsen, and J. S. Coplantz. *SHRP Report SHRP-A-415: Permanent Deformation Response of Asphalt-Aggregate Mixes.* TRB, National Research Council, Washington, D.C., 1994.

Stuart, K. D., and W. S. Mogawer. *Modified Asphalt Binders in Mixtures: Permanent Deformation Using a Mixture with Diabase Aggregate.* Report No. FHWA-RD-02-042, Federal Highway Administration, Office of Infrastructure Research and Development, McLean,Virginia, 2002.

Transportation Research Board. *NCHRP Research Results Digest 283: Jackknife Testing—An Experimental Approach to Refine Model Calibration and Validation.* Transportation Research Board of the National Academies, Washington, D.C., 2003a.

Transportation Research Board. *NCHRP Research Results Digest 284: Refining the Calibration and Validation of Hot-Mix Asphalt Performance Models: An Experimental Plan and Database.* Transportation Research Board of the National Academies, Washington, D.C., 2003b.

Verstraeten, J., V. Veverka, and L. Francken. Rational and Practical Designs of Asphalt Pavements to Avoid Cracking and Rutting. *Proceedings,* 5th International Conference on the Structural Design of Asphalt Pavements, Ann Arbor, Michigan, 1982.

Von Quintus, H. L. Local Calibration Adjustments for the HMA Distress Prediction Models. Preliminary Draft Final Report for NCHRP Project 1-40B. Applied Research Associates, Inc., 2005.

Von Quintus, H. L. History and Hypothesis Behind the HMA Mixture Adjustment Factors for Rutting and Area Fatigue Cracking Predictions. White Paper prepared for NCHRP Project 1-40B, "User Manual and Local Calibration Guide for the Mechanistic–Empirical Pavement Design Guide and Software." Applied Research Associates, Inc., 2006.

Von Quintus, H. L., J. B. Rauhut, T. W. Kennedy, and P. J. Jordahl. *Cost Effectiveness of Current Sampling and Testing Programs for Paving Construction and Materials,* Report No. FHWA/RD-85/030, Federal Highway Administration, Washington, D.C., January 1985.

Von Quintus, H. L., J. A. Scherocman, C. S. Hughes, and T. W. Kennedy. *NCHRP Report No. 338: Asphalt-Aggregate Mixture Analysis System: AAMAS*. TRB, National Research Council; Washington, D.C., 1991.

Von Quintus, H. L. and B. Killingsworth. *Design Pamphlet for the Determination of Layered Elastic Moduli for Flexible Pavement Design.* Publication Number FHWA-RD-97-077, Federal Highway Administration, Turner-Fairbanks Highway Research Center, Washington, D.C., 1997a.

Von Quintus, H. L. and B. Killingsworth. *Design Pamphlet for the Backcalculation of Pavement Layer Moduli in Support of the 1993 AASHTO Guide for the Design of Pavement Structures.* Publication Number FHWA-RD-97-076, Federal Highway Administration, Turner-Fairbanks Highway Research Center, Washington, D.C., 1997b.

Von Quintus, H. L. and B. Killingsworth. *Analyses Relating to Pavement Material Characterizations and Their Effects on Pavement Performance.* Publication Number FHWA-RD-97-085, Federal Highway Administration, Turner-Fairbanks Highway Research Center, Washington, D.C., 1998.

Von Quintus, H. L. and A. L. Simpson. *Structural Factors for Flexible Pavements—Initial Evaluation of the SPS-1 Experiment.* Report No. FHWA-RD-01-166, Federal Highway Administration, Office of Engineering Research and Development, Washington, D.C., 2000.

Von Quintus, H. L., A. L. Simpson, and A. A. Eltahan. *Rehabilitation of Asphalt Concrete Pavements—Initial Evaluation of the SPS-5 Experiment.* Federal Highway Administration, Office of Engineering Research and Development, Washington, D.C., 2000.

Von Quintus, H. L. and A. Yau. *Evaluation of Resilient Modulus Test Data in LTPP Database.* Report Number FHWA/RD-01-158, Federal Highway Administration, Office of Infrastructure Research and Development, Washington, D.C., 2001.

Von Quintus, H. L., C. Schwartz, R. McCuen, and D. Andrei. Experimental Plan for Calibration and Validation of Hot-Mix Asphalt Performance Models for Mix and Structural Design. Draft Final Report for NCHRP Project 9-30. Fugro Consultants LLP, 2004.

Von Quintus, H. L., D. Andrei, and C. Schwartz. Conduct Two Pre-Implementation Studies and Expand Population of M-E_DPM Database. Draft Report for NCHRP Project 9-30(01). Washington, D.C., Applied Research Associates and Fugro Consultants LLP, 2005.

Von Quintus, H. L., and J. S. Moulthrop. *Performance Prediction Models: Volume I—Research Report.* Publication Number FHWA/MT-06-014/8158-1, Montana Department of Transportation, Helena, MT, 2007.

Von Quintus, H. L., J. Mallela, and L. Titus-Glover. *Calibration Factors for Polymer Modified Asphalts Using M-E Based Design Methods.* Report Number 17985-1/1, Applied Research Associates, Inc.,

Prepared for the Affiliate Committee of the Asphalt Institute, Lexington, Kentucky, 2007.

Von Quintus, H. L., C. Rao, R. Minchin, S. Nazarian, K. Maser, and B. Prowell. *NCHRP Report 626: NDT Technology for Quality Assurance of HMA Pavement Construction.* Transportation Research Board of the National Academies, Washington, D.C., 2009.

Witczak, M. W. *NCHRP Report 580: Simple Performance Tests for Permanent Deformation of Hot Mix Asphalt, Volume II: Flow Number and Flow Time.* Transportation Research Board of the National Academies, Washington, D.C., 2007.

Witczak, M. W., K. Kaloush, T. Pellinen, M. El-Basyouny, and H. L. Von Quintus. *NCHRP Report 465: Simple Performance Test for Superpave Mix Design.* TRB, National Research Council, Washington, D.C., 2002.

Zang J., A. Cooley, and P. S. Kandhal. Comparison of Fundamental and Simulative Test Methods for Evaluating Permanent Deformation of Hot-Mix Asphalt. *Transportation Research Record: Journal of the Transportation Research Board, No. 1789.* Transportation Research Board of the National Academies, Washington, D.C., 2002, pp. 91–100.

Abbreviations and acronyms used without definitions in TRB publications:

AAAE	American Association of Airport Executives
AASHO	American Association of State Highway Officials
AASHTO	American Association of State Highway and Transportation Officials
ACI–NA	Airports Council International–North America
ACRP	Airport Cooperative Research Program
ADA	Americans with Disabilities Act
APTA	American Public Transportation Association
ASCE	American Society of Civil Engineers
ASME	American Society of Mechanical Engineers
ASTM	American Society for Testing and Materials
ATA	American Trucking Associations
CTAA	Community Transportation Association of America
CTBSSP	Commercial Truck and Bus Safety Synthesis Program
DHS	Department of Homeland Security
DOE	Department of Energy
EPA	Environmental Protection Agency
FAA	Federal Aviation Administration
FHWA	Federal Highway Administration
FMCSA	Federal Motor Carrier Safety Administration
FRA	Federal Railroad Administration
FTA	Federal Transit Administration
HMCRP	Hazardous Materials Cooperative Research Program
IEEE	Institute of Electrical and Electronics Engineers
ISTEA	Intermodal Surface Transportation Efficiency Act of 1991
ITE	Institute of Transportation Engineers
NASA	National Aeronautics and Space Administration
NASAO	National Association of State Aviation Officials
NCFRP	National Cooperative Freight Research Program
NCHRP	National Cooperative Highway Research Program
NHTSA	National Highway Traffic Safety Administration
NTSB	National Transportation Safety Board
PHMSA	Pipeline and Hazardous Materials Safety Administration
RITA	Research and Innovative Technology Administration
SAE	Society of Automotive Engineers
SAFETEA-LU	Safe, Accountable, Flexible, Efficient Transportation Equity Act: A Legacy for Users (2005)
TCRP	Transit Cooperative Research Program
TEA-21	Transportation Equity Act for the 21st Century (1998)
TRB	Transportation Research Board
TSA	Transportation Security Administration
U.S.DOT	United States Department of Transportation